Università degli studi di Roma

Tor Vergata

Facoltà di Scienze Matematiche, Fisiche e Naturali

Corso di laurea magistrale in Fisica

HOMOGENEOUS METALLICITY SCALE FOR GALACTIC CLASSICAL CEPHEIDS

SCALA DI METALLICITÀ OMOGENEA PER CEFEIDI CLASSICHE GALATTICHE

SUPERVISOR:
Prof. Giuseppe Bono

CO-SUPERVISOR:
Prof. Roberto Buonanno

CANDIDATE:

Bastian Proxauf

A thesis submitted in partial fulfilment of the requirements for the degree of Master of Science at the University of Rome Tor Vergata

Academic year 2015/2016

Contents

List of Tables

List of Figures

Sommario

In questa tesi viene presentata una scala di metallicità omogenea per Cefeidi classiche Galattiche. Cominciando da spettri astronomici preridotti ottenuti da diversi spettrografi, un trattamento preliminare dei dati è necessario. Inizialmente viene eseguita una normalizzazione del continuo con IRAF, un software per l'analisi dati. Dopodichè la velocità radiale degli oggetti viene determinata, utilizzando lo stesso programma, tramite uno spettro di riferimento già corretto per velocità radiale e traslando gli spettri dei target in quel quadro di riferimento.

In seguito ad una verifica del rapporto segnale/rumore basato sulle regioni del continuo e su una ispezione visiva degli intervalli di lunghezza d'onda selezionati, viene stabilita l'idoneità degli spettri per l'analisi seguente. In questo processo alcuni di essi vengono esclusi dalla determinazione della metallicità. Dopodichè le ampiezze equivalenti di una vasta selezione di righe spettrali (~ 900) vengono misurate fittandone i profili. ARES è un codice sofisticato per eseguire il fitting in modo semi-automatico per un gran numero di spettri. Per alcuni spettri la velocità radiale viene calcolata utilizzando questo programma invece di IRAF.

La temperatura efficace dell'oggetto viene poi calcolata usando delle coppie specifiche di righe e trasformando il rapporto delle ampiezze equivalenti ottenute in precedenza tramite delle funzioni di base analitiche (calibrazioni). Questo cosiddetto *line-depth-ratio method*, oltre ad essere facile da usare, è statisticamente robusto e capace di fornire le temperature efficaci con elevata accuratezza. Tuttavia, le calibrazioni possono essere utilizzate solo in un certo intervallo di temperature. Quindi, mancando la conoscenza iniziale sul valore corretto della temperatura efficace, viene usato un metodo iterativo che esclude man mano gli oggetti più lontani dal valore medio della distribuzione di temperature.

Sulla base delle temperature efficaci, le ampiezze equivalenti di oggetti selezionati vengono ricontrollate e il fitting viene in alcuni casi raffinato, riducendo così la dispersione della distribuzione di temperature ottenuta dalla procedura precedente. Dunque, un'elevata attenzione viene dedicata all'incertezza sulle temperature efficaci, visto che esse costituiscono il fattore più importante per la fase seguente di questo lavoro, la determinazione della metallicità.

Per poter determinare l'abbondanza di ferro delle Cefeidi, vengono usati dei modelli atmosferici ottenuti sia dal database MARCS che da quello di Kurucz/Castelli. Un'interpolazione viene poi eseguita, utilizzando i modelli, con lo scopo di creare un grigliato ad alta risoluzione che copre uno spazio 3D di parametri definito da quantità stellari importanti: la temperatura efficace, la gravità superficiale e la metallicità. La dipendenza da un ulteriore parametro, la microturbulenza, è di importanza secondaria.

Queste atmosfere, assieme alle ampiezze equivalenti già misurate, permettono il calcolo delle abbondanze per le singole righe usando il programma MOOG. In questo processo, i modelli MARCS mostrano discontinuità nonfisiche e vengono quindi esclusi, lasciando quelli di Kurucz per la determinazione della metallicità.

Non sapendo i valori corretti di alcuni dei parametri stellari che definiscono il trattamento dell'opacità atmosferica, c'è bisogno di un approccio iterativo, in cui vengono minimizzate le differenze tra lo spettro osservato e quello predetto. La massa di dati rende quasi impossibile una procedura manuale, per questo delle routine automatizzate diventano indispensabili. È stato scritto un codice basato su *Python* nel quale - dato un insieme di parametri iniziali -

l'input viene raffinato ad ogni passo. Questa ottimizzazione dei parametri viene stabilita da alcune condizioni fisiche che devono essere soddisfatte per gli spettri individuali.

Con l'approccio attuale, assieme alla temperatura efficace, la gravità superficiale e la microturbulenza, vengono ricavate le abbondanze di Fe I (neutro) e Fe II (prima ionizzazione). Avendo ottenuto le metallicità per i vari spettri ed eseguito alcune validazioni, se ne determina la media sugli oggetti e i risultati dei diversi spettrografi vengono uniti. Stime della metallicità per 216 Cefeidi (quindi più del 40 % di quelle attualmente note) vengono fornite.

Le abbondanze di ferro in letteratura possono poi essere adattate alla scala di metallicità definita dai target di questa tesi, aumentando così naturalmente l'ampiezza del campione. Le informazioni aggiuntive sul raggio Galattocentrico del campione permettono la determinazione del gradiente (profilo) radiale di metallicità della Via Lattea. Guardando la distribuzione polare dei target, l'esistenza di asimmetrie nell'abbondanza di ferro nelle vicinanze del Sole può essere validata. Infine, dei gradienti di metallicità di riferimento ottenuti da diversi tipi di oggetti (Cefeidi, ammassi aperti, regioni HII) vengono confrontati con il profilo radiale ricavato in precedenza.

I risultati ottenuti in questo modo sono in perfetto accordo con gli studi preesistenti e confermano l'esaurimento del ferro nelle regioni esterne della Galassia. Il database omogeneo della metallicità di Cefeidi classiche Galattiche costruito in questa tesi è quello più grande finora.

Abstract

In this thesis a homogeneous metallicity scale for Galactic classical Cepheids is presented. Starting from astronomical prereduced spectra taken by various spectrographs, a preliminary treatment of the data is necessary. First a continuum normalization is performed with the IRAF data analysis software. Afterwards the radial velocity for the objects is determined using the same program by means of a radial-velocity-free template spectrum and shifting the target spectra to that frame of reference.

Following a signal-to-noise check based on continuum regions and visual inspection of selected wavelength blocks, the suitability of the spectra for the later analysis may be validated. Hence, in this process several of them are discarded for the metallicity determination. Then the equivalent widths of a huge set of spectral lines (~ 900) are measured by fitting the line profiles. ARES is a sophisticated program for performing these fits in a semi-automatized way for a large number of spectra. For several spectra the radial velocity is calculated using this program instead of IRAF.

The effective temperature of the object is then calculated taking specific pairs of lines and transforming the ratios of the previously obtained equivalent widths using basic analytic functions (calibrations). This so-called line-depth-ratio method, besides being simple to use, is statistically solid and able to yield the effective temperatures with a very high accuracy. All calibrations, however, have a certain range in temperature where they may be used. Therefore, in absence of knowledge about the true value of the effective temperature, an iterative method is being applied, excluding outliers of the temperature distribution.

On the basis of the effective temperatures the equivalent widths of selected objects are rechecked and the fits are in some cases refined, thereby reducing the scatter of the temperature distribution obtained from the previous approach. Hence, special attention is dedicated to the uncertainty of the effective temperatures since they constitute the most important factor for the next phase of this work, the metallicity determination.

In order to be able to determine the iron abundance of the Cepheids, atmospheric models are used, taken both from the MARCS as well as the Kurucz/Castelli database. Using the models an interpolation is performed in order to create a finite, high resolution grid that spans a three-dimensional parameter space defined by important stellar quantities, i.e. the effective temperature, the surface gravity and the metallicity. The dependence on another parameter, the microturbulence velocity, is of minor concern.

These atmospheres together with the measured equivalent widths allow the calculation of single line abundances using the program MOOG. The MARCS models show spurious discontinuities in this process and are therefore discarded, leaving the Kurucz models for abundance determination.

Without knowledge about the correct values of some of the stellar parameters that define the atmospheric opacity treatment, however, an iterative approach is required, within which the differences between the observed and the predicted spectrum are minimized. The amount of data makes a manual procedure almost impossible, therefore automatized routines become necessary. A *Python*-based wrapper has been written in which - based on a collection of initial parameters - the input is refined in each step. This optimization of the parameters is guided by several physical conditions that are to be satisfied for the individual spectra.

With the current approach, besides the effective temperature, surface gravity and microturbulence velocity, the abundances of Fe I (neutral) and Fe II (once ionized) are yielded. After having obtained the metallicities for the various spectra and having performed a few sanity checks, they are averaged over the objects and the results from the different spectrographs are combined. Metallicity estimates for 216 Cepheids (thus more than 40 % of the currently known ones) are provided.

Iron abundances from the literature then may be transformed into the metallicity scale defined by the targets of this thesis, increasing naturally the sample size. Additional information about the Galactocentric radius of the sample enables a determination of the radial metallicity gradient (profile) of the Milky Way. Looking at the polar target distribution, the existence of possible iron abundance asymmetries in the solar vicinity can be checked. Finally, reference metallicity gradients from different types of objects (Cepheids, open clusters, HII regions) are compared with the previously derived radial profile.

The results obtained this way are well in agreement with former studies and confirm the picture of iron depletion towards the outer regions of the Galaxy. The homogeneous metallicity database of Galactic classical Cepheids that has been built in this study is the largest up to date.

Chapter 1

Introduction

Cepheids have a long and prominent history in the field of astrophysics and are widely used by researchers all over the world. They are stars of intermediate mass (4 - 10 solar masses) and relatively young (5 - 300 Myr). Their main source of energy is the triple-alpha process, transforming helium into carbon, together with their hydrogen-burning shell, and they are mostly located on the thin disk (with a scale height of typically 350 pc).

Their most important property, however, is their variable nature. Cepheids undergo changes in luminosity and therefore naturally also in apparent brightness in a regular, sinusoidal (but asymmetric) pattern, i.e. there is a fixed time interval in which a full cycle from brightest to faintest magnitude takes place. One of the models that tries to explain these variations is the κ-mechanism in which they are a consequence of the radial expansions and contractions (hence oscillations) of spherical shells caused by changes in the temperature-density structure of the star and the opacity that describes how much of the radiation is able to leave the star's atmosphere [1].

The formerly mentioned time interval, the period, is one of the key properties of Cepheids. Already in 1912, H. Leavitt discovered that there is a relation between that quantity and the absolute magnitude (hence intrinsic brightness) of the stars [2]. This discovery, the so-called period-luminosity-relation (PLR), once calibrated, made it possible to determine the distance to an object just on the basis of the light variation pattern (light curve) together with the measured apparent brightness and the reddening and has therefore revolutionized astrometry.

While it has been prominently used by E. Hubble in 1929 to determine his own constant (although with a wrong value) and therefore find the homonymous law [3], which itself deeply impacted modern cosmology, the popularity and usage of the PLR has not ceased at all till now and Cepheids therefore constitute without doubt one of the most important steps in the so-called cosmic distance ladder.

Although their distance measurement applicability is limited owing to technical reasons (flux limits), being primary distance indicators, Cepheids serve to calibrate the next-higher steps in the ladder such as supernovae Ia, the Tully-Fisher- and Faber-Jackson-relations, Globular Cluster Luminosity Functions (GCLFs) and Planetary Nebulae Luminosity Functions (PNLFs).

In recent years Cepheids are also being used together with supernovae Ia to constrain cosmological parameters. Indeed, 2011 saw a nobel prize for the expansive nature of the universe based on related measurements [4][5].

It is therefore easily understandable why much effort is made to still refine the PLR even nowadays [6][7][8][9]. The upcoming GAIA data releases containing parallax information for a vast number of objects will cause another jump in this respect due to better PLR calibrations.

There are also versions of the PLR where the luminosity further depends on temperature (or colour), hence extending the one-dimensional framework which is then regarded as the collapsed or projected description of a multi-parameter dependency. Recent research projects have been dedicated to additional possible metallicity effects on this dependency that may ex-

ist as well [10][11]. The metallicity dependence of so-called period-wesenheit-relations (PWRs, these have the advantage of being reddening-free) is another subject of interest [12].

This work focuses thus on a closely related aspect of Cepheids, their chemical structure, hereby restricting itself to the metallicity (the iron content) of these variables. As suggested in the title, the aim of the thesis is to create a homogeneous metallicity scale for classical Cepheids located within our galaxy, the Milky Way.

How can that be of scientific interest? First of all, Cepheids, being stellar tracers, allow us to study the chemical enrichment of the thin disk of the Galaxy. Using these stars, one may draw conclusions about the chemical composition of their surroundings. Cepheid metallicities can also be used to study the transition between the inner and outer Galactic regions [13][14][15] or age effects (despite their relatively small range of ages) [10][16].

With the distance info in combination with the Cepheid metallicities the radial metallicity profile of the Milky Way can be traced and thus the recent chemical enrichment can be studied [17][18]. Needless to say, this requires a uniform, identical treatment for all the objects that are to be considered.

Finally, within the Galactic disk there are also several open clusters. Although the number of Cepheids located in such clusters is limited - currently not more than a few dozens of cluster Cepheids are known - their usefulness is undisputed since the objects of the cluster all have comparable ages and chemistry. The metallicity of Cepheids therefore not only gives information about other cluster targets, but moreover the homogeneous iron abundance scale imposed by the objects of this study puts the field variables and the clusters themselves into a common frame of reference [19][20][21]. Due to the small age range of Cepheids compared to that of open clusters, this is of special relevance for investigations of the assumed age dependence of the radial metallicity gradient. Radial migration may be studied as well [22][23].

The list of possible uses shown above demonstrates the scientific relevance of the current work, but is nonetheless incomplete. With the other parameters determined in this study, the Galactic Cepheid temperature scale or surface gravity variation etc. could be investigated. Hopefully, the material provided in this thesis provokes thus a few ideas on how to use its results as a possible basis or subject of interest for future studies.

Chapter 2

Datasets and Instruments

2.1 Overview

I will define which instruments have been used for the analysis performed in the later chapters. A description of the datasets that have been used for the thesis and of the basis on which these samples have been built is given. A chapter on how the different spectra have been obtained follows, while the last part, concluding this chapter about preliminaries, explains how a basic database containing valuable properties of Galactic Cepheids, including the objects in this thesis, has been constructed.

2.2 Instrument Description

The main data used are spectra collected at three different telescopes of the *European Southern Observatory* (ESO from now onward). The instruments of these telescopes include the *Ultraviolet and Visual Echelle Spectrograph* (UVES), the *High Accuracy Radial velocity Planet Searcher* (HARPS) and the *Fiber-fed Extended Range Optical Spectrograph* (FEROS).

2.2.1 Ultraviolet and Visual Echelle Spectrograph - UVES

UVES is an echelle spectrograph situated at the Cerro Paranal site on board of the Very Large Telescope (VLT) in Chile. The light that reaches this spectrograph can be split at a certain wavelength (that depends on the instrument setup, especially on the dispersing element (the grating) that has been used), and follows then two different arms (blue and red). Hence by means of a so-called beam splitter the UV component of the spectrum is directed towards the blue arm, whereas the visual photons go to the red arm. At the end of the light path through the instrument, the photons are measured by two different Charge-Coupled-Device (CCD) detectors, one for the shorter (bluer) and one for the longer (redder) wavelengths. UVES offers a broad wavelength coverage from 3000 up to almost 11000 Å, depending on the grating/grism configuration, and a very high spectral resolution of typically R $\left(= \frac{\Delta\lambda}{\lambda}\right) \sim$ 40000, while having a nominal maximum resolution of R $\sim$ 80000 in the blue and $\sim$ 110000 in the red [24].

2.2.2 High Accuracy Radial velocity Planet Searcher - HARPS

The HARPS instrument, located at the La Silla Observatory in Chile, is mounted on the ESO La Silla 3.6m telescope and has been designed specifically with the purpose of being a state-of-the-art instrument capable of measuring the radial velocity of stars very accurately ($\sim$ 1 m/s) on the basis of the Doppler shift. It is thus extensively used by researchers all over the world especially for exoplanet detection. In order to achieve the high thermal stability required to obtain such precise measurements, and to prevent thermal line broadening, HARPS needs to

be constantly cooled using a cryostat, to maintain its temperature within a certain range, on the order of +/- 0.1 K [25]. The spectra that are collected with this instrument are thus very precise in wavelength. They range from 3780 to 6910 Å and have a small gap due to the detector being composed of two CCDs combined as a mosaic. Concerning the spectral resolution, the instrument reaches a value of R $\sim$ 115000 [26].

2.2.3 Fiber-fed Extended Range Optical Spectrograph - FEROS

Also set at the La Silla site, FEROS is another important echelle spectrograph, installed however on the MPG/ESO-2.20m telescope, after having been transferred from its original host in the period before 2002, the ESO-1.52m telescope. Main characteristics of FEROS include a rather high resolving power of R $\sim$ 48000 as well as a wavelength regime of 3500 to 9200 Å. Moreover, the instrument receives light from two fibers and can be operated in two different modes, one being the *object-sky* configuration, whereas the other, the *object-calibration* setup, allows for an exposure of the target to be taken together with either wavelength calibration spectra or so-called flatfields [27]. This makes it possible to get calibration spectra and target data at exactly the same environmental and instrumental conditions. FEROS's primary advantage, however, is that the spectra do not have any central gap and that spectral analysis can therefore be performed over the whole lambda range, as will be seen later [28].

2.3 Target Selection

The first step of the thesis was to define a list of stars that should be analyzed. All of the objects that were examined in the process of the master thesis are Cepheid variables. Due to their pulsating nature, one prime interest is the phase dependence of several relevant stellar quantities which I derived in this thesis.

Bearing this in mind, HARPS and the initial UVES objects have been chosen on the basis of availability of various spectra at different observation times (multi-epoch objects). Table 2.1 shows the list of selected objects together with the spectrograph and the number of spectra that have been studied during the course of the thesis (see also sect. 2.4).

Table 2.1: HARPS and UVES objects with the number of spectra.

Object	Spectrograph	N_S
S Cru	HARPS	12
β Dor	HARPS	46
ζ Gem	HARPS	47
Y Oph	HARPS	8
RS Pup	HARPS	15
X Sgr	HARPS	26
Y Sgr	HARPS	20
R TrA	HARPS	14
RZ Vel	HARPS	11
ER Car	UVES	12
BF Oph	UVES	10
BB Sgr	UVES	10

Additionally, the list was extended for UVES including also the objects of table 2 from Genovali (2015, [29]), with the exception of two variables (BB Gem and GQ Ori) for reasons mentioned in section 2.1 of the paper. The motivation behind this increase in sample size is to be in grade of comparing the results obtained in this thesis with recent literature values.

Near the end of the thesis data analysis phase, another batch of spectra, this time from an ESO observation program of L. Inno (Program ID 093.D-0816(A)) has been downloaded, with the aim of further increasing the number of different objects.

For FEROS the Cepheids were chosen on a different basis. From G. Bono I received a table (called FEROS base table from now on) that was built from information in the Genovali papers and that contains almost the entire sample of known Galactic Cepheids ($\sim$ 560) together with some important stellar parameters, including e.g. RA and DEC coordinates or Galactocentric distances. Using this table all downloadable spectra for these objects have been used. A complete list of all spectra and objects used in this thesis will be given in sect. 6.4 and appendix A.

2.4 Data Retrieval

For the selected objects the spectra now had to be obtained. Since all three spectrographs are ESO instruments, the ESO data archive easily provides data for the targets. However, before any retrieved spectrum can be further studied, it usually needs to undergo a certain number of processing steps (refer to sect. 3.1). In the case of FEROS there were only raw data and this process had to be performed by me. For HARPS and UVES, however, there do exist also certain spectra that have already been processed (phase-3 spectra, for UVES see [30]). Hence, for the latter spectrographs it has been verified that each raw spectrum had a phase-3 counterpart, so that only those had to be taken into consideration, simplifying the subsequent analysis in that way. In total, I downloaded 32 spectra for 3 UVES targets (defined at this point as the UVES TS sample, TS abbreviating *This Study*), 199 belonging to 9 HARPS objects, and 486 spectra of 169 FEROS Cepheids.

The additional 73 Genovali objects make up for 120 spectra that have been directly requested from the authors of the respective paper [29]. Those data are already preprocessed as will be explained later. The 154 Inno spectra belong to 46 stars and are prereduced, like UVES and HARPS. As such they underwent all steps similarly to those datasets, unless stated otherwise. Finally, 2 FEROS (raw) spectra and 9 UVES (phase-3) spectra from 2 and 1 targets that have been recently described in Kovtyukh (2016, [31]) were added. 134 preprocessed STELLA spectra for 5 different objects, collected by J. Storm, were included as well.

Not considering multiplicity of the objects among different spectrographs, the sample that has been studied consists therefore of 1002 spectra (32 UVES TS + 120 UVES Genovali + 9 UVES Kovtyukh + 154 UVES Inno + 199 HARPS + 486 FEROS (TS) + 2 FEROS Kovtyukh) from 249 Cepheid variables. The STELLA spectra are omitted from this count because they are a sample of their own. Please note that the final number of spectra and objects considered for the metallicity determination is actually smaller, for reasons indicated later.

2.5 Cepheid Catalogue

In the next step a compilation of the majority of known Galactic Cepheids has been created in the form of a Cepheid catalogue. Its purpose is to serve as a quick source of information for various variables. Consequently I can retrieve these data in a simple, homogeneous way. It provides a general database of the objects that have been studied in this thesis and enables easy sorting according to various criteria and columns. However it should be clear that several columns only have entries for some of the Cepheids.

Important data for 558 different targets are comprised in the aforementioned catalogue which has been built from quantities included in the FEROS base table mentioned previously. The information taken from this table includes RA, DEC and Galactic coordinates as well as J, H and K magnitudes and the extinction coefficients in the V, B, J, H and K bands. Also the mean J magnitude taken from the 2MASS survey [32][33] is given therein. Data shown in table 4 of Genovali (2014, [10]) were used to combine the present info with general parameters like the Cepheid type, the period, other magnitude but also metallicity estimates and the (Galactocentric) distance. Table 2 from Genovali (2015, [29]) served as the primary source for spectra where the metallicity had not been given in the previous paper, extending the chemical composition info by adding certain α-element abundances, while da Silva (2016, [34]) gave helpful insight into the newest r- and s-element estimates for a huge number of pulsating stars. Additionally, further information about position (RA, DEC), Cepheid classification, spectral type and magnitudes has been taken from the SIMBAD archive [35][36]. Further sources that have been used include Turner (2010a, [19]) and Majaess (2013a, [20] and 2013b, [21]), where the membership of several variables to open clusters is described. Finally, I added the number of spectra for different spectrographs or the amount of reduced spectra for the objects in my sample.

2.5.1 Priority Groups

When looking at the various targets listed in the catalogue, several of them have interesting properties that qualify these variables as being preferential candidates for further analysis. These objects have been put into so-called priority groups, i.e. while the subsequent studies have been performed for all stars in the dataset, special attention should be paid to those Cepheids being a member of such a group.

The first priority group is that of multi-epoch Cepheids, i.e. those with multiple spectra (≥ 2) available. The reason why these *calibrators* are being focused upon is of course the possibility to study how various parameters like effective temperature, radial velocity etc. change along the pulsation cycle. It should be clear that a high number of spectra is not a sufficient, however a necessary criterion for the object to have a good phase coverage. The cepheids for which the pulsation cycle is well-covered (within at least one spectrograph) are listed in table 2.2.

Table 2.2: Calibrators with the number of spectra for different datasets. Only the Cepheids with a good phase coverage within at least one spectrograph are shown. N_F, N_H, N_{U_G} and N_S denote the number of FEROS, HARPS, UVES Genovali and STELLA spectra.

Object	Spectrograph	N_F	N_H	N_{U_G}	N_S	N_{tot}
S Cru	FEROS/HARPS	1	12	-	-	13
β Dor	FEROS/HARPS	1	46	-	-	47
R TrA	FEROS/HARPS	1	14	-	-	15
RZ Vel	FEROS/HARPS	1	11	-	-	12
X Sgr	FEROS/HARPS/STELLA	2	26	-	24	52
V340 Ara	FEROS/UVES	28	-	6	-	34
XX Sgr	FEROS/UVES	4	-	5	-	9
EV Sct	FEROS/UVES	25	-	1	-	26
UZ Sct	FEROS/UVES	28	-	6	-	34
AV Sgr	FEROS/UVES	28	-	5	-	33
VY Sgr	FEROS/UVES	30	-	4	-	34
Y Oph	HARPS	-	8	-	-	8
RS Pup	HARPS	-	15	-	-	15
ζ Gem	HARPS/STELLA	-	47	-	81	128
Y Sgr	HARPS/STELLA	-	20	-	3	23
η Aql	STELLA	-	-	-	11	11
δ Cep	STELLA	-	-	-	15	15

Targets in the second priority group are united by their status as members of an open cluster. Since all stars that belong to the same open cluster are of a similar age and chemistry, such variables provide an important input on the metallicity and other abundances of the other cluster members and therefore put strong constraints on stellar evolution, one of the main points why open clusters are extensively examined by researchers. Out of all pulsators listed in my catalogue, 28 are *cluster Cepheids*, of which 14 are in the sample of this study (given in table 2.3):

Table 2.3: Cluster Cepheids with the number of spectra for different datasets. N_F, N_H, $N_{U_{TS}}$, N_{U_G} and N_S denote the number of FEROS, HARPS, UVES TS, UVES Genovali and STELLA spectra. Used references are Turner (2010a, [19], TUR), Majaess (2013a, [20], MAJa) and Majaess (2013b, [21], MAJb).

Object	Spectrograph	N_F	N_H	$N_{U_{TS}}$	N_{U_G}	N_S	N_{tot}	Cluster	Source
V Cen	FEROS	2	-	-	-	-	2	NGC 5662	TUR
S Nor	FEROS	2	-	-	-	-	2	NGC 6087	TUR
SZ Tau	FEROS	1	-	-	-	-	1	NGC 1674	TUR
CS Vel	FEROS	3	-	-	-	-	3	Ruprecht 79	TUR
SW Vel	FEROS	2	-	-	-	-	2	Vel OB5	TUR
CV Mon	FEROS/UVES	23	-	-	1	-	24	van den Bergh 1	TUR
GU Nor	FEROS/UVES	1	-	-	1	-	2	NGC 6067	MAJa
TW Nor	FEROS/UVES	3	-	-	1	-	4	Lyngå 6	TUR
RU Sct	FEROS/UVES	1	-	-	2	-	3	Trumpler 35	TUR
V367 Sct	FEROS/UVES	3	-	-	4	-	7	NGC 6649	TUR
WZ Sgr	FEROS/UVES	1	-	-	5	-	6	Turner 2	TUR
ζ Gem	HARPS/STELLA	-	47	-	-	81	128	ADS 5742	TUR
V340 Nor	UVES	-	-	-	1	-	1	NGC 6067	TUR/MAJa
BB Sgr	UVES	-	-	10	-	-	10	Collinder 394	TUR
CE A Cas	-	-	-	-	-	-	-	NGC 7790	MAJb
CE B Cas	-	-	-	-	-	-	-	NGC 7790	MAJb
CF Cas	-	-	-	-	-	-	-	NGC 7790	MAJb

CG Cas	-	-	-	-	-	-	-	Berkeley 58	TUR
DL Cas	-	-	-	-	-	-	-	NGC 129	TUR
SU Cas	-	-	-	-	-	-	-	Cas R2	TUR
SU Cyg	-	-	-	-	-	-	-	Turner 9	TUR
V1334 Cyg	-	-	-	-	-	-	-	Dolidze 45	TUR
V1726 Cyg	-	-	-	-	-	-	-	Platais 1	TUR
X Cyg	-	-	-	-	-	-	-	Ruprecht 175	TUR
U Sgr	-	-	-	-	-	-	-	IC 4725 (M25)	TUR/MAJb
α Umi	-	-	-	-	-	-	-	ADS 1477	TUR
S Vul	-	-	-	-	-	-	-	Anon Vul OB	TUR
SV Vul	-	-	-	-	-	-	-	Vul OB1	TUR

Recent metallicity results were published in Genovali (2013, [37], 2014, [10] and 2015, [29]) for a large fraction of the known Galactic classical Cepheids. In these papers estimates from other sources are also listed. It is therefore a prime interest to check whether among the targets of the current sample there are variables whose metallicities are not mentioned in these works. Indeed 50 objects do not have a value for the iron abundance yet, most of them belonging to the UVES Inno dataset (another reason for including the dataset in the overall sample). They have been put into the *nometal* group and are listed in table 2.4.

Table 2.4: Cepheids for which no previous metallicity estimate exists, with the number of spectra for different datasets. N_F, N_H, N_{U_I} and N_S denote the number of FEROS, HARPS, UVES Inno and STELLA spectra.

Object	Spectrograph	N_F	N_H	N_{U_I}	N_S	N_{tot}
DZ Cma	FEROS	1	-	-	-	1
CE Pup	FEROS	3	-	-	-	3
EK Pup	FEROS	1	-	-	-	1
CP Vel	FEROS	3	-	-	-	3
DD Vel	FEROS	4	-	-	-	4
X Sgr	FEROS/HARPS/STELLA	2	26	-	24	52
FO Car	FEROS/UVES	8	-	2	-	10
SU Cru	FEROS/UVES	2	-	2	-	4
IU Aql	UVES	-	-	3	-	3
V800 Aql	UVES	-	-	8	-	8
V912 Aql	UVES	-	-	3	-	3
V475 Ara	UVES	-	-	4	-	4
CC Car	UVES	-	-	3	-	3
CF Car	UVES	-	-	3	-	3
FF Car	UVES	-	-	1	-	1
FH Car	UVES	-	-	4	-	4
FK Car	UVES	-	-	3	-	3
FM Car	UVES	-	-	4	-	4
FN Car	UVES	-	-	2	-	2
FQ Car	UVES	-	-	3	-	3
GS Car	UVES	-	-	3	-	3
GT Car	UVES	-	-	3	-	3
HK Car	UVES	-	-	2	-	2
II Car	UVES	-	-	4	-	4
IK Car	UVES	-	-	4	-	4
IM Car	UVES	-	-	3	-	3
IP Car	UVES	-	-	4	-	4
IU Cen	UVES	-	-	3	-	3
IZ Cen	UVES	-	-	6	-	6

LV Cen	UVES	-	-	3	-	3
MY Cen	UVES	-	-	3	-	3
V553 Cen	UVES	-	-	2	-	2
V686 Cen	UVES	-	-	3	-	3
V782 Cen	UVES	-	-	4	-	4
SV Cru	UVES	-	-	4	-	4
TY Cru	UVES	-	-	4	-	4
VV Cru	UVES	-	-	3	-	3
VX Cru	UVES	-	-	3	-	3
DW Mus	UVES	-	-	3	-	3
UX Mus	UVES	-	-	4	-	4
V507 Sco	UVES	-	-	4	-	4
V567 Sco	UVES	-	-	3	-	3
V706 Sco	UVES	-	-	4	-	4
V708 Sco	UVES	-	-	4	-	4
V742 Sco	UVES	-	-	4	-	4
SU Sct	UVES	-	-	4	-	4
GK Sgr	UVES	-	-	4	-	4
V504 Sgr	UVES	-	-	4	-	4
BR Vul	UVES	-	-	4	-	4
GQ Vul	UVES	-	-	3	-	3

Note that, if a Cepheid belongs to one group, it does not mean that it is excluded from the other two. Although there is no overlap between the *cluster* and *nometal* variables, there are quite many *calibrators* in both groups.

Chapter 3

Data Reduction and Analysis

3.1 Preliminary Data Reduction

The spectra that are to be analyzed have to be preprocessed before they are ready for use. In a common framework this so-called preliminary data reduction consists of several parts that will be shortly discussed on the basis of usual UVES calibrations [38][39][40][41].

First, parts of the data that are not needed are removed. These include, for instance, overscan regions. Often the exposure is also rotated so as to put the frame into the right orientation.

Then typically a bias frame is subtracted from the spectrum. Bias frames are exposures with the telescope shutter closed and zero exposure time. As the name suggests, they give an artificial offset (bias) from zero that should prevent negative count rates for photons. In the ESO framework the bias frame is normally derived as a *master bias* from the average of several single bias exposures.

Together with the bias sometimes also *dark* spectra are subtracted. These are frames taken with a very long integration time, e.g. 1 h (still having the shutter of the telescope closed), and serve to determine the influence of thermal noise (thermal photons) inside the instrument. The thermal noise is pixel-dependent and increases over time. This calibration step is of bigger importance for long wavelengths (i.e. the IR regime).

Next, the background between the orders is subtracted, by means of fitting procedures that determine this contribution. Also the sky background level, i.e. the amount of light that does not come directly from the target has to be removed.

Subsequently, the orders of the echelle spectrum are extracted, i.e. from the pixel-pixel frame the location of the orders are estimated and the orders are traced along the image.

From averaged flatfields a *master flat* is created. Flatfields are continuum spectra, i.e. exposures without any spectral absorption or emission lines and generated by either taking a featureless light source (flatfield lamp, e.g. halogen lamp for UVES [41]) that illuminates the telescope aperture or by using the illuminated, closed dome of the telescope (dome flat). After having extracted the master flat exactly in the same way as the science spectrum, the latter is divided by the flatfield in order to remove differences between the various CCD pixels, for each one of them has a different response (gain) to the continuum source.

Furthermore, using so-called *wave* exposures, the now 1D-spectra (pixels as the coordinates and flux as the corresponding values) need to be transformed into wavelength space by getting a dispersion solution, i.e. a function $\lambda(x)$, usually in the form a polynomial. The wavelength frames are taken from a lamp that has emission lines with precise known (lab) wavelengths. In the case of UVES a ThAr lamp is usually used for this purpose.

The wavelength-flux parts for the different spectral orders are merged together. If there is an overlap between adjacent orders, a suitable weighted average of the fluxes from the two orders is performed.

Finally, the instrument characteristics are taken into consideration. In this step, the atmospheric extinction is corrected for, thus considering the light path through the Earth's atmosphere. Afterwards, if present, a *std* spectrum, taken from reference (standard) stars, enables a flux calibration, i.e. a transformation from arbitrary units (photon counts, adu) to physical fluxes. The instrument response curve created from the standard star spectrum can be thought of as a λ-dependent multiplicative factor that is applied to the science frame.

The presented scheme may differ slightly from instrument to instrument but is generally followed. On the internet, there are several programs offering commands for such reduction recipes, e.g. IRAF [42][43][44] (*doecslit*, [45]), ESO-MIDAS [46] (*echelle*, [47]) and many others. However, all of these have a decisive drawback. The reduction has to be done manually for each spectrum, a quite time-consuming and complicated process. A more sophisticated approach is the use of regularly updated dedicated pipelines, which exist e.g. for UVES [48] as well as other VLT-ESO instruments and are available on the ESO website. Graphical front ends for these pipelines may be used as well, enhancing user-friendliness and visualization of the workflow (the most famous example being *Reflex* [49]). They allow the user to perform relatively quick reductions of a large number of spectra, setting various parameters within the pipeline easily [50].

The most prominent parameter is the choice of the extraction mode. If set to *linear*, the pipeline sums the fluxes along the slit for each order. The *average* extraction is the same process, additionally dividing the total flux by the number of pixels. The recommended mode, however, is *optimal*, which fits the fluxes along the slit with a Gaussian or Moffat function and also removes exposure defects resulting from cosmic ray impacts. The algorithm is based on the papers of Horne (1986, [51]), Marsh (1989, [52]) and Mukai (1990, [53]) as explained in the pipeline manual [54].

HARPS has its own pipeline, which, however, is not available for download and may only be used directly at the La Silla observatory when observing the targets in visitor mode.

The aforementioned phase-3 spectra are quality-controlled data that have been processed using these codes [30] and stored in the science archive. In my sample the UVES spectra were all extracted with the optimal extraction mode. Of course no preprocessing was necessary either for the HARPS phase-3 data and the Genovali spectra were prereduced as well (manually). STELLA spectra do not require any initial treatment, for they had already been reduced when I received them.

The biggest part of the spectra taken with FEROS, however, cannot be reduced using official software, since there is no pipeline available. While an ESO-MIDAS-based quick-look tool for fast checks of spectral quality when observing stars at the FEROS site exists, the use of this *FEROS Data Reduction System* [55] for accurate homogeneous reductions of large samples is not recommended. During my internship at ESO in Garching, which formed the first part of the present thesis, I received an unofficial version of the FEROS-DRS from J. Pritchard which has been heavily improved by him and has now reached quite high quality standards [56]. It should be noted that the FEROS spectra present in the ESO archive are supposed to be collectively and homogeneously processed in the near future.

In order to process the science spectra, several calibration spectra had to be downloaded first. For this purpose a self-written script read the date of observation from the filename of the spectrum (e.g. FEROS.2001-11-29T03:29:26.000.fits) and passed the previous and the next

day to a code received from J. Pritchard that automatically got the filenames of the calibration files taken in that period from the ESO archive and downloaded them one by one. This way, 5048 calibration exposures have been retrieved for the 486 science spectra. Then soft links to the science and calibration spectra had to be created, separate for each observation night. The FEROS-DRS now automatically associated the correct calib files to the science spectra and put them into two distinct catalogues, whose contents were consequently reduced, following the above routine.

It should be noted, that at first several spectra taken before 2004 could not be reduced using the FEROS-DRS. This was due to a problem caused by the fact that the CCD software architecture was changed in October 2003 from the BIAS controller adopted from the Danish 1.54 m telescope (at La Silla) [57] to another one, FIERA [58], in addition to a contemporaneous change in the fits headers to comply with ESO standards. Having a different fits structure, the DRS could not read the files as intended. Another problem that arose was the sparse and lenient calibration plan of the FEROS instrument back in the year 2001, resulting in very few calibrations for the science spectra. For some of them no bias frames were present. Additional frames taken further away from the observation night could be used in combination with a manual file association to reduce these spectra. The current FEROS sample comprises 355 spectra, with the remaining 131 currently not being prereduced due to the above reasons (those are not included in the further analysis). I want to stress that none of these problems affected the quality of the results that have been yielded by the subsequent studies. Finally, it should be mentioned that the 2 FEROS Kovtyukh spectra have not been reduced yet, either.

3.2 Continuum Normalization

Once all spectra had been precalibrated, the next step was to continuum-normalize them, i.e. to make spectra with different flux levels comparable by setting the global continuum level to 1 so that various lines that are the subject of the later analysis can be compared independently of the absolute strength but in terms of the relative fluxes with respect to the continuum background at the specific wavelength. This continuum normalization was required for UVES, HARPS and FEROS, but not for STELLA, as those had already undergone the process when I received them. Also the UVES spectra from Genovali had already been normalized at the point when they were included in the sample.

In case of UVES and HARPS, the spectra had to be split due to the big gap between the blue and red parts of the frame. Otherwise, the continuum normalization would have inevitably failed, at least when used over the whole wavelength range. Therefore, for those instruments the zero flux pixels at the beginning, the end and those of the central gap of each exposure were detected and the spectra were cut in two pieces, by transforming them first into an ascii file and afterwards changing the extracted parts back into fits format. This essentially doubled the amount of work that had to be done for UVES and HARPS.

In order to perform this continuum normalization there are various programs that may be used, but the approach that quickly came to mind was to take IRAF's *continuum* command. As an input *continuum* receives a spectrum and outputs the normalized frame, offering advanced parameter control and making use of a broad range of individual options that can be passed together with the spectrum.

Among the most notable ones there are e.g. the *function* used for fitting the background level, allowing the user to choose between Legendre and Chebyshev polynomials as well as linear and cubic splines (the default). It has been verified that indeed cubic splines give the most suitable and reliable fits also in case of complex spectral shapes.

Another relevant parameter is the *order* of the function used, i.e. the degree of the polynomials and the spline pieces. The higher this parameter gets, the closer the continuum will follow the shape of the spectrum. This may be desirable in case of an exposure that has relatively many (smooth) changes in the continuum also on smaller wavelength intervals, but gives rise to problems in case of very strong lines, e.g. in absorption, where the fitted curve will try to follow the line too closely instead of detecting the true continuum. Depending on the subject of interest, in case this affects only saturated lines which one may not want to measure, this behaviour might be tolerated. In my case, however, the continuum was sufficiently smooth, so that it was not necessary to increase the order to such high levels.

Moreover, the number of rejection iterations, *niterate*, having 10 as its standard value, can be adjusted. It influences naturally the computation time of the command, but more importantly defines how stable the result is. Contrary to what one would expect, in some cases when the other parameters are left with default values, the fits seem to get unstable only above a certain number of iterations, around 8 typically. This is due to too many flux points being discarded from the set of values that defines the continuum, giving rise to implausible fits. In those cases, reasonable normalizations may already be achieved with 6 iterations. This approach has been used for the UVES Kovtyukh spectra. It allows to process many similar spectra with almost the same parameters, once suitable values for the order and the iterations have been found.

For UVES, HARPS and FEROS, the number of iterations was left unchanged. As a result the fits were often unstable at the beginning as described above. Setting instead a different *low_reject*, in case of FEROS also a *high_reject*, value, very good normalizations could be obtained. The mentioned quantities define which interval in terms of sigma multiples above and below the fit in each iteration will be kept and is therefore not associated to lines. Increasing e.g. the *low_reject* parameter thus means that the range of the accepted flux values below the preliminary continuum estimates widens and consequently moves the resulting continuum downwards, especially when there are stronger absorption lines. Since the analysis treats stellar spectra, there are almost always only absorption lines. FEROS, however, made it necessary to change also *high_reject*, for some spectra appeared to have emission spikes in the red part of the frame. These do not originate from the target itself, but stem from the use of the *object-calibration* setup, feeding the light from an emission lamp into the second fibre. The investigators observing those targets were probably interested in getting the most accurate wavelength calibrations possible. On the other hand, this leads to contamination of the target spectrum due to so-called bleeding from the calibration to the object fibre [27]. The effect was that the continuum was placed too high at the affected wavelengths and could therefore be resolved by lowering *high_reject*.

Defaults for *low_* - and *high_reject* are 2 and 0 respectively. Typical ranges of *low_reject* are e.g. between 1 and 3 for UVES and HARPS, and between 0 and 1.5 for FEROS, using a different fitting order in that case. Figure 3.1 visualizes the effect of a good and a bad choice of *low_reject* on the continuum fit.

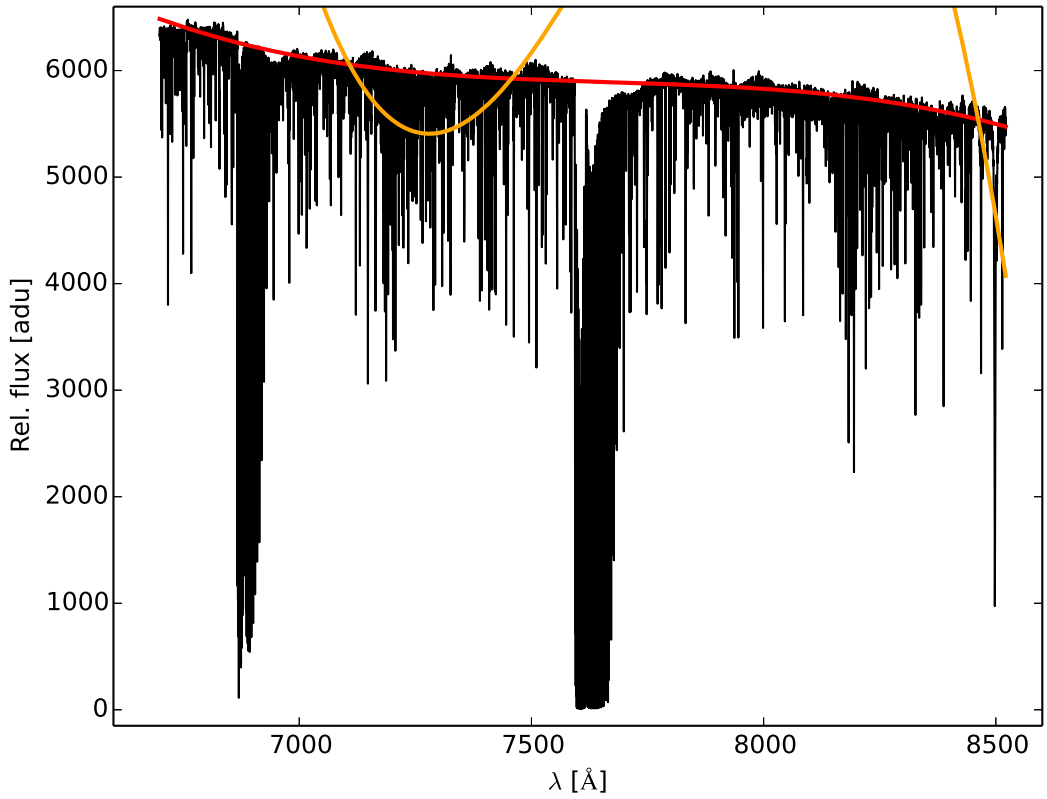

Figure 3.1: Different choices of the continuum rejection parameter for a sample spectrum. The original spectrum is plotted in black, with the continuum fits indicated in red ($low\_reject = 2.6$) respectively orange ($low\_reject = 1.7$) on top. While the red curve approximates the spectral shape very well, strong fluctuations are visible for the orange line. Please note that the fit linewidth has been increased for better visibility.

It has to be emphasized that the adjustment of those two parameters is equally crucial and time-consuming, since it requires an independent treatment of every spectrum. To complicate things, they are very sensitive options, meaning that an unstable fit at $low\_reject = 2$ could be corrected to a perfect continuum estimate at 2.05. What is more, the behaviour of the quantities is strongly non-linear, non-monotonic and consequently hardly predictable. If e.g. 1.99 shows a too high continuum, it is by no means guaranteed that 2.00 would result in a lower placement. Instead, the fit could reach slightly higher flux levels or, even worse, get unstable (rapidly oscillating). To cut a long matter short, there are some valleys of stability at different *low_ reject* positions but with very sharp borders. As a matter of fact, the parameters had to be selected individually and manually on a visual basis for every spectrum. A step size of 0.05 was chosen for this purpose.

The continuum normalization was a bit more difficult for the UVES Inno spectra since there were quite different spectral profiles and some of them could not be easily fitted. In a few cases even ripples or a strong, spurious, emission peak appeared. Such spectra were flagged to record difficulties during the subsequent normalization. All spectra were split into the different profile groups that I had defined and were normalized with common settings individually for

each of those groups. The basic approach was similar to that applied to the UVES Kovtyukh spectra. Some of the spectra additionally required slight modifications of either the fitting order or the number of iterations.

After the normalization the UVES Kovtyukh and Inno spectral parts were reassembled into single spectra for reasons of simplicity, since they had not been taken with a dichroic UVES grating. They thus differ conceptually from the UVES TS exposures.

3.3 Radial Velocity Determination

Having normalized the spectra, the next task was to determine the radial velocity of the objects for each exposure. In order to do this, there are usually many options. Two of them, that I used, will be presented in this section.

While UVES, HARPS and FEROS spectra are already 1D fits files, the STELLA ones were structured slightly differently. The spectral info therein was given in one out of three bands and the 82 different orders were separated in the file in the form of different apertures. In order to be able to measure the radial velocities, the 82 orders were written to separate fits files using the IRAF *scopy* command and subsequently combined into a 1D fits spectrum where the orders are properly merged using *scomb*. The spectra of one object could not be treated this way due to a different fits format and were left aside.

The first method for RV determination is based on IRAF. The package *rv* includes a variety of radial-velocity-related tasks, among others also *fxcor*. This command takes two spectra as input, the target spectrum that one wants to study and a template spectrum, i.e. an exposure in the lab frame (thus velocity-free). The produced output depends on the options given during command call.

In case of UVES Genovali, all frames had already been RV-corrected by the time I received them. Thus they could serve as template spectra. Back when performing the radial velocity determination, only a subsample of the Genovali spectra was present in my datasets, so the template sample consisted of a total of 92 exposures.

The estimation itself works by using a cross-correlation between the target and the template spectrum, i.e. by trying to match the two files as closely as possible. This is done by shifting one of the spectra for each radial velocity in a certain interval with sufficiently small step size and calculating the cross-correlation function (CCF). A very simplistic CCF could look as follows:

$$CCF(\Delta\lambda) = \int_{\lambda_1}^{\lambda_2} F_1(\lambda) * F_2(\lambda + \Delta\lambda) d\lambda$$

Here F_1 and F_2 are the fluxes of the template and the target spectrum respectively. λ_1 and λ_2 mark the interval borders of the wavelength region that is included in the CCF and $\Delta\lambda$ are wavelength shifts calculated using the non-relativistic Doppler shift formula, since the radial velocities of stars are always small compared to the velocity of light:

$$\Delta\lambda = \lambda * \left(1 + \frac{v}{c}\right)$$

As a result of this cross-correlation, when performing it in so-called interactive mode, IRAF prints out the shape of the CCF and performs a fit of it using a Gaussian. The function is expected to have a peak at the correct radial velocity, since the flux values of the two spectra amplify each other due to the multiplication. Assuming for simplicity that the spectra would look exactly the same when shifted by the correct radial velocity, wavelength intervals of almost arbitrarily large size could principally be taken and they would always yield the right velocity. Due to the different chemical compositions (elemental abundances) of the stars, however, the amount of blended lines may strongly vary. Therefore, when using a huge interval, one might run the risk of a very smeared out CCF function. Instead, small lambda intervals are preferred as they sharpen the distribution so that the peak of the cross-correlation curve is more pronounced.

IRAF also lets the user choose different wavelength regions in which to perform the RV determination for the target and the template frame (*o-* and *rsamples*). However, for simplicity I decided to take the same sample regions for both exposures. Of course, a certain lower limit for the interval size exists in this case as well, simply because it must be able to comprise both the radial-velocity-shifted and lab-frame wavelength, due to necessary statistics required owing to line blending, and to prevent a big influence of single saturated lines. Sample sizes between 30 and 100 Å e.g. have proven most useful for getting reasonable RV values. Additionally it should be clear that strong (but not saturated), isolated lines or characteristic line combinations preferably lie in the aforementioned intervals, as they are easy to match and facilitate the identification of the CCF peak. Examples for cross-correlation visualizations by IRAF are given in figures 3.2 and 3.3:

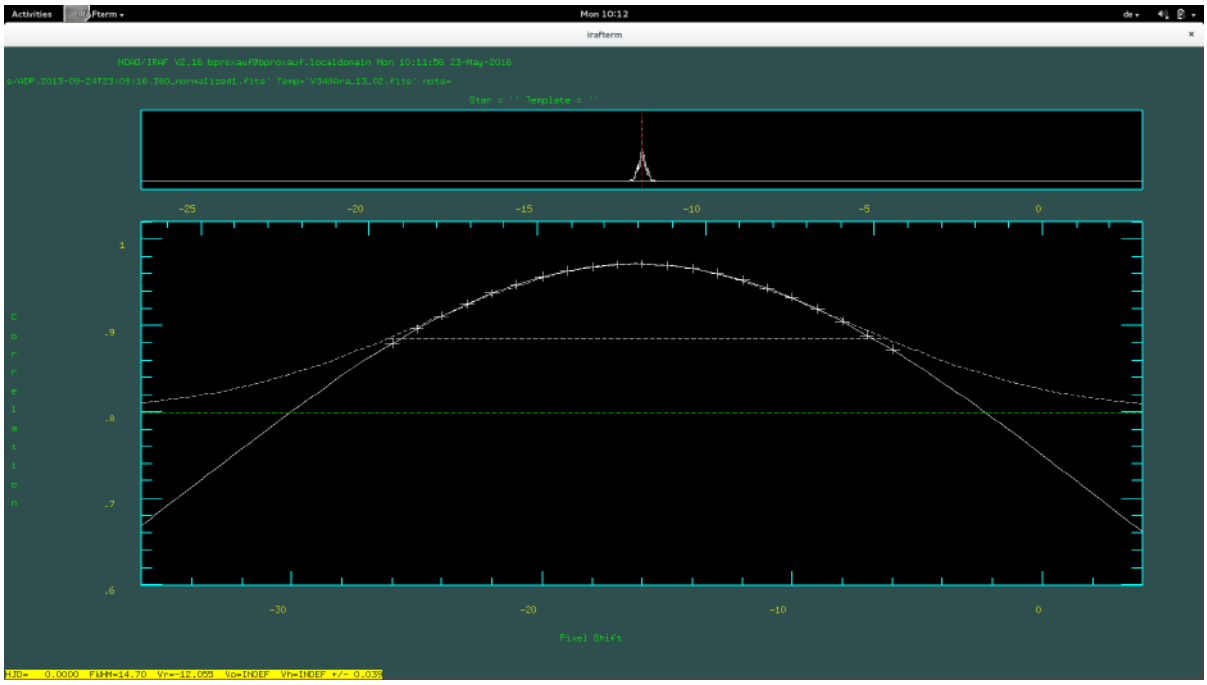

Figure 3.2: Correct choice of sample regions - *o-/r-samples* from 5680 to 5740 Å for a test spectrum.

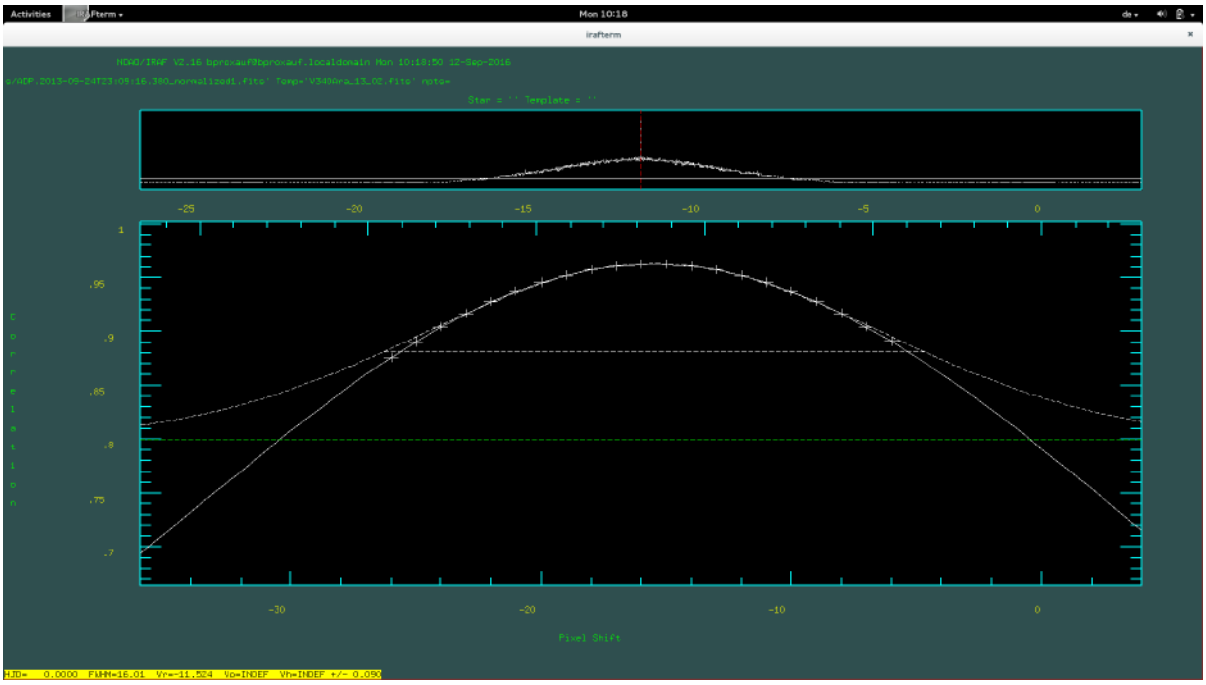

Figure 3.3: Bad choice of sample regions - *o-/r-samples* from $\sim$ 4900 to $\sim$ 5740 Å for a test spectrum. The smearing effect is visible in the upper part of the plot.

At this point it should be mentioned that IRAF internally normalizes the CCF to a maximum level of 1. The minimum of the function is 0. The user may also set a background to perform a Gaussian fit of the curve only above a certain level that can be chosen between these two limits. This was helpful in cases where with no background the fit did not converge, in spite of a sharp CCF peak. This parameter, however, does not affect the actual RV value significantly.

The large sample of spectra that had to be dealt with in this thesis forced me to process the spectra here in an automatic way (batch mode). To obtain the RV values, *fxcor* was launched using an output option, where the essential quantities are printed into a text file, omitting other possible output, e.g. the optional log for the fitting quantities and so-called graphics metacode files. The cross-correlation was performed for all spectra (or spectral parts, i.e. blue and red) and all templates, thus on the order of $\sim$ 90000 CCFs needed to be computed. From the output file, the individual velocity estimates from each target-template-spectrum-combination were taken and statistics giving min, max, mean, median and the range of the velocity distribution plus the number of successful CCFs have been created for each spectrum.

IRAF's main drawback is definitely the computation time. Getting RV estimates for the 199 HARPS spectra took more than 10 hours. Choosing suitable o- and rsample regions is crucial for the success or failure of the process. Often, IRAF would give out "indefinite", indicating that it could not calculate the radial velocity. The mentioned disadvantage limits success validation (quick-checks) to a few test templates, on which one has to make extrapolations for the whole template set. Nonetheless, this is balanced by the statistical power that is achieved once the parameters are set correctly. For each spectrum up to 92 independent estimates of the radial velocity have been obtained, agreeing very well with each other, with delta ranges (max - min) being normally less than 10 km/s. This demonstrates that the radial velocities yielded by IRAF are very stable.

The second method that I would like to introduce is the RV estimation using ARES [59]. ARES, an *Automatic Routine for line Equivalent widths in stellar Spectra*, is a code that, as the name suggests, serves to measure equivalent widths (EWs) of spectra [60][61]. Normally, a list of lines that should be measured has to be passed to the code, but in case one is interested only in the radial velocity, a fake list may be chosen for input. The program will be explained later in further detail, but in any case has a built-in functionality to shift spectra to the lab-frame. To do this, in the config file that is part of the input to the script, an *rvmask* (i.e. a set of lines) can be given, and the program then does a cross-correlation using a slightly different definition that is described in the paper by Sousa (2015, [62]). The developers of the code claim a precision of 0.1 km/s on the resulting radial velocities.

ARES usually prints out quite a lot of information about the equivalent line fitting onto the terminal, but among the initial data put out by the code, there is also the radial velocity. This output can now of course be easily redirected into a file and the RV values of different spectra may be collected this way. The advantage of this method is clearly the better computation time - hundreds of spectra can be processed within less than 5 minutes easily. Also its simplicity favors ARES over IRAF. The output data depend rather critically on the number of lines given, e.g. differences of +/- 3 km/s could be common for values taken from 5 respectively 11 lines, but it can be assumed that these arise solely from a too low number of lines used. Furthermore there is another quantity giving the space around each line in which the CC will be performed. It turned out that this parameter is relatively insensitive, but below a certain threshold bugs related to an interpolation mechanism in the *GNU Software Library* called from within ARES may break the calculation. What is more, exceeding a certain width results in the values not being printed either, since according to the logfile in those cases ARES cannot reliably calculate the velocity.

Overall the radial velocities taken from IRAF are more reliable than those from ARES (also thanks to the statistical basis of the template approach). The differences are usually within +/- 5 km/s, but the typical uncertainty attributed to the radial velocity measurements should be much smaller ($\lesssim$ 1 km/s). For UVES, HARPS and STELLA the IRAF results have subsequently been used, while during the equivalent width measurements it became apparent for FEROS that the lines were positioned closely but not exactly at the correct wavelength. This left ARES incapable of associating the fitted lines to the lab-frame ones, so that many EWs were not measured in the first place (see sect. 4). The bleeding from the wavelength calibration fibre [27] could be responsible for this. Consequently, for FEROS the velocity has later been taken from ARES.

While stars usually have just a single (constant) radial velocity, variable stars also have different radial velocities at different phases due to their intrinsic changes in structure (expanding and contracting shells). This leads to radial velocity curves, which have a mean called Γ-velocity (the star's barycentric relative velocity) and a periodic oscillation overlaid on this value. An example of such an RV curve is given in sect. 5. It may be worthwhile noting that the object X Sgr has a higher spread in the derived curve. This is very likely due to this object being classified as a binary in several papers [63][64][65][66] and databases, among them a collection of Cepheid binaries and the nature of their binarity (spectroscopic, photometric, visual) that was presented in Szabados (2003, [67]).

According to recent theories, the radial velocity curve of a variable star may change as a function of the wavelength from which it has been derived [68][69]. Specifically it is stated that the amplitude of the curve decreases with increasing wavelength, since deeper layers in the star's structure are traced, where the velocity oscillations are less pronounced. The mean velocity and overall shape should remain the same, assuming that the star's atmosphere behaves linearly. To test this statement, for all objects from the HARPS sample radial velocities were taken with ARES from line sets at approx. 4500, 5500 and 6300 Å and the radial velocity curves were overplotted one with each other for the 3 estimates derived. The result is shown in figure 3.4.

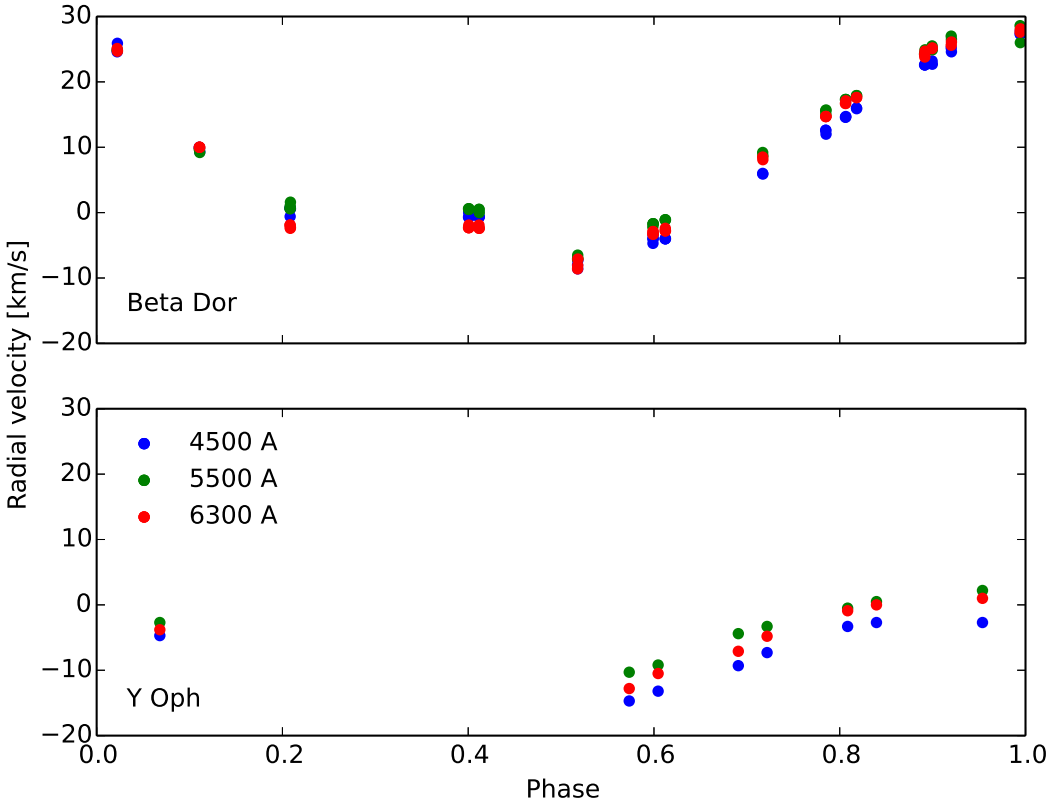

Figure 3.4: Radial velocity curves at different wavelengths for β Dor (top panel) and Y Oph (bottom panel). Blue respectively. green respectively red points indicate radial velocities derived from lines around 4500 respectively 5500 respectively 6300 Å, as indicated in the legend. The y-axis ranges have common limits for easier comparison of radial velocities.

As already mentioned, we can expect the 3 different curves to have the same mean, so that the red points always lie on the inside of the green curve, which itself should lie inside the blue curve. Also there would have to be a crossing of the curves both on the rising and the decreasing branches. However, this was the case only for some objects, whereas in other targets, as can be seen, the curves seem to be well-separated over the entire pulsation period. The reader should take note that no uncertainties have been plotted, since no data regarding error budget is given by ARES, but it can be assumed to be certainly smaller than 1 km/s.

Considering the errors on the data points, no obvious trend is visible from the plots and it can be stated that the theory can neither be proved nor disproved using the applied method.

3.4 S/N Analysis

3.4.1 Overview

Having determined the radial velocities for all the spectra, the next part of the thesis was to examine the spectra for EW measurement suitability. This analysis made use of the S/N which could once more be taken from ARES. Using a very simple choice of the continuum regions in our spectra, preliminary S/N estimates could be made. On a statistical basis in combination with a visual check, the used continuum regions have been optimally chosen so that a refined S/N estimate was possible. Considering again the wavelength regions used for retrieving that value, this enabled me to classify the different spectra as low, intermediate or high quality exposures and to evaluate the usability of these frames for further analysis, especially the metallicity determination. The focus here is not set as much on theoretical rigidity and an optimal approach to determine the S/N with very high accuracy as on showing a relatively simple way with which the results can be obtained with a precision high enough to allow the mentioned classification.

The subsequent analysis was performed separately for FEROS priority, non-priority, HARPS and UVES TS spectra. Exposures included in the Genovali sample did not undergo this treatment though, since they had been received later in the course of this thesis and they had already been marked with sufficient S/N by the original authors. The Kovtyukh and Inno spectra were also excluded from this analysis. For those frames the S/N ratio could be taken directly from the ESO archive where it was indicated (this was not possible for the other data, since it is a phase-3-exclusive feature that has only recently been introduced). Unlike for the other UVES exposures, the Kovtyukh and Inno S/N check did not have a direct impact on the later selection for the metallicity determination. Arguments shown in subsection 3.4.2 refer to the FEROS priority group, but are valid also for the other samples with different numbers.

3.4.2 Method

In order to get the signal-to-noise ratio, continuum blocks were detected in each spectrum using a self-written script that records all consecutive blocks of pixels that remain within a user-defined range around the continuum level of 1 for a minimum wavelength interval chosen by the user. The detected blocks were then sorted by size and the five biggest ones were printed out, assuming that the continuum normalization had been performed well enough with the continuum actually lying in the formerly defined interval. The minimum block size and the interval limits were selected in a way that for the majority of spectra blocks could be found, also having imposed a certain tolerance limit that could not be exceeded. Otherwise also line pixels would have been included in the detected block.

Then for each spectrum the S/N ratio based on these individual blocks was estimated using ARES. This was achieved in the following way:

When performing EW measurements with ARES, the input spectra have to be globally continuum-normalized. ARES nonetheless performs a local normalization. The user typically gives a rejection parameter (*rejt*) in the configuration file that has a similar function as the ones used in IRAF's continuum command. *rejt* thus determines at which flux level the continuum will be placed. Between that parameter and the S/N ratio there is the following simple relation, described in the paper [62]:

$$\text{rejt} = 1 - \frac{1}{\text{S/N}}$$

Usually, this equation is used to estimate the rejection value for a spectrum. However, there is the possibility of giving a set of continuum regions to ARES and letting it determine the correct number itself. In this process the S/N ratio and consequently *rejt* is calculated internally inside ARES based on a median of the S/N values of the single regions. The program then prints the calculated quantities onto the terminal. Redirecting this output into a file, an estimate of the S/N value could be made for all UVES TS, HARPS and FEROS spectra.

For a single spectrum the approach to detect the continuum blocks that has been presented may appear quite arbitrary. The method suffers from the fact that due to the different stellar chemistry, also non-continuum regions may be found if the lines in that region are either absent or weak enough. When put on a statistical basis, however, common wavelength regimes may be extracted among the five biggest blocks of each spectrum. Since statistically some regions would appear more often than others, those wavelength ranges may be regarded as candidate continuum proxies. The ten most common blocks were taken into consideration then. From this list each of the blocks was separately extracted for ten random high-S/N spectra from the FEROS sample (it was the first that was dealt with and had the biggest ranges in the preliminary S/N estimate), distributing them relatively well over the whole observational period to ensure a homogeneous, unbiased approach. Using a high-S/N ratio was essential here, since only in that case, when having a look at the continuum blocks, it is possible to tell whether those blocks actually represent "good" regions. Low S/N spectra make it very hard to disentangle the suitability as a continuum region from the high noise level. Even, if the region was a continuum region, the noise level would swallow this property in the plots.

Consequently out of the ten spectra eight were chosen from the S/N regime between 280 and 460. Two more spectra with S/N of ~ 135 respectively ~ 170 were added to improve the temporal coverage of the sample. Examining the extracted wavelength regions for the different spectra and making use of the number of spectra for which the respective region actually represented the continuum, common good continuum regions could be found and a hierarchy in terms of suitability for S/N estimates was defined. The order of the continuum blocks built that way coincided very well with the number of occurrences of the wavelength regions among all spectra, in the sense that those found for the highest number of spectra also proved to be the best proxies for a proper S/N estimation.

On the basis of these results, the 5 highest-ranked continuum blocks (5860 - 5890, 6675 - 6695, 7530 - 7555, 7725 - 7745, 7810 - 7835 Å) were selected for all spectra. Then, another estimate was made using these common, *fixed* blocks for each exposure. It could be seen

that the S/N ratio from the fixed blocks was systematically a bit lower than the numbers obtained from individual (*dynamical*) blocks. This was expected since the dynamical blocks were "tailored" to maximize the value for each frame. However, to estimate the effective differences, the spectra were ranked according to their S/N estimate from the fixed blocks and a second time similarly for the value yielded from the dynamical-block-approach. Both the positions and the S/N ratios were then fitted using a linear function with both free and zero intercept (a*x + b respectively a*x). Also the fixed-block approach gave intrinsically more S/N values since the dynamical blocks could not be found for all spectra in the first place. Thus, in a second step, only the common spectra were taken into account, the fixed-block estimates were reordered and the same fits were performed. It is worth noting that in such a case a zero-intercept is physically more plausible, because the sum of all positions is constant and the average difference has to be zero by definition.

The resulting fit parameters were a = 0.94, b = 6.73 (correlation 0.79) respectively a = 1.00 (correlation 0.94) for the case fixed vs. dynamical blocks and a = 0.90, b = 8.66 (correlation 0.80) respectively a = 0.97 (correlation 0.95) for the case fixed (subsample) vs. dynamical blocks. Figure 3.5 visualizes these fits.

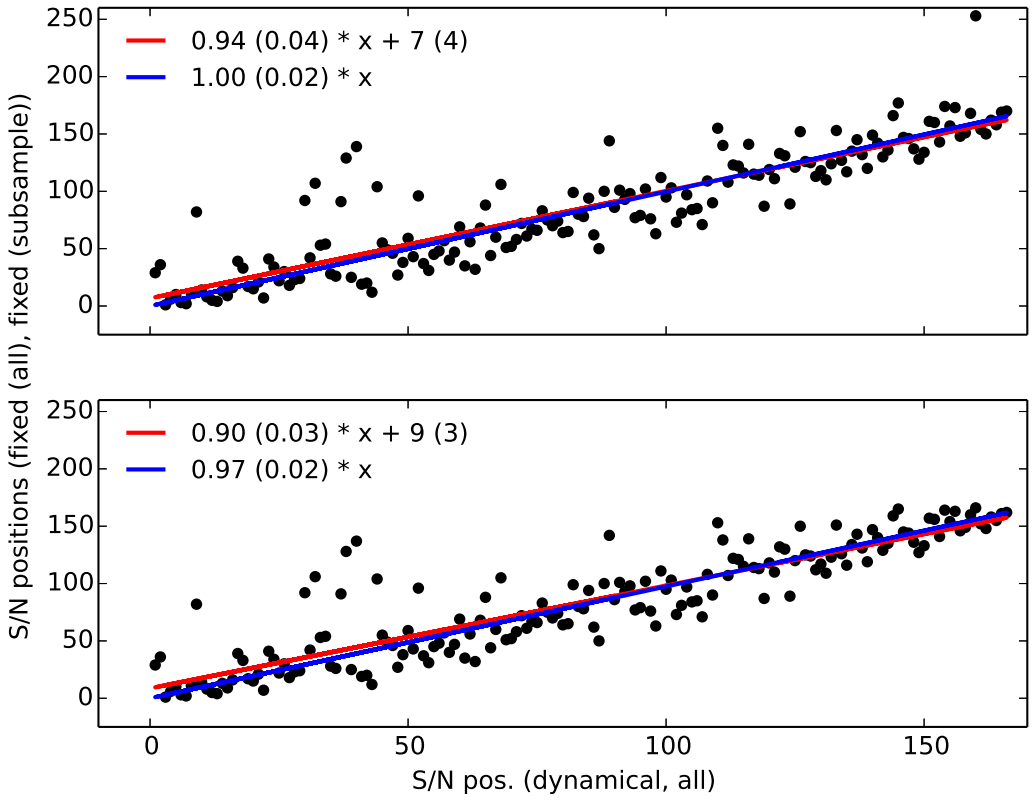

Figure 3.5: Comparison of the S/N positions between dynamical and fixed blocks (all (top panel) respectively a subsample (bottom panel), see text). The fit parameters are indicated on the plots, together with their respective errors (given in brackets).

Similarly, there was a relatively good correlation in the S/N ratios themselves, again with both fit functions. The small differences in the fit parameters when using all spectra respectively only the ones where also dynamical blocks have been found demonstrate that the spectra where the dynamical S/N could not be estimated (mostly frames from 2005) are actually among the low S/N in the new, fixed-approach results. In any case, the differences were generally not too large and, what is more important, the overall trend was kept over the entire sample. Therefore, having received evidence that the dynamical blocks themselves allow a determination of the S/N with sufficient accuracy, the results from that method have been adopted as the final S/N ratios. Nonetheless, the visual check was performed on the fixed blocks.

Together with a visual check of the wavelength regions that had been plotted and saved for all spectra individually, the S/N data made it possible for me to decide which spectra were of higher quality and thus eligible for a metallicity estimation and for which of them probably only radial velocities would be reliably measurable. Cases where it was difficult to judge their suitability were discussed with G. Bono and R. da Silva, another researcher. Many cases were added to the list of the accepted frames in this process. Examples for the 5 wavelength regions for spectra with different S/N estimates are depicted in figure 3.6.

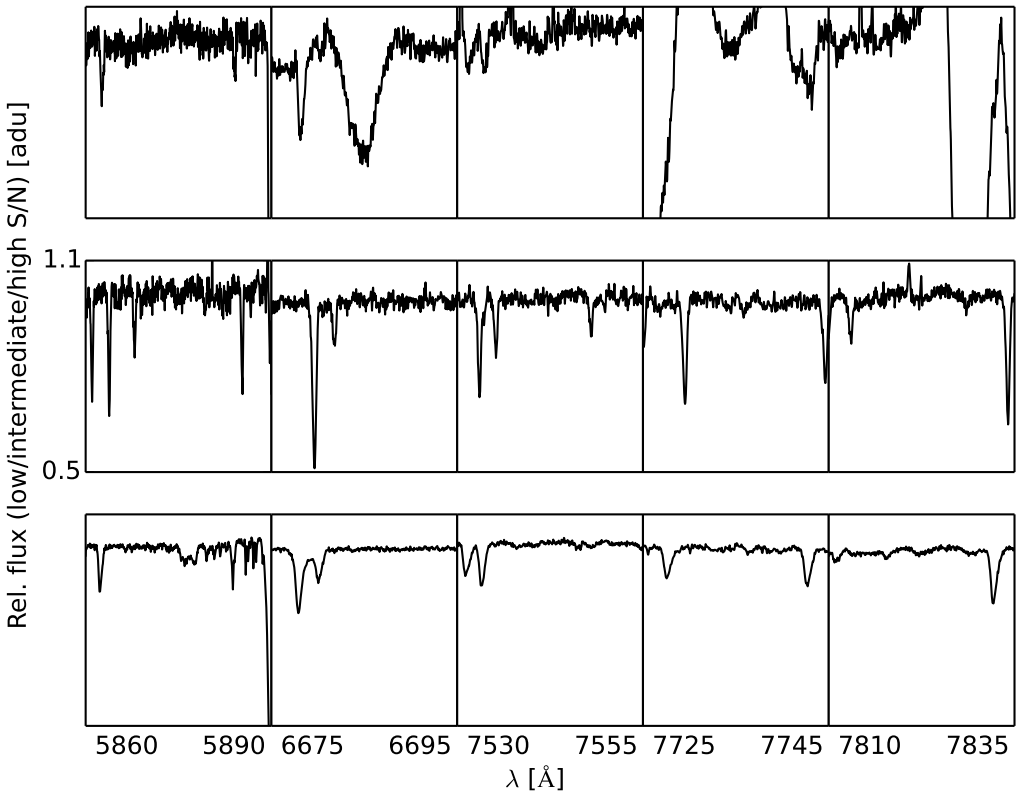

Figure 3.6: Extracted wavelength regions for spectra with different signal-to-noise-ratios. The top respectively middle respectively bottom panels show the (fixed) continuum blocks for low (not estimated), intermediate ($\sim$ 100) and high ($\sim$ 375) S/N values. Please note that panels 3 - 5 in the top row exceed the y-axis range and that the spectral regions are not radial-velocity-corrected (see text).

3.4.3 Continuum Blocks

To extend the discussion about the continuum blocks a bit further, another check was made. The minimum block size that had been used for FEROS to record a continuum block was 3 Å. It was now checked which tolerance level around 1 would have to be set by the user to get over the 50 % detection threshold, so that for more than half of the spectra blocks beyond the above minimum size could be found. For this purpose, a few tolerance levels were checked both for HARPS and UVES TS and the number of detections as well as the maximum and a typical size for the biggest dynamical blocks found for the spectra were recorded.

For UVES I found that the number of detections was decreasing rapidly below 1.5 % tolerance, while above this value a plateau was reached where practically only the length of the biggest blocks was changing. Based on a chosen value for the length of a suitable continuum region ($\sim$ 10 Å), the most reasonable tolerance was 2.5 % then. HARPS suffers from the problem that the blue spectral parts present a huge number of spectral lines and therefore display large variations in the flux. It was hence extremely difficult to detect blocks for those parts. In any case a steep increase in detections between 2.0 and 2.5 % could be noticed, so that 2.5 % was selected here as well.

From the continuum blocks that had been derived, also for HARPS and UVES common wavelength ranges could be extracted. While FEROS exposures showed some continuum blocks also beyond 7000 Å, those could not be found in HARPS, for the spectra do not cover that regime. The statistics for UVES are generally a bit shaky, since there are fewer spectra. A little more than a third of them lies in the extreme blue where no blocks can be found at all and as a consequence the highest number of occurrences for any block is generally lower. Considering that the blocks always have slightly different start and end wavelengths and me defining the common intervals that span the single similar blocks, there might also be an error on these numbers. Note that the common continuum blocks for HARPS, independent of the actual wavelength regimes, are much more reliable than those from UVES. Nonetheless, UVES showed overlap with FEROS and also HARPS blocks. It is worth mentioning that the selection of intervals that had been retrieved from HARPS appeared in FEROS as well. This fact indeed emphasizes the usability of these continuum regions as such and leads to the conclusion that the approach used here to define a continuum, although simplistic, is still correct in its result.

Finally, it should be noted that the wavelength regions were extracted from the spectra in their own reference frame, without any radial velocity correction being applied. Considering, however, that the typical radial velocities of Cepheids are relatively small ($\sim$ 0 - 100 km/s) and hence the small Doppler shifts $\left(z = \frac{v}{c}\right)$ compared to other kinds of stars as well as the relatively big size of the wavelength regions ($\sim$ 20 Å), the effective lambda shift ($\Delta\lambda = \lambda * z$) reaches between 1 - 3 Å at most in the optical/NIR regime covered by the spectra, such that the visual check or selection of common blocks was not endangered at all.

3.4.4 Results

From the analysis it became immediately clear that the visual check confirmed the S/N ratios by ARES, as smaller fluctuations (less noise) in the continuum blocks were well in agreement with a higher S/N.

For FEROS the S/N ranges were 25 - 475 and 120 - 330 in the priority group and non-priority group, respectively. In the non-priority group though, only one object had a lower estimate than 175. Estimated HARPS data varied between 145 and 400, while UVES TS covered the regime between 235 and 480.

While for 44 % of the FEROS spectra the S/N could not be estimated using dynamical blocks, almost half of the remaining ones were between S/N = 100 and 200. HARPS displayed an even higher fraction (51 %) of spectral parts without estimate, almost all being in the blue wavelength regime. In the end the decision was made to study only the red spectra and use the retrieved value also for the blue part for this part of the thesis, since we assume that the S/N ratio does not change too much over the wavelength range. Roughly half of the red spectral parts lie between 200 - 300 in S/N, while another significant fraction shows even higher numbers. UVES TS generally had very high S/N values as well. The only spectra where they were not written out by ARES were the purely blue frames.

A big part of the entire sample of spectra was of very high quality. This was especially evident for the HARPS dataset, where only one spectrum (out of 199) was discarded. Also for UVES TS all exposures have been taken. For UVES TS dynamical blocks could not be found only in some spectra in the extreme blue regime (14 out of 32), where a forest of lines is present. In case of FEROS, however, some spectra were relatively noisy, primarily (118 out of 128) ones from 2005, where the bleeding from the ThAr lamp severely impacts the data [27]. Most of those were disqualified for metallicity estimation also by the visual check. FEROS was furthermore the only spectrograph with a real transition region in the S/N check, i.e. where discarded and accepted spectra are separated by several ambiguous cases. The latter spanned a S/N range from $\sim$ 75 to 135. All spectra beyond the upper limit have been accepted. It should be noted that even some of the spectra without estimate were also of sufficient quality since the fluctuations present in the wavelength regions were due to lines instead of noise again. The typical S/N ratios of accepted FEROS, HARPS and UVES TS spectra were $\sim$ 200, $\sim$ 250 and $\sim$ 340, respectively.

As mentioned above, a strong trend in time could be seen for FEROS in the priority group objects. While all spectra from 2004 were accepted for S/N measurements, more than 92 % of those from 2005 were discarded. On the other hand, the year 2007 brought a relatively symmetric classification with a big part of ambiguous cases. 2010 offered almost a complete mirror distribution of 2005, with a 100 % degree of acceptance. The files from 2011 and 2012 (relatively few in total) were roughly equidistributed. The non-priority spectra were almost all accepted, with only two ambiguous cases and spectra generally were taken in the years 2010, 2011 and 2012, with one exception from 2005. UVES and HARPS did not present any temporal trend. Practically all of them were suitable for metallicity determination. It goes without saying, that no real trend in objects could be found, either. Nonetheless, the objects RS Pup and RZ Vel (two out of the nine HARPS Cepheids) constituted 10/15 HARPS red spectral parts without S/N estimate.

Below a summary of the final decision about metallicity determination suitability for the different spectrographs is given. A S/N status of *yes* marks the spectra as definitely having sufficient quality for equivalent width measurements and thus metallicity estimates, whereas the ambiguous cases (*maybe*) have a reasonable probability of doing so as well. Spectra belonging to the group *no* most probably will be usable only for radial velocity studies. Table 3.1 shows how many spectra were put into which group for each of the spectrographs.

Table 3.1: Number of spectra with different S/N classifications for FEROS, HARPS and UVES TS. The relative fractions refer to the different spectrographs respectively the entire sample.

Category	N_S	Fraction
FEROS S/N yes	206	58.03
FEROS S/N maybe	23	6.48
FEROS S/N no	126	35.49
HARPS S/N yes	196	98.49
HARPS S/N maybe	2	1.01
HARPS S/N no	1	0.50
UVES TS S/N yes	18	56.25
UVES TS S/N maybe	14	43.75
UVES TS S/N no	0	0.00
Total S/N yes	420	71.67
Total S/N maybe	39	6.66
Total S/N no	127	21.67
Total S/N	586	100.00

The discarded spectra underwent the same steps later as the accepted ones. Results, however, were put into separate files.

Chapter 4

Equivalent Width Measurements

4.1 Overview

With the S/N analysis being completed, the equivalent widths could now be measured. For this purpose, ARES has been used, which offers a sophisticated and at the same time user-friendly approach to this task in spite of relatively few adjustable parameters. By using first a global set of common input parameters for the three spectrographs UVES, HARPS and FEROS, an initial measurement of the equivalent widths could be performed. Problems that became apparent at this point helped adjusting these options for each spectrograph individually so that better equivalent width results were obtained in a second attempt.

4.2 Method

The options that decide how exactly the code performs the measurements are given in a configuration file [61][62]. Among those there are *specfits* and *readlinedat*, indicating the spectrum and a list of lines to measure on that exposure that are required as input by ARES. The main output file containing the equivalent widths can be set via *fileout* and the wavelength range to consider is given using the *lambdai* and *lambdaf* parameters. *rejt* and *rvmask* have been described earlier in this thesis and determine the continuum position and the radial velocity of the target for the respective spectrum. Further relevant settings include a minimum equivalent width below which no results are printed into the output file (*miniline*) and a certain wavelength interval describing which data to take into consideration for the computations (*space*). The value of *lineresol* is responsible for whether fitted lines are being associated to a particular feature. During the calculations, the data undergo a smoothing procedure by ARES, the degree of which is regulated by *smoothder*. Finally, *plots_flag* decides whether graphs of the lines and the fits that the code obtained should be displayed or not.

The dataset of this study comprises several hundred spectra. For each of them 3 linelists, received from R. da Silva, have been used. One of these lists includes specific lines (153) that were used later for determining the effective temperature of the object and had been built by combining four individual ones which had been received from Kovtyukh. Originally, there were only two lists which had been measured separately (45 + 94 lines). The other files included iron features (233) respectively lines belonging to other elements (113, α-, s- and r-elements).

Near the end of the thesis work, I received another linelist, based on the Gaia ESO Survey (GES), from B. Lemasle, which was combined with the former iron list to form the final set of iron features (615 lines). In order to have the latest values, this linelist has then been cross-checked with VALD 3 (*Vienna Atomic Line Database*, [70][71]). In case values would not agree (differences in wavelength or excitation potential occurred rarely and were minimal, similarly for the oscillation strengths log(gf)), the VALD ones were adopted. It should be noted that, contrary to R. da Silva's iron linelist, the newly added lines given in the final version have not been checked for blending.

All statements given in this section were made on the basis of measurements of the original two Kovtyukh lists for the effective temperature determination and R. da Silva's iron linelist, but they apply to the extended case (four Kovtyukh lists respectively the final iron list) as well. The complete list of lines used in this thesis can be found in appendix B. An example for typical information contained in a linelist is given in table 4.1.

Table 4.1: Partial linelist used in this thesis. Columns indicate the wavelength, excitation potential, oscillation strengths, element, atomic number/species and reference information. The oscillation strengths log(gf) are not given here, but they are relevant for the metallicity determination and therefore are present in the iron linelist. The source column describes the linelists from which the lines have been taken (see sect. 5).

λ	χ	log(gf)	Element	Num	Source
5348.30	1.00	-	CrI	24.00	KOV2
5373.71	4.47	-	FeI	26.00	KOV2
5410.91	4.47	-	FeI	26.00	KOV2
5497.52	1.01	-	FeI	26.00	KOV2
5501.46	0.96	-	FeI	26.00	KOV2
5506.78	0.99	-	FeI	26.00	KOV2
5554.89	4.55	-	FeI	26.00	KOV2
5565.71	4.61	-	FeI	26.00	KOV2
5578.72	1.68	-	NiI	28.00	KOV2
5633.97	4.99	-	FeI	26.00	KOV2

For each of the frames close to 500 lines would potentially be measured. Clearly, manual (individual) measurements of each spectrum with different input parameters and visual checks of every line fit are not at all feasible in this case. As a consequence a small script was written that prepares the configuration files and runs ARES for each spectrum. The terminal output of ARES, where quite important information is given, was redirected into individual logfiles. Problems of running the program with this redirected output and a plotting flag set to 1 so that graphs would be displayed forced the deactivation of the plots. This constraint does not affect the quality of the results in any way.

In order to become familiar with the code, a few spectra were input to ARES manually. Then in the first run of the whole sample all input parameters were set to the default ones given in the example configuration file of the ARES package (except the spectrum-specific ones like the wavelength range). The radial velocity was taken from the IRAF results obtained earlier, whereas the *rejt* parameter was left at its standard level. The common set of parameters was therefore:

- smoothder = 4
- space = 3.0
- rejt = 0.995
- lineresol = 0.1
- miniline = 2
- plotsflag = 0

It should be clear, that this method neglects the fact that different spectra require different parameters. However, since the sheer number of lines to measure per spectrum makes manual adjustment of the parameters almost impossible, the mentioned run may serve as a quick-check tool. Already at this point a few interesting issues became apparent. First of all, the computation time for HARPS was very long compared to UVES or FEROS. Although the routine used is generally fast and able to process UVES within a couple of minutes and FEROS within 2 hours, the above procedure took roughly 11.5 hours in case of that spectrograph. The ratio in the number of spectra is not sufficient to explain this difference. What is more, HARPS spectra generally do not differ much in terms of number of pixels per spectrum (resolution) from those of FEROS and also the size of the created files was very well compatible, indicating that the number of detected lines should be comparable at least on an order-of-magnitude scale.

By checking a few affected frames manually it was found that ARES in case of HARPS fitted too many lines. This is common when the spectrum has a higher noise level since the program erroneously interprets the fluctuations as absorption features. In fact, the big number of fits tremendously slowed down the calculations. Due to the contributions of these unreal lines to the total flux, the equivalent width of the actual feature that was to be measured is significantly reduced from its true value. Moreover, often the centers of the small lines would be away more than *lineresol* from the target absorption dip, leaving the program unable to match any line to the main feature. In such a case, the routine would print -0.0 for the equivalent width. Luckily, such results are never recorded in the output file due to *miniline*. Thus possible measurements on the remaining lines are not contaminated, with the amount of actual data being greatly reduced.

The solution to overcome the overall problem is quite simple. The smoothing that is being done by ARES to determine the line centers in the spectrum can be enhanced by increasing *smoothder*. This helps in eliminating noise from the derivatives which are calculated in the procedure (see Sousa (2007, [61])). The number of lines recorded in the output file shrinks with a too low smoothing parameter (too many lines and therefore resulting fitting errors). This is also true for a too high smoothing parameter, where the Gaussian profiles span the whole plot range and the (fit) line center is often more than *lineresol* away from the feature of interest. Consequently, the number of measured lines may be regarded as a good proxy for a plausible choice of the smoothing value. Nonetheless, it has to be stressed that in the end the only reliable, valid check is a visual inspection of at least several lines in a couple of spectra, a procedure, which consequently I followed. Figures 4.1- 4.3 visualize the effect of *smoothder* on the lines.

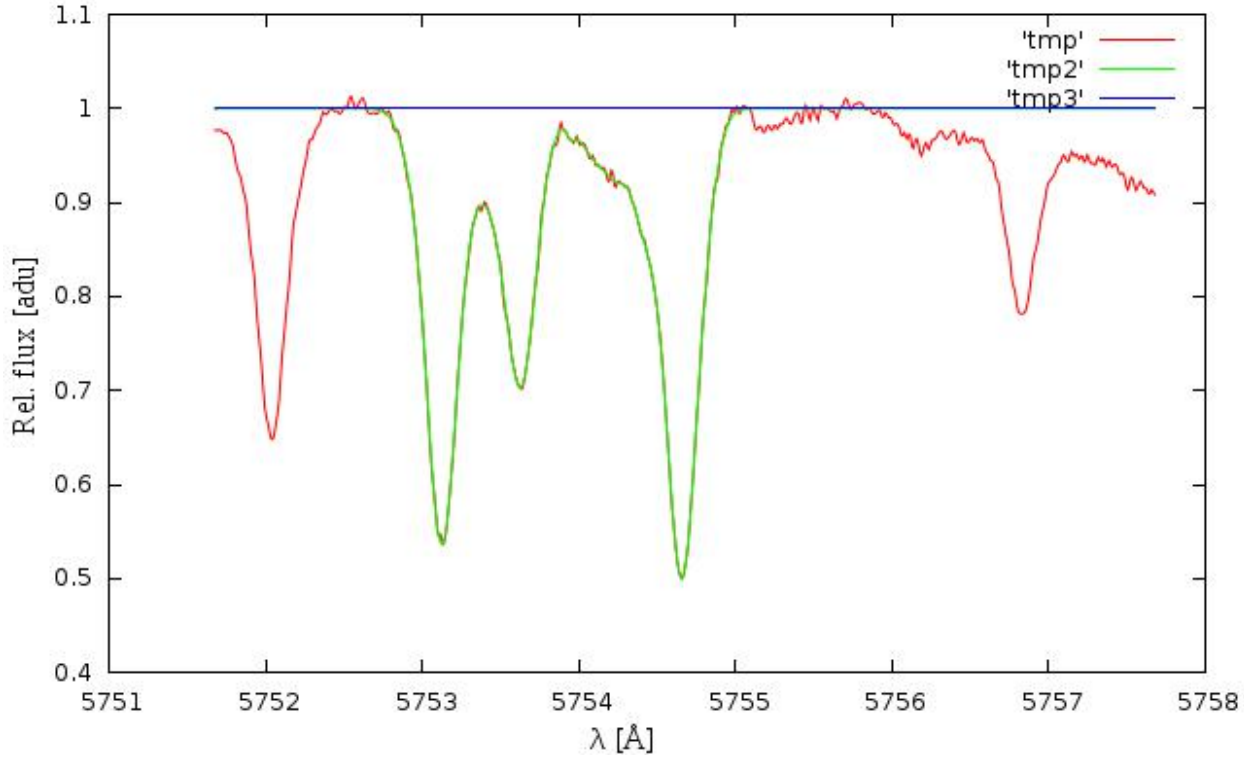

Figure 4.1: Too low smoothing parameter for test spectrum (object ζ Gem) - smoothder = 2. The spectrum is clearly overfitted.

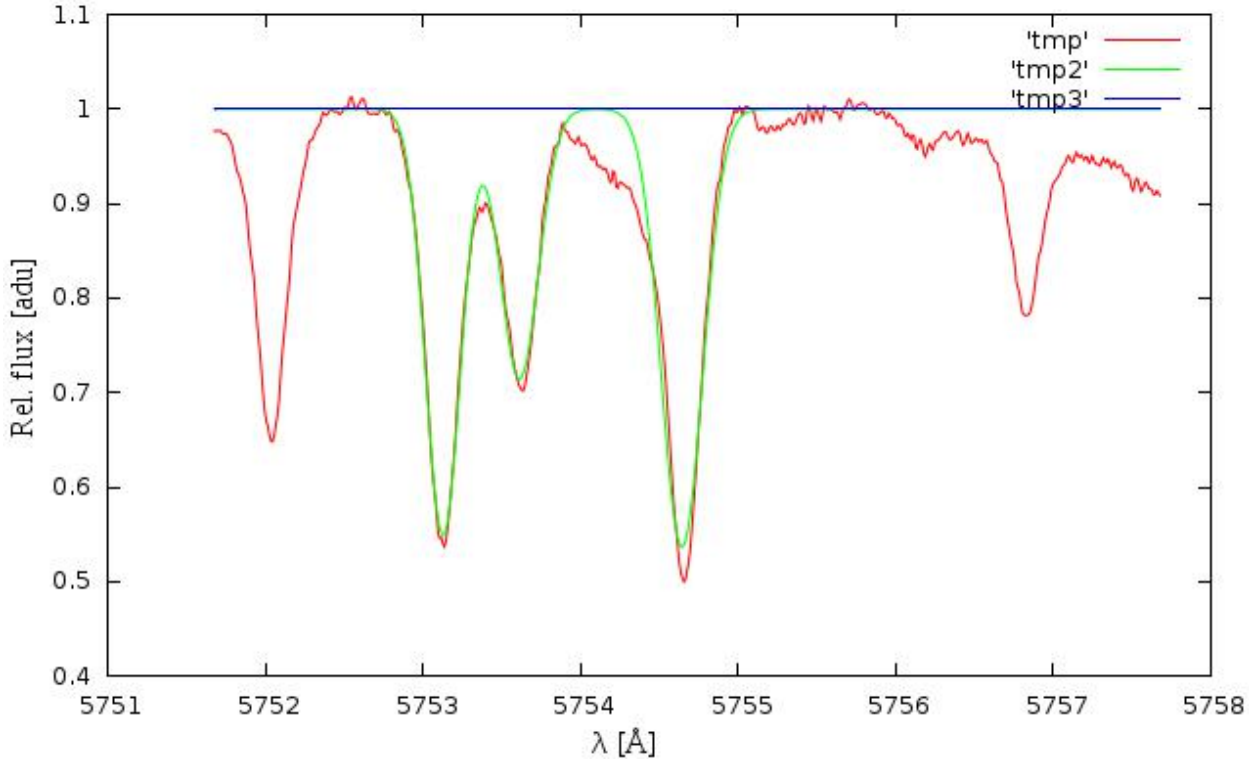

Figure 4.2: Optimal smoothing parameter for test spectrum (object ζ Gem) - smoothder = 20.

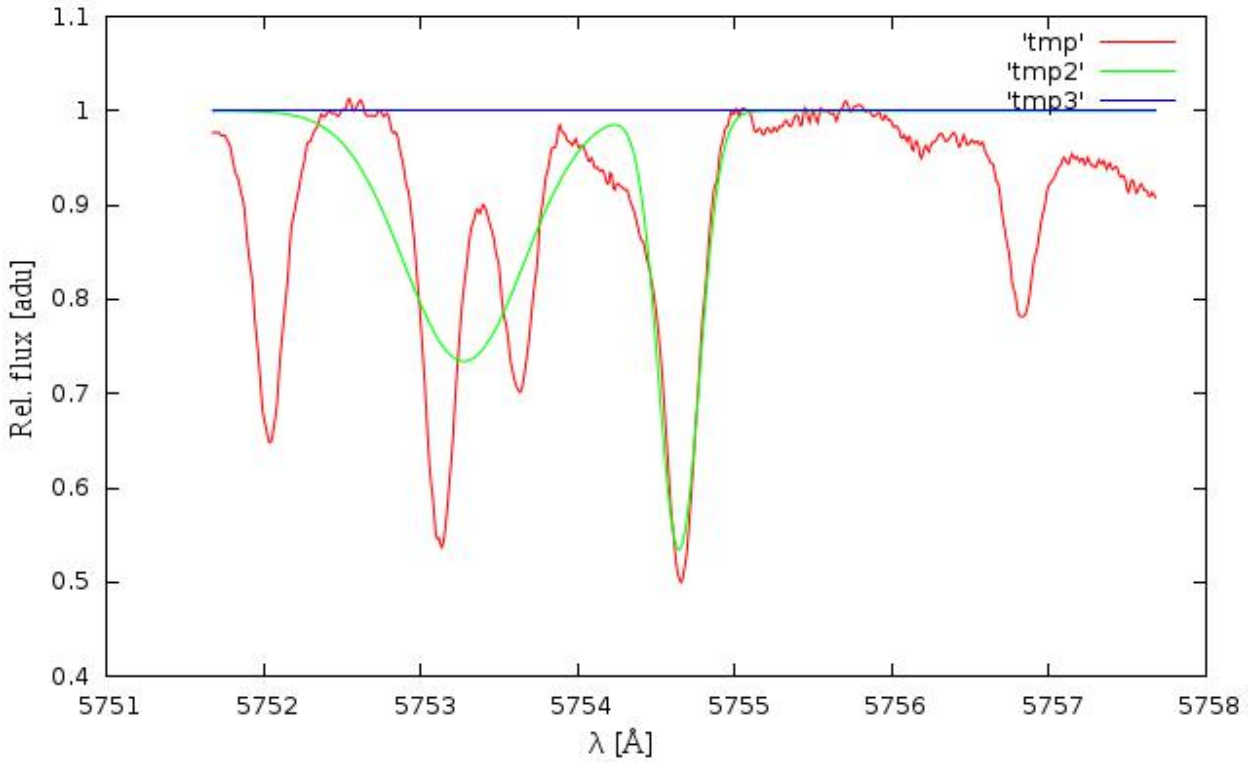

Figure 4.3: Too high smoothing parameter for test spectrum (object ζ Gem) - smoothder = 40. ARES does not manage to discriminate the two left lines from each other any more.

For HARPS, a correct smoothing parameter was found to be 20. This number was valid for practically all spectra. The computation time was reduced to below 1 hour. Some UVES ESO spectra required a slightly changed *smoothder* of 10 and Genovali spectra could be fitted well with a value of 20, whereas the default of 4 was sufficient for the FEROS exposures.

4.3 Fitting Problems

At this point let me state, that there are various critical situations that may appear during the equivalent width fittings in ARES. Figures 4.4-4.6 show problems with line matching, plotting and blended lines that occurred in some of the spectra. However, I would like to emphasize that most EW measurements performed with the routine are very reliable, stable and also have small recorded errors (a functionality built in the latest release, ARES v2 [62]) and that the results are generally of high quality.

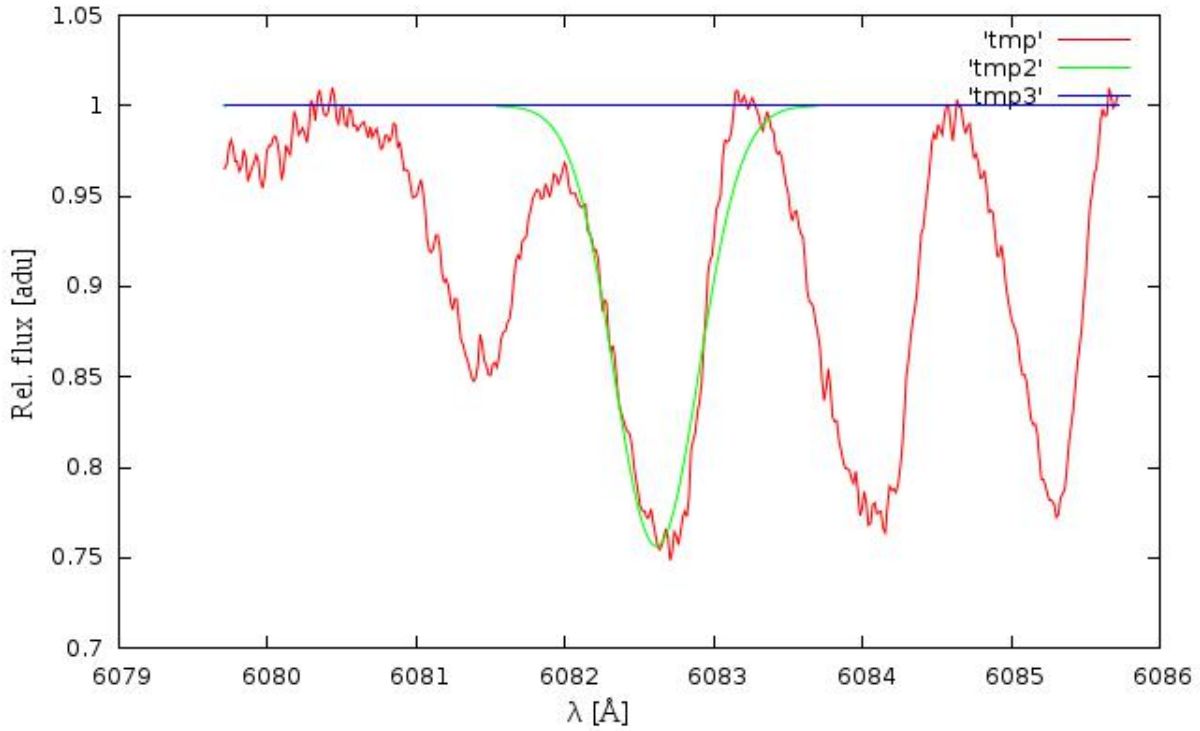

Figure 4.4: Line alignment problems in a test spectrum (object Z Sct). Such a slight misalignment (either because of a slightly wrong radial velocity or due to other factors) may already induce obstacles for ARES which accordingly does not associate the lines.

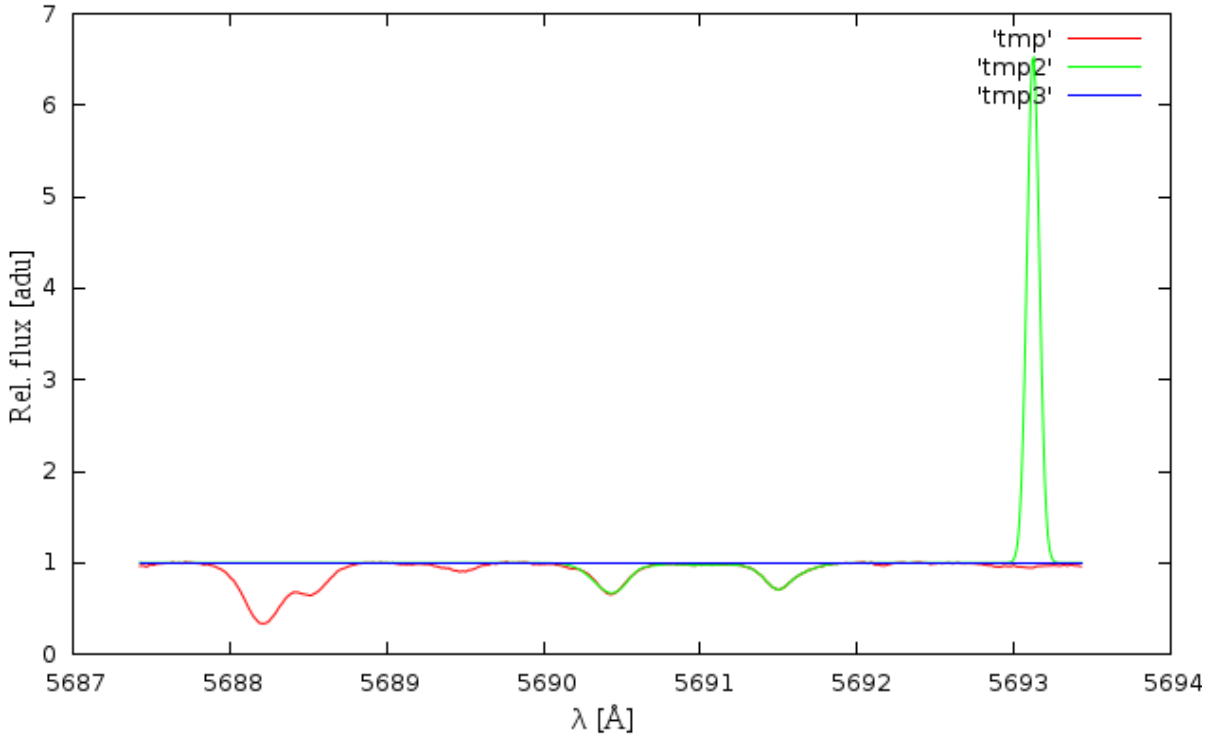

Figure 4.5: Plotting errors in a test spectrum (object ζ Gem). The resulting equivalent widths are still correct.

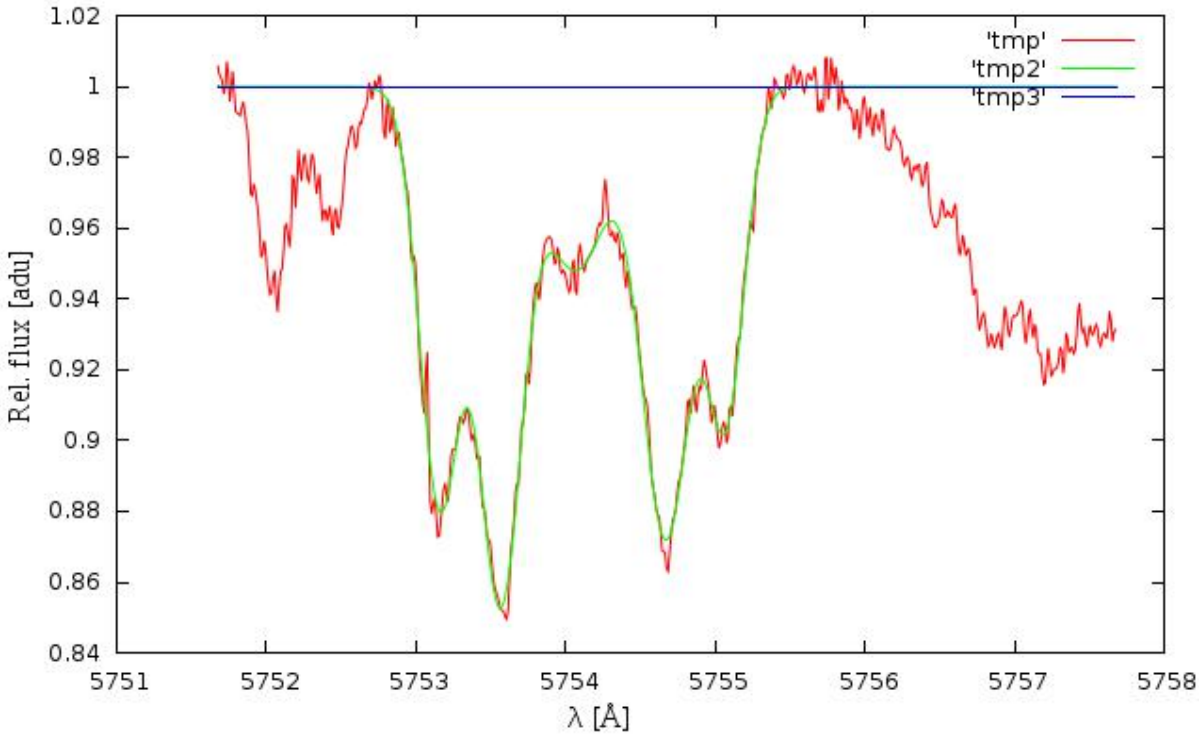

Figure 4.6: Blended lines apparent in a test spectrum (object X Sgr). Although ARES is capable of fitting them, the resulting equivalent widths do not stem from a single target in this case.

If problems appear with respect to line matching, they may not only be due to the spectra themselves. Other causes include e.g. errors in the wavelength scale. This occurred, for instance, for FEROS, where ARES at first tried to fit a line, where none was visible in the spectrum. By having a look at a specific line in a test spectrum, it could be seen that ARES was shifting the spectrum by 1.5 Å too far to the blue. After having checked that the radial velocity for this spectrum was correct by comparing the line in the original exposure to template frames, I found that this additional shift occurred consistently among the FEROS spectra, with exception of the ones taken in 2004. Due to the fact, that HARPS and UVES spectra were fitted correctly, either a problem with the pipeline reduction or a fault in the original spectra was assumed. The first option could be quickly eliminated since all spectra had been almost at the same time, using the same pipeline version.

The solution became clear after a sample fits file had been converted to ascii format, where the fitting was done in the right way, and after having compared the fits headers of files from different spectrographs. The reference pixel from which the wavelengths at each point were calculated was set to -49 instead of the usual one, with the correct starting wavelength that would be attributed to this pixel. However, ARES internally reads only this starting wavelength from the header without the pixel number (for which it takes 1). The underlying reason for this shift of 50 pixels was explained by J. Pritchard. FEROS spectra are read out with a pre-/post-overscan of 50 pixels. Due to a software upgrade at the VLT, from 2005-04-16 onward the reference pixels have already been changed in the raw data from 51 to 1, a modification which propagates through the DRS reduction.

An easy solution to this feature is to adjust the keywords for the reference pixel and its wavelength (CRPIX1, CRVAL1) accordingly so that ARES does a correct wavelength transformation. It is needless to say, that with the correct lambda scale, the results for practically all the spectra, where previously no or few (wrong) lines were measured, improved drastically.

Often the main culprit behind problems with line matching is in fact the radial velocity itself. This has also been found for many FEROS spectra, where IRAF's radial velocity was moved the target line quite close but not exactly to the rest frame. The typical velocity difference is on the order of less than 5 km/s, but the wavelength difference is sufficiently large to position the line more than 0.1 Å away from the lab frame. This obstacle was overcome by using the radial velocity from ARES for the whole FEROS sample instead, since the IRAF values might have been unreliable.

The plotting problem occurs primarily in combination with erroneous fits and does of course not influence the value of the EW result. Furthermore, ARES is well capable of fitting blended lines. Depending on the degree of blending, the error may, however, be larger for the equivalent widths of the isolated lines. The reason for the fitting problem in case of figure 4.6 is the binary nature of the object under consideration, X Sgr [63][64][65][66].

The chemical composition naturally plays a non-negligible role on the uncertainties of the results attributed to measurements made with ARES. Metal-rich objects present a forest of lines, with therefore more prominent occurrences of blended lines as well, increasing the uncertainty due to the Gaussian fits interfering with each other, whereas metal-poor ones may have a perfect continuum, but their tiny lines make it difficult to distinguish them from the noise background which therefore increases the (fractional) error.

Chapter 5

Effective Temperature Estimation

5.1 Overview

The results of the equivalent width measurements enabled me to obtain an estimate of the effective temperature of the target star for each spectrum. Line-depth ratios that can be built from the equivalent widths that had already been measured serve as estimators of this quantity. By means of looking at the effective temperature distribution for each spectrum and specifically the dispersion as its representative, outlying spectra may be found. Checking the ARES routine manually for those, the fitting process could be greatly improved and became physically more sensible. As a side benefit, the standard deviations became smaller, which allowed more precise statements about the actual temperature of the star in each phase for many cases.

5.2 Method

5.2.1 Initial Temperature Estimates

Kovtyukh & Gorlova (2000, [72]) developed the approach followed here. It is based on the pairwise calculation of the ratios of the depth of several particular absorption lines (line-depth-ratios). The lines forming these pairs should come from the same element, be close in wavelength to each other and neutral in order to minimize the influence of the abundance, the continuum placement and the surface gravity of the stars on the measured line depths.

The depth of the lines could be taken from the ARES results, where together with the wavelength of the line, the value of the equivalent width and its estimated error, also the Gaussian used for fitting the line and specifically the depth of the dip was stored. Using 32 pairs of lines that are located in the commonly used wavelength range between 5670 and 6850 Å, calculating their line-depth-ratios and transforming these numbers into an effective temperature by means of the functions in the mentioned publication, 32 independent estimates could be obtained.

From these 32 effective temperatures, several calibrations may be removed, for some of them could give results far away from the remaining ones. Such outliers may be caused by wrong line-depth-ratios or the use of the corresponding calibration in a regime of the effective temperature where it is not allowed. For each calibration there is a certain range of validity indicated in the paper where the function can be used and others where it is not possible, since the fits performed by Kovtyukh cover specific temperature ranges. At the beginning these temperature constraints of the calibrations were not noticed and therefore not taken into account. A discussion of the effect will be given later.

Generally speaking, the outliers can be cut by imposing that the calibrations pass a sigma-clipping, i.e. that their individual estimate is within e.g. the mean +/- a threshold value.

At each cycle of the sigma-clipping the standard deviation σ was calculated as a proxy of the scatter of the distribution and 2σ was adopted as the allowed interval around the mean. The sigma-clipping ended if either all points had an effective temperature estimate within the mean +/- 2σ and/or if the standard deviation was lower than 100 K. The latter criterion was introduced in order to avoid cutting away (discarding) too many calibrations.

Once the sigma-clipping was finished, the mean and median temperature was computed from the remaining values. As results showed, the effective temperatures seemed very plausible, the number of calibrations that survived the sigma-clipping was typically quite high (~ 20) so that a solid statistical basis was present and the standard deviations were relatively low for most of the spectra.

Nonetheless, for some spectra the effective temperature could not be retrieved this way. Among the affected frames there were a few from the UVES spectrograph, whose wavelength range did not have any overlap with the linelist, respectively also partial UVES TS spectra, where it was quite small (either blue spectra that barely reached the lower limit or red parts if the blue regime covered the wavelengths of the lines that had been measured). For many FEROS spectra a temperature determination was impossible at first, since the radial velocity was not exact (see sect. 4). Other spectra from FEROS, HARPS and UVES TS had very high standard deviations. A limit of 150 K for σ was set, based on the usual uncertainties given in the literature, above which the spectra underwent a manual check to see what caused the bigger dispersion.

5.2.2 Refinement of Equivalent Widths

Let me emphasize that when checking the parameters used by ARES and modifying them the goal was to reach a better (more plausible) fitting of the lines and hence improved equivalent widths. If later the dispersion when recalculating the effective temperatures was smaller, this would be a positive side effect indicating a more realistic measurement of the equivalent width respectively the line depth. It is of utmost importance not to try to modify the fitting in a way that the standard deviations were lower but instead in a way that the fitting itself is performed in a better way. Although the spectra with a very high σ indicated that maybe there was a problem in the ARES measurements, reducing the dispersion was always considered a consequence of a better fitting process, not its scope. Let me add that arbitrary modifications were also prevented by the fact that all concerned spectra of a spectrograph had been "optimized" before the temperatures for the whole sample would be recomputed. Moreover, all outlying spectra of the same object were reduced with the same parameters. Additionally, owing to the complex polynomials that constitute the calibrations that transform the line-depth ratios into the temperatures it is not possible to estimate the effect of a changed parameter in advance, also preventing arbitrarily changing ARES options in order to obtain a smaller dispersion.

In case of UVES, only the Genovali spectra had outliers in terms of a high σ. It was found, that for some of them the *smoothder* value had been set too low. Sometimes the line-matching was not performed well in spite of the correct smoothing parameter, which made me increase *lineresol* slightly. For some spectra the minimum threshold below which equivalent widths were not recorded was set higher to avoid having very weak lines in the output, where the fractional error is typically much bigger than for the strong lines.

The HARPS outliers offered a still too high number of fitted lines, which could be decreased by enlarging the smoothing option. Other than that, X Sgr was measured using the ARES radial velocity, since the spread of the IRAF values was bigger for this binary Cepheid.

FEROS had the highest fraction of spectra beyond $\sigma = 150$ K. The reasons seemed to be manifold, the primary one being the wrong radial velocity. Other reasons might have been related to *smoothder*. For some spectra no apparent reason for the high standard deviations could be detected. These spectra were left unchanged, except for the use of ARES RV values to guarantee a homogeneous treatment of the dataset.

With these optimizations performed, the T_{eff} of the targets was recomputed. It turned out that although some spectra had even higher standard deviations, the changes brought the benefit of a smaller temperature distribution for the majority. The mean and median temperatures changed of course, but the median's statistical robustness prevented any bigger changes in the value. Those would have shown only if the majority of the measurements was systematically at a too high or too low temperature, a situation prevented by the estimates' independence.

5.2.3 Additional Calibrations

Later, several more, currently new calibrations from Kovtyukh (2007, [73]) were added to the sample, using not only polynomials but also other kinds of fitting functions. The extended temperature ranges of the new calibrations allow temperature determinations up to 7000 K and naturally improve the statistical reliability of the derived data. A full list of all used calibrations can be found in the appendix C of this master thesis.

In order to yield the new effective temperatures, the additional lines had to be measured by ARES and combined with the old sample. Using the new calibrations, the temperature validity ranges were noticed for the first time. The treatment of the calibrations became slightly more difficult, for in advance it was impossible to tell whether the use of the concerned function was allowed at all. This would have required the knowledge about the effective temperature which could not be acquired without the calibrations. Unfortunately, one can only make a statement about the validity of the calibration after having used it. Usually, such a dilemma can be overcome through iterative processes. This had been realized as follows:

At first the sigma-clipping was left untouched, but a new part was implemented in the script, according to which a calibration would be accepted only if the median temperature plus and minus three times the dispersion fell entirely within the temperature range. It turned out, that practically no calibrations remained, due to this restrictive criterion. A less stringent requirement was to allow all calibrations where the median +/- 3σ at least touched the boundaries of the temperature range of the calibration of interest. The two clippings (sigma and temperature exclusion) were set within a while-loop until no more calibrations were cut away by the temperature discarding process.

This procedure was then also used once more exclusively for the old Kovtyukh functions to see which impact it would have on the results. Most interestingly, the effective temperatures (both mean and median) did not change at all, neither did the related standard deviations. An explanation can be found by looking at the derived effective temperatures. First of all, the old Kovtyukh calibrations had quite big and what is more common validity "valleys" and

second, the derived temperatures fell within that range. Apparently, the sigma clipping had already removed all implausible estimates from the set of used values so that an additional temperature exclusion was redundant. Thus, a reexamination of the spectra where previously ARES parameters had been changed on the basis of suspiciously high standard deviations was not necessary. Nevertheless, in an example spectrum it was checked that the new lines had been properly fitted as well, similarly to the already measured ones.

Comparing the new and the old results, however, showed that the new ones seemingly attributed higher errors to the data that were yielded in the routine. The median temperatures, on the other hand, were very well compatible with the old ones. By changing the admission criterion for temperature calibrations, the standard deviations were significantly reduced. Especially in the first cycles 3σ appeared to be an overly lenient interval, thus only few calibrations were discarded, even if they were actually quite far away from the median. In the next iteration, since the calibrations were still among the accepted ones, the standard dispersion barely changed and they were again left in the sample.

Therefore the results were recomputed using 2σ, σ and 0 as the interval range around the median. Soon it became obvious that the choice between 1 and 0 times the standard deviation practically did not influence the output. More importantly though, the errors on the temperature became significantly smaller in the general trend when tightening the requirements on used calibrations. This was even more true for the spectra with the highest standard dispersions according to the new set of lines. The majority of spectra fell now below a 45 ° line in a plot comparing the standard deviations. This is well illustrated by figures 5.1-5.3.

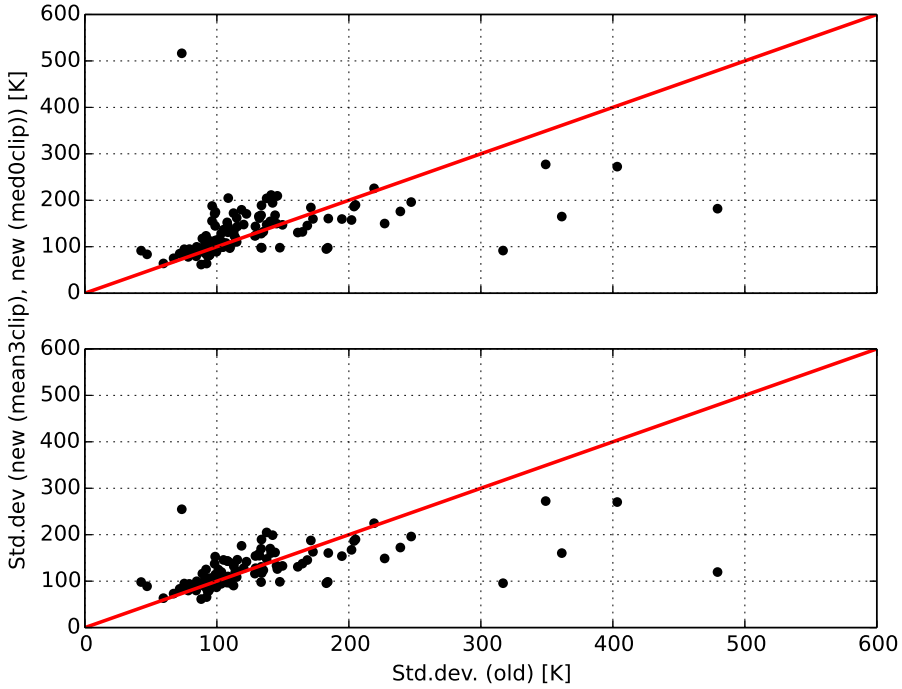

Figure 5.1: Comparison of standard deviations between old and new Kovtyukh lines for UVES spectra. A mean respectively median sigma clipping has been performed together with a median +/- 3σ respectively median +/- 0σ temperature exclusion (top respectively bottom panel).

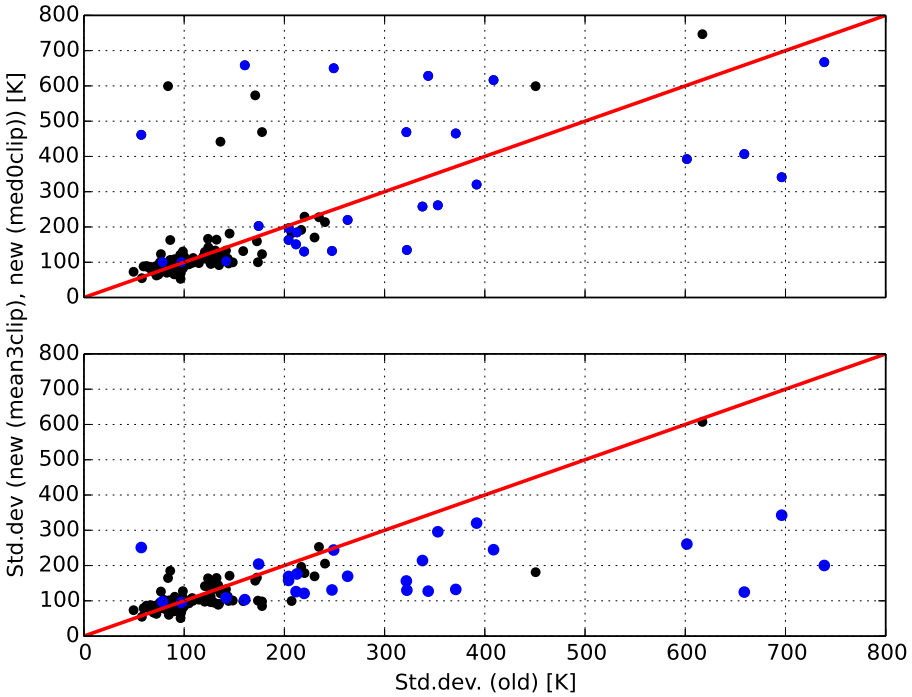

Figure 5.2: Same as figure 5.1, but for HARPS. Blue points are attributed to X Sgr.

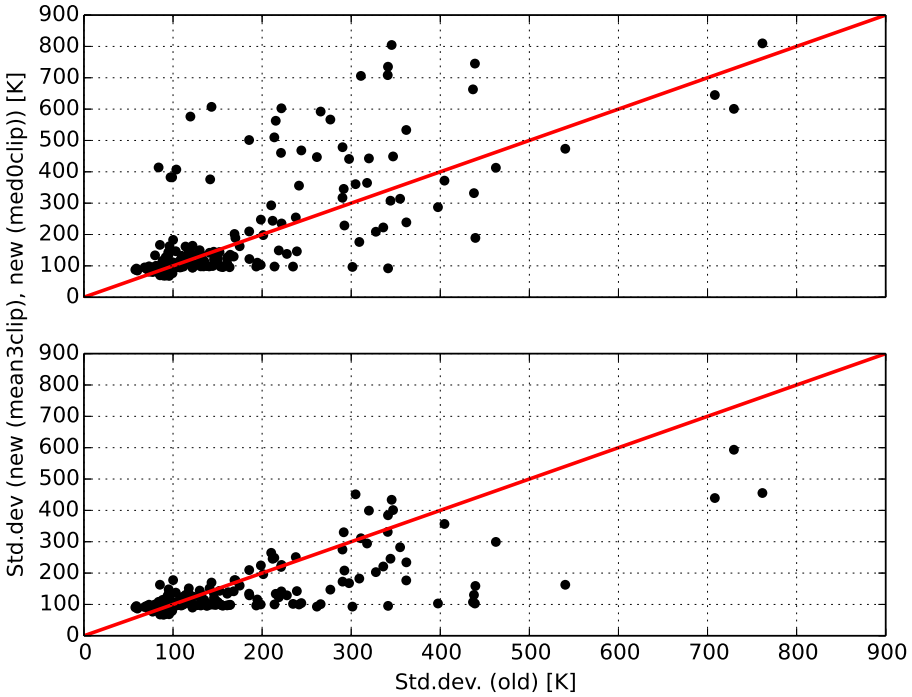

Figure 5.3: Same as figure 5.1, but for FEROS.

In the end, the decision was made to use 0σ for the temperature determination. The fact that the temperatures themselves did not change with different temperature exclusion rules merely confirmed that indeed the outliers had already been removed from the array of temperatures correctly or that statistically they were not relevant.

As another check, the interquartile range (IQR) was used instead of the standard deviation for the clipping processes, since it is principally a more suitable estimator for the spread when dealing with asymmetric distributions. However, it could be seen that the results behaved almost identically to the former ones, giving the smallest uncertainties at 0*IQR. For simplicity reasons the clipping rules were left unchanged and the standard deviation was kept.

Later, even more calibrations were received from Kovtyukh. They were given in two sets, one for the visual regime, the other for the IR. Naturally, the wavelength range of the functions was now extended and lines between 7000 and 8000 Å were used as well. Furthermore, the temperature validity range had improved as well, allowing the use of the estimators in a bigger interval of effective temperature. Due to the different format of the calibrations, all sets that had been taken for temperature determination were homogenized, so that they e.g. contained the columns in the same order.

In total, there were 4 distinct sets of calibrations, taking the two new ones into account. They are marked as KOV1 (2000, [72]), KOV2 (2007, [73]), KOV3 (2016, new) and KOV4 (2016, new) and they contain 32, 131, 110 and 41 calibrations, respectively. The lines that belong to these functions were merged and the multiplicity was removed. It was found that in some cases the wavelength had changed slightly (0.01 Å) between different sets, similarly for the excitation potential (0.01 eV), which was most probably caused by more accurate data. In such cases the newer values were preferred, and the older ones were modified accordingly. The list of unique lines that needed to be measured thus included 153 lines.

Also in the different calibration sets, often functions with identical wavelengths for the line ratios would be used. The older sets and KOV4 did not have any common wavelengths. Whether any calibration would be removed, depended now on the temperature range in which the fit was valid. In case of no overlap, all calibrations remained in the list, independently whether they originated from different sets or not. Moreover, if there was an overlap in the newest set, all of them were kept. In case of an overlap between the most recent sources and others, the older ones were removed, assuming that the latest functions were based on the most reliable data.

A different method could have been to shrink the temperature ranges of the older calibrations so that there would not be any common region anymore. The more restrictive procedure presented here was followed because certainly the approach of Kovtyukh, who performed the fit to shrink the range in the given way, was physically motivated and thus a reliable source. Generally speaking, the statistics were not severely affected by this, so 257 line-depth-ratios could then be used to determine the effective temperature independently.

With the new lines having been measured, the distributions in terms of effective temperature were recomputed for all spectra. It could be seen that the comparison between the latest data and the oldest ones was not much different from the graphs shown previously. This became evident from the plots that were created.

For the new lines, some further validation checks were performed. Concerning the standard deviations, one may distinguish three different and independent factors. First, there is the choice of the ARES parameters that determine the EWs that are used for obtaining the temperatures. The second factor is the choice of the sigma clipping and temperature exclusion procedure/rules, represented by the width of the intervals within which calibrations are kept. The number of calibrations also plays an important role.

Going from 3 to 0 sigma in the temperature exclusion, the same trend of removed outliers could be seen with the new calibrations, so that the conclusions reached previously were also applicable here. The figures created there were similar in appearance to figures 5.1-5.3 and are therefore not displayed below. The other two factors will be exemplarily shown in figure 5.4 for the HARPS sample, but of course the statements made are valid for UVES and FEROS as well.

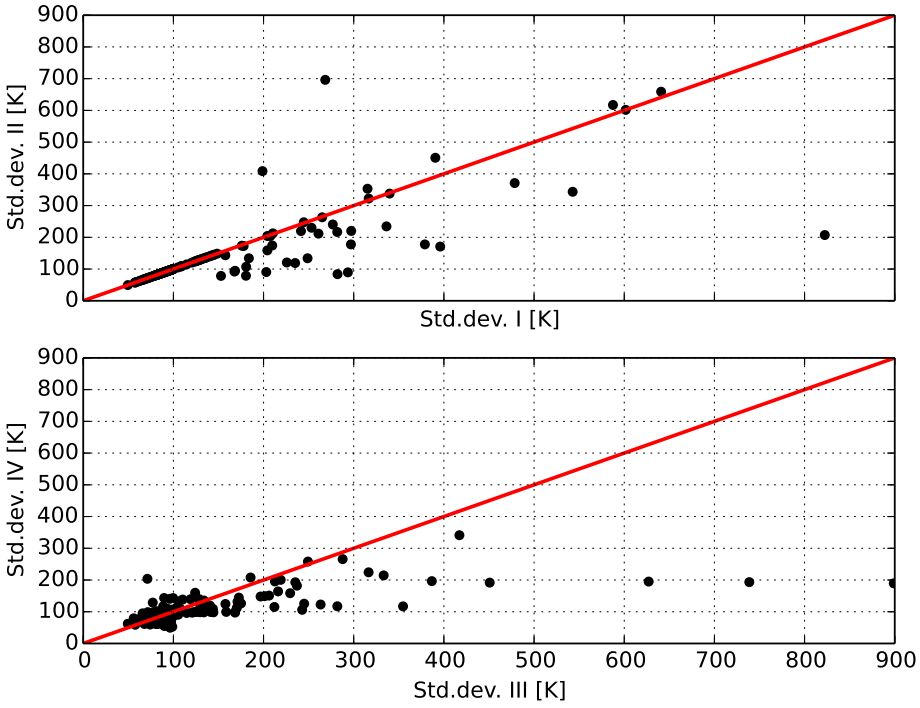

Figure 5.4: Top panel: comparison of standard deviations of KOV1 calibrations for HARPS spectra after (Std. dev. I) respectively before (Std. dev. II) refining the ARES parameters. Please note that ARES parameters were changed only for exposures with $\sigma >= 150$ K. Only a mean sigma clipping had been applied to get the temperatures (no temperature exclusion). Bottom panel: comparison of standard deviations between KOV1 (Std. dev III) and all Kovtyukh (Std. dev IV) calibrations for HARPS spectra. A median sigma clipping had been performed together with a median +/- 3σ temperature exclusion.

As can be seen, refining the ARES parameters indeed reduced the standard deviation for many spectra. This effect was a bit weaker in case of FEROS and UVES, but present there as well. The inclusion of further lines improved the statistical power of the LDR approach and, as described, gave rise to a newly accessible temperature regime. Standard deviations were once more decreased, especially for spectra with high values in the former analysis.

The fact that the new standard deviations were not much smaller than before, in some cases even a bit higher, could indicate that the physically intrinsic lower limit (due to the dispersion contributions from the spectra and thus the line ratios themselves, and from the fit) was relatively close.

5.2.4 Phase Dependency

It is worth saying at this point that high standard deviations are not automatically linked to problems in the line-depth measurements. First of all, ARES sometimes does not detect a line, even when it is actually present in the spectrum, therefore impairing the statistical foundation for any effective temperature arguments. More importantly though, spectra of stars in the rising phase of their pulsation cycle (i.e. when their effective temperature is increasing) present themselves with intrinsically higher dispersions due to the star's variable nature (they are thus fixed by the physical structure). This could be checked only for the spectra with multiple measurements. At that point in the analysis only HARPS had sufficiently good phase coverage for its spectra, since in particular all of the UVES TS spectra downloaded from the ESO archive were taken at the same phase.

The phase points were calculated by using the Modified Julian Date (MJD) of the spectra, which had been extracted from the header of the respective fits files. From this the Heliocentric Julian Date (HJD) was computed by adding 2400000.5. Additionally, the period of the target was used. This period was taken from the *astro toronto catalogue* [74][75]. If not found, I used the *General Catalogue of Variable Stars* (GCVS) [76][77] or the FEROS base table. As a reference point an HJD of 0.0 was chosen, for the epoch of maximum or any other notable phase in the pulsation cycle of the targets was not known (the papers by Groenewegen (2008a, [78]) and Storm (2011, [79]) were checked but did not contain that info). This, of course, only amounted to a shift of the x-axis, but did not affect in any way the shape of any phase-dependent curves. Examples for HARPS effective temperature and radial velocity curves are given in figure 5.5. Please note that no errors are given for the radial velocity on that plot.

It can be seen from the plots that Y Sgr and ζ Gem had a very well-defined sinusoidal, asymmetric phase behaviour, both in radial velocity and in effective temperature. X Sgr, being a binary star, did not show these clear trends. Otherwise, standard deviations were typically relatively small and the temperature curves followed mostly the usual pattern. With the exception of X Sgr for all HARPS objects the effective temperature curves were well-shaped.

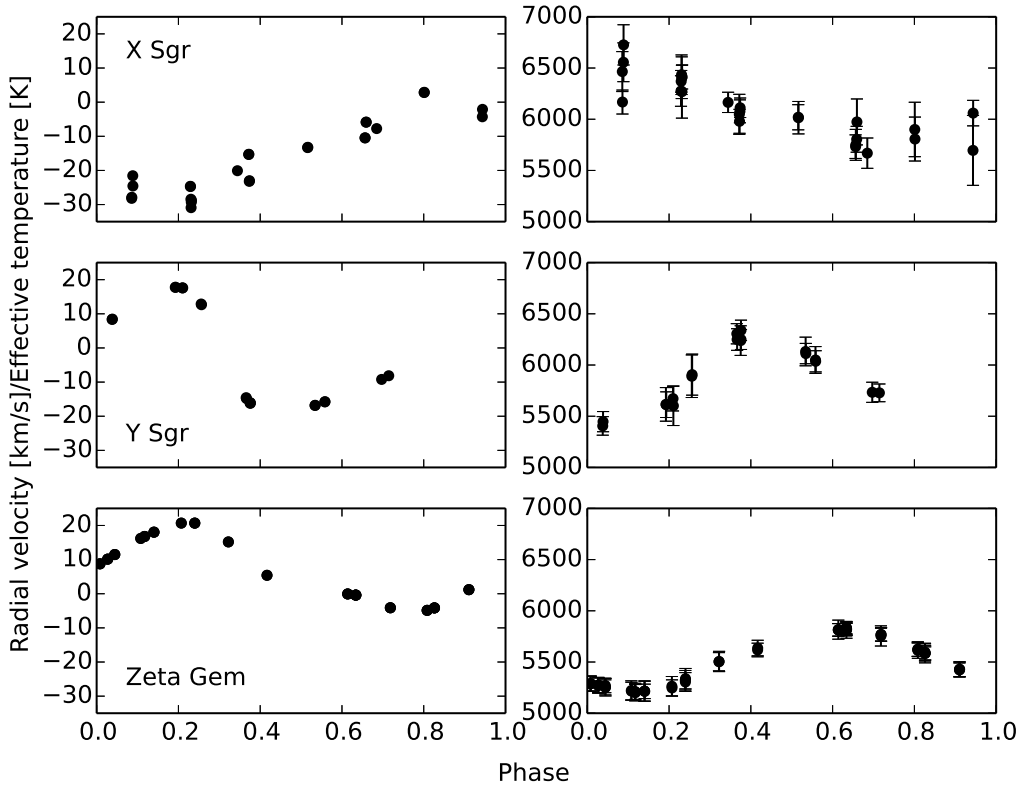

Figure 5.5: Phase dependence of radial velocity and temperature for X Sgr (top panels), Y Sgr (middle panels) and ζ Gem (bottom panels). A relatively high spread in the derived temperatures is apparent for X Sgr, while Y Sgr displays a moderate dispersion. Overall, ζ Gem has very small standard deviations.

5.3 Results

Using the line-depth-ratio approach the effective temperatures could be estimated for all spectra or spectral parts that had reached the current phase in the thesis, i.e. 50 UVES TS spectral parts, 120 UVES Genovali spectra, 9 UVES Kovtyukh spectra and 154 UVES Inno spectra, 398 HARPS spectral parts and 355 FEROS spectra (this means that $T_{\rm eff}$ was not obtained for the 131 FEROS TS and 2 FEROS Kovtyukh spectra that had not been reduced). Most of the effective temperatures were accepted (considering still the S/N of the spectra and the sigma of $T_{\rm eff}$) and therefore used for the metallicity determination. Their exact values can be found in sect. 6.4.

In order to validate the obtained effective temperatures, comparisons with independent temperature scales are necessary. Such determinations are provided e.g. through spectral synthesis [80], interferometry [81] or the Baade-Wesselink method [82][83]. For several of the Genovali spectra, effective temperatures were estimated by M. Urbaneja on the basis of a treatment without the assumption of local thermodynamic equilibrium (a non-LTE approach), intrinsically underlying the method followed in this study. However, a detailed comparison cannot be given here, since it requires detailed knowledge about the differences of the physical assumptions adopted in the two different approaches.

Chapter 6

Metallicity Determination

6.1 Overview

Having gone through the previous steps, the metallicity and other parameters could finally be determined. *MOOG*, a sophisticated code for yielding such results, made use of the already calculated equivalent widths as well as atmospheric models for the targets of interest. A self-written complex wrapper surrounding this program allowed the treatment of the spectra analyzed so far in an automated way, consisting of several steps. The atmospheric models, spanning a multi-dimensional parameter space, were interpolated so that a sufficiently fine grid of files could be constructed. Based on this grid, the spectra underwent a series of multiple iterations. Using this approach, essential stellar parameters such as gravity or microturbulence velocity and of course the metallicity could be retrieved at the end.

Please note that there are already several available projects having a similar scope and setup. Among the most notable ones I want to mention FAMA (Fast Automatic Moog Analysis, [84]) by L. Magrini and StePar [85][86] by H. Tabernero. I noticed the existence of these sophisticated tools when my wrapper was already in a very late phase and therefore did not make use of them.

Of course, the routine proposed here works for a manual analysis of a single spectrum as well. Owing to the huge number of spectra and a lot of iterations that had to be performed, however, automation techniques were inevitable, as should become clear in the following paragraphs. The whole source code of this automatized approach can be electronically received from the author.

6.2 Method

6.2.1 Initial Steps

In order to determine the main quantities of interest, a dedicated program called *MOOG* [87] was downloaded. Its installation required further codes, *X11* and *SuperMongo*. Apart from this, it is else a stand-alone routine.

Necessary input files included a file containing spectroscopic line parameters such as wavelength, a number identifying the atom or molecule, from which the line has been formed, the excitation potential and log(gf) values of the feature, and the equivalent width. The error on the equivalent width can be given as well but is not used by the program.

The ARES equivalent width results already contained part of this information, the remaining data were extracted by matching the wavelengths of the lines with the linelist showing those quantities. In this way, the data were prepared, i.e. converted to a MOOG-readable format.

The other main input consisted of an atmospheric model, i.e a theoretical description of how the spectrum respectively the shape of the lines that were measured had changed from the location where it had been formed due to the path of the light through the star's atmosphere. Various models exist on the internet, among others *Kurucz* [88] with its extensions by *Castelli* [89][90] and *MARCS* [91][92], both of them including a complex opacity treatment.

Initially, for this thesis the choice fell on MARCS. Searching this database which comprises $\sim$ 52000 models, different parameters can be set, among them the chemical composition. Different choices are being offered, e.g. standard composition, i.e. where the ratios in the abundances of different elements follow closely those of the Sun, or alpha-enhanced/negative, meaning that the fraction of alpha-elements is increased/diminished w.r.t. solar values.

Another option concerns the geometry of the atmosphere. While plane-parallel works reasonably well for dwarf or main sequence stars, giants and thus also Cepheids require a spherical description. Next, ranges for the effective temperature, the gravity (log g), the metallicity ([Fe/H]), the microturbulence velocity v_t and the mass can be given. The MARCS database allows values for these quantities between [2500, 8000] K, [-0.5, 5.5] dex, [-5.0, 1.0] dex, [1, 5] km/s, [0.5, 15] $M_\odot$, with regime-dependent respective resolutions and specific further constraints set by the chemical composition and the geometry.

It was checked which regime in effective temperature was covered by the different objects to be studied. The gravity range was set by the typical values expected for Cepheids. Metallicity data from Genovali (2014, [10]) for several pulsators helped setting the appropriate interval, into which my targets were assumed to fall. The maximal range was chosen for v_t, while the mass was again based on common Cepheid values (4 - 10 $M_\odot$). All ranges were extended to the next closest points (steps) in the MARCS set. All in all, 130 models were downloaded for the following intervals/values, all for a scaled solar composition and spherical geometry:

- T_{eff} [K] = [4000, 7000], resolution 1000
- log(g) [dex] = [-0.5, 2.0], resolution 0.5
- [Fe/H] [dex] = [-0.75, 0.75], resolution 0.25
- v_t [m/s] = [1, 2, 5]
- M [$M_\odot$] = 5

6.2.2 Interpolation of Atmospheric Models

The ranges that were then covered by the models themselves were identical to the ones above, with one exception, the gravity:

- log(g) [dex] = [0.0, 2.0], resolution 1.0

There were 11 parameters describing each of the downloaded models, namely T_{eff}, log(g), M, v_t, and finally z, a, c, n, o, r, s, the abundances of iron respectively of alpha-elements, carbon, nitrogen, oxygen, r- and s-elements w.r.t. iron. Since the chosen chemical composition coupled the last six to iron and there was only a single value for the mass, 4 parameters remained free.

The resolutions of the different quantities were apparently much too large to allow scientific statements with high accuracy. Due to this coarse sampling of the models, an interpolation of these data points to smaller intervals became necessary. Directly on the MARCS webpage a tool written by T. Masseron that provides this function is offered [93][94]. It is capable of interpolating three quantities at once.

Fortunately, MOOG can calculate a new microturbulence velocity internally in the program, so that v_t is removed from the free parameters as well. Since typical microturbulence parameters lie between 3 and 4 km/s for most Cepheids (see Genovali (2014, [10])), both 2 and 5 km/s were equally close to the range and the former value was fixed for simplicity. The natural representation of the space, in which the remaining quantities lived, became a cube. This cube consisted of the different combinations of temperature, gravity and metallicity, i.e. there were 4 * 3 * 7 = 84 grid points.

It should be stated here, that besides the coarseness of the grid, there is another problem, holes, i.e. grid points where no model exists. Holes that lie fully inside the cube, even when extended, are not problematic, since they can be filled via interpolation, whereas those at the borders or corners cannot be recovered by any means. For this study 59 models with the correct mass and v_t were present.

In order to conduct the interpolation, 8 models have to be given to the routine, forming the 8 corner points of a cuboid, in which the desired interpolated model should lie. All of these grid points are then used for the interpolation process. It should be clear, that the closer the corner points are to the desired values, the more accurate the interpolation will be. Also the strict geometry of the routine intrinsically creates a cuboid-like substructure, as will be seen later.

The output contains a subsample of the columns from the input files (optical depth, temperature, electron as well as gas pressure and a linear density). If some identical corner points are given, the program can also do 2D- or 1D-interpolations. Using the same model as input eight times, the program even performs a kind of "0D-interpolation" on a point that is already in the grid (a so-called *pivot*). Despite this unusual terminology and unorthodox use of the interpolator, the model is reasonably converted into a format identical to that of actual interpolations. In order to check the validity of the interpolation, a 3D cuboid around a pivot was used to interpolate a model that had the same parameters as the pivot. Furthermore, in a second check, a 0D "cuboid", i.e the pivot itself, was used to "interpolate" to the same point. The results are shown in figures 6.1 and 6.2 for the temperature structure.

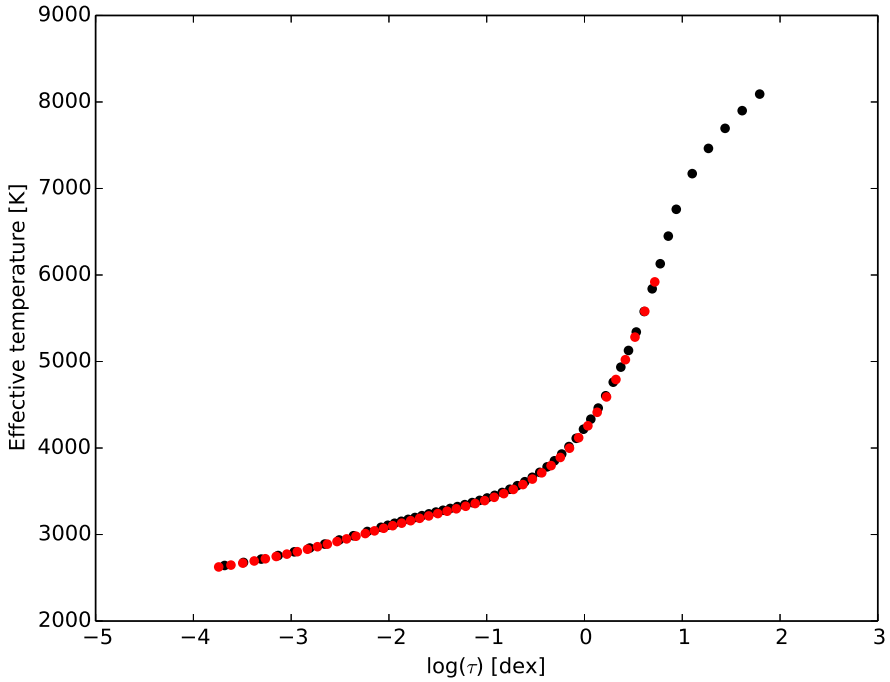

Figure 6.1: Temperature structure (effective temperature vs. optical depth) for an atmosphere created by 3D-interpolation of a test model. The red and points show the interpolated and original atmospheres, respectively.

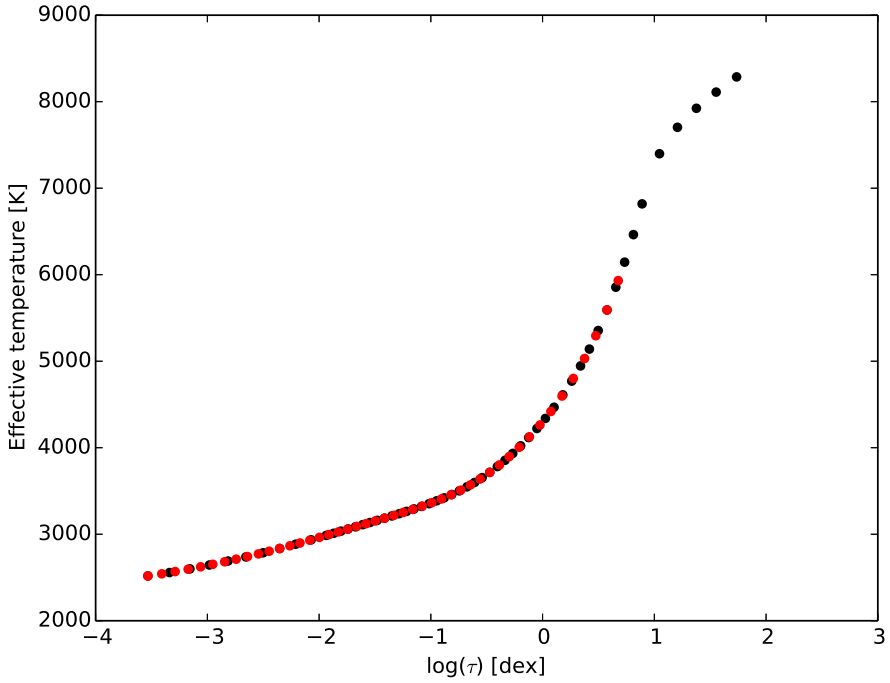

Figure 6.2: Same as figure 6.1 for an atmosphere created by 0D/self-"interpolation" of another test model.

The plots demonstrate clearly that both a 3D and a 0D interpolation are reliably performed and that the interpolation routine works as expected. Naturally, checks for the other quantities in the interpolated models were performed as well, confirming this statement.

At first, I tried to perform interpolations only one-dimensionally, i.e. by interpolating one parameter at a time. In order to reach points on the inside of the cube, this would have to be done repeatedly and would have required interpolating files that themselves had been created from interpolating others.

However, it was found that the interpolation routine was not capable of recognizing the format of its own output files as input, thus excluding this possibility and making 3D interpolation for arbitrary grid points inside the cube inevitable. As has been mentioned above, the best way to do this is to select pivots as close to the desired point as possible, thus achieving the most precise results. Geometrically speaking, the task is to find the cuboid with the smallest volume whose 8 (pivot) corner points are present among the set of models and which surrounds the model that has to be calculated.

After several different attempts, a brute-force technique seemed most appropriate for dealing with this situation. By its nature, the cuboid structure is compatible with the use of for-loops over the different quantities, programming-wise. Consequently, all different 1D intervals that included the output model each for T_{eff}, log(g) and [Fe/H] were put together in every possible combination. Then it could be checked whether the models had been downloaded. Among the possible cuboids that had been recorded the one with the smallest volume was selected and interpolation was performed using the pivots belonging to it.

It is important at this point to mention that the terms *cuboid* and *volume* should be regarded in the context of N-dimensional spaces. Since the models that should be interpolated can lie as well inside the cube, on a plane where only e.g. temperature and gravity would not be among the values covered by all pivots, or similarly on a line, in such cases 2D or 1D interpolations are preferable, as the degree of freedom is reduced. The 2D/1D analogues of the upper expressions are of course *rectangle* and *area* respectively *interval* and *length*. As evaluated previously even interpolations of pivots to themselves are allowed. Hence, in case of multiple dimensions, the N-cuboid with the smallest N-volume was chosen among the ones with the lowest-dimensional geometry.

As interpolation step sizes for T_{eff}, log(g) and metallicity, 100 K respectively 0.1 dex respectively 0.05 dex, were initially used. Together with a refinement of the original grid by the factors 10, 10 and 5 respectively, this brought the number of potential output models up to 31 * 21 * 31 = 20181. Despite the interpolation itself being the bottleneck of the code in terms of computation time, T. Masseron's routine was extremely fast and could create all possible atmosphere models within $\sim$ 6 min. Bearing the holes in mind, the 10381 models that were calculated are visualized in figures 6.3 and 6.4. Please note that later the temperature step size was changed to 50 K, in order to further improve the temperature resolution.

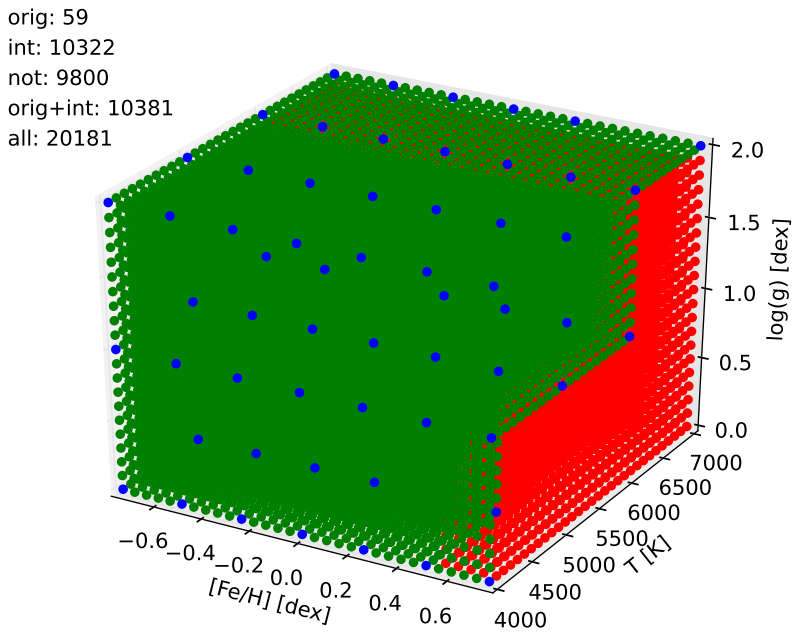

Figure 6.3: Interpolated grid for the MARCS models. Pivots are marked in blue, interpolated models (excluding pivots) in green, holes in red.

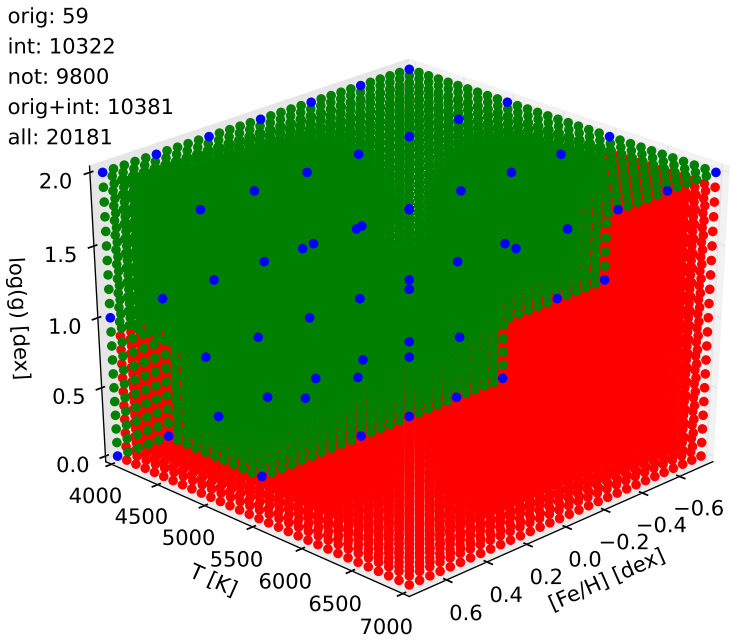

Figure 6.4: Same as figure 6.3 under an azimuth viewing angle of 45°.

The semi-transparent *Python* plot allows a look through the outermost layers of models on the border faces of the cuboid and a look at the inner composition. As explained previously, cuboid- or stair-like substructures are clearly visible. All models that could potentially be interpolated were, in fact, computed: Points strictly inside green cuboids are all automatically present since they have the same pivot origin as others. The main limitation of the grid responsible for the non-interpolatable models are the combinations of high temperature and low gravity. Blue loop stars (such as Cepheids) constitute the only exception in the Hertzsprung-Russell-diagram where such a configuration is physically realized, although only some of them fall into that regime.

Specific interest has been given to the question whether at the fixed mass, these holes could be filled by extending the grid in either direction of temperature, gravity or metallicity. However, since there are no models with log(g) < 0.0 dex at M = 5 $M_{\odot}$, gravity can be excluded here. Furthermore, as expected, beyond 7000 K, only gravities bigger than 2.0 dex are covered. Last but not least, the grid points with metallicity beyond 0.75 dex provide only a perfect continuation of the stairs that had been seen so far without adding pivots in the critical area, whereas those with [Fe/H] < -0.75 dex, temperatures in the interval [4000, 7000] K and gravities within [-0.5, 2.0] dex do not yield relevant models, either.

In the 45°-azimuth plot a small red cuboid is visible "inside" one of the stairs. This is due to the model with z = 0.75, log(g) = 0.0 and $T_{\rm eff}$ = 5000 K being absent at v_t = 2 km/s. There is no atmosphere with z = 1.0 and identical other parameters, either. Additionally, there are also 3 further, single and not interpolation-critical holes visible. The pivots of the models at v_t = 5 km/s, however, include all of the aforementioned missing points, while they have only one non-critical hole. Hence, the values in the respective intervals around the holes are slightly more reliable since the interpolation cuboid is smaller.

Another possible approach is to interpolate between models with different v_t, but it is unclear whether the automatic script would allow such an interpolation and furthermore for reasons of homogeneity it is preferable not to mix different models. Since the typical value for Cepheids (between 3-4 km/s) is equally far away from 2 and 5, we could also choose the latter directly and thus improve the grid coverage.

6.2.3 Parameter and Input Control

For iterative methods initial values need to be defined, of course. The objects given in Genovali (2014, [10] and 2015, [29]) cover a major part of the ones used here. For each target as a starting metallicity the value presented in that paper (literature results or author estimates) may be taken, thanks to this overlap. The effective temperature can be retrieved from the values yielded by the previous analysis. In case that no data are present for a specific spectral part (e.g. blue arm of UVES) - reasons could be too small common wavelength regions with the linelists etc. - the temperature from the other region (e.g. red arm) may be used instead. The objects without temperature or metallicity estimates force adopting arbitrary initial values such as e.g. 5500 K respectively 0.0 dex. Their counterpart for gravity is 1.0 dex, used for all spectra, similarly 2 km/s for v_t.

Every time these initial values are defined or whenever reference values are modified via iterations, the corresponding atmospheric model needs to be given as input for MOOG. Analogously, at the beginning of the metallicity determination, the equivalent width file is specified so that the routine knows from where to take these values. Next a configuration file is written where several MOOG input parameters are stored. An example is given below:

```
abfind
terminal          'X11'
standard_out      '../output/standard.dat'
summary_out       '../output/summary.dat'
model_in          '../input/atm/tempmodel.MOOG'
lines_in          '../input/obs/tempmoogfile.dat'
atmosphere        1
molecules         2
lines             1
freeform          1
flux/int          0
damping           1
plot              3
```

The task that the code should perform is defined by the so-called driver, *abfind*. It tells the program to perform a standard metallicity analysis. There are many other possibilities as well, though. *Terminal*, as the name suggests, sets the terminal environment that is to be used, whereas *standard_out* and *summary_out* regulate output filenames. Their input counterparts are given via *model_in* (atmospheric model) respectively *lines_in* (equivalent width file). The level of detail for atmospheric output info is contained in *atmosphere.Molecules* decides whether molecular equilibrium calculations will be performed and *lines* is responsible for the amount of output data concerning the various lines. Flexible input formats for the EW file can be read by the routine if *freeform* is set appropriately. Moreover flux or intensity calculations can be switched using *flux/int* while *damping* changes of course the way line damping processes are treated in the program. Plotting options can be given by means of *plot*. The above parameters orient themselves on the examples given in the MOOG manual [95].

With these configurations done, the program can be run. During that process several diagnostic graphs are shown. They are used to find the correct stellar parameters for the respective spectrum (see sect. 6.2.5). When those are displayed, the user may also set a different microturbulence velocity inside the code, which is then adopted and the abundances are recalculated using that value. What is more, MOOG in general asks the user several times during a run to provide answers to its questions, whether, for instance, output should be shown on the terminal or whether further elements among those from the equivalent width file should be treated.

However, in an automated approach clearly this input has to be given by the computer itself as well. A terminal command called *expect*, based on the *Tool Command Language* (TCL), which has a C-like syntax, was used. This task enables interaction between various scripts where otherwise manual input would be required. In this case, the user, pressing keyboard buttons is replaced as a dialogue counterpart for the abundance routine and the computer reacts to text output answering MOOG's questions accordingly.

It should be noted that adapting v_t is impossible when the plot option is deactivated in the parameter file. Due to the plotting procedures being forced, the diagrams are shown in a single program run, but they are always displayed in the foreground, which makes working on the respective device very difficult. As a matter of fact, solely the command calls responsible for showing the images were disabled directly in the source code of the routine. Once a single run is finished, the code prints out a list of the lines that have been used together with the individual abundance of the respective element yielded by the calculations as well as average values, uncertainties and a few other potentially useful quantities.

6.2.4 Line Clippings

Before the iterative refinement of the various stellar parameters can start, specific steps have to be followed for each spectrum. First all lines from the original equivalent width file are read and those above a set threshold are removed. This limit was set to 120 and 180 mÅ for Fe I and Fe II respectively, following the suggestions given in the paper of Genovali (2014, [10]). This EW-clipping is done in order to prevent the use of saturated lines whose derived abundances are not reliable. The relatively small number of Fe II lines in the linelist (45) compared to the Fe I ones (570) made it necessary to slightly loosen the criterion for saturated lines, but the lines were still in a safe regime, where the so-called curve of growth (the diagram of line abundances vs. reduced width) was still linear.

With the smaller EW file, the closest model to the initial stellar parameters was taken and Moog was run once with this configuration so that the abundances of the different lines were retrieved. Using a sigma-clipping (median +/- 2 sigma) to separate outliers from the bulk of the abundances, further lines were removed from the set of Fe I/Fe II lines. It should be noted that typically this sigma-clipping excluded only a small number of lines. The major fraction had been discarded in the former EW-clipping.

Under the assumption that the initial parameters are actually already the true values for that star, the definition of outliers makes sense. Since, however, some certainty is present only about the LDR-derived temperature and the metallicity, but not about the surface gravity or the microturbulence, the abundance distribution may be different and the sigma-clipping could remove points that are actually centrally amidst the abundances for the correct configuration of stellar parameters. On the other hand, in the course of several test runs it was found that the temperature had the strongest influence on the abundances, so that even being at a greater distance from the actual log(g) and v_t of the star - supposing the effect of those parameters being sufficiently small - the proposed clipping was justified. Repeated runs using the final output of the automatic routine as the new input parameters could help approach the correct values in an iterative way even in case the sigma clipping cut the "wrong" points due to wrong initial parameters, as long as the disturbance introduced was small enough.

6.2.5 Optimizing Stellar Parameters

The spectrum then had to undergo a certain procedure for finding the correct metallicity. Since the atmospheric models also had the effective temperature, the gravity and the micro-turbulence as parameters and all of them influenced the abundances yielded by MOOG as

well, they all needed to be at their correct values in order to retrieve the actual iron content of the star.

It could be seen from some test runs later and the results of Genovali that the parameters were not independent from each other in terms of their effects on the output metallicity. Especially T_{eff} and log(g) showed a strong coupling, so that different solutions (combinations of these parameters) could have led to the same abundances, whereas the microturbulence seemed to be relatively unaffected by the two former quantities. Despite the coupling of the variables, the sets of changes of their values to find the correct configuration (the so-called optimizations) were performed one-dimensionally, with alternating quantities in each of them.

The *effective temperature* can be found by means of the excitation potential of the lines in combination with the respective abundance. When plotting these against each other, the slope of a linear fit should be small, so that the straight line gets as flat as possible. Physically this means, that independent of the excitation potential of the lines, the abundance is constant. On the other hand, if a wrong temperature is given, the populations of the different atomic levels from which the lines originate, set principally by the Boltzmann and Saha equations with an inverse exponential temperature behaviour, will be such that different abundance contributions will be required as compensation to explain the measured equivalent widths. By demanding the metallicity to be constant across all lines, as is the case in the star, the part of the line shapes that comes from the chemical composition is accounted for and the temperature giving that metallicity is then the one closest to the correct one, considering the current set of parameters. Since the Fe I lines were statistically many more than the Fe II ones, abundances of the former species were used for the determination of the effective temperature.

To determine the *gravity* of the object, it was necessary to consider the abundances of Fe I and Fe II. The higher the surface gravity, the more often collisions of electrons and ions occur, leading to recombination to Fe I. The larger the value of log(g), the larger the abundance of Fe I. Only when the abundances yielded by MOOG were (almost) equal (i.e. ionization equilibrium has been reached), the correct gravity could be found.

The *microturbulence* could be estimated on the basis of the slope of Fe I abundance vs. the reduced width (RW). The latter quantity can be computed from the EW by dividing it through the wavelength of the line. Microturbulence provides a broadening contribution to the spectroscopic lines. Naturally, the EW and through it the reduced width becomes larger with higher velocities. Similarly, as in the case of temperature, the slope of metallicity vs. RW should get as small as possible, meaning that independent of the width of different lines, the iron content is a constant.

The optimizations of these parameters occur in a certain linear order of log(g), v_t and T_{eff} and are performed by looping at constant other parameters over the quantity of interest and then determining by means of a fit the minimum slope or iron abundance difference. As could be seen later, leaving the temperature as a variable parameter causes instability in the program due to degenerate solutions. Since, however, the temperatures derived from the line-depth-ratios are solid, they may be set constant, with only log(g) and v_t varying.

The model inside the grid closest to the (current) reference values was taken, and the next parameter was optimized. Once all parameters had been modified, a new iteration began, until at one point the difference in (Fe I) abundance between two consecutive loops became

smaller than a user-defined threshold, 0.05 in this case, or until a certain upper limit for the number of loops was reached. The metallicity that had been retrieved was set as a new input parameter for the atmospheric models and the inner loop was started anew.

In case that the triplet of effective temperature, surface gravity and microturbulence of the latest iteration was identical to that of the previous cycle and if the output abundance equaled the reference (input) metallicity for the current run, convergence was achieved and all loops could be stopped at that point. Similarly, if for some reason a configuration appeared even earlier in the sequence of MOOG runs, the program quitted analyzing the current spectrum since the optimizations fell into a loop pattern.

Note that such jumps/sequences most prominently occur as a consequence of the discrete grid: Since we cannot reach an infinitely fine sampling of models, the fitting processes could principally under-/overshoot e.g. in temperature in case the actual stellar parameters are close to the average of two adjacent grid points (assume as an example models at 6000 and 6050 K and a true value around 6025 K). Because of the coupling of the different quantities, a change in T_{eff} can cause another change in log(g) in the subsequent optimization loop, which can again lead to a different temperature minimum.

In such a case the minimum and maximum values (the range) of effective temperature, surface gravity, velocity and metallicity were given as output to indicate the space within which these quantities varied, since no statement can be made about the precise configuration. A three-dimensional fitting where all parameters are varied at the same time could possibly prevent cause-effect chains like the one described for the "linearized" optimizations, but probably may still lead to loop patterns in case that the minimum is only defined weakly and cannot avoid single-parameter under- and overshooting.

6.3 Problems

During the course of all tests and MOOG runs, a few major problems were encountered. A description of what their effects were and how they could be solved respectively avoided is given in this section.

6.3.1 MOOG Compilation Bug

By coincidence, it was found that in a test spectrum, MOOG gave two different sets of output abundances when using the same atmospheric model, EW file, microturbulence velocity and even identical MOOG versions on different computers. Runs on the two devices were performed manually to ensure independence from automatic scripts/wrappers like the one presented in the thesis at hand. When the error was first discovered, the atmospheric model that had been used was part of the optimization sequences, but not necessarily giving the true stellar parameters for that star. Specifically the abundances that I had retrieved from MOOG were significantly higher than those obtained by R. da Silva, M. Fabrizio, D. Magurno (researchers in the group of Prof. Bono) and Prof. C. Sneden, the author of MOOG. Apparently, this affected only the broad lines (see figure 6.5).

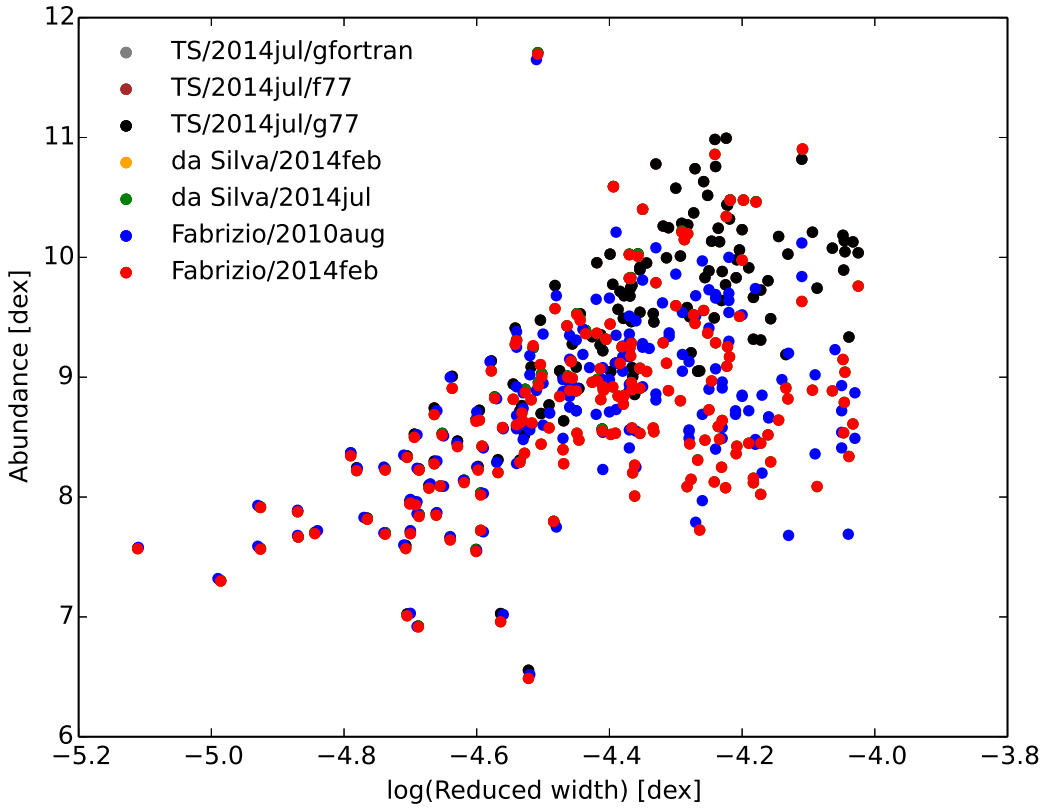

Figure 6.5: MOOG output abundances as a function of log(reduced width) for identical input obtained on different machines by me (TS), R. da Silva and M. Fabrizio. The MOOG versions that were used are indicated. In case of TS additional compiler info is given as well (see text). Effectively there are 3 sets of points that can properly be distinguished (TS, reference values (MOOG 2010), reference values (MOOG 2014).

Around a certain, maybe sharp, value of log(RW) the two sets of data points begin to deviate from each other when looking at lines broader than that limit. The numbers obtained on my device, other than being generally larger, presented also a smaller spread. Different MOOG versions were also tried to check their effect on the numbers yielded by the program. Indeed, between the versions of August 2010 and July 2014 noticeable abundance differences were found while the February and July 2014 ones were almost indistinguishable. It was checked furthermore that the results did not change when using different FORTRAN compilers for the MOOG setup files or library paths in the installation makefiles. By chance, after having installed a virtual machine and MOOG freshly on the OS there, my results all of a sudden agreed with those of the other researchers.

In the end it was found that I had not specified the folder of the MOOG files in the compilation path, but a folder higher in the file structure. Most interestingly the compilation worked, nonetheless, but clearly some files were either not considered or certain calculations skipped, in any case not performed correctly. The bug was reproducible by switching between different folder paths and together with some other small suggestions was reported to C. Sneden, who agreed on its relevance for MOOG working in the expected way.

6.3.2 MARCS Abundance Discontinuities

Several info plots created by my wrapper revealed that in the (linear) fits of log(g) and T_{eff} some data points were slightly different from the others (which followed a straight line very well). Those points formed small straight segments that seemed practically offset from the rest by a shift. However, this offset was small enough so that the fits still reasonably reproduced the data and was thus ignored at first.

This was a mistake in as far as when running the optimization code with different test spectra, it appeared that the fits would not get stable. Therefore no solid output values for the effective temperature, surface gravity or microturbulence velocity and hence neither for the metallicity could be obtained. It was found that while the above fits were not noticeably affected by the shifts, the abundances were. In terms of log(g) or T_{eff}, the iron content (both in Fe I and Fe II) showed severe, abrupt discontinuities. An example of this is given in figure 6.6.

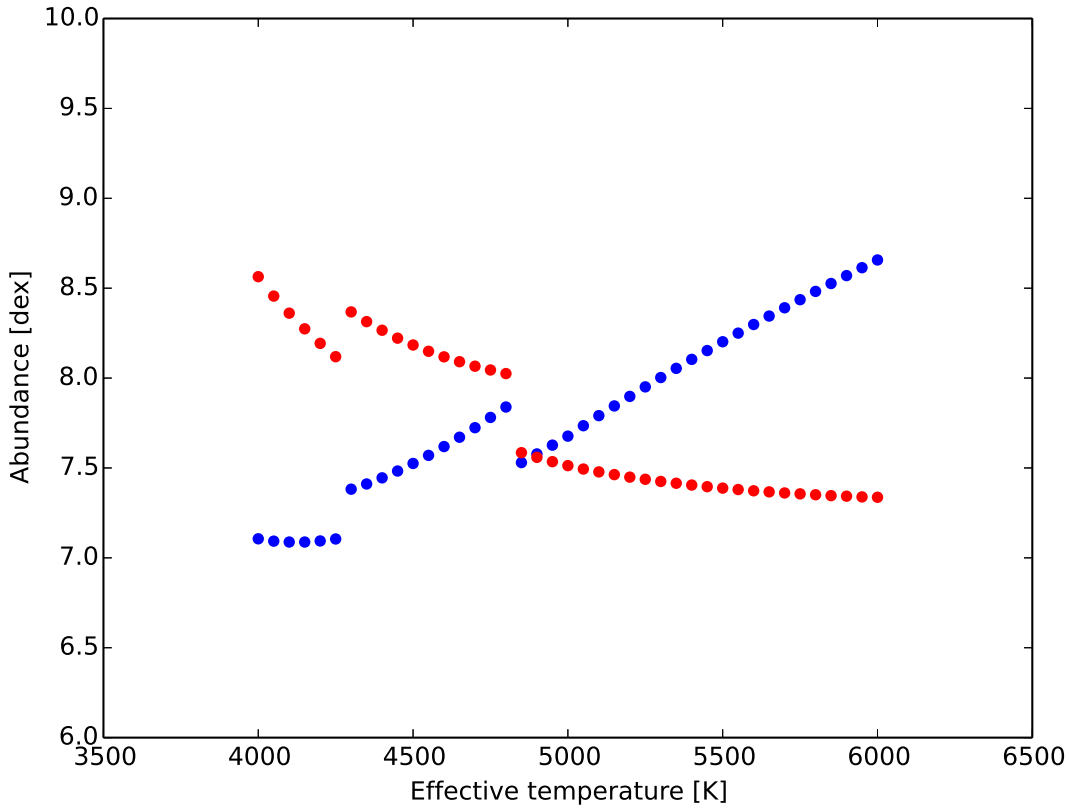

Figure 6.6: MOOG output abundances as a function of effective temperature at log(g) = 1.0, [Fe/H] = 0.25 for a test spectrum. Clear discontinuities are visible between 4000 and 5000 K. The blue points indicate Fe I, the red ones Fe II.

The discontinuities unfortunately occurred independent of the input EW file used and at different positions in the parameter space. It should be noted that the size of the jumps became bigger at larger effective temperatures (for the surface gravity there was no obvious trend)

and that the discontinuity positions were at larger temperatures when the input metallicity was smaller. It was checked that the jumps were indeed discontinuities by increasing the resolution to a finer grid around the critical regions by a factor of 5. This showed again a similar picture, eliminating the possibility of a smooth transition in the curve on smaller scales. Jumps did not occur at every parameter combination, but for most of them. Although it might have been possible to detect the jumps based on plots like the above one, the effort of doing this for a large number of input files would have been immense. Also the discontinuity region might have included the correct stellar parameters like in the test case where the true effective temperature on the basis of the LDR measurements was around 4750 K.

The reason as to why these gaps were present has not been found yet. It is obvious that the results cannot be trusted, as long as there is no way of examining the nature of the problem and subsequently resolving it. The equivalent widths cannot be responsible since when comparing my EWs to those of R. da Silva, the points were quite close to the 1:1-line (i.e. the identity line), with different size of scattering (this was confirmed by both the average and the median values). For the test spectrum, the structure of the input MARCS models was studied by plotting the dependent model quantities such as $T_{\rm eff}$, the electron and the gas pressure as well as the linear density against the independent one, i.e. the optical depth. The models revealed a seemingly smooth appearance, both for a single curve but also between different models. It was checked specifically that also the interpolated models did not produce any artificial artifacts or jumps.

Another test was performed by using the script *readmarcs.f* offered on the MARCS website with which it is possible to extract different columns from the original models. Small modifications enabled me to get the same data as that used in interpolated models, so that, by adding the header and footer lines of their self-interpolated counterparts, MOOG could be tricked into using the original models directly. This was made necessary by the fact that the program was incapable of processing pivot models due to a different format which was not properly recognized. Using this test I could verify that the "interpolation" also of the original models to themselves once again was reasonable and that hence discontinuities, if they were due to the model structure, were already present in the pivots. Note that this neither excludes the possibility that the MARCS models were flawless and that the jumps arose solely from MOOG, nor that exclusively the models were responsible for the observed behaviour. Most probably, however, the problem came up from the usage of MARCS models in combination with MOOG.

R. da Silva, using his own interpolated models and MOOG installation together with my test EW files could independently reproduce the MARCS discontinuities and hence confirmed the problem. C. Sneden, the author of MOOG, was once more contacted, but has currently not responded yet. On the basis of this work, users of the program are advised to carefully double-check each step when dealing with blue loop stars.

The solution to this problem was to switch to other atmospheric models. Therefore the Kurucz models were used from then on. The original, old Kurucz models offer a grid in parameter space for different temperatures and surface gravities at various metallicities, i.e. slices in the iron abundance [88]. Additionally, F. Castelli offers newer models for a part of the metallicities, based on the latest opacity distribution functions (ODFs) [89][90], on her website. According to her, the differences to the former ones should be relatively small in most cases, but at some $T_{\rm eff}$, the new atmospheres give more reliable results.

Unfortunately, the grids offered have a relatively low resolution in both cases, so that interpolation is inevitable. While a program to compute Kurucz models is offered on the websites (the so-called ATLAS-9/12 code), an interpolator could not be found. From R. da Silva I got a FORTRAN-based interpolator (not written by him), capable of using the old Kurucz models for interpolation. It uses a fixed grid in parameter space. Interpolating only between the Castelli models, the interpolation cube thus had a much too small coverage. This was not the case for the Kurucz models. In the end, however, the decision was made to use the Castelli atmospheres where present and the Kurucz ones otherwise and performing the interpolation on the newly formed set of models, considering that this should effectively improve the results or at least not be worse than using only the Kurucz models.

Since the preparatory procedure is actually composed of two scripts, one for the actual interpolation and another one which transforms the format of the file (also including the possibility to change v_t, which was not used), contrary to the MARCS case here self-interpolation was not necessary and the original models could, with minor format manipulations, be passed directly to the second routine. The resulting grid showed similar or even better parameter coverage than the MARCS output cube. Let me add, that the change from MARCS to Kurucz was also accompanied by switching from a linear to a quadratic fit in T_{eff} since the new respectively better accessible regime of high temperatures (at low gravities) showed that the (decreasing) excitation potential slope vs. T_{eff} curve flattened off.

6.3.3 MOOG Wavelength Step Size Error

For certain combinations of atmospheric models, equivalent width files, and v_t, MOOG would not run properly and break down without writing any output. In such a case a message was displayed on the terminal that said: "CANNOT DECIDE ON LINE WAVELENGTH STEP SIZE FOR XXXX.XX I QUIT!". At this point XXXX.XX was a wavelength that critically blocked the program from working as usual. Although a short look was taken at the program source code of the tool, no direct info was found there and further information was not present in the manual, either. C. Sneden attributed this error to very broad lines, i.e. those with a large reduced width. However, the largest ones should not have been included anymore after the EW-clipping. So far no convincing explanation has been found for this error message. As long as the error affected only a few atmospheric models, however, the fit quality was not endangered and therefore those models were simply skipped.

While the MARCS models as mentioned above showed limitations for determining the stellar parameters and the iron abundance of the different targets, the mentioned step size error was affected only a few atmospheres for the test EW files. Kurucz models, on the other hand, were subject to this bug as well. For the majority of stars this would not be critical but at quite extreme metallicities below -0.5 or above 0.5 dex, entire slices of temperatures, gravities or microturbulence parameters would fail during program execution. Whether this is due to some actual physical restriction or simply due to the program design of MOOG is unclear and impossible to check without deassembling the source code.

It is a matter of fact that this error was the main (computational) obstacle for determining the stellar parameters, since at a few phases in the wrapper it was crucial to run MOOG for a specific parameter set, i.e. for example after fitting the minimum or even already before performing the sigma-clipping at the beginning. In case of the microturbulence having

to be optimized a non-working model might prevent changing v_t, thus impeding the entire optimization of this quantity at least in the respective iteration cycle. In some cases a certain tolerance approach was pursued by taking the next closest model and using that instead, up to two times.

However, if even this fails, the original parameter set was restored and a flag for quality control was set accordingly. Also flags describing whether the EW or the sigma clipping had worked were stored and facilitated judging the reliability of results, at least from the computational point of view. Results where e.g. the sigma clipping did not work or where (sufficiently small) jump sequences (i.e. non-convergence) of parameters appeared should principally be usable since uncertainty in the form of a standard deviation is expected to be automatically higher. Critical step size errors occurred very rarely (only in the case of KN Cen, i.e. for 2 spectra) but the results for these spectra have to be treated with due caution and are not very reliable.

6.4 Results

Finally, the results of the analysis were obtained, i.e. the effective temperature, the surface gravity, the microturbulence velocity and the iron abundance. They are presented in table 6.1 for the spectra where such a treatment was possible and sensible (for example where a sufficient number of measured line EWs was present etc.). Please note that the 2 spectra from KN Cen are excluded because of the aforementioned MOOG wavelength step size problem.

Input parameters were the LDR temperature, the Genovali metallicity for the objects (where it was available) and as formerly mentioned 1.0 dex respectively 3.5 km/s for log(g) and v_t. Please note that the output effective temperature yielded by the program was equal to the input since that parameter had been fixed, for we knew that the LDR measurements were reliable. The error given there was the standard deviation of the single T_{eff} estimates from the various calibrations.

No uncertainties are presented for the other stellar parameters, the surface gravity and the microturbulence velocity, since these quantities were as mentioned determined by the fits to the minimum. An in-depth error analysis is beyond the scope of this thesis. The diverse uncertainty contributions in the different phases from output to input are manifold and include the error on the fit itself, the error on the single output abundances given by MOOG (that cannot be properly estimated, although the standard deviation of the lines is well defined), the uncertainty (applicability) of the conceptual approach (by this I mean the sigma as well as the EW clipping, the linearization of the multi-dimensional optimization etc.), the error on the EWs themselves and the error on the original atmospheric models as well as that of the interpolation. The resolution of the grid plays a role as well, since it limits the precision with which intrinsically the input can be given to MOOG.

Many of these factors are out of reach, would require a careful examination of the respective program source codes and/or are difficult to estimate. For this reason the only statement that can be easily made is that the error on log(g) and v_t cannot be smaller than the interpolation step sizes, hence 0.1 dex and 0.1 km/s, respectively. However, we typically expect quite larger uncertainties of the order of 0.5 dex and 1 km/s, respectively. The error on the Fe I and Fe II abundance is given by the standard deviation of the single abundances.

Table 6.1: All metallicity results for the single spectra used for iron determination. The last column gives the average of the Fe I and the Fe II abundance. Please note that the datasets UVES Kovtyukh and UVES Genovali have been abbreviated and that all abundances (and their uncertainties) carry dex units.

Spectrum	Object	Dataset	Spectral part	MJD [d]	T_{eff} [K]	$\Delta(T_{eff})$ [K]	log(g) [dex]	v_t [km/s]	Fe I	Δ(Fe I)	N_{FeI}	Fe II	Δ(Fe I)	N_{FeII}	[Fe/H]
ADP.2013-09-25T22:59:21.263	ER Car	UVES TS	blue	52675.38	5604	74	1.3	3.9	-0.03	0.24	153	-0.03	0.36	13	-0.03
ADP.2013-09-25T22:59:21.263	ER Car	UVES TS	red	52675.38	5604	74	1.3	3.6	-0.01	0.20	111	0.00	0.15	13	0.00
ADP.2013-09-25T22:59:21.203	ER Car	UVES TS	blue	52675.39	5608	73	1.5	4.2	-0.04	0.25	158	-0.05	0.31	12	-0.04
ADP.2013-09-25T22:59:21.203	ER Car	UVES TS	red	52675.39	5608	73	1.0	3.1	0.03	0.20	112	0.01	0.18	13	0.02
ADP.2013-09-25T22:59:21.317	ER Car	UVES TS	blue	52675.39	5608	77	1.1	4.2	-0.03	0.25	158	-0.06	0.36	12	-0.04
ADP.2013-09-25T22:59:21.317	ER Car	UVES TS	red	52675.39	5608	77	1.2	3.5	0.00	0.22	113	-0.04	0.22	13	-0.02
ADP.2013-09-24T23:09:16.747	BF Oph	UVES TS	blue	52080.28	5528	97	1.9	4.3	-0.05	0.29	155	-0.07	0.35	14	-0.06
ADP.2013-09-24T23:09:16.747	BF Oph	UVES TS	red	52080.28	5528	97	1.2	2.9	0.10	0.21	106	0.08	0.16	15	0.09
ADP.2013-09-24T23:09:16.380	BF Oph	UVES TS	blue	52080.29	5545	87	1.8	4.0	-0.02	0.29	146	-0.04	0.40	13	-0.03
ADP.2013-09-24T23:09:16.380	BF Oph	UVES TS	red	52080.29	5545	87	1.2	2.8	0.10	0.19	106	0.12	0.19	15	0.11
ADP.2013-09-24T23:09:16.520	BF Oph	UVES TS	blue	52080.30	5546	84	1.7	4.1	-0.05	0.29	151	-0.07	0.39	15	-0.06
ADP.2013-09-24T23:09:16.520	BF Oph	UVES TS	red	52080.30	5546	84	1.3	3.0	0.03	0.20	108	0.03	0.20	14	0.03
ADP.2013-09-24T23:09:16.413	BB Sgr	UVES TS	blue	52080.34	5742	121	1.3	4.9	-0.04	0.25	121	-0.03	0.40	10	-0.04
ADP.2013-09-24T23:09:16.413	BB Sgr	UVES TS	red	52080.34	5742	121	1.8	4.9	-0.08	0.26	93	-0.07	0.14	9	-0.08
ADP.2013-09-24T23:09:16.653	BB Sgr	UVES TS	blue	52080.35	5745	108	1.3	4.9	-0.05	0.28	125	-0.07	0.30	12	-0.06
ADP.2013-09-24T23:09:16.653	BB Sgr	UVES TS	red	52080.35	5745	108	1.7	4.9	-0.09	0.28	89	-0.07	0.14	11	-0.08
ADP.2013-09-24T23:09:16.873	BB Sgr	UVES TS	blue	52080.35	5743	110	1.3	4.9	-0.03	0.27	121	-0.01	0.39	11	-0.02
ADP.2013-09-24T23:09:16.873	BB Sgr	UVES TS	red	52080.35	5743	110	1.7	4.9	-0.09	0.27	90	-0.10	0.15	8	-0.09
ADP.2014-05-16T05:42:40.330	VX Pup	UVES Kov	single	56749.99	5873	99	1.8	3.2	-0.10	0.25	232	-0.09	0.23	25	-0.09
ADP.2014-05-16T05:55:02.693	VX Pup	UVES Kov	single	56763.01	6438	81	1.9	2.4	-0.08	0.21	227	-0.08	0.30	31	-0.08
ADP.2014-05-16T05:55:02.647	VX Pup	UVES Kov	single	56763.09	6485	92	1.9	2.6	-0.10	0.21	224	-0.09	0.28	31	-0.10
ADP.2014-05-16T05:55:36.240	VX Pup	UVES Kov	single	56764.01	6128	83	1.8	2.2	-0.03	0.24	276	-0.02	0.23	34	-0.02
ADP.2014-05-16T05:55:36.253	VX Pup	UVES Kov	single	56764.13	6053	75	1.8	2.4	-0.09	0.22	281	-0.08	0.30	34	-0.09
ADP.2014-05-16T06:11:56.963	VX Pup	UVES Kov	single	56773.02	5967	97	1.8	2.3	-0.06	0.23	292	-0.05	0.31	33	-0.06
ADP.2014-05-16T06:11:56.970	VX Pup	UVES Kov	single	56773.09	5923	89	1.7	2.3	-0.07	0.24	284	-0.05	0.24	31	-0.06
ADP.2014-05-22T09:33:18.130	VX Pup	UVES Kov	single	56778.99	6141	74	1.7	2.1	-0.04	0.22	287	-0.05	0.23	34	-0.04
ADP.2014-05-22T09:33:18.123	VX Pup	UVES Kov	single	56779.02	6111	81	1.7	2.3	-0.08	0.25	294	-0.10	0.21	34	-0.09
ADP.2014-05-16T06:16:34.843	V912 Aql	UVES Inno	single	56775.39	5982	116	1.8	3.5	0.12	0.25	191	0.11	0.24	18	0.12
ADP.2014-05-16T06:16:34.830	V912 Aql	UVES Inno	single	56775.40	5975	99	2.0	4.2	0.13	0.26	187	0.12	0.20	20	0.13
ADP.2014-05-16T06:16:34.837	V912 Aql	UVES Inno	single	56775.40	5991	98	2.0	3.6	0.11	0.23	188	0.13	0.20	19	0.12
ADP.2014-04-07T15:35:11.853	CC Car	UVES Inno	single	56739.05	5933	80	1.3	2.5	0.18	0.25	227	0.21	0.32	27	0.20
ADP.2014-04-07T15:35:11.680	CC Car	UVES Inno	single	56739.06	5935	99	1.4	2.6	0.20	0.25	226	0.19	0.26	26	0.19
ADP.2014-04-07T15:35:11.927	CC Car	UVES Inno	single	56739.06	5960	98	1.4	2.6	0.17	0.25	232	0.20	0.36	24	0.19
ADP.2014-04-07T15:35:11.873	CF Car	UVES Inno	single	56739.09	5429	98	1.8	4.9	-0.02	0.27	188	-0.02	0.33	21	-0.02
ADP.2014-04-07T15:35:11.960	CF Car	UVES Inno	single	56739.09	5411	98	1.8	4.5	-0.04	0.25	191	-0.02	0.31	22	-0.03
ADP.2014-04-07T15:35:11.953	CF Car	UVES Inno	single	56739.10	5401	96	1.6	4.9	-0.04	0.28	194	-0.03	0.22	22	-0.03
ADP.2014-04-07T15:30:10.930	FF Car	UVES Inno	single	56732.25	5250	84	0.9	3.5	-0.01	0.25	199	-0.01	0.29	21	-0.01
ADP.2014-04-07T15:35:11.807	FK Car	UVES Inno	single	56739.03	5240	97	1.0	4.9	-0.05	0.28	195	-0.04	0.32	16	-0.04
ADP.2014-04-07T15:35:11.913	FK Car	UVES Inno	single	56739.04	5243	94	1.0	4.9	-0.05	0.29	194	-0.04	0.32	15	-0.04
ADP.2014-04-07T15:35:11.893	FK Car	UVES Inno	single	56739.05	5232	99	0.8	4.0	-0.02	0.29	204	-0.03	0.27	16	-0.02
ADP.2014-04-07T15:34:03.817	FM Car	UVES Inno	single	56738.22	6188	97	1.7	3.3	0.02	0.24	184	-0.01	0.25	23	0.01
ADP.2014-04-07T15:34:03.723	FM Car	UVES Inno	single	56738.23	6208	104	1.6	2.7	0.15	0.22	194	0.14	0.35	21	0.14
ADP.2014-04-07T15:34:03.823	FM Car	UVES Inno	single	56738.24	6186	119	1.7	3.0	0.15	0.24	188	0.14	0.28	24	0.15
ADP.2014-04-07T15:34:03.937	FM Car	UVES Inno	single	56738.25	6195	102	1.7	3.1	0.01	0.25	188	0.01	0.28	24	0.01
ADP.2014-04-07T15:35:11.733	FN Car	UVES Inno	single	56739.12	5546	94	1.6	3.8	-0.05	0.27	180	-0.05	0.26	23	-0.05
ADP.2014-04-07T15:35:11.847	FN Car	UVES Inno	single	56739.12	5531	99	1.5	3.7	-0.04	0.26	194	-0.03	0.28	22	-0.04
ADP.2014-04-07T15:35:11.687	FO Car	UVES Inno	single	56739.13	5189	95	1.2	4.9	-0.04	0.23	142	-0.04	0.25	16	-0.04
ADP.2014-04-07T15:35:11.760	FO Car	UVES Inno	single	56739.13	5155	99	0.8	4.9	-0.09	0.29	155	-0.10	0.24	12	-0.10
ADP.2014-04-07T15:35:11.673	FQ Car	UVES Inno	single	56739.15	5175	85	0.8	3.4	0.10	0.25	188	0.11	0.29	21	0.10
ADP.2014-04-07T15:35:11.787	FQ Car	UVES Inno	single	56739.15	5186	94	1.2	3.4	0.06	0.25	188	0.07	0.33	22	0.06
ADP.2014-04-07T15:35:11.700	FQ Car	UVES Inno	single	56739.16	5190	85	1.0	3.6	0.06	0.25	185	0.04	0.27	21	0.05
ADP.2014-04-07T15:34:03.997	GS Car	UVES Inno	single	56738.19	5614	96	1.4	2.5	0.11	0.24	254	0.12	0.25	26	0.12
ADP.2014-04-07T15:34:03.770	GS Car	UVES Inno	single	56738.20	5620	100	1.2	2.5	0.07	0.23	242	0.06	0.28	26	0.06
ADP.2014-04-07T15:34:04.010	GS Car	UVES Inno	single	56738.21	5629	88	1.5	2.5	0.11	0.22	235	0.16	0.26	26	0.13
ADP.2014-04-07T15:35:11.707	GT Car	UVES Inno	single	56739.11	5688	99	1.1	2.8	-0.03	0.31	237	-0.03	0.24	19	-0.03
ADP.2014-04-07T15:35:11.767	GT Car	UVES Inno	single	56739.11	5766	102	0.9	2.4	0.13	0.30	243	0.13	0.32	20	0.13
ADP.2014-04-07T15:35:11.827	GT Car	UVES Inno	single	56739.11	5671	142	1.0	3.0	-0.10	0.32	234	-0.10	0.27	19	-0.10
ADP.2014-04-07T15:35:11.617	HK Car	UVES Inno	single	56739.14	6126	75	1.2	3.0	0.07	0.24	208	0.06	0.27	19	0.06
ADP.2014-04-07T15:35:11.813	HK Car	UVES Inno	single	56739.14	6119	75	1.1	2.9	0.11	0.23	224	0.08	0.30	22	0.09
ADP.2014-04-07T15:34:03.883	II Car	UVES Inno	single	56738.10	5505	98	0.8	4.9	-0.06	0.29	167	-0.07	0.31	12	-0.06
ADP.2014-04-07T15:34:03.857	II Car	UVES Inno	single	56738.11	5493	99	0.6	4.0	-0.03	0.28	160	-0.04	0.28	10	-0.04
ADP.2014-04-07T15:34:03.930	II Car	UVES Inno	single	56738.12	5503	97	0.5	4.4	-0.04	0.29	152	-0.03	0.27	11	-0.04
ADP.2014-04-07T15:34:03.843	II Car	UVES Inno	single	56738.13	5462	117	0.6	3.8	-0.05	0.28	167	-0.06	0.27	14	-0.06
ADP.2014-04-07T15:35:12.000	IM Car	UVES Inno	single	56739.07	5539	102	1.3	4.4	0.02	0.27	161	0.00	0.17	15	0.01
ADP.2014-04-07T15:35:11.713	IM Car	UVES Inno	single	56739.08	5490	99	1.3	4.9	-0.05	0.28	184	-0.05	0.20	17	-0.05
ADP.2014-04-07T15:35:11.907	IM Car	UVES Inno	single	56739.08	5529	100	1.1	3.8	0.11	0.25	166	0.10	0.24	17	0.11
ADP.2014-04-07T15:34:03.810	IP Car	UVES Inno	single	56738.26	5671	137	1.3	3.0	-0.17	0.32	242	-0.19	0.28	27	-0.18
ADP.2014-04-07T15:34:03.730	IP Car	UVES Inno	single	56738.27	5672	150	1.3	2.6	-0.10	0.30	239	-0.09	0.27	26	-0.10
ADP.2014-04-07T15:34:03.777	IP Car	UVES Inno	single	56738.29	5645	164	1.6	2.6	-0.08	0.32	226	-0.06	0.35	26	-0.07
ADP.2014-04-07T15:34:03.697	IP Car	UVES Inno	single	56738.30	5628	161	1.4	2.8	-0.11	0.36	225	-0.11	0.25	23	-0.11
ADP.2014-04-07T15:39:53.843	BK Cen	UVES Inno	single	56748.08	5886	96	2.0	3.2	0.16	0.29	245	0.15	0.22	25	0.15
ADP.2014-04-07T15:39:53.877	BK Cen	UVES Inno	single	56748.08	5865	92	1.6	2.8	0.16	0.27	224	0.17	0.23	24	0.16
ADP.2014-04-07T15:36:11.707	IZ Cen	UVES Inno	single	56740.06	6100	99	1.8	3.4	0.10	0.28	213	0.12	0.27	21	0.11
ADP.2014-04-07T15:36:11.567	IZ Cen	UVES Inno	single	56740.07	6069	95	1.5	3.6	0.15	0.28	204	0.12	0.30	22	0.13
ADP.2014-04-07T15:36:11.780	IZ Cen	UVES Inno	single	56740.15	6069	100	1.8	3.8	0.13	0.32	216	0.13	0.26	22	0.13
ADP.2014-04-07T15:36:11.573	IZ Cen	UVES Inno	single	56740.16	6046	99	1.4	2.6	0.18	0.26	210	0.19	0.28	23	0.18
ADP.2014-04-07T15:36:11.627	IZ Cen	UVES Inno	single	56740.16	6000	100	1.7	3.8	0.07	0.32	217	0.06	0.22	22	0.07
ADP.2014-04-07T15:36:11.553	IZ Cen	UVES Inno	single	56740.17	6084	98	1.8	4.7	0.02	0.32	213	0.00	0.26	26	0.01
ADP.2014-04-07T15:35:11.753	LV Cen	UVES Inno	single	56739.29	5775	73	1.5	3.2	0.13	0.24	235	0.12	0.23	23	0.13
ADP.2014-04-07T15:35:11.980	LV Cen	UVES Inno	single	56739.30	5805	86	1.3	2.9	0.13	0.23	240	0.12	0.33	24	0.12
ADP.2014-04-07T15:35:11.653	LV Cen	UVES Inno	single	56739.31	5790	83	1.5	3.2	0.13	0.24	234	0.13	0.29	25	0.13
ADP.2014-04-07T15:39:53.770	MY Cen	UVES Inno	single	56748.12	5697	99	2.0	4.9	0.11	0.31	188	0.09	0.30	19	0.10
ADP.2014-04-07T15:39:53.857	MY Cen	UVES Inno	single	56748.12	5637	139	1.6	4.9	-0.02	0.34	170	-0.02	0.37	21	-0.02
ADP.2014-04-07T15:39:53.960	MY Cen	UVES Inno	single	56748.12	5696	100	2.0	4.9	0.02	0.38	178	-0.07	0.36	18	-0.02
ADP.2014-04-07T15:39:54.037	UZ Cen	UVES Inno	single	56748.08	5840	97	1.5	2.5	0.10	0.23	263	0.08	0.29	27	0.09
ADP.2014-04-07T15:39:53.890	V553 Cen	UVES Inno	single	56748.15	6020	146	1.9	2.7	0.00	0.29	211	-0.02	0.29	27	-0.01
ADP.2014-04-07T15:39:54.003	V553 Cen	UVES Inno	single	56748.16	6097	139	1.9	2.4	0.10	0.29	218	0.09	0.25	27	0.10
ADP.2014-04-07T15:35:11.747	V782 Cen	UVES Inno	single	56739.17	6146	150	1.9	4.5	0.16	0.36	226	0.15	0.22	16	0.15
ADP.2014-04-07T15:35:11.647	V782 Cen	UVES Inno	single	56739.18	6206	99	1.5	3.7	0.17	0.34	228	0.18	0.33	20	0.18
ADP.2014-04-07T15:35:11.880	V782 Cen	UVES Inno	single	56739.18	6151	97	1.2	3.4	0.13	0.34	235	0.11	0.23	17	0.12
ADP.2014-04-07T15:35:11.940	V782 Cen	UVES Inno	single	56739.19	6078	117	1.3	3.8	0.13	0.35	226	0.13	0.28	14	0.13
ADP.2014-04-07T15:30:11.023	SV Cru	UVES Inno	single	56732.30	5616	98	1.3	3.2	0.14	0.24	170	0.16	0.20	18	0.15
ADP.2014-04-07T15:36:11.580	SV Cru	UVES Inno	single	56740.17	5458	90	1.4	4.9	0.01	0.33	163	0.02	0.22	18	0.02
ADP.2014-04-07T15:36:11.653	SV Cru	UVES Inno	single	56740.18	5442	81	1.3	4.9	0.00	0.31	150	0.00	0.19	17	0.00
ADP.2014-04-07T15:36:11.720	SV Cru	UVES Inno	single	56740.18	5448	97	1.4	4.3	0.07	0.27	155	0.09	0.21	17	0.08
ADP.2014-04-07T15:35:11.693	TY Cru	UVES Inno	single	56739.32	5976	102	1.8	4.9	0.18	0.35	143	0.16	0.24	16	0.17
ADP.2014-04-07T15:35:11.840	TY Cru	UVES Inno	single	56739.32	6015	156	2.0	4.9	0.15	0.28	153	0.14	0.28	17	0.15
ADP.2014-04-07T15:35:11.800	TY Cru	UVES Inno	single	56739.33	5966	135	1.7	4.9	0.12	0.26	148	0.12	0.29	17	0.12
ADP.2014-04-07T15:35:11.860	TY Cru	UVES Inno	single	56739.34	5998	96	1.7	4.9	0.13	0.27	149	0.12	0.28	14	0.13

ADP.2014-04-07T15:35:11.887	VV Cru	UVES Inno	single	56739.34	5517	88	1.3	3.1	0.11	0.26	228	0.11	0.25	24	0.11
ADP.2014-04-07T15:35:11.793	VV Cru	UVES Inno	single	56739.35	5532	81	1.3	3.1	0.12	0.24	218	0.13	0.27	23	0.12
ADP.2014-04-07T15:35:11.967	VV Cru	UVES Inno	single	56739.36	5521	75	1.2	3.0	0.12	0.23	223	0.13	0.26	21	0.12
ADP.2014-04-07T15:38:45.510	VX Cru	UVES Inno	single	56745.09	6226	98	1.3	3.1	0.30	0.31	226	0.30	0.24	16	0.30
ADP.2014-04-07T15:38:45.523	VX Cru	UVES Inno	single	56745.09	6172	92	1.2	3.0	0.17	0.28	222	0.21	0.30	15	0.19
ADP.2014-04-07T15:38:45.627	VX Cru	UVES Inno	single	56745.09	6185	96	1.2	3.2	0.18	0.29	221	0.20	0.27	17	0.19
ADP.2014-05-16T05:52:31.610	V507 Sco	UVES Inno	single	56759.24	5606	153	1.6	2.9	-0.29	0.33	214	-0.28	0.24	25	-0.29
ADP.2014-05-16T05:52:31.590	V507 Sco	UVES Inno	single	56759.25	5530	172	1.8	3.7	-0.35	0.35	201	-0.33	0.27	29	-0.34
ADP.2014-05-16T05:52:31.503	V507 Sco	UVES Inno	single	56759.26	5579	170	1.8	3.5	-0.38	0.35	216	-0.34	0.21	28	-0.36
ADP.2014-05-16T05:52:31.723	V507 Sco	UVES Inno	single	56759.26	5639	155	1.9	3.7	-0.29	0.34	226	-0.30	0.22	27	-0.29
ADP.2014-05-16T06:14:54.917	V504 Sgr	UVES Inno	single	56774.24	6150	97	2.0	2.6	0.16	0.26	225	-0.06	0.24	31	0.05
ADP.2014-05-16T06:14:55.370	V504 Sgr	UVES Inno	single	56774.24	6182	101	2.0	2.4	0.20	0.25	215	-0.03	0.32	28	0.09
ADP.2014-05-16T06:14:55.097	V504 Sgr	UVES Inno	single	56774.25	6231	109	2.0	2.5	0.20	0.22	206	-0.03	0.28	31	0.09
ADP.2014-05-16T06:14:55.337	V504 Sgr	UVES Inno	single	56774.26	6158	168	2.0	2.7	0.17	0.27	208	-0.03	0.29	28	0.07
ADP.2014-05-16T06:21:15.773	BR Vul	UVES Inno	single	56778.40	5821	100	1.1	2.3	0.20	0.24	242	0.22	0.31	26	0.21
ADP.2014-05-16T06:21:15.833	BR Vul	UVES Inno	single	56778.40	5828	90	1.4	2.4	0.21	0.24	236	0.23	0.33	25	0.22
ADP.2014-05-16T06:21:15.853	BR Vul	UVES Inno	single	56778.40	5823	96	1.4	2.6	0.17	0.27	236	0.20	0.32	25	0.18
ADP.2014-05-16T06:21:16.040	BR Vul	UVES Inno	single	56778.40	5830	98	1.5	2.5	0.23	0.29	233	0.22	0.32	25	0.22
ADP.2014-06-05T06:37:02.577	GQ Vul	UVES Inno	single	56781.38	6140	96	1.6	4.9	0.16	0.29	172	0.17	0.21	13	0.17
ADP.2014-06-05T06:37:02.570	GQ Vul	UVES Inno	single	56781.39	6174	98	1.3	4.9	0.18	0.30	168	0.16	0.22	12	0.17
ADP.2014-06-05T06:37:02.583	GQ Vul	UVES Inno	single	56781.40	6200	107	1.5	4.9	0.19	0.35	186	0.18	0.21	12	0.19
V340Ara_35_58	V340 Ara	UVES Geno	single	54708.07	5181	99	0.9	4.3	0.25	0.28	106	0.24	0.26	7	0.24
V340Ara_37_46	V340 Ara	UVES Geno	single	54709.08	5095	99	0.7	4.8	0.20	0.31	104	0.20	0.26	6	0.20
V340Ara_13_02	V340 Ara	UVES Geno	single	56137.14	5172	99	0.8	4.8	0.19	0.29	136	0.17	0.30	6	0.18
V340Ara_15_24	V340 Ara	UVES Geno	single	56138.09	5578	119	0.9	4.9	0.23	0.24	163	0.21	0.16	11	0.22
V340Ara_17_25	V340 Ara	UVES Geno	single	56139.19	6083	133	1.6	4.9	0.32	0.30	177	0.34	0.30	17	0.33
V340Ara_25_34	V340 Ara	UVES Geno	single	56152.05	4742	108	1.1	4.8	0.10	0.32	95	0.12	0.84	9	0.11
ASAur_59_43	AS Aur	UVES Geno	single	54845.14	5670	148	1.4	2.8	-0.07	0.26	135	-0.06	0.23	15	-0.06
MZCen_57_15	MZ Cen	UVES Geno	single	54584.29	5508	99	1.2	4.9	0.11	0.25	123	0.12	0.21	10	0.12
OOCen_58_58	OO Cen	UVES Geno	single	54585.07	5945	122	1.5	4.2	0.14	0.28	121	0.13	0.20	10	0.13
TXCen_15_00	TX Cen	UVES Geno	single	54862.36	5360	94	0.9	4.9	0.18	0.30	99	0.18	0.22	7	0.18
V339Cen_57_15	V339 Cen	UVES Geno	single	54584.30	5217	90	1.2	4.9	-0.07	0.26	131	-0.09	0.32	9	-0.08
VWCen_15_00	VW Cen	UVES Geno	single	54862.36	5180	100	0.7	4.9	0.13	0.35	67	0.15	0.44	5	0.14
AOCma_54_36	AO Cma	UVES Geno	single	54839.06	5804	92	1.1	2.1	0.11	0.24	200	0.13	0.26	16	0.12
RWCma_54_37	RW Cma	UVES Geno	single	54839.14	6111	79	1.3	2.6	0.06	0.24	180	0.06	0.23	17	0.06
SSCma_54_37	SS Cma	UVES Geno	single	54839.07	5704	98	1.2	3.2	0.10	0.30	191	0.09	0.18	16	0.09
TVCma_03_08	TV Cma	UVES Geno	single	54847.25	5561	82	1.4	3.3	0.06	0.28	182	0.07	0.22	16	0.06
TWCma_54_37	TW Cma	UVES Geno	single	54839.08	5884	466	2.0	4.9	-0.13	0.37	161	-0.16	0.22	14	-0.15
AAGem_01_19	AA Gem	UVES Geno	single	54846.15	5565	131	1.3	4.4	-0.17	0.27	154	-0.18	0.23	12	-0.18
ADGem_01_19	AD Gem	UVES Geno	single	54846.22	6240	172	1.7	2.4	-0.10	0.27	145	-0.08	0.22	17	-0.09
BWGem_59_43	BW Gem	UVES Geno	single	54845.13	5853	120	1.8	2.0	-0.08	0.26	215	-0.07	0.22	18	-0.07
DXGem_01_19	DX Gem	UVES Geno	single	54846.20	6201	98	1.9	2.4	-0.10	0.27	133	-0.12	0.21	16	-0.11
RZGem_59_43	RZ Gem	UVES Geno	single	54845.10	6713	255	1.2	2.0	-0.26	0.30	80	-0.24	0.29	15	-0.25
BEMon_01_19	BE Mon	UVES Geno	single	54846.20	5703	112	1.6	2.9	0.06	0.25	181	0.06	0.25	16	0.06
CVMon_01_19	CV Mon	UVES Geno	single	54846.18	5500	111	1.5	4.9	-0.10	0.30	146	-0.09	0.22	15	-0.10
FTMon_59_43	FT Mon	UVES Geno	single	54845.11	5832	135	2.0	3.4	-0.05	0.32	156	-0.11	0.23	16	-0.08
SVMon_59_43	SV Mon	UVES Geno	single	54845.12	5115	86	1.0	3.9	-0.02	0.25	152	-0.02	0.26	12	-0.02
TWMon_39_42	TW Mon	UVES Geno	single	54796.35	5949	111	1.3	2.6	-0.02	0.28	176	-0.04	0.23	17	-0.03
TXMon_40_39	TX Mon	UVES Geno	single	54798.35	6014	121	1.4	3.3	-0.06	0.29	183	-0.05	0.17	16	-0.05
TYMon_01_19	TY Mon	UVES Geno	single	54846.14	6169	111	1.5	2.8	-0.11	0.29	177	-0.10	0.20	17	-0.10
TZMon_03_08	TZ Mon	UVES Geno	single	54847.24	5606	93	1.2	3.0	-0.01	0.25	186	-0.02	0.22	16	-0.02
V465Mon_03_08	V465 Mon	UVES Geno	single	54847.24	6219	95	1.9	2.8	-0.08	0.25	170	-0.06	0.23	18	-0.07
V495Mon_01_19	V495 Mon	UVES Geno	single	54846.17	5543	158	1.3	3.0	-0.08	0.27	167	-0.09	0.24	17	-0.09
V508Mon_03_08	V508 Mon	UVES Geno	single	54847.23	6007	195	1.8	3.0	-0.12	0.27	179	-0.10	0.17	16	-0.11
V510Mon_01_19	V510 Mon	UVES Geno	single	54846.16	5457	123	1.3	3.6	-0.12	0.28	177	-0.14	0.17	16	-0.13
XXMon_40_39	XX Mon	UVES Geno	single	54798.34	5478	97	1.8	4.9	-0.08	0.28	148	-0.07	0.18	14	-0.07
GUNor_41_39	GU Nor	UVES Geno	single	54667.21	6246	90	1.5	2.3	0.18	0.21	179	0.17	0.26	17	0.17
IQNor_57_15	IQ Nor	UVES Geno	single	54584.30	6019	95	1.6	4.9	0.15	0.30	135	0.16	0.20	10	0.15
QZNor_17_35	QZ Nor	UVES Geno	single	54863.37	5749	121	1.3	3.0	0.34	0.27	177	0.33	0.25	15	0.34
QZNor_13_36	QZ Nor	UVES Geno	single	54923.34	5799	98	1.3	2.7	0.35	0.25	193	0.34	0.20	14	0.34
RSNor_17_35	RS Nor	UVES Geno	single	54863.36	6160	92	1.4	2.6	0.33	0.23	174	0.34	0.18	11	0.33
SYNor_35_58	SY Nor	UVES Geno	single	54708.06	5531	99	1.1	4.9	0.18	0.31	128	0.21	0.20	9	0.19
SYNor_37_46	SY Nor	UVES Geno	single	54709.08	5664	94	1.2	4.9	0.17	0.26	149	0.19	0.16	10	0.18
TWNor_40_53	TW Nor	UVES Geno	single	54666.13	5105	86	0.9	4.8	0.10	0.34	110	0.11	0.35	8	0.10
V340Nor_31_12	V340 Nor	UVES Geno	single	54873.38	5726	106	1.7	4.9	0.01	0.30	133	0.00	0.21	13	0.01
CSOri_59_43	CS Ori	UVES Geno	single	54845.09	6497	145	1.7	2.0	-0.12	0.26	147	-0.12	0.24	20	-0.12
RSOri_59_43	RS Ori	UVES Geno	single	54845.10	6206	91	1.5	3.1	-0.03	0.28	168	-0.03	0.22	17	-0.03
AQPup_54_36	AQ Pup	UVES Geno	single	54839.07	5091	225	1.3	4.9	-0.21	0.48	88	-0.19	0.63	7	-0.20
BCPup_54_37	BC Pup	UVES Geno	single	54839.16	5751	158	2.0	4.9	-0.18	0.31	164	-0.20	0.23	14	-0.19
BMPup_54_37	BM Pup	UVES Geno	single	54839.09	5453	109	1.1	3.2	-0.09	0.31	176	-0.08	0.23	17	-0.08
BNPup_54_36	BN Pup	UVES Geno	single	54839.11	5378	86	0.9	2.8	0.14	0.25	174	0.15	0.21	15	0.14
CKPup_54_37a	CK Pup	UVES Geno	single	54839.12	6149	118	1.2	2.3	-0.07	0.28	203	-0.09	0.22	18	-0.08
CKPup_54_37b	CK Pup	UVES Geno	single	54839.18	6142	98	1.1	2.0	-0.07	0.26	193	-0.09	0.25	18	-0.08
HWPup_35_32	HW Pup	UVES Geno	single	54792.25	5276	100	0.9	2.9	-0.12	0.24	169	-0.10	0.27	16	-0.11
LSPup_54_37	LS Pup	UVES Geno	single	54839.08	5299	117	1.3	4.9	-0.19	0.30	88	-0.21	0.14	7	-0.20
VWPup_49_43	VW Pup	UVES Geno	single	54832.33	5562	203	1.8	4.9	-0.24	0.28	167	-0.25	0.18	15	-0.25
VZPup_54_36	VZ Pup	UVES Geno	single	54839.10	6326	165	1.5	5.0	-0.17	0.32	103	-0.16	0.12	10	-0.17
WWPup_54_37	WW Pup	UVES Geno	single	54839.09	6261	103	1.3	2.0	-0.01	0.26	186	-0.01	0.29	16	-0.01
WYPup_54_37	WY Pup	UVES Geno	single	54839.10	6001	203	1.4	2.7	-0.06	0.26	108	-0.06	0.18	11	-0.06
WZPup_54_37	WZ Pup	UVES Geno	single	54839.11	5661	96	1.4	2.7	-0.01	0.26	196	-0.01	0.16	15	-0.01
XPup_54_37	X Pup	UVES Geno	single	54839.07	5032	163	0.6	4.9	-0.14	0.39	90	-0.14	0.88	7	-0.14
KQSco_31_11	KQ Sco	UVES Geno	single	54873.38	4917	100	0.3	4.9	0.08	0.39	57	0.08	0.59	3	0.08
KQSco_17_25	KQ Sco	UVES Geno	single	56139.02	5084	114	0.3	4.8	0.16	0.35	116	0.14	0.45	9	0.15
KQSco_25_34	KQ Sco	UVES Geno	single	56152.10	4916	93	1.0	4.8	0.14	0.25	134	0.15	0.50	14	0.15
KQSco_31_36	KQ Sco	UVES Geno	single	56163.00	4797	103	0.2	4.8	0.04	0.35	86	0.02	0.43	8	0.03
KQSco_33_38	KQ Sco	UVES Geno	single	56166.01	4930	96	1.7	4.9	0.06	0.36	97	0.08	0.74	8	0.07
RYSco_04_58	RY Sco	UVES Geno	single	54599.41	5324	99	0.8	4.9	0.05	0.29	150	0.07	0.24	9	0.06
RYSco_19_04	RY Sco	UVES Geno	single	56140.19	5582	97	0.7	3.4	0.17	0.25	230	0.18	0.25	12	0.18
RYSco_25_34	RY Sco	UVES Geno	single	56152.14	6256	95	0.9	3.0	0.17	0.24	219	0.19	0.29	17	0.18
RYSco_30_52	RY Sco	UVES Geno	single	56162.17	5431	99	0.6	4.2	0.13	0.27	217	0.11	0.27	13	0.12
RYSco_34_12	RY Sco	UVES Geno	single	56167.08	5309	97	0.9	4.9	-0.03	0.29	183	-0.03	0.30	12	-0.03
V470Sco_35_58	V470 Sco	UVES Geno	single	54708.08	5711	83	1.2	4.9	0.16	0.24	138	0.16	0.14	9	0.16
V500Sco_19_04	V500 Sco	UVES Geno	single	56140.19	5986	79	1.1	2.6	0.15	0.23	257	0.15	0.34	25	0.15
V500Sco_25_34	V500 Sco	UVES Geno	single	56152.09	5394	83	1.1	3.0	0.07	0.24	252	0.07	0.30	27	0.07
V500Sco_31_36	V500 Sco	UVES Geno	single	56163.00	5283	97	1.2	4.0	-0.06	0.28	203	-0.08	0.36	24	-0.07
V500Sco_34_12	V500 Sco	UVES Geno	single	56167.08	6061	59	1.0	2.6	0.11	0.23	264	0.09	0.27	26	0.10
EVSct_35_58	EV Sct	UVES Geno	single	54708.09	6057	90	1.7	3.1	-0.05	0.29	125	-0.05	0.21	16	-0.05
RUSct_58_47	RU Sct	UVES Geno	single	54906.41	5266	77	0.6	4.0	0.05	0.26	143	0.06	0.24	8	0.06
RUSct_13_36	RU Sct	UVES Geno	single	54923.38	5541	98	0.9	3.5	0.13	0.27	151	0.12	0.22	9	0.13
UZSct_58_47	UZ Sct	UVES Geno	single	54906.40	5382	100	1.1	4.9	0.15	0.29	137	0.15	0.26	10	0.15
UZSct_13_36	UZ Sct	UVES Geno	single	54923.37	5088	99	1.6	4.8	0.14	0.29	114	0.12	0.38	10	0.13
UZSct_13_02	UZ Sct	UVES Geno	single	56137.16	4797	98	0.9	4.8	0.08	0.36	110	0.08	0.44	12	0.08
UZSct_25_34	UZ Sct	UVES Geno	single	56152.07	4769	98	0.9	4.8	0.02	0.34	109	0.00	0.54	14	0.01
UZSct_29_57	UZ Sct	UVES Geno	single	56160.16	5295	99	1.3	4.9	0.14	0.29	191	0.15	0.28	15	0.14
UZSct_36_29	UZ Sct	UVES Geno	single	56175.05	5275	99	1.5	4.9	0.18	0.28	181	0.15	0.33	17	0.17
V367Sct_37_46	V367 Sct	UVES Geno	single	54709.13	5712	99	1.7	4.3	-0.03	0.29	153	-0.01	0.27	12	-0.02
V367Sct_13_02	V367 Sct	UVES Geno	single	56137.14	5697	84	1.4	3.0	0.19	0.24	231	0.19	0.30	25	0.19
V367Sct_36_29	V367 Sct	UVES Geno	single	56175.11	5959	93	1.8	4.9	0.10	0.31	190	0.10	0.23	19	0.10

V367Sct_41_10	V367 Sct	UVES Geno	single	56184.00	6262	106	1.1	2.4	0.12	0.27	218	0.14	0.38	26	0.13
XSct_37_46	X Sct	UVES Geno	single	54709.12	5814	69	1.4	2.5	0.13	0.25	155	0.12	0.27	14	0.12
ZSct_47_31	Z Sct	UVES Geno	single	54678.09	5025	98	0.5	4.8	-0.05	0.32	91	-0.07	0.23	6	-0.06
ZSct_13_02	Z Sct	UVES Geno	single	56137.12	5125	97	0.7	4.9	-0.10	0.32	95	-0.09	0.22	9	-0.10
ZSct_25_34	Z Sct	UVES Geno	single	56152.07	5664	89	1.4	4.9	0.04	0.27	164	0.02	0.15	17	0.03
ZSct_28_56	Z Sct	UVES Geno	single	56159.18	5199	99	1.2	4.8	0.12	0.28	176	0.11	0.33	18	0.12
ZSct_36_29	Z Sct	UVES Geno	single	56175.04	5094	151	0.6	4.8	-0.02	0.32	121	-0.02	0.32	7	-0.02
AASer_35_58	AA Ser	UVES Geno	single	54708.05	4808	98	0.7	4.8	0.11	0.32	66	0.09	0.56	7	0.10
CRSer_37_46	CR Ser	UVES Geno	single	54709.12	5434	97	1.6	4.9	0.04	0.31	137	0.05	0.17	10	0.04
AVSgr_13_36	AV Sgr	UVES Geno	single	54923.35	5062	99	0.1	4.9	0.16	0.30	62	0.18	0.16	4	0.17
AVSgr_11_11a	AV Sgr	UVES Geno	single	56136.17	5036	98	1.6	4.8	0.22	0.26	155	0.23	0.50	14	0.22
AVSgr_11_11b	AV Sgr	UVES Geno	single	56136.20	5051	100	1.3	4.8	0.19	0.29	153	0.20	0.45	12	0.20
AVSgr_25_34	AV Sgr	UVES Geno	single	56152.08	4999	97	1.3	4.8	0.20	0.28	153	0.20	0.55	14	0.20
AVSgr_34_37	AV Sgr	UVES Geno	single	56168.05	4991	99	1.6	4.8	0.22	0.28	142	0.23	0.68	16	0.22
AYSgr_04_58	AY Sgr	UVES Geno	single	54599.40	5771	84	1.2	2.6	0.16	0.24	174	0.18	0.20	15	0.17
V1954Sgr_04_58	V1954 Sgr	UVES Geno	single	54599.39	6110	89	1.5	3.0	0.35	0.27	177	0.35	0.19	11	0.35
V773Sgr_42_25	V773 Sgr	UVES Geno	single	54669.22	6208	137	2.0	3.4	0.20	0.27	92	0.20	0.20	15	0.20
VYSgr_13_36	VY Sgr	UVES Geno	single	54923.36	5107	112	1.3	3.8	0.20	0.29	122	0.21	0.33	10	0.20
VYSgr_29_57	VY Sgr	UVES Geno	single	56160.18	4882	86	0.3	4.8	0.09	0.36	122	0.08	0.51	6	0.08
VYSgr_30_52	VY Sgr	UVES Geno	single	56162.16	5202	97	0.3	4.9	0.08	0.32	104	0.08	0.20	8	0.08
VYSgr_34_37	VY Sgr	UVES Geno	single	56168.06	5419	99	0.9	3.8	0.20	0.31	195	0.21	0.45	15	0.21
WZSgr_04_58	WZ Sgr	UVES Geno	single	54599.40	5147	123	2.0	4.9	0.09	0.38	77	0.10	0.54	5	0.10
WZSgr_06_58	WZ Sgr	UVES Geno	single	56132.19	6011	94	1.4	4.9	0.16	0.29	173	0.15	0.15	14	0.16
WZSgr_11_11	WZ Sgr	UVES Geno	single	56136.21	5452	99	0.8	4.9	0.12	0.30	188	0.11	0.34	15	0.11
WZSgr_25_34	WZ Sgr	UVES Geno	single	56152.04	5182	95	0.5	4.9	0.15	0.33	138	0.15	0.44	8	0.15
WZSgr_28_56	WZ Sgr	UVES Geno	single	56159.12	5315	86	0.6	4.9	0.14	0.28	179	0.13	0.22	13	0.14
XXSgr_04_58	XX Sgr	UVES Geno	single	54599.40	6313	167	1.8	3.5	-0.06	0.27	153	-0.07	0.16	16	-0.06
XXSgr_49_23	XX Sgr	UVES Geno	single	56054.23	5867	91	1.3	2.6	0.14	0.25	264	0.16	0.27	25	0.15
XXSgr_11_11	XX Sgr	UVES Geno	single	56136.22	6259	76	1.1	2.3	0.07	0.25	218	0.09	0.31	30	0.08
XXSgr_25_34	XX Sgr	UVES Geno	single	56152.05	5511	86	1.2	3.0	0.10	0.28	225	0.11	0.31	22	0.10
XXSgr_28_56	XX Sgr	UVES Geno	single	56159.13	5465	90	1.1	3.5	-0.06	0.29	201	-0.08	0.28	24	-0.07
EZVel_19_12	EZ Vel	UVES Geno	single	54759.35	4814	118	0.4	4.9	-0.26	0.36	99	-0.24	0.34	7	-0.25
ADP.2014-10-01T10:23:13.380	S Cru	HARPS	red	53150.13	6158	182	1.7	2.9	0.20	0.31	217	0.20	0.22	17	0.20
ADP.2014-10-01T10:23:25.600	S Cru	HARPS	red	53151.06	6222	61	1.7	3.0	0.11	0.25	226	0.09	0.18	22	0.10
ADP.2014-10-01T10:21:29.113	S Cru	HARPS	red	53152.13	5732	63	1.2	2.3	0.15	0.20	251	0.14	0.24	21	0.15
ADP.2014-10-01T10:20:16.920	S Cru	HARPS	red	53153.07	5556	100	1.4	3.0	-0.01	0.23	227	-0.02	0.21	20	-0.01
ADP.2014-10-01T10:21:37.650	S Cru	HARPS	red	53154.13	5612	99	1.7	4.5	-0.06	0.26	195	-0.05	0.18	15	-0.06
ADP.2014-10-01T10:20:12.610	S Cru	HARPS	red	53156.12	6013	50	1.7	2.8	0.12	0.23	240	0.11	0.19	19	0.11
ADP.2014-10-01T10:21:37.017	S Cru	HARPS	red	53201.99	6482	98	1.9	2.8	0.12	0.22	191	0.10	0.22	22	0.11
ADP.2014-10-01T10:22:39.377	S Cru	HARPS	red	53202.98	6058	53	1.5	2.5	0.16	0.21	236	0.17	0.19	21	0.16
ADP.2014-10-01T10:19:57.310	S Cru	HARPS	red	53202.99	6051	55	1.6	2.7	0.14	0.21	232	0.14	0.19	20	0.14
ADP.2014-10-01T10:21:41.723	S Cru	HARPS	red	53204.97	5517	97	1.4	3.6	-0.06	0.24	210	-0.05	0.17	20	-0.06
ADP.2014-10-01T10:20:19.233	S Cru	HARPS	red	53205.98	5784	106	1.9	4.2	-0.02	0.25	183	-0.03	0.16	16	-0.02
ADP.2014-10-01T10:23:08.910	S Cru	HARPS	red	53206.95	6418	98	1.7	2.7	0.08	0.23	188	0.09	0.23	22	0.09
ADP.2014-10-01T10:21:34.170	β Dor	HARPS	red	53015.12	5248	93	1.5	3.9	-0.06	0.22	221	-0.08	0.24	19	-0.07
ADP.2014-10-01T10:22:31.197	β Dor	HARPS	red	53015.12	5236	91	1.4	3.6	-0.05	0.22	223	-0.03	0.27	21	-0.04
ADP.2014-10-01T10:21:15.450	β Dor	HARPS	red	53015.13	5249	90	1.5	3.9	-0.05	0.22	221	-0.06	0.27	21	-0.06
ADP.2014-10-01T10:19:44.810	β Dor	HARPS	red	53016.17	5186	98	1.4	4.9	-0.14	0.28	199	-0.16	0.30	18	-0.15
ADP.2014-10-01T10:22:41.257	β Dor	HARPS	red	53016.17	5195	98	1.4	4.9	-0.13	0.26	194	-0.15	0.30	18	-0.14
ADP.2014-10-01T10:20:43.897	β Dor	HARPS	red	53016.18	5203	95	1.3	4.9	-0.14	0.27	194	-0.15	0.27	18	-0.15
ADP.2014-10-01T10:23:39.770	β Dor	HARPS	red	53017.18	5398	160	1.1	3.7	-0.10	0.22	162	-0.07	0.28	15	-0.08
ADP.2014-10-01T10:19:36.430	β Dor	HARPS	red	53017.19	5392	113	1.1	4.2	-0.11	0.22	167	-0.11	0.18	12	-0.11
ADP.2014-10-01T10:20:17.523	β Dor	HARPS	red	53017.19	5388	139	1.1	4.9	-0.12	0.26	160	-0.14	0.26	13	-0.13
ADP.2014-10-01T10:20:18.303	β Dor	HARPS	red	53021.18	5992	77	1.1	2.8	-0.02	0.21	230	-0.01	0.21	18	-0.01
ADP.2014-10-01T10:21:03.290	β Dor	HARPS	red	53021.18	5994	90	1.3	3.3	-0.01	0.22	233	-0.04	0.19	20	-0.03
ADP.2014-10-01T10:21:47.523	β Dor	HARPS	red	53021.18	6006	75	1.2	3.0	0.01	0.21	234	-0.01	0.18	16	0.00
ADP.2014-10-01T10:23:09.210	β Dor	HARPS	red	53021.19	6001	85	1.2	2.8	-0.02	0.21	232	-0.02	0.20	17	-0.02
ADP.2014-10-01T10:23:11.353	β Dor	HARPS	red	53023.13	5563	73	1.5	3.7	-0.06	0.22	236	-0.07	0.19	20	-0.06
ADP.2014-10-01T10:19:34.827	β Dor	HARPS	red	53023.14	5559	82	1.5	3.7	-0.05	0.22	231	-0.05	0.19	20	-0.05
ADP.2014-10-01T10:21:20.960	β Dor	HARPS	red	53023.14	5560	69	1.4	3.4	-0.04	0.20	236	-0.03	0.17	20	-0.03
ADP.2014-10-01T10:23:23.900	β Dor	HARPS	red	53023.14	5556	71	1.3	3.2	-0.02	0.20	234	-0.02	0.18	21	-0.02
ADP.2014-10-01T10:23:08.883	β Dor	HARPS	red	53025.17	5229	93	1.3	3.6	-0.04	0.23	217	-0.02	0.25	20	-0.03
ADP.2014-10-01T10:19:12.130	β Dor	HARPS	red	53025.18	5227	90	1.2	3.5	-0.03	0.23	216	-0.05	0.26	21	-0.04
ADP.2014-10-01T10:22:01.160	β Dor	HARPS	red	53025.18	5229	92	1.2	3.6	-0.04	0.23	216	-0.04	0.25	21	-0.04
ADP.2014-10-01T10:20:15.947	β Dor	HARPS	red	53026.09	5207	97	1.5	4.9	-0.15	0.26	195	-0.13	0.29	19	-0.14
ADP.2014-10-01T10:21:08.847	β Dor	HARPS	red	53026.10	5203	99	1.4	4.9	-0.16	0.27	193	-0.15	0.30	19	-0.15
ADP.2014-10-01T10:20:14.110	β Dor	HARPS	red	53028.17	5692	110	1.5	3.9	-0.05	0.20	193	-0.05	0.24	12	-0.05
ADP.2014-10-01T10:22:32.210	β Dor	HARPS	red	53028.17	5684	129	1.5	3.8	-0.03	0.19	190	-0.04	0.17	13	-0.04
ADP.2014-10-01T10:19:29.217	β Dor	HARPS	red	53028.18	5689	99	1.7	4.9	-0.09	0.22	190	-0.11	0.16	13	-0.10
ADP.2014-10-01T10:22:19.807	β Dor	HARPS	red	53029.13	5814	90	1.4	3.3	-0.02	0.20	215	0.00	0.27	14	-0.01
ADP.2014-10-01T10:22:36.720	β Dor	HARPS	red	53029.13	5810	84	1.3	3.3	-0.01	0.20	216	0.00	0.16	15	-0.01
ADP.2014-10-01T10:23:17.653	β Dor	HARPS	red	53029.13	5809	83	1.3	3.4	-0.02	0.21	215	-0.03	0.16	15	-0.03
ADP.2014-10-01T10:20:37.623	β Dor	HARPS	red	53029.14	5793	86	1.4	3.5	-0.03	0.22	220	-0.03	0.16	15	-0.03
ADP.2014-10-01T10:21:53.153	β Dor	HARPS	red	53031.13	5971	89	1.3	3.0	-0.01	0.22	234	-0.01	0.18	14	-0.01
ADP.2014-10-01T10:21:04.103	β Dor	HARPS	red	53031.14	5991	85	1.2	2.9	0.04	0.23	238	0.02	0.18	15	0.03
ADP.2014-10-01T10:21:53.427	β Dor	HARPS	red	53031.14	5981	80	1.3	3.0	-0.02	0.23	241	0.00	0.17	16	-0.01
ADP.2014-10-01T10:21:23.637	β Dor	HARPS	red	53032.18	5714	81	1.3	3.4	-0.05	0.22	239	-0.07	0.16	19	-0.06
ADP.2014-10-01T10:21:42.837	β Dor	HARPS	red	53032.18	5732	75	1.6	3.8	-0.04	0.23	240	-0.03	0.20	19	-0.03
ADP.2014-10-01T10:22:19.253	β Dor	HARPS	red	53032.18	5730	73	1.6	3.7	-0.04	0.23	231	-0.03	0.18	19	-0.03
ADP.2014-10-01T10:20:32.310	β Dor	HARPS	red	53033.11	5525	78	1.3	3.3	-0.04	0.21	230	-0.02	0.18	21	-0.03
ADP.2014-10-01T10:23:26.587	β Dor	HARPS	red	53033.11	5531	76	1.3	3.2	0.01	0.21	240	-0.05	0.18	21	-0.02
ADP.2014-10-01T10:23:38.710	β Dor	HARPS	red	53033.11	5526	74	1.4	3.2	0.00	0.20	235	-0.01	0.18	21	0.00
ADP.2014-10-01T10:22:36.283	β Dor	HARPS	red	53034.14	5340	81	1.3	3.4	-0.01	0.20	231	-0.04	0.23	20	-0.02
ADP.2014-10-01T10:22:43.283	β Dor	HARPS	red	53034.14	5331	74	1.3	3.3	-0.02	0.21	234	-0.01	0.22	21	-0.02
ADP.2014-10-01T10:21:20.153	β Dor	HARPS	red	53035.13	5227	92	1.5	3.8	-0.03	0.24	221	-0.02	0.27	20	-0.02
ADP.2014-10-01T10:23:36.690	β Dor	HARPS	red	53035.14	5219	86	1.4	4.1	-0.09	0.24	218	-0.11	0.27	21	-0.10
ADP.2014-10-01T10:19:39.697	β Dor	HARPS	red	53036.14	5210	91	1.0	4.0	-0.11	0.27	195	-0.13	0.24	17	-0.12
ADP.2014-10-01T10:22:52.313	β Dor	HARPS	red	53036.14	5213	96	1.3	4.9	-0.17	0.26	187	-0.18	0.27	15	-0.18
ADP.2014-10-01T10:20:15.307	β Dor	HARPS	red	53037.14	5521	141	1.4	4.9	-0.10	0.24	161	-0.10	0.17	10	-0.10
ADP.2014-10-01T10:19:47.440	β Dor	HARPS	red	53037.15	5494	140	1.4	4.6	-0.09	0.25	140	-0.09	0.15	11	-0.09
ADP.2014-10-01T10:20:04.377	ζ Gem	HARPS	red	53015.21	5253	74	1.6	4.0	-0.01	0.22	215	-0.03	0.30	20	-0.02
ADP.2014-10-01T10:21:33.270	ζ Gem	HARPS	red	53015.21	5254	86	1.5	3.5	0.06	0.21	217	0.05	0.30	19	0.05
ADP.2014-10-01T10:22:45.030	ζ Gem	HARPS	red	53015.21	5271	71	1.4	3.8	0.05	0.23	219	0.06	0.29	20	0.05
ADP.2014-10-01T10:21:42.857	ζ Gem	HARPS	red	53016.18	5216	97	1.2	4.4	-0.05	0.24	190	-0.05	0.28	17	-0.05
ADP.2014-10-01T10:23:38.027	ζ Gem	HARPS	red	53016.18	5216	100	1.4	4.9	-0.02	0.25	195	-0.01	0.29	15	-0.02
ADP.2014-10-01T10:21:48.930	ζ Gem	HARPS	red	53016.19	5213	71	1.6	4.9	-0.05	0.25	196	-0.03	0.30	17	-0.04
ADP.2014-10-01T10:23:27.827	ζ Gem	HARPS	red	53017.19	5322	96	1.2	4.9	-0.06	0.23	167	-0.06	0.24	12	-0.06
ADP.2014-10-01T10:20:09.707	ζ Gem	HARPS	red	53017.20	5305	92	1.1	4.9	-0.05	0.23	162	-0.05	0.22	13	-0.05
ADP.2014-10-01T10:21:59.757	ζ Gem	HARPS	red	53017.20	5337	100	1.3	4.9	-0.01	0.24	170	-0.01	0.22	13	-0.01
ADP.2014-10-01T10:19:42.483	ζ Gem	HARPS	red	53021.19	5818	64	1.1	3.0	0.09	0.21	249	0.09	0.19	15	0.09
ADP.2014-10-01T10:20:41.893	ζ Gem	HARPS	red	53021.19	5812	80	1.1	3.0	0.12	0.23	256	0.11	0.19	15	0.11
ADP.2014-10-01T10:23:13.893	ζ Gem	HARPS	red	53021.19	5837	60	1.2	3.1	0.15	0.24	251	0.13	0.18	13	0.14
ADP.2014-10-01T10:19:06.560	ζ Gem	HARPS	red	53021.20	5819	59	1.2	3.0	0.13	0.22	251	0.12	0.17	13	0.12
ADP.2014-10-01T10:23:24.320	ζ Gem	HARPS	red	53021.20	5829	61	1.3	2.8	0.13	0.21	246	0.12	0.21	14	0.13
ADP.2014-10-01T10:19:16.990	ζ Gem	HARPS	red	53023.14	5597	86	1.4	3.3	0.11	0.22	236	0.12	0.18	18	0.11
ADP.2014-10-01T10:19:38.267	ζ Gem	HARPS	red	53023.15	5586	74	1.4	3.5	0.05	0.22	236	0.05	0.19	17	0.05
ADP.2014-10-01T10:20:19.793	ζ Gem	HARPS	red	53023.15	5585	63	1.5	3.6	0.03	0.21	232	0.05	0.19	18	0.04
ADP.2014-10-01T10:23:34.070	ζ Gem	HARPS	red	53023.15	5585	93	1.5	3.7	0.04	0.23	236	0.04	0.19	17	0.04

ADP.2014-10-01T10:22:55.680	ζ Gem	HARPS	red	53025.18	5270	74	1.1	3.2	0.07	0.21	218	0.06	0.28	20	0.06
ADP.2014-10-01T10:20:48.893	ζ Gem	HARPS	red	53025.19	5276	74	1.4	3.6	0.09	0.22	220	0.08	0.26	20	0.08
ADP.2014-10-01T10:21:12.867	ζ Gem	HARPS	red	53025.19	5272	74	1.3	3.4	0.04	0.22	222	0.05	0.27	20	0.04
ADP.2014-10-01T10:19:31.800	ζ Gem	HARPS	red	53026.10	5209	74	1.6	4.9	-0.05	0.25	198	-0.05	0.29	18	-0.05
ADP.2014-10-01T10:22:38.720	ζ Gem	HARPS	red	53026.10	5210	83	1.3	3.6	-0.01	0.24	193	0.00	0.30	20	0.00
ADP.2014-10-01T10:22:42.490	ζ Gem	HARPS	red	53026.10	5200	80	1.7	4.9	-0.06	0.26	198	-0.04	0.29	19	-0.05
ADP.2014-10-01T10:19:40.910	ζ Gem	HARPS	red	53028.18	5505	99	1.5	4.9	-0.04	0.22	181	-0.05	0.19	13	-0.04
ADP.2014-10-01T10:20:13.530	ζ Gem	HARPS	red	53028.18	5503	89	1.3	4.9	-0.02	0.23	180	-0.04	0.18	14	-0.03
ADP.2014-10-01T10:19:45.937	ζ Gem	HARPS	red	53029.14	5617	67	1.0	3.3	0.12	0.20	201	0.10	0.19	14	0.11
ADP.2014-10-01T10:19:52.113	ζ Gem	HARPS	red	53029.14	5637	76	1.4	4.1	0.10	0.23	218	0.10	0.18	15	0.10
ADP.2014-10-01T10:19:55.463	ζ Gem	HARPS	red	53031.14	5813	62	1.2	3.1	0.11	0.21	243	0.09	0.18	14	0.10
ADP.2014-10-01T10:22:57.410	ζ Gem	HARPS	red	53031.14	5816	93	1.3	3.1	0.11	0.21	242	0.13	0.18	14	0.12
ADP.2014-10-01T10:20:48.933	ζ Gem	HARPS	red	53031.15	5814	61	1.2	3.0	0.12	0.21	249	0.11	0.18	12	0.11
ADP.2014-10-01T10:21:06.883	ζ Gem	HARPS	red	53032.20	5767	62	1.4	3.0	0.12	0.23	248	0.12	0.18	13	0.12
ADP.2014-10-01T10:22:48.073	ζ Gem	HARPS	red	53032.20	5755	99	1.2	3.1	0.13	0.25	248	0.12	0.17	15	0.12
ADP.2014-10-01T10:22:35.563	ζ Gem	HARPS	red	53032.21	5770	67	1.2	3.0	0.12	0.22	250	0.14	0.26	15	0.13
ADP.2014-10-01T10:19:36.583	ζ Gem	HARPS	red	53033.12	5613	77	1.5	3.7	-0.02	0.24	247	-0.03	0.18	16	-0.03
ADP.2014-10-01T10:20:24.990	ζ Gem	HARPS	red	53033.12	5626	72	1.4	3.4	0.10	0.23	239	0.09	0.19	16	0.10
ADP.2014-10-01T10:21:51.400	ζ Gem	HARPS	red	53033.12	5621	65	1.3	3.2	0.04	0.22	232	0.05	0.18	18	0.05
ADP.2014-10-01T10:19:05.720	ζ Gem	HARPS	red	53034.15	5422	68	1.4	3.3	0.03	0.20	241	0.06	0.21	20	0.04
ADP.2014-10-01T10:22:42.557	ζ Gem	HARPS	red	53034.15	5429	74	1.5	3.5	0.08	0.21	235	0.08	0.22	19	0.08
ADP.2014-10-01T10:23:01.643	ζ Gem	HARPS	red	53034.16	5428	71	1.2	3.0	0.12	0.19	239	0.10	0.20	18	0.11
ADP.2014-10-01T10:20:04.450	ζ Gem	HARPS	red	53035.14	5289	74	1.3	3.2	0.10	0.21	232	0.11	0.26	21	0.10
ADP.2014-10-01T10:20:54.450	ζ Gem	HARPS	red	53035.14	5288	73	1.4	3.6	0.05	0.21	231	0.05	0.26	20	0.05
ADP.2014-10-01T10:22:40.883	ζ Gem	HARPS	red	53035.15	5288	73	1.2	3.1	0.10	0.21	234	0.09	0.26	21	0.09
ADP.2014-10-01T10:21:17.743	ζ Gem	HARPS	red	53036.16	5222	95	1.4	3.6	0.00	0.23	206	0.00	0.28	19	0.00
ADP.2014-10-01T10:21:34.773	ζ Gem	HARPS	red	53036.16	5216	86	1.1	3.3	0.04	0.22	205	0.02	0.28	19	0.03
ADP.2014-10-01T10:19:13.987	ζ Gem	HARPS	red	53037.16	5264	95	1.3	4.9	-0.06	0.26	175	-0.05	0.28	11	-0.06
ADP.2014-10-01T10:23:25.193	ζ Gem	HARPS	red	53037.17	5247	79	1.3	4.9	-0.05	0.25	178	-0.06	0.29	16	-0.05
ADP.2014-10-01T10:20:35.397	Y Oph	HARPS	red	53150.28	5540	96	1.1	3.1	-0.01	0.23	247	0.01	0.27	14	0.00
ADP.2014-10-01T10:19:23.977	Y Oph	HARPS	red	53152.29	5564	100	1.4	3.9	-0.02	0.24	242	-0.01	0.23	12	-0.02
ADP.2014-10-01T10:20:19.440	Y Oph	HARPS	red	53154.25	5628	94	1.3	3.6	-0.02	0.25	235	-0.01	0.24	14	-0.02
ADP.2014-10-01T10:21:38.427	Y Oph	HARPS	red	53156.21	5758	91	1.1	3.6	0.08	0.25	251	0.09	0.24	14	0.08
ADP.2014-10-01T10:20:24.870	Y Oph	HARPS	red	53201.13	5562	99	0.8	2.9	0.13	0.25	246	0.11	0.26	15	0.12
ADP.2014-10-01T10:21:56.237	Y Oph	HARPS	red	53203.14	5524	75	1.1	3.2	-0.02	0.23	241	-0.02	0.27	14	-0.02
ADP.2014-10-01T10:20:27.810	Y Oph	HARPS	red	53216.24	5707	106	0.6	2.8	0.14	0.23	264	0.12	0.24	15	0.13
ADP.2014-09-26T16:54:13.337	Y Oph	HARPS	red	56213.98	5663	99	0.5	2.7	0.13	0.23	254	0.12	0.24	15	0.13
ADP.2014-10-01T10:21:04.037	RS Pup	HARPS	red	53048.11	5083	103	0.4	4.9	-0.03	0.35	107	-0.02	0.34	8	-0.03
ADP.2014-10-01T10:19:21.580	RS Pup	HARPS	red	53052.13	6238	132	2.0	4.9	-0.01	0.34	135	-0.07	0.28	15	-0.04
ADP.2014-10-01T10:20:02.840	RS Pup	HARPS	red	53054.16	6184	135	1.0	3.6	0.18	0.26	160	0.19	0.29	10	0.18
ADP.2014-10-01T10:20:50.620	RS Pup	HARPS	red	53056.18	6037	121	0.8	3.7	0.21	0.24	173	0.22	0.19	8	0.22
ADP.2014-10-01T10:21:40.103	RS Pup	HARPS	red	53058.19	5769	133	0.8	4.9	0.12	0.28	189	0.12	0.27	10	0.12
ADP.2014-10-01T10:23:13.800	RS Pup	HARPS	red	53060.19	5593	100	0.6	4.9	0.13	0.24	188	0.15	0.20	8	0.14
ADP.2014-10-01T10:19:59.250	RS Pup	HARPS	red	53062.17	5438	98	0.5	4.9	0.14	0.28	191	0.14	0.17	10	0.14
ADP.2014-10-01T10:20:47.857	RS Pup	HARPS	red	53064.18	5346	99	0.6	4.9	0.12	0.26	185	0.14	0.22	12	0.13
ADP.2014-10-01T10:19:28.643	RS Pup	HARPS	red	53066.16	5266	97	0.7	4.9	0.10	0.26	199	0.10	0.27	12	0.10
ADP.2014-10-01T10:23:29.943	RS Pup	HARPS	red	53149.98	5206	100	0.6	4.9	0.10	0.24	181	0.09	0.25	10	0.10
ADP.2014-10-01T10:23:14.640	RS Pup	HARPS	red	53151.98	5171	82	0.8	4.9	0.07	0.23	178	0.08	0.25	11	0.07
ADP.2014-10-01T10:22:43.703	RS Pup	HARPS	red	53153.99	5135	99	1.0	4.0	0.14	0.22	179	0.13	0.23	10	0.14
ADP.2014-10-01T10:22:24.580	RS Pup	HARPS	red	53155.97	5089	90	1.0	4.9	0.12	0.24	175	0.14	0.28	13	0.13
ADP.2014-10-01T10:23:15.737	RS Pup	HARPS	red	53155.98	5085	95	0.9	4.9	0.11	0.25	174	0.12	0.27	11	0.11
ADP.2014-10-01T10:20:28.523	X Sgr	HARPS	red	53055.40	6556	190	2.0	2.7	-0.33	0.45	106	-0.44	0.32	15	-0.38
ADP.2014-10-01T10:22:51.013	X Sgr	HARPS	red	53055.41	6726	197	2.0	5.0	-0.38	0.48	112	-0.60	0.23	15	-0.49
ADP.2014-10-01T10:21:38.447	X Sgr	HARPS	red	53056.40	6435	193	2.0	2.0	-0.60	0.44	169	-0.64	0.21	20	-0.62
ADP.2014-10-01T10:22:08.730	X Sgr	HARPS	red	53056.40	6405	204	2.0	3.0	-0.43	0.50	86	-0.55	0.30	15	-0.49
ADP.2014-10-01T10:21:28.753	X Sgr	HARPS	red	53056.41	6412	117	2.0	2.6	-0.62	0.44	173	-0.73	0.29	21	-0.67
ADP.2014-10-01T10:23:10.033	X Sgr	HARPS	red	53056.41	6269	258	1.8	2.1	-0.68	0.45	179	-0.69	0.24	18	-0.68
ADP.2014-10-01T10:22:07.723	X Sgr	HARPS	red	53057.40	6077	112	1.8	2.5	-0.45	0.36	191	-0.46	0.25	23	-0.45
ADP.2014-10-01T10:23:39.343	X Sgr	HARPS	red	53057.41	6112	95	1.7	2.6	-0.46	0.38	196	-0.47	0.19	21	-0.46
ADP.2014-10-01T10:19:16.363	X Sgr	HARPS	red	53058.40	6019	123	2.0	3.9	-0.65	0.50	199	-0.65	0.44	21	-0.65
ADP.2014-10-01T10:20:23.927	X Sgr	HARPS	red	53058.41	6015	158	2.0	3.6	-0.61	0.49	203	-0.64	0.45	20	-0.63
ADP.2014-10-01T10:22:18.243	X Sgr	HARPS	red	53059.41	5974	224	2.0	4.9	-0.33	0.37	164	-0.56	0.36	20	-0.44
ADP.2014-10-01T10:23:20.607	X Sgr	HARPS	red	53059.41	5804	126	2.0	4.9	-0.39	0.42	182	-0.45	0.30	21	-0.42
ADP.2014-10-01T10:19:21.627	X Sgr	HARPS	red	53060.40	5900	266	2.0	2.8	-0.24	0.32	176	-0.49	0.24	17	-0.36
ADP.2014-10-01T10:20:17.583	X Sgr	HARPS	red	53060.40	5807	215	2.0	3.1	-0.40	0.35	180	-0.65	0.29	20	-0.53
ADP.2014-10-01T10:20:45.297	X Sgr	HARPS	red	53061.40	5696	341	2.0	3.4	-0.72	0.49	99	-0.91	0.13	11	-0.82
ADP.2014-10-01T10:22:09.283	X Sgr	HARPS	red	53061.40	6060	125	2.0	3.0	-0.68	0.53	156	-0.84	0.22	12	-0.76
ADP.2014-10-01T10:22:51.900	X Sgr	HARPS	red	53062.40	6168	117	1.3	2.8	-0.58	0.36	143	-0.59	0.28	18	-0.58
ADP.2014-10-01T10:23:18.883	X Sgr	HARPS	red	53062.40	6465	195	2.0	4.9	-0.54	0.43	150	-0.57	0.26	22	-0.55
ADP.2014-10-01T10:21:04.760	X Sgr	HARPS	red	53063.40	6275	149	2.0	2.0	-0.53	0.47	157	-0.82	0.25	16	-0.68
ADP.2014-10-01T10:21:10.540	X Sgr	HARPS	red	53063.41	6370	106	1.7	2.9	-0.56	0.51	171	-0.58	0.45	23	-0.57
ADP.2014-10-01T10:20:36.787	X Sgr	HARPS	red	53064.40	6048	196	1.8	2.0	-0.57	0.44	198	-0.56	0.36	20	-0.57
ADP.2014-10-01T10:20:42.153	X Sgr	HARPS	red	53064.41	5980	117	1.9	2.0	-0.60	0.42	184	-0.61	0.29	22	-0.61
ADP.2014-10-01T10:22:19.133	X Sgr	HARPS	red	53066.40	5750	151	2.0	4.9	-0.62	0.45	172	-0.68	0.26	17	-0.65
ADP.2014-10-01T10:22:39.410	X Sgr	HARPS	red	53066.40	5732	115	2.0	4.4	-0.63	0.42	189	-0.63	0.30	18	-0.63
ADP.2014-09-26T16:51:21.510	X Sgr	HARPS	red	56212.99	6165	99	2.0	2.0	-0.33	0.40	217	-0.42	0.43	21	-0.37
ADP.2014-10-06T10:05:39.787	X Sgr	HARPS	red	56552.00	5669	148	1.9	3.2	-0.62	0.45	185	-0.63	0.32	20	-0.63
ADP.2014-10-01T10:19:06.007	Y Sgr	HARPS	red	53149.29	5405	91	1.2	4.1	-0.06	0.30	147	-0.08	0.21	13	-0.07
ADP.2014-10-01T10:19:59.150	Y Sgr	HARPS	red	53149.30	5447	99	1.3	4.9	-0.03	0.32	149	-0.02	0.27	12	-0.03
ADP.2014-10-01T10:21:50.593	Y Sgr	HARPS	red	53150.29	5672	120	2.0	4.9	-0.04	0.31	106	-0.03	0.18	10	-0.04
ADP.2014-10-01T10:23:24.960	Y Sgr	HARPS	red	53150.29	5602	193	1.8	4.9	-0.04	0.24	105	-0.06	0.17	10	-0.05
ADP.2014-10-01T10:19:48.923	Y Sgr	HARPS	red	53151.24	6239	145	2.0	3.4	0.09	0.23	150	0.11	0.22	17	0.10
ADP.2014-10-01T10:23:22.147	Y Sgr	HARPS	red	53151.25	6339	100	2.0	3.1	0.17	0.23	143	0.13	0.11	14	0.15
ADP.2014-10-01T10:19:23.310	Y Sgr	HARPS	red	53152.30	6049	131	2.0	4.4	0.00	0.26	177	0.00	0.17	15	0.00
ADP.2014-10-01T10:19:26.353	Y Sgr	HARPS	red	53152.30	6036	104	2.0	4.2	-0.02	0.28	186	-0.03	0.20	17	-0.03
ADP.2014-10-01T10:19:57.397	Y Sgr	HARPS	red	53156.32	5891	208	1.9	4.9	0.08	0.23	109	0.10	0.23	9	0.09
ADP.2014-10-01T10:22:30.910	Y Sgr	HARPS	red	53156.33	5906	201	2.0	3.7	0.12	0.21	101	0.10	0.16	10	0.11
ADP.2014-10-01T10:20:13.170	Y Sgr	HARPS	red	53202.15	5616	164	1.8	4.9	-0.05	0.26	119	-0.06	0.15	11	-0.05
ADP.2014-10-01T10:20:36.747	Y Sgr	HARPS	red	53202.15	5613	125	1.6	4.4	-0.04	0.25	118	-0.03	0.11	8	-0.04
ADP.2014-10-01T10:19:57.470	Y Sgr	HARPS	red	53203.15	6305	99	2.0	3.3	0.16	0.23	146	0.10	0.21	15	0.13
ADP.2014-10-01T10:21:42.943	Y Sgr	HARPS	red	53203.15	6249	106	2.0	3.7	0.10	0.23	146	0.09	0.24	16	0.09
ADP.2014-10-01T10:19:33.267	Y Sgr	HARPS	red	53204.12	6112	99	1.9	4.1	0.11	0.32	191	0.11	0.15	16	0.11
ADP.2014-10-01T10:22:57.317	Y Sgr	HARPS	red	53204.12	6132	140	2.0	4.9	-0.06	0.33	181	-0.07	0.23	16	-0.07
ADP.2014-10-01T10:19:54.937	Y Sgr	HARPS	red	53205.16	5728	87	2.0	4.9	0.00	0.25	196	-0.13	0.23	16	-0.06
ADP.2014-09-26T16:54:49.173	Y Sgr	HARPS	red	56212.99	5734	98	1.9	4.9	-0.04	0.30	196	-0.06	0.25	17	-0.05
ADP.2014-09-26T16:52:07.950	Y Sgr	HARPS	red	56240.00	6249	97	2.0	5.0	0.08	0.31	184	-0.01	0.19	15	0.04
ADP.2014-10-01T10:23:03.403	R TrA	HARPS	red	53150.14	5934	143	2.0	4.9	0.01	0.24	138	-0.16	0.22	13	-0.08
ADP.2014-10-01T10:20:53.017	R TrA	HARPS	red	53150.15	5910	143	2.0	4.9	-0.01	0.23	129	-0.18	0.22	17	-0.10
ADP.2014-10-01T10:22:05.127	R TrA	HARPS	red	53152.14	5814	94	1.9	3.4	-0.02	0.23	196	-0.01	0.24	20	-0.02
ADP.2014-10-01T10:20:00.543	R TrA	HARPS	red	53152.15	5824	95	1.8	3.2	0.04	0.22	200	0.06	0.15	21	0.05
ADP.2014-10-01T10:20:49.807	R TrA	HARPS	red	53154.14	6467	84	2.0	3.7	-0.02	0.24	166	-0.11	0.20	21	-0.06
ADP.2014-10-01T10:22:04.773	R TrA	HARPS	red	53154.15	6452	96	2.0	2.9	0.06	0.23	168	-0.01	0.24	19	0.02
ADP.2014-10-01T10:19:19.927	R TrA	HARPS	red	53156.14	5698	102	2.0	4.9	-0.10	0.27	170	-0.07	0.24	19	-0.09
ADP.2014-10-01T10:20:01.507	R TrA	HARPS	red	53156.15	5745	96	2.0	4.8	-0.01	0.23	155	0.00	0.19	17	0.00
ADP.2014-10-01T10:23:31.460	R TrA	HARPS	red	53201.03	5966	109	2.0	4.3	0.03	0.22	129	0.00	0.21	16	0.01
ADP.2014-10-01T10:22:15.857	R TrA	HARPS	red	53202.03	6277	80	2.0	3.5	0.01	0.28	172	-0.08	0.25	21	-0.03
ADP.2014-10-01T10:20:44.903	R TrA	HARPS	red	53203.05	5799	100	2.0	3.5	0.00	0.24	200	0.02	0.16	21	0.01
ADP.2014-10-01T10:22:41.683	R TrA	HARPS	red	53204.01	5836	97	2.0	4.9	0.04	0.25	149	-0.11	0.18	14	-0.03

ADP.2014-10-01T10:20:37.110	R TrA	HARPS	red	53205.04	6450	98	2.0	3.5	0.00	0.24	167	-0.08	0.20	22	-0.04
ADP.2014-10-01T10:20:58.203	R TrA	HARPS	red	53206.03	5941	79	1.8	2.8	0.13	0.24	199	0.12	0.29	19	0.12
ADP.2014-10-01T10:23:31.687	RZ Vel	HARPS	red	53149.99	5321	97	0.7	3.3	0.12	0.22	218	0.15	0.29	13	0.14
ADP.2014-10-01T10:19:16.737	RZ Vel	HARPS	red	53152.01	5163	97	1.2	4.1	0.07	0.22	209	0.06	0.21	11	0.06
ADP.2014-10-01T10:21:54.067	RZ Vel	HARPS	red	53154.00	5041	78	1.3	4.9	0.05	0.25	175	0.05	0.31	13	0.05
ADP.2014-10-01T10:20:36.780	RZ Vel	HARPS	red	53155.99	4981	85	1.6	4.9	-0.03	0.30	138	-0.04	0.47	11	-0.03
ADP.2014-10-01T10:23:18.300	RZ Vel	HARPS	red	53200.95	5409	106	1.0	4.9	0.06	0.28	123	0.06	0.23	10	0.06
ADP.2014-10-01T10:20:20.600	RZ Vel	HARPS	red	53201.95	5422	100	0.9	4.9	0.04	0.28	171	0.07	0.17	10	0.06
ADP.2014-10-01T10:22:09.087	RZ Vel	HARPS	red	53202.95	6245	98	1.2	3.8	0.10	0.25	153	0.09	0.27	14	0.09
ADP.2014-10-01T10:19:17.420	RZ Vel	HARPS	red	53203.94	6314	192	1.2	5.0	0.05	0.36	182	0.05	0.31	10	0.05
ADP.2014-10-01T10:21:30.200	RZ Vel	HARPS	red	53204.94	6474	120	1.4	4.9	0.01	0.30	180	-0.01	0.21	12	0.00
ADP.2014-10-01T10:20:40.817	RZ Vel	HARPS	red	53205.94	6225	100	1.5	4.9	0.16	0.30	155	0.16	0.20	11	0.16
ADP.2014-10-06T10:07:21.373	RZ Vel	HARPS	red	56606.19	5308	110	1.6	4.9	0.10	0.46	99	0.11	0.49	8	0.10
FEROS.2010-03-29T02:24:34.361	T Ant	FEROS	single	55284.10	6301	183	2.0	5.0	-0.28	0.35	125	-0.29	0.31	10	-0.29
FEROS.2005-05-30T06:41:48.494	SZ Aql	FEROS	single	53520.28	4983	126	1.4	4.9	-0.14	0.46	113	-0.13	0.94	8	-0.13
FEROS.2005-09-07T01:27:47.700	V340 Ara	FEROS	single	53620.06	5921	154	2.0	4.9	0.13	0.56	163	0.00	0.41	6	0.07
FEROS.2010-03-31T05:40:43.377	AQ Car	FEROS	single	55286.24	5813	88	1.8	4.9	-0.05	0.33	160	-0.05	0.15	8	-0.05
FEROS.2010-03-31T04:47:58.864	CN Car	FEROS	single	55286.20	6284	100	2.0	5.0	-0.10	0.40	168	-0.16	0.31	16	-0.13
FEROS.2010-03-31T05:04:29.711	CN Car	FEROS	single	55286.21	6282	89	2.0	5.0	-0.08	0.40	161	-0.16	0.28	13	-0.12
FEROS.2010-03-31T05:21:00.699	CN Car	FEROS	single	55286.22	6292	95	2.0	5.0	0.03	0.40	164	-0.02	0.12	10	0.00
FEROS.2010-03-30T05:13:46.558	CY Car	FEROS	single	55285.22	6042	86	1.9	3.8	0.08	0.33	166	0.09	0.34	12	0.08
FEROS.2010-04-01T04:23:21.309	DY Car	FEROS	single	55287.18	6467	97	2.0	3.2	0.14	0.42	148	0.05	0.23	17	0.09
FEROS.2010-04-01T04:46:32.522	DY Car	FEROS	single	55287.20	6449	94	2.0	5.0	0.05	0.45	150	-0.11	0.19	12	-0.03
FEROS.2010-04-01T05:09:43.434	DY Car	FEROS	single	55287.22	6514	92	2.0	5.0	0.07	0.40	130	-0.08	0.30	12	0.00
FEROS.2010-03-26T05:59:52.394	ER Car	FEROS	single	55281.25	5828	98	1.8	4.3	-0.04	0.26	127	-0.03	0.11	12	-0.04
FEROS.2004-05-31T01:58:03.236	EY Car	FEROS	single	53156.08	6006	207	2.0	4.9	-0.10	0.43	183	-0.28	0.27	22	-0.19
FEROS.2004-06-02T01:14:50.908	EY Car	FEROS	single	53158.05	5863	172	2.0	3.4	-0.05	0.34	169	-0.06	0.28	14	-0.06
FEROS.2010-03-28T04:22:09.822	FI Car	FEROS	single	55283.18	5150	97	1.5	4.9	-0.12	0.48	126	-0.11	0.46	13	-0.11
FEROS.2010-03-28T04:53:46.308	FI Car	FEROS	single	55283.20	5139	104	1.6	4.9	-0.04	0.45	128	-0.06	0.39	9	-0.05
FEROS.2010-03-28T05:25:23.404	FI Car	FEROS	single	55283.23	5152	99	1.5	4.9	-0.03	0.46	121	-0.02	0.31	11	-0.03
FEROS.2010-03-30T05:46:13.761	FO Car	FEROS	single	55285.24	3944	168	0.5	4.8	-0.82	0.53	187	-0.83	0.84	14	-0.82
FEROS.2010-03-30T06:07:06.048	FO Car	FEROS	single	55285.25	3959	161	0.5	2.1	-0.56	0.49	183	-0.56	0.93	13	-0.56
FEROS.2010-03-30T07:44:09.032	FO Car	FEROS	single	55285.32	3949	338	0.0	2.4	-0.72	0.48	188	-0.71	0.87	13	-0.71
FEROS.2010-03-30T08:08:19.640	FO Car	FEROS	single	55285.34	3927	136	0.0	2.6	-0.72	0.54	195	-0.40	0.77	15	-0.56
FEROS.2011-04-16T02:19:12.265	FO Car	FEROS	single	55667.10	5739	99	1.6	4.9	-0.03	0.46	178	-0.02	0.28	10	-0.03
FEROS.2011-04-17T02:32:42.006	FO Car	FEROS	single	55668.11	5491	99	1.3	4.0	0.02	0.38	169	0.01	0.18	10	0.02
FEROS.2011-04-18T03:59:32.921	FO Car	FEROS	single	55669.17	5273	78	1.7	4.9	-0.02	0.39	162	-0.01	0.37	16	-0.01
FEROS.2011-04-19T06:44:04.166	FO Car	FEROS	single	55670.28	5092	86	1.3	4.9	-0.06	0.45	150	-0.06	0.32	12	-0.06
FEROS.2010-03-25T05:45:03.243	FR Car	FEROS	single	55280.24	5909	98	1.8	4.9	0.00	0.34	143	-0.01	0.16	8	-0.01
FEROS.2010-03-25T04:58:17.988	GH Car	FEROS	single	55280.21	6329	100	1.8	5.0	-0.06	0.36	146	-0.08	0.06	7	-0.07
FEROS.2010-03-30T04:24:09.084	GX Car	FEROS	single	55285.18	6304	94	1.7	3.3	-0.03	0.35	144	0.00	0.11	11	-0.02
FEROS.2004-05-31T01:21:01.473	GZ Car	FEROS	single	53156.06	5983	99	1.4	2.5	0.15	0.23	363	0.15	0.24	31	0.15
FEROS.2004-06-02T01:52:07.763	GZ Car	FEROS	single	53158.08	5884	100	1.6	2.5	0.11	0.23	373	0.12	0.31	31	0.11
FEROS.2010-03-26T05:07:06.000	HW Car	FEROS	single	55281.21	5686	97	1.4	3.7	0.00	0.33	159	0.00	0.58	13	0.00
FEROS.2010-03-27T04:48:50.085	IO Car	FEROS	single	55282.20	6148	100	1.2	2.5	0.17	0.33	193	0.16	0.14	7	0.16
FEROS.2010-03-27T05:08:02.631	IO Car	FEROS	single	55282.21	6055	100	1.2	3.0	0.09	0.35	192	0.10	0.11	8	0.09
FEROS.2010-03-27T05:27:13.156	IO Car	FEROS	single	55282.23	6074	99	1.8	4.9	-0.06	0.41	203	-0.08	0.13	9	-0.07
FEROS.2010-03-25T05:35:45.372	IT Car	FEROS	single	55280.23	5795	81	1.8	4.9	0.03	0.34	152	0.03	0.12	10	0.03
FEROS.2010-03-25T03:22:02.130	l Car	FEROS	single	55280.14	5277	99	1.2	4.9	-0.01	0.31	132	0.00	1.14	10	-0.01
FEROS.2010-03-31T06:59:30.281	SX Car	FEROS	single	55286.29	6505	86	1.8	2.4	0.01	0.35	128	0.02	0.28	14	0.01
FEROS.2010-03-25T05:14:27.544	U Car	FEROS	single	55280.22	4966	132	0.9	4.9	-0.18	0.47	96	-0.17	0.53	9	-0.17
FEROS.2010-03-25T04:02:02.560	UW Car	FEROS	single	55280.17	6562	92	2.0	3.9	-0.11	0.36	129	-0.10	0.29	12	-0.10
FEROS.2010-04-01T04:07:37.036	UX Car	FEROS	single	55287.17	6426	98	2.0	3.1	0.11	0.32	152	0.07	0.11	12	0.09
FEROS.2010-03-30T04:58:29.048	UY Car	FEROS	single	55285.21	6383	112	2.0	5.0	-0.04	0.39	123	-0.17	0.31	13	-0.10
FEROS.2010-03-31T06:23:33.917	UZ Car	FEROS	single	55286.27	6042	95	2.0	4.9	-0.05	0.45	139	-0.06	0.55	12	-0.06
FEROS.2010-03-31T00:47:14.614	V Car	FEROS	single	55286.03	5912	99	1.9	4.9	-0.06	0.29	138	-0.04	0.11	9	-0.05
FEROS.2010-03-25T03:41:12.012	V397 Car	FEROS	single	55280.15	6021	95	2.0	4.9	-0.02	0.39	152	-0.03	0.19	13	-0.03
FEROS.2010-03-31T06:45:11.048	VY Car	FEROS	single	55286.28	4868	101	0.3	4.9	0.05	0.47	57	0.03	0.22	6	0.04
FEROS.2010-03-31T06:52:12.633	VY Car	FEROS	single	55286.29	4864	103	0.4	4.9	0.03	0.37	52	0.02	0.30	6	0.03
FEROS.2010-03-27T02:28:41.363	WW Car	FEROS	single	55282.10	5913	134	2.0	4.9	-0.10	0.40	145	-0.13	0.18	14	-0.11
FEROS.2010-03-26T05:39:29.861	WZ Car	FEROS	single	55281.24	5666	202	1.0	4.9	-0.20	0.49	133	-0.20	0.18	8	-0.20
FEROS.2010-03-25T04:22:48.137	XX Car	FEROS	single	55280.18	5926	113	1.1	4.9	0.05	0.37	160	0.06	0.06	5	0.05
FEROS.2010-03-25T04:40:17.350	XY Car	FEROS	single	55280.19	5769	99	1.7	4.9	-0.10	0.41	157	-0.08	0.58	11	-0.09
FEROS.2010-04-01T05:37:29.936	XZ Car	FEROS	single	55287.23	6203	91	2.0	4.9	0.10	0.36	127	0.11	0.24	11	0.11
FEROS.2004-05-30T22:52:42.838	Y Car	FEROS	single	53155.95	5888	100	1.7	2.2	0.04	0.21	400	0.06	0.24	34	0.05
FEROS.2004-06-02T03:12:50.643	Y Car	FEROS	single	53158.13	6613	109	1.6	2.6	-0.05	0.27	302	-0.05	0.32	34	-0.05
FEROS.2010-03-31T05:55:07.812	YZ Car	FEROS	single	55286.25	5611	99	1.2	4.9	-0.08	0.36	147	-0.06	0.16	9	-0.07
FEROS.2010-03-30T06:31:17.266	AY Cen	FEROS	single	55285.27	5895	67	1.5	3.7	0.00	0.37	164	-0.03	0.09	12	-0.02
FEROS.2010-03-27T05:50:26.417	AZ Cen	FEROS	single	55282.24	6387	76	1.8	2.1	0.10	0.32	164	0.12	0.21	12	0.11
FEROS.2010-03-31T07:53:01.181	BB Cen	FEROS	single	55286.33	6157	99	1.3	2.8	0.15	0.31	181	0.14	0.25	13	0.15
FEROS.2004-05-31T03:15:16.240	BK Cen	FEROS	single	53156.14	5893	98	2.0	3.8	0.06	0.29	325	0.07	0.31	30	0.06
FEROS.2004-06-02T05:04:53.367	BK Cen	FEROS	single	53158.21	5778	99	1.7	2.7	0.15	0.26	362	0.16	0.26	31	0.16
FEROS.2010-03-25T06:08:17.415	KK Cen	FEROS	single	55280.26	5838	100	1.5	4.9	0.00	0.39	161	0.00	0.52	10	0.00
FEROS.2010-03-25T06:34:49.718	KK Cen	FEROS	single	55280.27	5862	98	1.8	4.9	-0.01	0.37	153	0.00	0.26	10	-0.01
FEROS.2010-03-25T07:01:21.771	KK Cen	FEROS	single	55280.29	5884	99	1.5	5.0	0.14	0.37	180	0.12	0.39	8	0.13
FEROS.2010-03-26T06:29:40.579	MZ Cen	FEROS	single	55281.27	5720	105	1.0	4.9	0.10	0.44	159	0.09	1.04	10	0.09
FEROS.2010-03-26T07:01:12.674	MZ Cen	FEROS	single	55281.29	5763	115	1.3	4.9	0.11	0.44	145	0.09	0.11	9	0.10
FEROS.2010-03-26T07:32:43.099	MZ Cen	FEROS	single	55281.31	5754	99	1.3	4.9	0.11	0.48	162	0.11	0.29	10	0.11
FEROS.2010-03-27T07:10:04.046	QY Cen	FEROS	single	55282.30	6210	98	1.8	4.9	0.14	0.38	126	0.14	0.25	6	0.14
FEROS.2010-03-27T07:45:06.574	QY Cen	FEROS	single	55282.32	6244	99	2.0	4.9	0.19	0.37	128	0.17	0.12	6	0.18
FEROS.2010-03-27T08:20:07.282	QY Cen	FEROS	single	55282.35	6228	97	1.6	4.9	0.11	0.38	118	0.12	0.25	8	0.11
FEROS.2007-03-31T06:30:15.282	TX Cen	FEROS	single	54190.27	4841	93	0.0	4.9	0.16	0.42	87	0.24	0.38	6	0.20
FEROS.2007-03-31T07:01:05.471	TX Cen	FEROS	single	54190.29	4830	89	0.2	4.9	0.18	0.37	98	0.16	0.47	7	0.17
FEROS.2004-05-31T03:55:48.499	UZ Cen	FEROS	single	53156.16	6313	97	1.4	2.2	0.06	0.24	342	0.05	0.32	34	0.05
FEROS.2004-06-02T03:43:11.313	UZ Cen	FEROS	single	53158.15	5840	96	1.8	3.4	-0.01	0.24	316	0.00	0.28	33	-0.01
FEROS.2010-03-28T09:42:34.409	V Cen	FEROS	single	55283.40	5504	139	1.5	4.9	-0.18	0.39	148	-0.16	0.21	14	-0.17
FEROS.2010-03-29T08:15:47.770	V Cen	FEROS	single	55284.34	6452	93	2.0	3.9	-0.01	0.35	132	-0.06	0.23	15	-0.04
FEROS.2010-03-25T08:44:40.216	V339 Cen	FEROS	single	55280.36	5918	89	1.2	3.3	0.12	0.28	159	0.12	0.59	9	0.12
FEROS.2010-03-30T08:48:22.522	V378 Cen	FEROS	single	55285.37	6168	75	1.3	3.1	0.03	0.35	183	0.02	0.39	12	0.02
FEROS.2010-04-01T06:28:32.252	V381 Cen	FEROS	single	55287.27	6232	105	2.0	4.9	-0.04	0.35	145	-0.14	0.09	9	-0.09
FEROS.2010-04-01T05:50:30.612	V419 Cen	FEROS	single	55287.24	6291	96	1.6	5.0	-0.01	0.48	147	-0.01	0.24	6	-0.01
FEROS.2010-03-29T07:39:23.022	V496 Cen	FEROS	single	55284.32	6193	94	2.0	4.0	0.00	0.39	153	-0.03	0.13	11	-0.01
FEROS.2010-04-01T06:23:41.569	V659 Cen	FEROS	single	55287.27	6072	80	1.7	4.9	-0.06	0.42	152	-0.05	0.12	12	-0.06
FEROS.2010-04-01T06:35:12.135	V737 Cen	FEROS	single	55287.27	5845	80	1.6	4.1	0.09	0.29	155	0.07	0.10	8	0.08
FEROS.2007-03-27T04:16:22.763	VW Cen	FEROS	single	54186.18	5311	107	1.4	4.9	-0.04	0.52	123	-0.06	0.64	12	-0.05
FEROS.2010-03-30T09:03:51.703	XX Cen	FEROS	single	55285.38	5924	98	1.8	4.9	0.10	0.35	150	0.11	0.46	7	0.10
FEROS.2010-03-30T09:14:22.452	AV Cir	FEROS	single	55285.38	6143	97	1.6	2.0	0.18	0.28	189	0.17	0.21	17	0.18
FEROS.2010-03-28T10:07:23.359	AX Cir	FEROS	single	55283.42	5576	130	1.7	4.9	-0.26	0.42	128	-0.26	0.14	15	-0.26
FEROS.2010-03-30T09:22:26.125	AX Cir	FEROS	single	55285.39	5745	79	1.5	3.1	-0.09	0.35	158	-0.07	0.11	10	-0.08
FEROS.2010-04-01T06:46:04.847	BP Cir	FEROS	single	55287.28	6549	102	2.0	2.3	-0.09	0.37	166	-0.07	0.17	18	-0.08
FEROS.2007-04-01T02:22:23.845	AO Cma	FEROS	single	54191.10	5875	250	1.9	5.0	-0.23	0.52	190	-0.22	0.26	9	-0.23
FEROS.2012-12-28T07:01:31.754	SS Cma	FEROS	single	56289.29	5378	97	1.4	4.9	-0.20	0.51	192	-0.21	0.24	12	-0.21
FEROS.2012-12-28T06:46:59.520	TV Cma	FEROS	single	56289.28	5702	100	1.8	3.9	-0.01	0.44	190	-0.02	0.18	18	-0.01
FEROS.2010-03-27T06:03:31.532	AD Cru	FEROS	single	55282.25	5961	96	1.6	3.5	0.09	0.33	183	0.11	0.08	11	0.10
FEROS.2010-03-27T06:27:02.376	AD Cru	FEROS	single	55282.27	5957	93	1.7	4.9	-0.07	0.35	177	-0.09	0.18	13	-0.08
FEROS.2010-03-27T06:45:54.458	AD Cru	FEROS	single	55282.28	5962	94	1.9	4.1	-0.02	0.36	186	-0.02	0.12	11	-0.02
FEROS.2010-03-29T07:18:38.828	AG Cru	FEROS	single	55284.30	6672	80	2.0	4.7	-0.09	0.33	132	-0.23	0.24	11	-0.16
FEROS.2010-03-28T08:00:43.295	R Cru	FEROS	single	55283.33	6214	65	1.4	2.5	0.14	0.25	145	0.15	0.18	11	0.14

FEROS.2010-03-29T07:33:59.167	S Cru	FEROS	single	55284.32	6472	93	1.9	3.1	-0.04	0.38	137	-0.04	0.33	13	-0.04
FEROS.2010-03-29T06:13:39.144	SU Cru	FEROS	single	55284.26	4039	175	0.0	4.8	-0.99	0.61	165	-0.98	0.68	15	-0.98
FEROS.2011-04-17T05:03:50.372	SU Cru	FEROS	single	55668.21	3984	182	1.1	4.9	-0.78	0.65	152	-0.78	0.65	13	-0.78
FEROS.2010-03-30T07:24:04.421	T Cru	FEROS	single	55285.31	5929	86	1.7	4.9	0.08	0.35	143	0.06	0.09	7	0.07
FEROS.2010-03-29T06:54:28.129	VW Cru	FEROS	single	55284.29	5830	64	1.9	4.9	-0.03	0.33	150	-0.04	0.22	12	-0.04
FEROS.2010-03-30T08:35:22.467	X Cru	FEROS	single	55285.36	5919	84	1.7	3.8	-0.02	0.37	160	-0.01	0.10	9	-0.02
FEROS.2010-03-28T08:19:39.978	GH Lup	FEROS	single	55283.35	5420	92	1.4	4.9	-0.02	0.33	137	-0.02	0.19	10	-0.02
FEROS.2007-04-01T01:16:15.131	TW Mon	FEROS	single	54191.05	5593	487	1.9	4.9	-0.27	0.63	214	-0.27	0.39	13	-0.27
FEROS.2007-04-01T01:47:05.849	TW Mon	FEROS	single	54191.07	5667	215	2.0	5.0	-0.31	0.65	214	-0.41	0.57	16	-0.36
FEROS.2007-04-01T00:12:06.041	V510 Mon	FEROS	single	54191.01	5342	98	1.6	4.9	-0.19	0.53	193	-0.18	0.61	13	-0.19
FEROS.2007-04-01T00:42:57.418	V510 Mon	FEROS	single	54191.03	5345	98	1.6	4.9	-0.23	0.48	164	-0.24	0.36	15	-0.23
FEROS.2010-03-29T07:28:47.954	R Mus	FEROS	single	55284.31	5957	85	1.5	3.4	0.04	0.30	142	0.03	0.25	11	0.03
FEROS.2010-03-31T07:18:48.517	RT Mus	FEROS	single	55286.30	6237	85	1.8	2.1	0.16	0.30	162	0.17	0.17	12	0.17
FEROS.2010-03-29T06:02:51.874	S Mus	FEROS	single	55284.25	5725	91	1.2	3.4	-0.01	0.31	153	0.01	0.15	11	0.00
FEROS.2010-03-29T06:07:11.012	S Mus	FEROS	single	55284.25	5743	73	1.5	4.9	-0.07	0.37	150	-0.08	0.15	11	-0.08
FEROS.2010-03-28T06:17:20.291	TZ Mus	FEROS	single	55283.26	6376	109	1.9	5.0	-0.11	0.48	172	-0.12	0.30	10	-0.11
FEROS.2010-03-28T06:49:50.993	TZ Mus	FEROS	single	55283.28	6304	157	2.0	5.0	-0.09	0.50	183	-0.12	0.30	13	-0.10
FEROS.2010-03-28T07:22:36.917	TZ Mus	FEROS	single	55283.31	6268	189	2.0	5.0	-0.03	0.54	169	-0.10	0.32	13	-0.07
FEROS.2010-03-25T07:31:25.197	UU Mus	FEROS	single	55280.31	6138	97	2.0	4.9	-0.11	0.40	128	-0.39	0.71	15	-0.25
FEROS.2010-03-27T09:09:00.240	GU Nor	FEROS	single	55282.38	6011	98	1.6	2.9	0.20	0.32	176	0.21	0.19	11	0.20
FEROS.2007-03-30T05:05:10.103	QZ Nor	FEROS	single	54189.21	5742	111	2.0	4.9	0.11	0.42	164	0.03	0.28	18	0.07
FEROS.2007-03-31T07:34:08.233	RS Nor	FEROS	single	54190.32	5463	75	1.8	4.9	0.10	0.35	153	0.12	0.21	13	0.11
FEROS.2007-03-31T08:04:59.882	RS Nor	FEROS	single	54190.34	5469	90	1.4	3.8	0.15	0.36	149	0.13	0.20	12	0.14
FEROS.2010-03-30T09:33:02.694	S Nor	FEROS	single	55285.40	5842	67	1.5	3.5	0.18	0.30	151	0.19	0.09	7	0.18
FEROS.2010-03-26T08:21:32.307	SY Nor	FEROS	single	55281.35	5480	97	1.0	4.9	0.04	0.39	141	0.04	0.51	8	0.04
FEROS.2010-04-01T07:10:52.140	TW Nor	FEROS	single	55287.30	5932	151	1.4	4.9	0.14	0.38	145	0.15	0.14	6	0.14
FEROS.2010-04-01T07:42:44.849	TW Nor	FEROS	single	55287.32	5979	97	1.7	4.9	0.34	0.34	109	0.32	0.07	5	0.33
FEROS.2010-04-01T08:14:35.438	TW Nor	FEROS	single	55287.34	5928	113	1.7	4.9	0.31	0.36	124	0.32	0.26	6	0.32
FEROS.2010-04-01T06:52:35.300	U Nor	FEROS	single	55287.29	5377	99	1.0	3.1	0.15	0.36	181	0.15	0.27	13	0.15
FEROS.2010-04-01T08:50:31.264	BF Oph	FEROS	single	55287.37	6255	92	2.0	4.1	-0.05	0.35	153	-0.10	0.21	11	-0.08
FEROS.2010-03-31T00:40:12.588	AP Pup	FEROS	single	55286.03	6229	98	1.8	3.8	-0.07	0.37	153	-0.07	0.15	15	-0.07
FEROS.2010-03-29T00:30:11.116	AT Pup	FEROS	single	55284.02	6428	98	1.9	3.7	-0.07	0.29	132	-0.05	0.22	14	-0.06
FEROS.2010-03-31T01:22:52.056	CE Pup	FEROS	single	55286.06	5750	115	1.0	4.9	-0.08	0.36	121	-0.08	0.22	8	-0.08
FEROS.2010-03-31T01:58:44.451	CE Pup	FEROS	single	55286.08	5826	192	0.6	3.7	-0.02	0.43	114	-0.06	0.22	7	-0.04
FEROS.2010-03-31T02:34:37.174	CE Pup	FEROS	single	55286.11	5818	173	1.3	4.9	-0.05	0.39	127	-0.05	0.32	7	-0.05
FEROS.2012-12-28T07:10:51.685	EK Pup	FEROS	single	56289.30	6262	268	2.0	3.6	-0.08	0.47	209	-0.21	0.25	15	-0.15
FEROS.2007-03-30T01:57:14.897	HW Pup	FEROS	single	54189.08	5326	210	1.7	4.9	-0.50	0.65	205	-0.49	0.42	14	-0.49
FEROS.2010-03-25T01:57:22.397	MY Pup	FEROS	single	55280.08	6304	100	1.2	2.0	0.00	0.28	163	-0.02	0.33	15	-0.01
FEROS.2010-03-26T01:23:39.013	NT Pup	FEROS	single	55281.06	5545	102	1.5	4.9	-0.19	0.42	164	-0.18	0.52	13	-0.19
FEROS.2010-03-26T02:10:41.380	NT Pup	FEROS	single	55281.09	5589	121	1.5	4.9	-0.17	0.40	161	-0.18	0.39	12	-0.18
FEROS.2010-03-26T02:57:43.246	NT Pup	FEROS	single	55281.12	5556	98	1.3	4.9	-0.18	0.41	166	-0.20	0.25	10	-0.19
FEROS.2004-06-01T22:38:25.303	VX Pup	FEROS	single	53157.94	6426	98	1.9	2.6	-0.09	0.22	284	-0.08	0.31	32	-0.09
FEROS.2012-12-28T07:49:50.400	WY Pup	FEROS	single	56289.33	6248	273	2.0	5.0	-0.27	0.54	209	-0.32	0.31	14	-0.30
FEROS.2005-05-30T06:12:51.724	KQ Sco	FEROS	single	53520.26	4731	118	0.7	4.9	-0.06	0.60	86	-0.06	0.65	6	-0.06
FEROS.2007-03-30T06:13:41.984	KQ Sco	FEROS	single	54189.26	5540	145	1.2	4.9	0.00	0.46	107	0.01	0.79	10	0.00
FEROS.2010-03-29T08:22:48.895	RV Sco	FEROS	single	55284.35	6167	79	1.9	3.3	0.15	0.32	134	0.15	0.27	11	0.15
FEROS.2010-03-29T08:30:23.805	V482 Sco	FEROS	single	55284.35	6091	72	1.6	3.3	0.13	0.32	159	0.12	0.08	10	0.12
FEROS.2010-04-01T08:56:41.565	V636 Sco	FEROS	single	55287.37	5316	90	1.3	4.9	-0.07	0.41	152	-0.07	0.30	14	-0.07
FEROS.2010-03-30T09:38:47.951	V950 Sco	FEROS	single	55285.40	6310	93	1.4	2.7	0.07	0.32	178	0.08	0.17	14	0.08
FEROS.2011-05-14T06:39:50.297	CN Sct	FEROS	single	55695.28	5309	194	0.7	4.9	-0.17	0.66	180	-0.17	0.70	11	-0.17
FEROS.2005-08-20T03:21:42.361	EV Sct	FEROS	single	53602.14	5898	566	2.0	5.0	-0.19	0.73	243	-0.42	1.05	17	-0.30
FEROS.2005-08-21T03:23:22.751	EV Sct	FEROS	single	53603.14	6409	670	2.0	5.0	0.10	0.72	223	-0.40	0.47	15	-0.15
FEROS.2005-09-03T02:33:14.680	EV Sct	FEROS	single	53616.11	5839	419	2.0	5.0	-0.25	0.76	236	-0.90	0.65	13	-0.58
FEROS.2005-09-08T00:46:20.011	EV Sct	FEROS	single	53621.03	6037	260	2.0	5.0	-0.24	0.65	227	-0.64	0.50	15	-0.44
FEROS.2007-03-30T08:29:16.644	EV Sct	FEROS	single	54189.35	6070	121	2.0	5.0	-0.21	0.44	141	-0.36	0.27	14	-0.28
FEROS.2007-03-30T09:00:09.012	EV Sct	FEROS	single	54189.38	6146	98	2.0	5.0	-0.09	0.50	148	-0.17	0.29	15	-0.13
FEROS.2004-05-31T07:28:43.848	EW Sct	FEROS	single	53156.31	5686	71	1.5	3.2	0.04	0.26	316	0.04	0.25	29	0.04
FEROS.2004-06-01T10:29:26.199	EW Sct	FEROS	single	53157.44	5970	79	1.5	3.2	-0.04	0.25	276	-0.03	0.27	28	-0.04
FEROS.2004-06-02T10:00:20.131	EW Sct	FEROS	single	53158.42	6372	84	1.6	2.8	0.03	0.27	290	0.02	0.22	32	0.03
FEROS.2011-05-14T06:26:43.910	RU Sct	FEROS	single	55695.27	5226	100	0.9	4.9	-0.01	0.39	141	-0.01	0.41	10	-0.01
FEROS.2011-05-14T06:52:56.591	TY Sct	FEROS	single	55695.29	5490	144	1.8	4.9	0.15	0.45	171	0.18	0.51	8	0.16
FEROS.2007-03-31T08:38:46.919	UZ Sct	FEROS	single	54190.36	4824	121	1.3	4.9	0.07	0.43	83	0.08	0.49	11	0.07
FEROS.2007-03-31T09:09:39.317	UZ Sct	FEROS	single	54190.38	4822	99	1.3	4.9	0.00	0.42	87	0.02	0.41	9	0.01
FEROS.2004-05-31T08:06:00.321	V367 Sct	FEROS	single	53156.34	6089	107	2.0	4.9	-0.02	0.36	304	-0.09	0.33	25	-0.06
FEROS.2004-05-31T08:36:53.705	V367 Sct	FEROS	single	53156.36	6050	135	1.7	4.9	-0.02	0.34	298	-0.01	0.24	23	-0.02
FEROS.2004-06-01T09:17:17.779	V367 Sct	FEROS	single	53157.39	6201	97	1.8	3.8	0.01	0.34	264	0.00	0.31	25	0.01
FEROS.2004-05-31T06:12:02.552	V458 Sct	FEROS	single	53156.26	6143	98	1.8	3.3	-0.02	0.26	240	-0.02	0.25	26	-0.02
FEROS.2004-06-01T07:28:59.993	V458 Sct	FEROS	single	53157.31	5952	94	1.4	2.8	0.14	0.25	314	0.10	0.29	31	0.12
FEROS.2004-05-31T06:51:36.376	BQ Ser	FEROS	single	53156.29	5876	175	1.9	4.9	-0.13	0.34	237	-0.13	0.23	22	-0.13
FEROS.2004-06-01T09:53:34.668	BQ Ser	FEROS	single	53157.41	6270	149	2.0	4.5	-0.08	0.31	233	-0.10	0.19	28	-0.09
FEROS.2004-06-02T09:20:53.516	BQ Ser	FEROS	single	53158.39	6214	110	1.7	3.0	-0.07	0.28	247	-0.05	0.25	28	-0.06
FEROS.2005-08-19T04:07:29.730	AV Sgr	FEROS	single	53601.17	6091	159	1.3	4.9	0.35	0.49	122	0.35	0.16	8	0.35
FEROS.2005-08-20T02:52:01.461	AV Sgr	FEROS	single	53602.12	6259	149	1.4	5.0	0.38	0.49	127	0.37	0.20	9	0.37
FEROS.2007-03-26T08:38:58.450	AV Sgr	FEROS	single	54185.36	5442	98	0.8	4.9	0.14	0.35	119	0.13	0.34	6	0.13
FEROS.2005-06-01T05:28:26.262	VY Sgr	FEROS	single	53522.23	6136	150	1.6	5.0	0.34	0.45	139	0.33	0.05	5	0.33
FEROS.2005-06-29T03:56:18.121	VY Sgr	FEROS	single	53550.16	5678	146	1.0	4.9	0.19	0.47	104	0.18	0.39	8	0.19
FEROS.2005-06-30T05:16:19.841	VY Sgr	FEROS	single	53551.22	5388	122	0.8	4.9	0.28	0.41	99	0.28	0.38	6	0.28
FEROS.2005-09-03T02:13:22.130	VY Sgr	FEROS	single	53616.09	6269	149	1.9	5.0	0.33	0.44	118	0.33	0.22	5	0.33
FEROS.2007-03-30T06:56:38.009	VY Sgr	FEROS	single	54189.29	5317	118	0.9	4.9	0.24	0.38	145	0.22	0.50	5	0.23
FEROS.2007-03-30T07:27:28.207	VY Sgr	FEROS	single	54189.31	5269	99	0.8	3.9	0.17	0.34	147	0.18	0.39	6	0.18
FEROS.2005-05-30T06:33:46.049	WZ Sgr	FEROS	single	53520.27	4974	109	1.3	4.8	0.15	0.33	111	0.15	0.73	10	0.15
FEROS.2010-03-31T09:01:42.139	X Sgr	FEROS	single	55286.38	6415	156	2.0	2.0	-0.38	0.52	106	-0.47	0.34	18	-0.43
FEROS.2010-03-28T08:27:13.457	LR TrA	FEROS	single	55283.35	5756	179	2.0	4.9	-0.23	0.59	151	-0.21	0.53	14	-0.22
FEROS.2010-03-28T08:14:18.323	R TrA	FEROS	single	55283.34	6096	90	2.0	4.9	-0.03	0.35	121	-0.22	0.43	13	-0.13
FEROS.2010-03-30T09:27:38.729	S TrA	FEROS	single	55285.39	5930	88	1.7	3.6	0.01	0.32	140	-0.01	0.43	11	0.00
FEROS.2004-05-31T05:30:07.493	U TrA	FEROS	single	53156.23	5941	100	1.9	3.0	-0.01	0.23	335	-0.02	0.29	32	-0.01
FEROS.2004-06-02T06:58:04.773	U TrA	FEROS	single	53158.29	6065	96	1.6	2.2	-0.03	0.22	352	-0.05	0.28	34	-0.04
FEROS.2010-04-01T03:37:36.859	AE Vel	FEROS	single	55287.15	5421	92	1.3	4.9	-0.17	0.44	146	-0.19	0.22	11	-0.18
FEROS.2004-05-30T23:17:17.176	AP Vel	FEROS	single	53155.97	5801	97	2.0	4.9	-0.07	0.28	229	-0.06	0.25	26	-0.06
FEROS.2004-06-02T00:14:28.622	AP Vel	FEROS	single	53158.01	5931	95	1.7	2.7	0.06	0.25	335	0.07	0.25	31	0.07
FEROS.2004-05-30T23:50:31.310	AX Vel	FEROS	single	53155.99	6235	95	1.7	2.7	-0.10	0.24	299	-0.12	0.28	33	-0.11
FEROS.2004-06-02T00:51:31.715	AX Vel	FEROS	single	53158.04	6260	115	1.7	2.8	-0.10	0.25	281	-0.12	0.24	30	-0.11
FEROS.2010-04-01T01:44:24.786	BG Vel	FEROS	single	55287.07	5803	115	1.8	4.2	-0.02	0.34	133	-0.04	0.67	12	-0.03
FEROS.2010-03-30T02:02:16.646	CS Vel	FEROS	single	55285.08	5462	94	0.9	4.9	-0.11	0.52	149	-0.09	0.39	10	-0.10
FEROS.2010-03-30T02:44:46.634	CS Vel	FEROS	single	55285.11	5390	97	1.9	4.9	0.00	0.46	94	-0.01	0.32	10	0.00
FEROS.2010-03-30T03:27:19.152	CS Vel	FEROS	single	55285.14	5411	100	1.5	4.9	-0.02	0.36	88	-0.01	0.37	12	-0.02
FEROS.2010-03-29T01:06:31.372	CX Vel	FEROS	single	55284.05	6149	102	2.0	4.9	0.00	0.33	141	-0.02	0.36	10	-0.01
FEROS.2010-03-29T01:31:27.655	CX Vel	FEROS	single	55284.06	6215	100	1.9	3.8	0.05	0.32	136	0.06	0.30	13	0.06
FEROS.2010-03-29T01:56:25.238	CX Vel	FEROS	single	55284.08	6174	92	1.8	5.0	-0.04	0.44	160	-0.04	0.32	11	-0.04
FEROS.2007-03-27T02:09:50.650	DD Vel	FEROS	single	54186.09	5679	157	2.0	4.9	-0.13	0.46	135	-0.21	0.20	11	-0.17
FEROS.2007-03-27T02:40:42.529	DD Vel	FEROS	single	54186.11	5451	156	0.9	4.9	-0.45	0.45	129	-0.47	0.25	8	-0.46
FEROS.2007-03-27T03:11:32.687	DD Vel	FEROS	single	54186.13	5436	181	1.2	4.9	-0.51	0.56	227	-0.50	0.23	11	-0.50
FEROS.2007-03-27T03:42:22.665	DD Vel	FEROS	single	54186.15	5698	170	1.8	4.9	-0.14	0.50	136	-0.13	0.28	14	-0.13
FEROS.2010-03-25T02:38:09.504	DK Vel	FEROS	single	55280.11	6451	99	1.5	2.0	0.19	0.34	169	0.19	0.25	11	0.19
FEROS.2010-03-25T02:51:45.292	DK Vel	FEROS	single	55280.12	6393	100	1.7	2.0	0.19	0.36	168	0.18	0.22	12	0.18
FEROS.2010-03-25T03:05:22.801	DK Vel	FEROS	single	55280.13	6361	97	2.0	2.9	0.12	0.40	200	0.08	0.17	12	0.10
FEROS.2010-03-26T04:03:34.125	DR Vel	FEROS	single	55281.17	5443	93	0.9	3.1	0.11	0.28	152	0.12	0.17	10	0.12
FEROS.2010-04-01T01:51:57.565	EX Vel	FEROS	single	55287.08	5851	94	1.7	4.9	-0.08	0.43	172	-0.07	0.83	14	-0.08

FEROS.2010-04-01T02:21:24.829	EX Vel	FEROS	single	55287.10	5833	98	1.5	4.9	-0.09	0.41	180	-0.08	0.17	11	-0.08
FEROS.2010-04-01T02:50:50.422	EX Vel	FEROS	single	55287.12	5891	92	1.7	4.9	-0.03	0.37	168	-0.03	0.56	10	-0.03
FEROS.2007-03-26T23:52:55.721	EZ Vel	FEROS	single	54186.00	6063	126	1.5	5.0	-0.24	0.58	201	-0.25	0.49	12	-0.25
FEROS.2007-03-27T00:23:47.359	EZ Vel	FEROS	single	54186.02	6178	422	2.0	5.0	-0.05	0.59	234	-0.14	0.99	15	-0.10
FEROS.2007-03-27T00:54:39.217	EZ Vel	FEROS	single	54186.04	5763	332	1.6	4.9	-0.64	0.58	221	-0.64	1.09	14	-0.64
FEROS.2007-03-27T01:25:31.535	EZ Vel	FEROS	single	54186.06	6005	278	1.4	5.0	-0.30	0.60	209	-0.28	0.93	13	-0.29
FEROS.2007-03-31T04:53:21.900	EZ Vel	FEROS	single	54190.20	5763	128	0.7	4.9	-0.08	0.47	175	-0.09	0.71	6	-0.08
FEROS.2007-03-31T05:24:14.178	EZ Vel	FEROS	single	54190.23	5617	169	0.8	4.9	-0.14	0.55	189	-0.13	0.65	8	-0.14
FEROS.2007-03-31T05:55:06.237	EZ Vel	FEROS	single	54190.25	5662	186	1.4	4.9	-0.10	0.56	173	-0.10	0.65	12	-0.10
FEROS.2010-03-27T00:32:17.936	FG Vel	FEROS	single	55282.02	5434	104	1.5	4.9	-0.17	0.40	139	-0.16	0.38	12	-0.16
FEROS.2010-03-27T01:09:04.005	FG Vel	FEROS	single	55282.05	5435	112	1.1	4.9	-0.04	0.41	105	-0.05	0.33	11	-0.04
FEROS.2010-03-27T01:45:49.994	FG Vel	FEROS	single	55282.07	5430	115	1.1	4.9	-0.03	0.42	100	-0.02	0.26	11	-0.03
FEROS.2010-03-28T01:52:43.501	FN Vel	FEROS	single	55283.08	5775	99	1.8	4.9	-0.10	0.42	157	-0.11	0.27	12	-0.10
FEROS.2010-03-28T02:11:04.399	FN Vel	FEROS	single	55283.09	5769	99	1.7	4.9	-0.07	0.38	168	-0.06	0.23	10	-0.06
FEROS.2010-03-25T03:51:24.102	RY Vel	FEROS	single	55280.16	5443	99	0.6	3.9	0.10	0.32	171	0.10	0.52	9	0.10
FEROS.2010-03-25T02:04:02.131	RZ Vel	FEROS	single	55280.09	5199	99	1.2	4.9	-0.11	0.45	123	-0.11	0.52	9	-0.11
FEROS.2010-03-29T00:39:51.089	ST Vel	FEROS	single	55284.03	6211	98	1.7	3.3	-0.03	0.31	137	-0.02	0.17	9	-0.02
FEROS.2010-03-26T05:26:52.949	SV Vel	FEROS	single	55281.23	6042	80	1.4	3.8	0.10	0.32	148	0.08	0.82	11	0.09
FEROS.2010-03-30T01:22:44.578	SW Vel	FEROS	single	55285.06	6537	216	1.8	5.0	-0.12	0.44	90	-0.12	0.23	12	-0.12
FEROS.2010-03-25T02:10:09.101	SX Vel	FEROS	single	55280.09	6275	89	1.0	2.3	0.07	0.27	145	0.06	0.33	12	0.07
FEROS.2010-03-25T23:34:33.289	T Vel	FEROS	single	55280.98	5714	110	2.0	4.9	-0.12	0.42	137	-0.09	0.15	13	-0.10
FEROS.2010-04-01T03:23:26.365	V Vel	FEROS	single	55287.14	6321	99	1.9	3.3	-0.13	0.31	136	-0.11	0.30	13	-0.12
FEROS.2010-03-28T02:59:39.115	XX Vel	FEROS	single	55283.12	6486	188	2.0	5.0	0.01	0.42	162	-0.11	0.28	12	-0.05
FEROS.2010-03-28T03:15:31.479	XX Vel	FEROS	single	55283.14	6467	96	2.0	5.0	-0.05	0.43	164	-0.06	0.20	14	-0.06
FEROS.2010-03-28T03:31:23.372	XX Vel	FEROS	single	55283.15	6479	98	2.0	5.0	-0.05	0.44	170	-0.08	0.20	9	-0.07

Chapter 7

Discussion and Comparison with Literature Results

7.1 Overview

Now that the main results of the thesis had been obtained, the last step was to set them in relation to already existing ones. For this purpose several confidence tests (validity checks) and comparisons were performed. The main source of reference was the paper by Genovali, since first of all a reasonable number of spectra was identical and furthermore the target list had a significant overlap as well. Further references can be found in the respective sections where they were used.

7.2 Convergence and Sigma Clipping

While my wrapper takes a set of parameters and changes them so that different criteria are met (flat excitation potential and reduced width slopes, ionization equilibrium), leading to changes in the output metallicities, it is interesting to see what happens when the output values are taken as the new input. This way it is possible to check whether the output (input) parameters were close or far away from the true numbers (assuming that large distances complicate the fitting process) and validate the convergence.

Taking the UVES sample and running the program once (the zeroth iteration) using the default configuration and then two more times with input values based on the former results, it became apparent that between iteration 0 and 1 there was only a minor fraction of the spectra (10-20 %) where the output values changed at all. These small variations for log(g) and v_t were, however, on the scale of 0.1 dex and 0.1-0.2 km/s, respectively, causing slight abundance changes of < 0.05 dex and may hence be ignored considering the overall error budget. The second iteration confirmed this, as there were no fluctuations anymore. Although the study was performed only for the former interpolation cube based exclusively on the old Kurucz models, the results are assumed to be generalizable to the Kurucz-Castelli grid. The conclusion that may be drawn from this is, that running the program once is sufficient for the accuracy that can be achieved intrinsically.

R. da Silva sent me a few results for some UVES test EW files from an independent analysis based on his own code for determining the quantities of interest. He used my EWs and the same MOOG version but his own models (Kurucz as well) and no sigma clipping at all. As input parameters once my output results were taken and fixed and a second time Genovali metallicities plus my LDR effective temperatures were assumed, leaving log(g) and v_t free (the usual setup). Comparing his results to mine, differences were visible, but they did not exceed the error budget. Therefore, while isolating the effect of the sigma clipping from the remaining code is difficult, this gave us a hint that the effect of the sigma clipping is not too relevant.

Last but not least I compared results for the UVES sample based on active respectively deactivated sigma-clipping using solely my wrapper. The output values differed for some of the spectra, but typically on the order of less than 0.3 dex and 0.5 km/s, with minor changes in the abundances (< 0.05 dex). A large fraction of spectra was completely unaffected. This indicated that the sigma clipping indeed was safe (especially in terms of metallicity) and that it could be a matter of personal preference whether or not to include it.

7.3 Metallicity Sensitivity

Since the input stellar parameters are reasonable, but still arbitrary default values in case of log(g) and v_t, it is most interesting to check the effect of slightly changed values on the metallicity. This concerns naturally also the effective temperature, because despite this quantity being fixed, there is a certain error assigned to it within which the correct number should lie.

In order to study such effects on the iron abundances yielded by the program, first several test spectra from all 3 spectrographs (UVES, HARPS and FEROS) were given to the program and treated as usual, then their output was used as the new, fixed input and - with certain steps around these values - the metallicities were calculated. These were +/- 100 K for the effective temperature, +/- 0.3 dex for the surface gravity and +/- 0.5 km/s for the microturbulence velocity.

The results are given in table 7.1. Note please that the parameters of the spectra are capped at 4000/7000 K, 0.0/2.0 dex and 2.0/5.0 km/s for T_{eff}, log(g) and v_t respectively, such that changes beyond these limits do not alter the values of these quantities.

Table 7.1: All metallicity results for the sensitivity check. Columns 9 - 15 give the output metallicities in dex units for different sets of input parameters (see text). The first respectively second respectively third row indicates the Fe I respectively Fe II respectively averaged abundance. Units are generally the same as in table 6.1.

Spectrum	Object	Dataset	Spectral part	T_{eff}	log(g)	Fe I	v_t	Default	+100 K	-100 K	+0.3 dex	-0.3 dex	+0.5 km/s	-0.5 km/s
V340Ara_17_25	V340 Ara	UVES Geno	single	6100	1.6	0.30	4.9	0.32	0.25	0.38	0.32	0.31	0.34	0.31
								0.34	0.36	0.34	0.24	0.44	0.38	0.30
								0.33	0.30	0.36	0.28	0.38	0.36	0.31
V340Ara_25_34	V340 Ara	UVES Geno	single	4750	1.1	0.10	4.8	0.10	0.03	0.20	0.10	0.11	0.13	0.08
								0.12	0.21	0.04	0.01	0.25	0.14	0.11
								0.11	0.12	0.12	0.05	0.18	0.13	0.10
V510Mon_01_19	V510 Mon	UVES Geno	single	5450	1.3	-0.10	3.6	-0.12	-0.22	-0.04	-0.10	-0.14	-0.09	-0.16
								0.14	-0.12	-0.15	-0.25	-0.01	-0.01	-0.21
								0.13	-0.17	-0.09	-0.18	-0.08	-0.05	-0.18
ADP.2014-10-01T10:19:40.910	ζ Gem	HARPS	red	5500	1.5	-0.05	4.9	-0.04	-0.11	0.05	-0.02	-0.04	-0.02	-0.05
								0.05	-0.03	-0.06	-0.17	0.08	0.03	-0.10
								0.04	-0.07	-0.01	-0.09	0.02	0.01	-0.08
ADP.2014-10-01T10:23:13.893	ζ Gem	HARPS	red	5850	1.2	0.10	3.1	0.15	0.07	0.21	0.16	0.13	0.20	0.13
								0.13	0.13	0.13	0.02	0.24	0.21	0.01
								0.14	0.10	0.17	0.09	0.19	0.21	0.07
ADP.2014-10-01T10:20:19.793	ζ Gem	HARPS	red	5600	1.5	0.05	3.6	0.03	-0.05	0.11	0.05	0.02	0.06	0.01
								0.05	0.09	0.02	-0.06	0.16	0.13	-0.04
								0.04	0.02	0.06	-0.01	0.09	0.10	-0.01
ADP.2014-10-01T10:22:42.490	ζ Gem	HARPS	red	5200	1.7	-0.05	4.9	-0.06	-0.15	0.02	-0.06	-0.07	-0.04	-0.07
								0.04	0.00	-0.07	-0.17	0.10	0.06	-0.10
								0.05	-0.07	-0.03	-0.11	0.02	0.01	-0.08
ADP.2014-10-01T10:22:24.580	RS Pup	HARPS	red	5100	1.0	0.10	4.9	0.12	0.03	0.20	0.14	0.11	0.14	0.11
								0.14	0.16	0.09	0.02	0.27	0.22	0.12
								0.13	0.09	0.14	0.08	0.19	0.18	0.12
ADP.2014-10-01T10:23:14.640	RS Pup	HARPS	red	5150	0.8	0.05	4.9	0.07	-0.02	0.15	0.08	0.05	0.08	0.06
								0.08	0.14	0.04	-0.03	0.20	0.10	0.06
								0.07	0.06	0.09	0.03	0.13	0.09	0.06
ADP.2014-10-01T10:22:15.857	R TrA	HARPS	red	6300	2.0	-0.05	3.5	0.01	-0.05	0.08	0.02	0.01	0.06	-0.01
								0.08	-0.06	-0.07	-0.19	-0.08	-0.01	-0.14
								0.03	-0.05	0.00	-0.08	-0.03	0.02	-0.08
FEROS.2010-03-26T02:10:41.380	NT Pup	FEROS	single	5600	1.5	-0.15	4.9	-0.17	-0.24	-0.09	-0.15	-0.18	-0.16	-0.18
								0.18	-0.17	-0.18	-0.29	-0.06	-0.11	-0.22
								0.17	-0.20	-0.13	-0.22	-0.12	-0.13	-0.20
FEROS.2010-03-26T02:57:43.246	NT Pup	FEROS	single	5550	1.3	-0.20	4.9	-0.18	-0.27	-0.10	-0.16	-0.20	-0.17	-0.19
								0.20	-0.19	-0.21	-0.31	-0.09	-0.12	-0.27
								0.19	-0.23	-0.16	-0.24	-0.14	-0.14	-0.23
FEROS.2010-03-25T02:38:09.504	NT Pup	FEROS	single	6450	1.5	0.20	2.0	0.20	0.14	0.26	0.23	0.18	0.25	0.14
								0.19	0.17	0.21	0.10	0.28	0.21	-0.02
								0.19	0.15	0.23	0.16	0.23	0.23	0.06

At least two different objects with 3 spectra (in total) are being considered for each spectrograph. The UVES objects/spectra are identical to those of a similar check presented in table 2 of Genovali. RS Pup and R TrA are long-/short-period variables (41.39 vs. 3.39 d) for HARPS, similarly NT Pup and DK Vel for FEROS (15.57 vs. 2.48 d). ζ Gem was selected because it presents an excellent phase coverage with 47 HARPS spectra spanning the entire pulsation cycle. The ones indicated in the table were taken on the rising branch, at the maximum, on the decreasing branch and at the minimum of the effective temperature curve. Checking the sensitivity exemplarily at different phases may help reveal a potential dependency of the relevance of input parameter accuracy on the physical structure of the star, hence indirectly on the output (input) parameters themselves.

The table shows that changes in temperature of +/- 100 K affect the Fe I abundance much stronger (typically -/+ 0.08 dex) than the Fe II one (typically +/- 0.03 dex). The influence on [Fe/H] ([Fe/H] was built as an average of Fe I and Fe II) is then on the order of -/+ 0.03 dex. Changes in log(g) by +/- 0.3 dex, on the other hand, result in almost no effect on Fe I (+/- 0.01 dex), with more pronounced action on Fe II (-/+ 0.11 dex). The resulting change of [Fe/H] amounts to -/+ 0.05 dex. The trend with the microturbulence for +/- 0.5 km/s is more difficult to establish, but changes of Fe I (+/- 0.03 dex) are in most cases smaller than the variations in Fe II (+/- 0.08 dex).

All numbers described above should be treated as order-of-magnitude values. It is interesting to see that the temperature influences Fe I much stronger, whereas log(g) constitutes the Fe II analogue. In both cases the stronger effect has a minus sign for bigger values of the input parameter (anti-correlation) and an opposite behaviour for the opposite species. This is not the case for the microturbulence where both Fe I and Fe II positively correlate with the velocity change. Whether the stronger effect of v_t on Fe II than on Fe I is real or just due to the smaller number of lines available for Fe II and therefore is owing to a less solid statistical footing is difficult to verify, since input variations are more difficult to validate for that parameter owing to the larger dispersion of the sensitivity.

Concerning a period dependency on the strength of the changes, no trends, neither in Fe I nor in Fe II for any parameter, are apparent, maybe also due to the small sample size. On the other hand, regarding the spectra of ζ Gem in the given order of rising branch, maximum, decreasing branch and minimum of the temperature curve, there is no obvious correlation with phase, either. One may speculate about the temperature being most important at minimum and least important near the maximum (less apparent for Fe I than Fe II), the gravity having its strongest effect near the minimum as well and being less critical slightly after the maximum (for both species) and the microturbulence acting strongest near the smallest temperature and weakest at the biggest one, at least for Fe I (Fe II is almost random there).

Taking into account the equal sign of T_{eff} and log(g), one could also imagine a coupling in terms of a phase behaviour of their effectiveness. Although ζ Gem is of extraordinary spectral quality considering the spectra available, having also the most precise LDR temperatures for the whole HARPS sample, if the dispersion of the sensitivity would be considered, any trend could be swallowed within internal fluctuations. Taking into account that the effective temperature is the only quantity for which the regular pattern in the literature is typically clearly visible, the temperature accuracy behaviour with phase and as a consequence anticorrelation with the temperature itself may be the only justifiable dependency. It could also be that the effect on Fe I/II is bigger simply because the relative change of T_{eff} is bigger as well.

7.4 Comparison with Genovali

Due to the spectra given in Genovali being included in my sample as well, it is worth putting the stellar parameters given in the aforementioned paper into context with those retrieved by the analysis of this study. For this purpose the spectra have been matched and the respective quantities have been pairwise compared in a threefold way by overplotting the two values against a sequential index number, plotting them against each other and finally showing their difference as a function of my own result. The latter plots are depicted in figure 7.1.

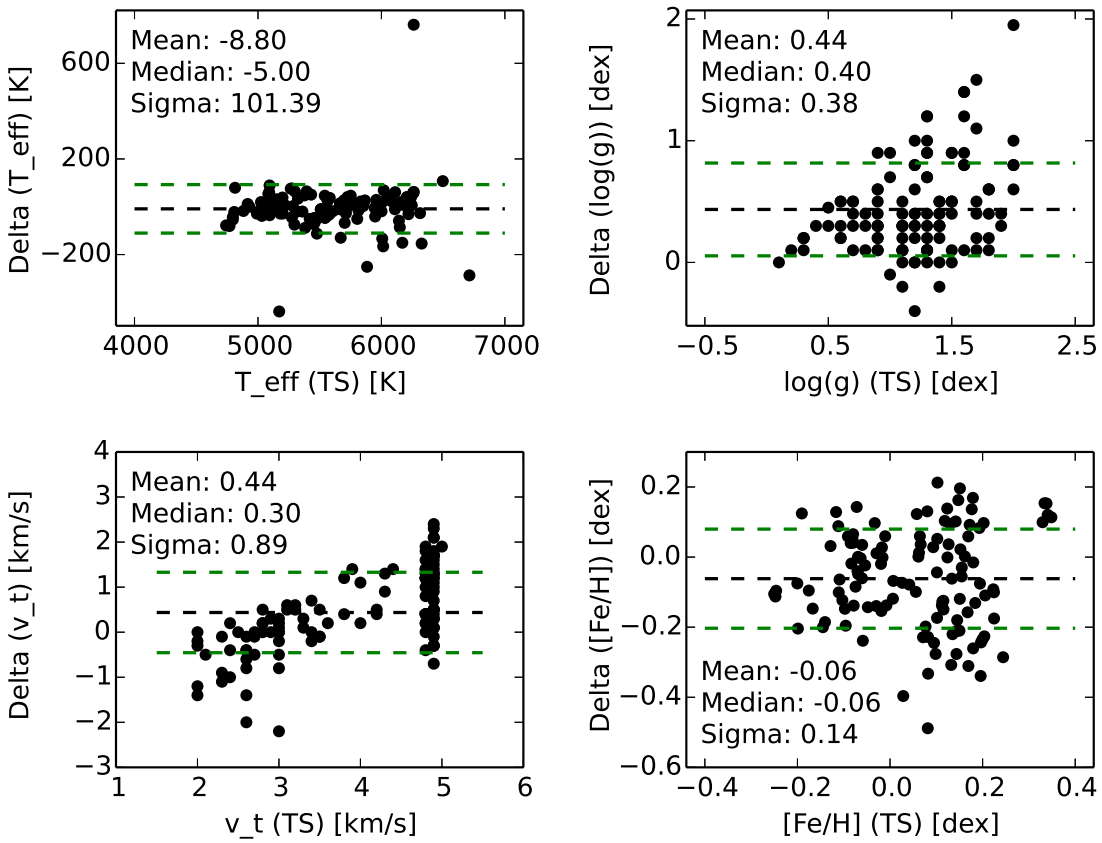

Figure 7.1: Comparison of the main stellar parameters (T_{eff}, log(g), v_t) and the metallicity between TS and Genovali's results. The mean, median and standard deviation are indicated on the plots. The black lines show the mean values, the green ones define a 1-sigma interval around the mean.

As can be seen a so-called cumulative effect is apparent for the microturbulence velocity, where my program clips all values above 5.0 km/s to this upper edge. Genovali gives in the paper sometimes slightly larger values. The effective temperatures, with exception of a few outliers, agree very well with each other, as mentioned earlier. Concerning the mean and the median differences, offsets to Genovali are apparent, maybe owing to the different approach. However they are typically still within the error indicated by the sigmas, which themselves are not larger than expected (indicated in sect. 6.4).

7.5 Homogeneous Metallicity Scale

With those steps completed and having all the abundances (both for Fe I and II) for all the spectra, it was now possible to build a large database of Cepheids and calculate the metallicity of the objects (effective temperature, surface gravity and microturbulence are phase-dependent quantities). Spectral parts (i.e. blue and red) were combined first individually by averaging the output abundances, where both parts were measured, else the single part was taken directly. Then the abundances from the spectra themselves were averaged within the same object and the same spectrograph so that for UVES, HARPS and FEROS individual lists of objects and their abundances were obtained. Of course there was some overlap between these datasets. Consequently, since UVES had the largest number of both objects and spectra, with FEROS and especially HARPS being smaller in this respect, a certain order in which the results were combined was naturally imposed (it especially helped to prevent difference outliers).

First the objects that were common between UVES and FEROS were matched and the difference in abundance was computed. Next the mean difference and the sigma was calculated. After that this shift was applied exclusively to the FEROS spectra that were not present in the UVES sample, bringing them to the UVES reference frame. The UVES-exclusive metallicities were kept, while common objects were treated by averaging the UVES and FEROS metallicities. This constituted the UVES-FEROS catalogue. A similar procedure was applied to include HARPS in the final metallicity database, comprising only objects for which the abundance analysis was performed.

It should be clear, that this list of Cepheids, although based on a large set of objects, is still incomplete. In order to get a larger coverage of the Galactic classical Cepheids, literature references were used. They include Lemasle (2013, [96], LEM13 (65 objects)), Lemasle (2008, [97], LEM08 (33 objects)), Lemasle (2007, [98], LEM07 (30 objects)), Luck (2011a, [99], LIII (339 objects)), Luck (2011b, [100], LII (270 objects)), Martin(2015, [101], MAR (27 objects)), Szilàdi (2007, [102], SZI (17 objects)) and Yong (2006, [103], YON (24 objects)). The papers by Romaniello (2008, [11], ROM (32 objects)) and Pedicelli (2010, [104], PED (4 objects)) were also checked, but the objects listed therein are all present among the ones of this study, so no new information could be gained. Please note that the LEM13 dataset comprises all objects from LEM08 (except for two targets) and LEM07 as well as those from PED. LEM13, LEM08 and LEM07 are from the same author, B. Lemasle, and were therefore merged into the LEM dataset, taking for each object the latest metallicity available.

All of these references except for MAR were mentioned in Genovali (2014, [10] and 2015, [29]). The primary metallicity data given in the papers were gathered. Within an iterative framework, it is possible to evaluate in each cycle the number of common objects between the reference and this study and shift the sample with the largest overlap to the reference frame of the new metallicity measurements. However, in this thesis, the samples were added in a fixed order, namely LEM, LIII, LII, MAR, SZI and YON (as described in Genovali). The MAR sample was added directly after LII because the metallicities are close to the ones from Luck (LIII and LII).

The order defined above automatically set a hierarchy for the finally adopted metallicity values. The shifts were applied like in the FEROS and HARPS cases, the only difference being that for common objects, the "highest-priority" estimate would be taken instead of averaging between datasets.

It is worthwhile to plot the iron abundance differences between the metallicity database at each stage and the next literature sample that had been included. Any trends of abundance differences with metallicity can thus easily be revealed. Defining TS as the P0 sample, TS + LEM as P1, TS + LEM + LIII as P2 etc., the resulting shifts can be seen in figure 7.2.

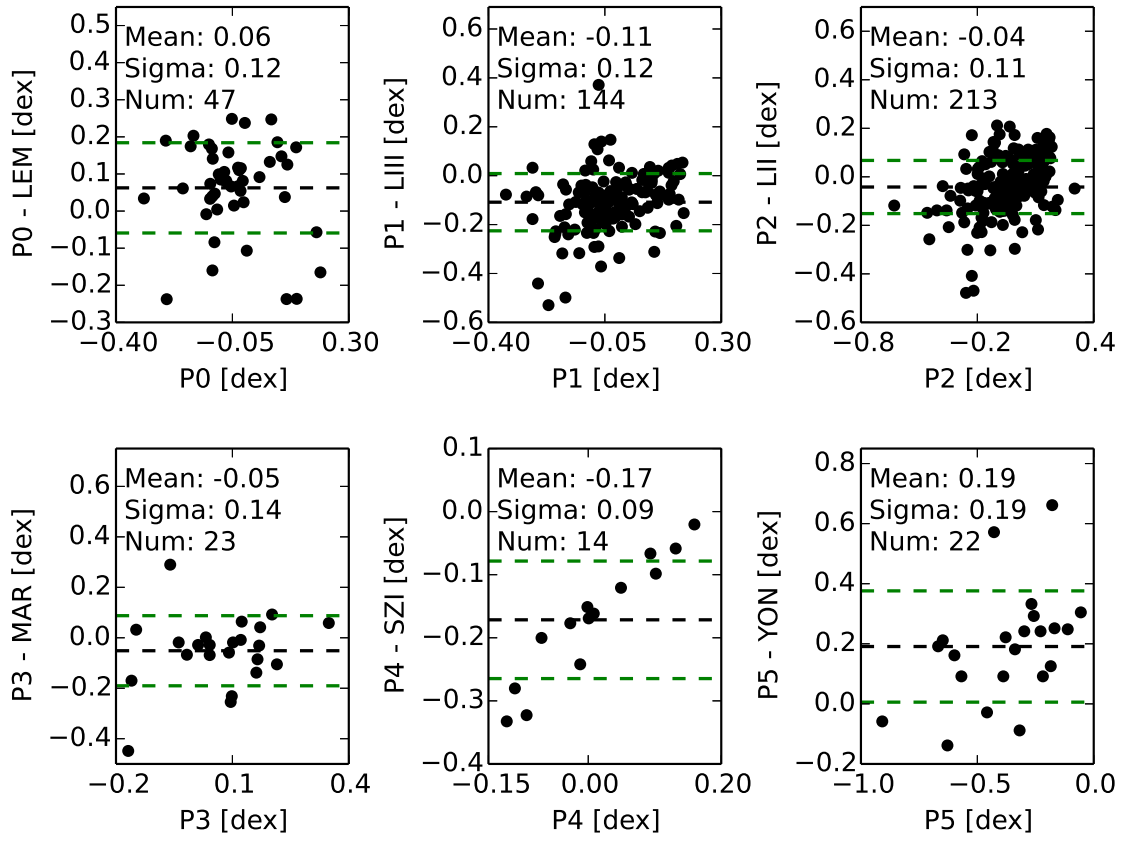

Figure 7.2: Abundance residuals between the Px and the following reference sample as a function of metallicity. The adopted metallicity shifts, given by the average differences, are indicated by the black lines, while the green ones define a 1-sigma interval around the mean. The number of objects used to determine the shifts is given as well.

As can be seen, there are no trends of metallicity residuals with metallicity, except for P4 - SZI. A thorough study of the behaviour goes beyond the scope of this thesis. However, due to SZI being a low-priority sample (as defined in the sample hierarchy mentioned above) and the small number of objects in that dataset, only 3 targets (V701 Car, V1048 Cen, V1210 Cen) were affected by possible systematics (if at all). The uncertainty of these objects is higher than the average one given by the standard deviation.

This way a very extensive list of targets and their iron abundances (almost reaching the totality of known Cepheids) was generated, given in table 7.2. Please note that some *Guide Star Catalogue* (GSC, [105]) objects given in LIII and SZI are listed under their variable star (GCVS) name, taken from the SIMBAD archive ([35][36]). One target, GSC 03725-00174, was not associated by SIMBAD, but identified with the star PV Cam because of identical coordinates. All object names are thus equal to those given in Genovali.

Table 7.2: All metallicity results for the sample objects - homogeneous metallicity scale. References are Lemasle (2013, [96], 2008, [97] and 2007, [98], LEM), Luck (2011a, [99], LIII), Luck (2011b, [100], LII), Martin (2015, [101], MAR), Szilàdi (2007, [102], SZI) and Yong (2006, [103], YON) (see text). The columns show the original (left) and shifted (right) literature metallicities. The finally adopted metallicity and its corresponding sample are indicated as well.

Object	P [d]	TS	LEM		LIII		LII		MAR		SZI		YON		final	Source
V912 Aql	4.40	0.12	-	-	-	-	-	-	-	-	-	-	-	-	0.12	TS
CC Car	4.76	0.19	-	-	-	-	-	-	-	-	-	-	-	-	0.19	TS
CF Car	5.49	-0.03	-	-	-	-	-	-	-	-	-	-	-	-	-0.03	TS
FF Car	16.33	-0.01	-	-	-	-	-	-	-	-	-	-	-	-	-0.01	TS
FK Car	23.25	-0.04	-	-	-	-	-	-	-	-	-	-	-	-	-0.04	TS
FM Car	7.64	0.08	-	-	-	-	-	-	-	-	-	-	-	-	0.08	TS
FN Car	4.59	-0.04	-	-	-	-	-	-	-	-	-	-	-	-	-0.04	TS
FQ Car	10.27	0.07	-	-	-	-	-	-	-	-	-	-	-	-	0.07	TS
GS Car	4.06	0.10	-	-	-	-	-	-	-	-	-	-	-	-	0.10	TS
GT Car	13.16	0.00	-	-	-	-	-	-	-	-	-	-	-	-	0.00	TS
HK Car	6.70	0.08	-	-	-	-	-	-	-	-	-	-	-	-	0.08	TS
II Car	64.24	-0.05	-	-	-	-	-	-	-	-	-	-	-	-	-0.05	TS
IM Car	5.34	0.02	-	-	-	-	-	-	-	-	-	-	-	-	0.02	TS
IP Car	7.12	-0.11	-	-	-	-	-	-	-	-	-	-	-	-	-0.11	TS
IZ Cen	5.89	0.11	-	-	-	-	-	-	-	-	-	-	-	-	0.11	TS
LV Cen	4.98	0.13	-	-	-	-	-	-	-	-	-	-	-	-	0.13	TS
MY Cen	3.72	0.02	-	-	-	-	-	-	-	-	-	-	-	-	0.02	TS
OO Cen	12.88	0.13	-	-	-	-	-	-	-	-	-	-	-	-	0.13	TS
TX Cen	17.09	0.23	-	-	-	-	-	-	-	-	-	-	-	-	0.18	TS
V553 Cen	2.06	0.04	-	-	-	-	-	-	-	-	-	-	-	-	0.04	TS
V782 Cen	11.58	0.15	-	-	-	-	-	-	-	-	-	-	-	-	0.15	TS
VW Cen	15.04	0.10	-	-	-	-	-	-	-	-	-	-	-	-	0.14	TS
AO CMa	5.82	0.00	-	-	-	-	-	-	-	-	-	-	-	-	0.12	TS
RW CMa	5.73	0.06	-	-	-	-	-	-	-	-	-	-	-	-	0.06	TS
SS CMa	12.36	-0.01	-	-	-	-	-	-	-	-	-	-	-	-	0.09	TS
TV CMa	4.67	0.08	-	-	-	-	-	-	-	-	-	-	-	-	0.06	TS
TW CMa	7.00	-0.15	-	-	-	-	-	-	-	-	-	-	-	-	-0.15	TS
SU Cru	12.85	-0.78	-	-	-	-	-	-	-	-	-	-	-	-	-0.88	TS
SV Cru	7.00	0.06	-	-	-	-	-	-	-	-	-	-	-	-	0.06	TS
TY Cru	4.99	0.14	-	-	-	-	-	-	-	-	-	-	-	-	0.14	TS
VV Cru	6.12	0.12	-	-	-	-	-	-	-	-	-	-	-	-	0.12	TS
VX Cru	12.21	0.23	-	-	-	-	-	-	-	-	-	-	-	-	0.23	TS
IQ Nor	8.24	0.15	-	-	-	-	-	-	-	-	-	-	-	-	0.15	TS
QZ Nor	3.79	0.25	-	-	-	-	-	-	-	-	-	-	-	-	0.34	TS
RS Nor	6.20	0.28	-	-	-	-	-	-	-	-	-	-	-	-	0.33	TS
BM Pup	7.20	-0.08	-	-	-	-	-	-	-	-	-	-	-	-	-0.08	TS
CK Pup	7.42	-0.08	-	-	-	-	-	-	-	-	-	-	-	-	-0.08	TS
LS Pup	14.15	-0.20	-	-	-	-	-	-	-	-	-	-	-	-	-0.20	TS
WZ Pup	5.03	-0.01	-	-	-	-	-	-	-	-	-	-	-	-	-0.01	TS
V507 Sco	11.80	-0.32	-	-	-	-	-	-	-	-	-	-	-	-	-0.32	TS
V504 Sgr	1.50	0.07	-	-	-	-	-	-	-	-	-	-	-	-	0.07	TS
X Sgr	7.01	-0.43	-	-	-	-	-	-	-	-	-	-	-	-	-0.43	TS
BR Vul	5.20	0.21	-	-	-	-	-	-	-	-	-	-	-	-	0.21	TS
GQ Vul	12.64	0.17	-	-	-	-	-	-	-	-	-	-	-	-	0.17	TS
DD Vel	13.19	-0.21	-0.35	-0.29	-	-	-	-	-	-	-	-	-	-	-0.32	TS
EZ Vel	34.53	-0.19	-0.01	0.05	-	-	-	-	-	-	-	-	-	-	-0.25	TS
BE Mon	2.71	0.06	-0.07	-0.01	0.08	-0.03	-	-	-	-	-	-	-	-	0.06	TS
TY Mon	4.02	-0.10	-0.15	-0.09	0.02	-0.09	-	-	-	-	-	-	-	-	-0.10	TS
AQ Car	9.77	0.05	-0.30	-0.24	0.03	-0.08	0.06	0.02	-	-	-	-	-	-	-0.05	TS
l Car	35.55	0.09	0.10	0.16	0.13	0.02	0.05	0.01	-	-	-	-	-	-	-0.01	TS
UX Car	3.68	0.19	-0.10	-0.04	0.05	-0.06	0.02	-0.02	-	-	-	-	-	-	0.09	TS
V Car	6.70	0.06	-0.06	0.00	0.04	-0.07	0.01	-0.03	-	-	-	-	-	-	-0.05	TS
V397 Car	2.06	0.08	-0.08	-0.02	0.15	0.04	0.03	-0.01	-	-	-	-	-	-	-0.03	TS
VY Car	18.91	0.13	-0.06	0.00	0.02	-0.09	0.26	0.22	-	-	-	-	-	-	0.03	TS
AA Gem	11.30	-0.18	-0.35	-0.29	-0.14	-0.25	-0.24	-0.28	-	-	-	-	-	-	-0.18	TS
AD Gem	3.79	-0.09	-0.19	-0.13	-0.15	-0.26	-0.18	-0.22	-	-	-	-	-	-	-0.09	TS
RZ Gem	5.53	-0.25	-0.44	-0.38	-0.17	-0.28	-0.12	-0.16	-	-	-	-	-	-	-0.25	TS
CV Mon	5.38	-0.10	-0.10	-0.04	0.01	-0.10	-0.03	-0.07	-	-	-	-	-	-	-0.10	TS
TW Mon	7.10	-0.12	-0.15	-0.09	-0.18	-0.29	-0.24	-0.28	-	-	-	-	-	-	-0.03	TS
TX Mon	8.70	-0.05	-0.12	-0.06	-0.03	-0.14	-0.14	-0.18	-	-	-	-	-	-	-0.05	TS
TZ Mon	7.43	-0.02	-0.04	0.02	0.01	-0.10	-0.07	-0.11	-	-	-	-	-	-	-0.02	TS
V495 Mon	4.10	-0.09	-0.17	-0.11	-0.11	-0.22	-0.26	-0.30	-	-	-	-	-	-	-0.09	TS
V508 Mon	4.13	-0.11	-0.25	-0.19	-0.13	-0.24	-0.25	-0.29	-	-	-	-	-	-	-0.11	TS
V510 Mon	7.31	-0.12	-0.12	-0.06	-0.06	-0.17	-0.19	-0.23	-	-	-	-	-	-	-0.13	TS
XX Mon	5.46	-0.07	-0.18	-0.12	0.00	-0.11	-0.14	-0.18	-	-	-	-	-	-	-0.07	TS
AP Pup	5.08	0.03	-0.15	-0.09	0.08	-0.03	0.06	0.02	-	-	-	-	-	-	-0.07	TS
AQ Pup	30.10	-0.20	-0.26	-0.20	0.04	-0.07	-0.14	-0.18	-	-	-	-	-	-	-0.20	TS
AT Pup	6.66	0.04	-0.22	-0.16	0.05	-0.06	-0.14	-0.18	-	-	-	-	-	-	-0.06	TS
BN Pup	13.67	0.14	-0.03	0.03	0.11	0.00	0.01	-0.03	-	-	-	-	-	-	0.14	TS
MY Pup	5.70	0.09	-0.25	-0.19	0.04	-0.07	-0.13	-0.17	-	-	-	-	-	-	-0.01	TS
RS Pup	41.39	0.14	0.07	0.13	0.22	0.11	0.17	0.13	-	-	-	-	-	-	0.11	TS
VZ Pup	23.17	-0.17	-0.37	-0.31	-0.11	-0.22	-0.16	-0.20	-	-	-	-	-	-	-0.17	TS
BG Vel	6.92	0.07	-0.10	-0.04	0.03	-0.08	-0.01	-0.05	-	-	-	-	-	-	-0.03	TS
DR Vel	11.20	0.22	-0.01	0.05	0.18	0.07	0.08	0.04	-	-	-	-	-	-	0.12	TS
RY Vel	28.14	0.20	-0.05	0.01	0.09	-0.02	0.01	-0.03	-	-	-	-	-	-	0.10	TS
RZ Vel	20.40	0.05	0.05	0.11	0.04	-0.07	-0.02	-0.06	-	-	-	-	-	-	-0.11	TS
ST Vel	5.86	0.08	-0.14	-0.08	0.05	-0.06	0.00	-0.04	-	-	-	-	-	-	-0.02	TS
SW Vel	23.44	-0.02	-0.15	-0.09	0.00	-0.11	-0.07	-0.11	-	-	-	-	-	-	-0.12	TS
SX Vel	9.55	0.17	-0.18	-0.12	0.06	-0.05	-0.02	-0.06	-	-	-	-	-	-	0.07	TS
T Vel	4.64	0.00	-0.02	0.04	0.04	-0.07	-0.02	-0.06	-	-	-	-	-	-	-0.10	TS
V Vel	4.37	-0.02	-0.30	-0.24	-0.08	-0.19	-0.23	-0.27	-	-	-	-	-	-	-0.12	TS

VX Pup	3.01	-0.03	-0.15	-0.09	0.00	-0.11	-0.13	-0.17	-	-	0.13	-0.04	-	-	-0.07	TS
SV Mon	15.23	-0.02	-0.10	-0.04	-	-	-0.03	-0.07	-	-	-	-	-	-	-0.02	TS
CS Ori	3.89	-0.12	-0.19	-0.13	-	-	-0.26	-0.30	-	-	-	-	-	-	-0.12	TS
RS Ori	7.57	-0.03	-0.14	-0.08	-	-	-0.10	-0.14	-	-	-	-	-	-	-0.03	TS
UZ Sct	14.74	0.13	0.35	0.41	-	-	0.33	0.29	-	-	-	-	-	-	0.11	TS
AV Sgr	15.42	0.30	0.26	0.32	-	-	0.34	0.30	-	-	-	-	-	-	0.20	TS
VY Sgr	13.56	0.25	0.38	0.44	-	-	0.26	0.22	-	-	-	-	-	-	0.14	TS
V340 Ara	20.81	0.19	0.38	0.44	-	-	0.31	0.27	0.32	0.27	-	-	-	-	0.21	TS
HW Pup	13.45	-0.25	-0.28	-0.22	-	-	-0.25	-0.29	-	-	-	-	-0.36	-0.17	-0.11	TS
AX Vel	3.67	-0.01	-0.15	-0.09	-	-	-	-	-	-	0.17	0.00	-	-	-0.11	TS
AS Aur	3.18	-0.06	-	-	-0.20	-0.31	-	-	-	-	-	-	-	-	-0.06	TS
FO Car	10.36	-0.15	-	-	-0.44	-0.55	-	-	-	-	-	-	-	-	-0.07	TS
BW Gem	2.64	-0.07	-	-	-0.18	-0.29	-	-	-	-	-	-	-	-	-0.07	TS
FT Mon	3.42	-0.08	-	-	-0.21	-0.32	-	-	-	-	-	-	-	-	-0.08	TS
EV Sct	3.09	-0.13	-	-	0.15	0.04	-	-	-	-	-	-	-	-	-0.05	TS
T Ant	5.90	-0.18	-	-	-0.20	-0.31	-0.24	-0.28	-	-	-	-	-	-	-0.29	TS
CN Car	4.93	0.02	-	-	0.21	0.10	0.06	0.02	-	-	-	-	-	-	-0.08	TS
CY Car	4.27	0.18	-	-	0.11	0.00	0.10	0.06	-	-	-	-	-	-	0.08	TS
DY Car	4.67	0.12	-	-	0.07	-0.04	-0.07	-0.11	-	-	-	-	-	-	0.02	TS
ER Car	7.72	0.02	-	-	0.15	0.04	0.03	-0.01	-	-	-	-	-	-	-0.02	TS
FI Car	13.46	0.04	-	-	0.31	0.20	0.06	0.02	-	-	-	-	-	-	-0.06	TS
FR Car	10.72	0.10	-	-	0.11	0.00	0.02	-0.02	-	-	-	-	-	-	-0.01	TS
GH Car	5.73	0.03	-	-	0.22	0.11	-0.01	-0.05	-	-	-	-	-	-	-0.07	TS
GX Car	7.20	0.09	-	-	0.14	0.03	0.01	-0.03	-	-	-	-	-	-	-0.02	TS
HW Car	9.20	0.10	-	-	0.09	-0.02	0.04	0.00	-	-	-	-	-	-	0.00	TS
IO Car	12.69	0.16	-	-	0.13	0.02	-0.05	-0.09	-	-	-	-	-	-	0.06	TS
IT Car	7.53	0.13	-	-	0.14	0.03	0.06	0.02	-	-	-	-	-	-	0.03	TS
SX Car	4.86	0.12	-	-	0.05	-0.06	-0.09	-0.13	-	-	-	-	-	-	0.01	TS
U Car	38.77	-0.07	-	-	0.04	-0.07	0.01	-0.03	-	-	-	-	-	-	-0.17	TS
UW Car	5.35	0.00	-	-	0.09	-0.02	-0.06	-0.10	-	-	-	-	-	-	-0.10	TS
UY Car	5.54	0.00	-	-	0.13	0.02	0.03	-0.01	-	-	-	-	-	-	-0.10	TS
UZ Car	5.20	0.04	-	-	0.13	0.02	0.07	0.03	-	-	-	-	-	-	-0.06	TS
WW Car	4.68	-0.01	-	-	0.00	-0.11	-0.07	-0.11	-	-	-	-	-	-	-0.11	TS
WZ Car	23.01	-0.10	-	-	0.05	-0.06	0.03	-0.01	-	-	-	-	-	-	-0.20	TS
XX Car	15.72	0.16	-	-	0.20	0.09	0.11	0.07	-	-	-	-	-	-	0.05	TS
XY Car	12.43	0.01	-	-	0.07	-0.04	0.04	0.00	-	-	-	-	-	-	-0.09	TS
XZ Car	16.65	0.21	-	-	0.19	0.08	0.14	0.10	-	-	-	-	-	-	0.11	TS
YZ Car	18.17	0.03	-	-	0.00	-0.11	0.02	-0.02	-	-	-	-	-	-	-0.07	TS
AY Cen	5.31	0.08	-	-	0.08	-0.03	0.01	-0.03	-	-	-	-	-	-	-0.02	TS
AZ Cen	3.21	0.21	-	-	0.09	-0.02	-0.05	-0.09	-	-	-	-	-	-	0.11	TS
BB Cen	4.00	0.25	-	-	0.22	0.11	0.13	0.09	-	-	-	-	-	-	0.15	TS
KK Cen	12.18	0.14	-	-	0.24	0.13	0.12	0.08	-	-	-	-	-	-	0.04	TS
MZ Cen	10.35	0.16	-	-	0.35	0.24	0.20	0.16	-	-	-	-	-	-	0.12	TS
QY Cen	17.75	0.24	-	-	0.24	0.13	0.16	0.12	-	-	-	-	-	-	0.14	TS
V Cen	5.49	0.00	-	-	0.03	-0.08	-0.01	-0.05	-	-	-	-	-	-	-0.10	TS
V339 Cen	9.47	0.07	-	-	0.14	0.03	0.04	0.00	-	-	-	-	-	-	-0.08	TS
V378 Cen	6.46	0.12	-	-	0.08	-0.03	-0.02	-0.06	-	-	-	-	-	-	0.02	TS
V381 Cen	5.08	0.01	-	-	0.02	-0.09	0.02	-0.02	-	-	-	-	-	-	-0.09	TS
V419 Cen	5.51	0.10	-	-	0.14	0.03	0.07	0.03	-	-	-	-	-	-	-0.01	TS
V496 Cen	4.42	0.09	-	-	0.09	-0.02	0.00	-0.04	-	-	-	-	-	-	-0.01	TS
V659 Cen	5.62	0.05	-	-	0.09	-0.02	0.07	0.03	-	-	-	-	-	-	-0.06	TS
V737 Cen	7.07	0.18	-	-	0.14	0.03	0.13	0.09	-	-	-	-	-	-	0.08	TS
XX Cen	10.95	0.20	-	-	0.18	0.07	0.16	0.12	-	-	-	-	-	-	0.10	TS
AV Cir	3.07	0.28	-	-	0.17	0.06	0.10	0.06	-	-	-	-	-	-	0.18	TS
AX Cir	5.27	-0.07	-	-	-0.01	-0.12	-0.06	-0.10	-	-	-	-	-	-	-0.17	TS
BP Cir	2.40	0.02	-	-	0.02	-0.09	-0.06	-0.10	-	-	-	-	-	-	-0.08	TS
AD Cru	6.40	0.10	-	-	0.11	0.00	0.06	0.02	-	-	-	-	-	-	0.00	TS
R Cru	5.83	0.24	-	-	0.13	0.02	0.08	0.04	-	-	-	-	-	-	0.14	TS
S Cru	4.69	0.09	-	-	0.11	0.00	-0.12	-0.16	-	-	-	-	-	-	-0.04	TS
T Cru	6.73	0.17	-	-	0.14	0.03	0.09	0.05	-	-	-	-	-	-	0.07	TS
VW Cru	5.27	0.06	-	-	0.19	0.08	0.10	0.06	-	-	-	-	-	-	-0.04	TS
DX Gem	3.14	-0.11	-	-	-0.04	-0.15	-0.02	-0.06	-	-	-	-	-	-	-0.11	TS
ζ Gem	10.15	0.08	-	-	0.10	-0.01	0.00	-0.04	-	-	-	-	-	-	0.05	TS
GH Lup	9.28	0.08	-	-	0.13	0.02	0.08	0.04	-	-	-	-	-	-	-0.02	TS
V465 Mon	2.71	-0.07	-	-	0.02	-0.09	0.03	-0.01	-	-	-	-	-	-	-0.07	TS
R Mus	7.51	0.14	-	-	0.15	0.04	0.10	0.06	-	-	-	-	-	-	0.03	TS
RT Mus	3.09	0.27	-	-	0.12	0.01	0.02	-0.02	-	-	-	-	-	-	0.17	TS
S Mus	9.66	0.06	-	-	0.07	-0.04	-0.02	-0.06	-	-	-	-	-	-	-0.04	TS
TZ Mus	4.94	0.01	-	-	0.10	-0.01	-0.01	-0.05	-	-	-	-	-	-	-0.09	TS
UU Mus	11.64	-0.15	-	-	0.19	0.08	0.05	0.01	-	-	-	-	-	-	-0.25	TS
GU Nor	3.45	0.24	-	-	0.27	0.16	0.15	0.11	-	-	-	-	-	-	0.17	TS
S Nor	9.75	0.29	-	-	0.13	0.02	0.06	0.02	-	-	-	-	-	-	0.18	TS
SY Nor	12.65	0.17	-	-	0.34	0.23	0.31	0.27	-	-	-	-	-	-	0.19	TS
TW Nor	10.79	0.23	-	-	0.33	0.22	0.28	0.24	-	-	-	-	-	-	0.10	TS
U Nor	12.64	0.25	-	-	0.19	0.08	0.15	0.11	-	-	-	-	-	-	0.15	TS
V340 Nor	11.29	0.01	-	-	0.16	0.05	0.04	0.00	-	-	-	-	-	-	0.01	TS
BF Oph	4.07	0.02	-	-	0.14	0.03	0.03	-0.01	-	-	-	-	-	-	0.01	TS
X Pup	25.96	-0.14	-	-	0.08	-0.03	-0.03	-0.07	-	-	-	-	-	-	-0.14	TS
RV Sco	6.06	0.25	-	-	0.11	0.00	0.06	0.02	-	-	-	-	-	-	0.15	TS
V482 Sco	4.53	0.22	-	-	0.20	0.09	0.07	0.03	-	-	-	-	-	-	0.12	TS
V636 Sco	6.80	0.03	-	-	0.10	-0.01	0.07	0.03	-	-	-	-	-	-	-0.07	TS
V950 Sco	3.38	0.18	-	-	0.21	0.10	0.11	0.07	-	-	-	-	-	-	0.08	TS
Z Sct	12.90	-0.01	-	-	0.33	0.22	0.29	0.25	-	-	-	-	-	-	-0.01	TS
LR TrA	2.46	-0.12	-	-	0.31	0.20	0.25	0.21	-	-	-	-	-	-	-0.22	TS
R TrA	3.39	0.00	-	-	0.19	0.08	0.06	0.02	-	-	-	-	-	-	-0.13	TS
S TrA	6.32	0.10	-	-	0.21	0.10	0.12	0.08	-	-	-	-	-	-	0.00	TS
AE Vel	7.13	-0.08	-	-	0.14	0.03	0.05	0.01	-	-	-	-	-	-	-0.18	TS
CS Vel	5.90	0.06	-	-	0.12	0.01	0.08	0.04	-	-	-	-	-	-	-0.04	TS
CX Vel	6.26	0.10	-	-	0.16	0.05	0.06	0.02	-	-	-	-	-	-	0.00	TS
DK Vel	2.48	0.26	-	-	0.18	0.07	-0.02	-0.06	-	-	-	-	-	-	0.16	TS
EX Vel	13.23	0.04	-	-	0.07	-0.04	0.05	0.01	-	-	-	-	-	-	-0.06	TS
FG Vel	6.45	0.02	-	-	0.02	-0.09	-0.05	-0.09	-	-	-	-	-	-	-0.08	TS
FN Vel	5.32	0.02	-	-	0.15	0.04	0.06	0.02	-	-	-	-	-	-	-0.08	TS
SV Vel	14.10	0.19	-	-	0.12	0.01	0.08	0.04	-	-	-	-	-	-	0.09	TS
XX Vel	6.98	0.04	-	-	0.11	0.00	-0.05	-0.09	-	-	-	-	-	-	-0.06	TS
AG Cru	3.84	-0.06	-	-	0.08	-0.03	-0.13	-0.17	0.01	-0.04	-	-	-	-	-0.16	TS
X Cru	6.22	0.08	-	-	0.15	0.04	0.14	0.10	0.05	0.00	-	-	-	-	-0.02	TS
CE Pup	49.53	0.05	-	-	0.03	-0.08	-0.04	-0.08	-	-	-	-	-0.36	-0.17	-0.06	TS
NT Pup	15.57	-0.08	-	-	-0.02	-0.13	-0.15	-0.19	-	-	-	-	-0.31	-0.12	-0.18	TS
CN Sct	9.99	-0.07	-	-	0.33	0.22	-	-	0.28	0.23	-	-	-	-	-0.17	TS
RU Sct	19.70	0.09	-	-	0.11	0.00	-	-	0.15	0.10	-	-	-	-	0.09	TS
TY Sct	11.05	0.27	-	-	0.37	0.26	-	-	0.25	0.20	-	-	-	-	0.16	TS
AA Ser	17.14	0.10	-	-	0.41	0.30	-	-	0.33	0.28	-	-	-	-	0.10	TS
SZ Aql	17.14	-0.03	-	-	-	-	0.17	0.13	-	-	-	-	-	-	-0.13	TS
β Dor	9.84	-0.02	-	-	-	-	-0.01	-0.05	-	-	-	-	-	-	-0.06	TS
Y Oph	17.13	0.09	-	-	-	-	0.06	0.02	-	-	-	-	-	-	0.05	TS
BC Pup	3.54	-0.19	-	-	-	-	-0.23	-0.27	-	-	-	-	-	-	-0.19	TS
VW Pup	4.29	-0.25	-	-	-	-	-0.19	-0.23	-	-	-	-	-	-	-0.25	TS

WW Pup	5.52	-0.01	-	-	-	-	-0.18	-0.22	-	-	-	-	-	-	-0.01	TS
RY Sco	20.32	0.10	-	-	-	-	0.09	0.05	-	-	-	-	-	-	0.10	TS
V500 Sco	9.32	0.06	-	-	-	-	0.01	-0.03	-	-	-	-	-	-	0.06	TS
BB Sgr	6.64	-0.06	-	-	-	-	0.08	0.04	-	-	-	-	-	-	-0.06	TS
WZ Sgr	21.85	0.19	-	-	-	-	0.19	0.15	-	-	-	-	-	-	0.13	TS
XX Sgr	6.42	0.04	-	-	-	-	0.10	0.06	-	-	-	-	-	-	0.04	TS
Y Sgr	5.77	0.05	-	-	-	-	0.05	0.01	-	-	-	-	-	-	0.02	TS
KQ Sco	28.69	0.08	-	-	-	-	0.16	0.12	0.35	0.30	-	-	-	-	0.10	TS
EW Sct	5.82	0.11	-	-	-	-	0.04	0.00	-	-	0.17	0.00	-	-	0.01	TS
V367 Sct	6.29	0.09	-	-	-	-	-0.01	-0.05	-	-	0.20	0.03	-	-	0.10	TS
BQ Ser	4.27	0.01	-	-	-	-	-0.04	-0.08	-	-	0.23	0.06	-	-	-0.09	TS
EK Pup	2.63	-0.05	-	-	-	-	-	-	-0.18	-0.23	-	-	-	-	-0.15	TS
WY Pup	5.25	-0.13	-	-	-	-	-	-	-0.35	-0.40	-	-	-	-	-0.06	TS
V470 Sco	16.26	0.16	-	-	-	-	-	-	0.30	0.25	-	-	-	-	0.16	TS
X Sct	4.20	0.12	-	-	-	-	-	-	0.06	0.01	-	-	-	-	0.12	TS
CR Ser	5.30	0.04	-	-	-	-	-	-	0.11	0.06	-	-	-	-	0.04	TS
AY Sgr	6.57	0.17	-	-	-	-	-	-	0.20	0.15	-	-	-	-	0.17	TS
V1954 Sgr	6.18	0.35	-	-	-	-	-	-	0.29	0.24	-	-	-	-	0.35	TS
V773 Sgr	5.75	0.20	-	-	-	-	-	-	0.11	0.06	-	-	-	-	0.20	TS
EY Car	2.88	-0.02	-	-	-	-	-	-	-	-	0.21	0.04	-	-	-0.12	TS
GZ Car	4.16	0.23	-	-	-	-	-	-	-	-	0.19	0.02	-	-	0.13	TS
Y Car	3.64	0.10	-	-	-	-	-	-	-	-	0.15	-0.02	-	-	0.00	TS
BK Cen	3.17	0.19	-	-	-	-	-	-	-	-	0.18	0.01	-	-	0.16	TS
UZ Cen	3.33	0.11	-	-	-	-	-	-	-	-	0.16	-0.01	-	-	0.09	TS
V458 Sct	4.84	0.15	-	-	-	-	-	-	-	-	0.17	0.00	-	-	0.05	TS
U TrA	2.57	0.07	-	-	-	-	-	-	-	-	0.15	-0.02	-	-	-0.03	TS
AP Vel	3.13	0.10	-	-	-	-	-	-	-	-	0.17	0.00	-	-	0.00	TS
AO CMa	5.82	-	-0.04	0.02	-	-	-	-	-	-	-	-	-	-	0.02	LEM
AX Aur	3.05	-	-0.22	-0.16	-0.04	-0.15	-	-	-	-	-	-	-	-	-0.16	LEM
BV Mon	3.01	-	-0.10	-0.04	-0.10	-0.21	-	-	-	-	-	-	-	-	-0.04	LEM
WX Pup	8.94	-	-0.15	-0.09	-0.04	-0.15	-	-	-	-	-	-	-	-	-0.09	LEM
AV Tau	3.62	-	-0.17	-0.11	-0.07	-0.18	-	-	-	-	-	-	-	-	-0.11	LEM
AO Aur	6.76	-	-0.41	-0.35	-0.27	-0.38	-0.14	-0.18	-	-	-	-	-	-	-0.35	LEM
BK Aur	8.00	-	-0.07	-0.01	-0.04	-0.15	0.17	0.13	-	-	-	-	-	-	-0.01	LEM
SY Aur	10.14	-	-0.13	-0.07	0.04	-0.07	-0.02	-0.06	-	-	-	-	-	-	-0.07	LEM
Y Aur	3.86	-	-0.26	-0.20	0.03	-0.08	-0.23	-0.27	-	-	-	-	-	-	-0.20	LEM
EK Mon	3.96	-	-0.05	0.01	0.04	-0.07	-0.10	-0.14	-	-	-	-	-	-	0.01	LEM
UY Mon	2.40	-	-0.33	-0.27	-0.09	-0.20	-0.08	-0.12	-	-	-	-	-	-	-0.27	LEM
AD Pup	13.59	-	-0.20	-0.14	-0.03	-0.14	-0.24	-0.28	-	-	-	-	-	-	-0.14	LEM
ST Tau	4.03	-	-0.14	-0.08	0.00	-0.11	-0.05	-0.09	-	-	-	-	-	-	-0.08	LEM
AH Vel	4.23	-	-0.04	0.02	0.19	0.08	0.10	0.06	-	-	-	-	-	-	0.02	LEM
YZ Aur	18.19	-	-0.33	-0.27	-0.30	-0.41	-0.36	-0.40	-	-	-	-	-0.60	-0.41	-0.27	LEM
WW Mon	4.66	-	-0.32	-0.26	-0.19	-0.30	-0.29	-0.33	-	-	-	-	-0.55	-0.36	-0.26	LEM
RY CMa	4.68	-	-0.16	-0.10	-	-	0.02	-0.02	-	-	-	-	-	-	-0.10	LEM
RZ CMa	4.25	-	-0.20	-0.14	-	-	-0.03	-0.07	-	-	-	-	-	-	-0.14	LEM
TW CMa	7.00	-	-0.51	-0.45	-	-	-0.19	-0.23	-	-	-	-	-	-	-0.45	LEM
GQ Ori	8.62	-	0.11	0.17	-	-	0.01	-0.03	-	-	-	-	-	-	0.17	LEM
BC Aql	2.91	-	-	-	-0.28	-0.39	-	-	-	-	-	-	-	-	-0.39	LIII
EV Aql	38.71	-	-	-	0.06	-0.05	-	-	-	-	-	-	-	-	-0.05	LIII
KL Aql	6.11	-	-	-	0.33	0.22	-	-	-	-	-	-	-	-	0.22	LIII
U Aql	7.02	-	-	-	0.17	0.06	-	-	-	-	-	-	-	-	0.06	LIII
V1344 Aql	7.48	-	-	-	0.15	0.04	-	-	-	-	-	-	-	-	0.04	LIII
V336 Aql	7.30	-	-	-	0.18	0.07	-	-	-	-	-	-	-	-	0.07	LIII
V493 Aql	2.99	-	-	-	0.03	-0.08	-	-	-	-	-	-	-	-	-0.08	LIII
V526 Aql	4.21	-	-	-	0.50	0.39	-	-	-	-	-	-	-	-	0.39	LIII
V916 Aql	13.44	-	-	-	0.39	0.28	-	-	-	-	-	-	-	-	0.28	LIII
CO Aur	1.78	-	-	-	-0.01	-0.12	-	-	-	-	-	-	-	-	-0.12	LIII
FF Aur	2.12	-	-	-	-0.51	-0.62	-	-	-	-	-	-	-	-	-0.62	LIII
GT Aur	4.40	-	-	-	-0.02	-0.13	-	-	-	-	-	-	-	-	-0.13	LIII
V637 Aur	7.85	-	-	-	-0.15	-0.26	-	-	-	-	-	-	-	-	-0.26	LIII
AC Cam	4.16	-	-	-	-0.13	-0.24	-	-	-	-	-	-	-	-	-0.24	LIII
AM Cam	4.00	-	-	-	-0.13	-0.24	-	-	-	-	-	-	-	-	-0.24	LIII
CK Cam	3.29	-	-	-	0.07	-0.04	-	-	-	-	-	-	-	-	-0.04	LIII
LO Cam	12.64	-	-	-	-0.05	-0.16	-	-	-	-	-	-	-	-	-0.16	LIII
MN Cam	8.20	-	-	-	0.01	-0.10	-	-	-	-	-	-	-	-	-0.10	LIII
MQ Cam	6.60	-	-	-	-0.11	-0.22	-	-	-	-	-	-	-	-	-0.22	LIII
OX Cam	5.07	-	-	-	-0.01	-0.12	-	-	-	-	-	-	-	-	-0.12	LIII
PV Cam	3.09	-	-	-	-0.17	-0.28	-	-	-	-	-	-	-	-	-0.28	LIII
QS Cam	5.12	-	-	-	-0.22	-0.33	-	-	-	-	-	-	-	-	-0.33	LIII
V359 Cam	6.60	-	-	-	-0.16	-0.27	-	-	-	-	-	-	-	-	-0.27	LIII
AP Cas	6.85	-	-	-	0.05	-0.06	-	-	-	-	-	-	-	-	-0.06	LIII
AS Cas	3.02	-	-	-	0.02	-0.09	-	-	-	-	-	-	-	-	-0.09	LIII
AW Cas	4.28	-	-	-	0.03	-0.08	-	-	-	-	-	-	-	-	-0.08	LIII
AY Cas	2.87	-	-	-	0.02	-0.09	-	-	-	-	-	-	-	-	-0.09	LIII
BF Cas	3.63	-	-	-	-0.05	-0.16	-	-	-	-	-	-	-	-	-0.16	LIII
BP Cas	6.27	-	-	-	0.09	-0.02	-	-	-	-	-	-	-	-	-0.02	LIII
BV Cas	5.40	-	-	-	0.02	-0.09	-	-	-	-	-	-	-	-	-0.09	LIII
BY Cas	3.22	-	-	-	0.12	0.01	-	-	-	-	-	-	-	-	0.01	LIII
CD Cas	7.80	-	-	-	0.13	0.02	-	-	-	-	-	-	-	-	0.02	LIII
CG Cas	4.37	-	-	-	0.09	-0.02	-	-	-	-	-	-	-	-	-0.02	LIII
CT Cas	3.81	-	-	-	-0.05	-0.16	-	-	-	-	-	-	-	-	-0.16	LIII
CZ Cas	5.66	-	-	-	0.07	-0.04	-	-	-	-	-	-	-	-	-0.04	LIII
DW Cas	5.00	-	-	-	0.06	-0.05	-	-	-	-	-	-	-	-	-0.05	LIII
EX Cas	4.31	-	-	-	-0.07	-0.18	-	-	-	-	-	-	-	-	-0.18	LIII
FW Cas	6.24	-	-	-	-0.09	-0.20	-	-	-	-	-	-	-	-	-0.20	LIII
GL Cas	4.01	-	-	-	0.03	-0.08	-	-	-	-	-	-	-	-	-0.08	LIII
GM Cas	7.47	-	-	-	-0.10	-0.21	-	-	-	-	-	-	-	-	-0.21	LIII
GO Cas	3.24	-	-	-	0.12	0.01	-	-	-	-	-	-	-	-	0.01	LIII
HK Cas	2.50	-	-	-	0.45	0.34	-	-	-	-	-	-	-	-	0.34	LIII
KK Cas	8.19	-	-	-	0.13	0.02	-	-	-	-	-	-	-	-	0.02	LIII
LT Cas	5.90	-	-	-	-0.36	-0.47	-	-	-	-	-	-	-	-	-0.47	LIII
NP Cas	6.17	-	-	-	0.01	-0.10	-	-	-	-	-	-	-	-	-0.10	LIII
OP Cas	5.51	-	-	-	0.14	0.03	-	-	-	-	-	-	-	-	0.03	LIII
OZ Cas	5.08	-	-	-	0.06	-0.05	-	-	-	-	-	-	-	-	-0.05	LIII
PW Cas	4.00	-	-	-	-0.06	-0.17	-	-	-	-	-	-	-	-	-0.17	LIII
RS Cas	6.30	-	-	-	0.18	0.07	-	-	-	-	-	-	-	-	0.07	LIII
UZ Cas	4.26	-	-	-	-0.05	-0.16	-	-	-	-	-	-	-	-	-0.16	LIII
V1017 Cas	4.64	-	-	-	-0.18	-0.29	-	-	-	-	-	-	-	-	-0.29	LIII
V1019 Cas	3.62	-	-	-	0.07	-0.04	-	-	-	-	-	-	-	-	-0.04	LIII
V1020 Cas	4.74	-	-	-	0.15	0.04	-	-	-	-	-	-	-	-	0.04	LIII
V1100 Cas	4.71	-	-	-	0.02	-0.09	-	-	-	-	-	-	-	-	-0.09	LIII
V1154 Cas	2.11	-	-	-	-0.06	-0.17	-	-	-	-	-	-	-	-	-0.17	LIII
V1206 Cas	4.74	-	-	-	-0.16	-0.27	-	-	-	-	-	-	-	-	-0.27	LIII
V342 Cas	3.92	-	-	-	0.03	-0.08	-	-	-	-	-	-	-	-	-0.08	LIII
V395 Cas	4.04	-	-	-	0.02	-0.09	-	-	-	-	-	-	-	-	-0.09	LIII
V407 Cas	4.58	-	-	-	0.11	0.00	-	-	-	-	-	-	-	-	0.00	LIII
V556 Cas	6.03	-	-	-	-0.01	-0.12	-	-	-	-	-	-	-	-	-0.12	LIII
VV Cas	6.21	-	-	-	-0.04	-0.15	-	-	-	-	-	-	-	-	-0.15	LIII

VW Cas	5.99	-	-	-	0.19	0.08	-	-	-	-	-	-	-	-	0.08	LIII
AK Cep	7.23	-	-	-	0.05	-0.06	-	-	-	-	-	-	-	-	-0.06	LIII
CN Cep	9.50	-	-	-	0.06	-0.05	-	-	-	-	-	-	-	-	-0.05	LIII
DR Cep	19.08	-	-	-	-0.14	-0.25	-	-	-	-	-	-	-	-	-0.25	LIII
IY Cep	5.66	-	-	-	0.11	0.00	-	-	-	-	-	-	-	-	0.00	LIII
MU Cep	3.77	-	-	-	0.18	0.07	-	-	-	-	-	-	-	-	0.07	LIII
V901 Cep	9.00	-	-	-	0.04	-0.07	-	-	-	-	-	-	-	-	-0.07	LIII
V911 Cep	4.28	-	-	-	-0.02	-0.13	-	-	-	-	-	-	-	-	-0.13	LIII
EP Cyg	4.32	-	-	-	-0.06	-0.17	-	-	-	-	-	-	-	-	-0.17	LIII
EU Cyg	14.99	-	-	-	-0.20	-0.31	-	-	-	-	-	-	-	-	-0.31	LIII
EX Cyg	4.85	-	-	-	0.25	0.14	-	-	-	-	-	-	-	-	0.14	LIII
EZ Cyg	11.66	-	-	-	0.28	0.17	-	-	-	-	-	-	-	-	0.17	LIII
GH Cyg	7.82	-	-	-	0.21	0.10	-	-	-	-	-	-	-	-	0.10	LIII
GI Cyg	5.78	-	-	-	0.27	0.16	-	-	-	-	-	-	-	-	0.16	LIII
GL Cyg	3.37	-	-	-	0.05	-0.06	-	-	-	-	-	-	-	-	-0.06	LIII
IY Cyg	21.75	-	-	-	-0.09	-0.20	-	-	-	-	-	-	-	-	-0.20	LIII
KX Cyg	20.05	-	-	-	0.21	0.10	-	-	-	-	-	-	-	-	0.10	LIII
V1020 Cyg	4.92	-	-	-	0.29	0.18	-	-	-	-	-	-	-	-	0.18	LIII
V1025 Cyg	6.96	-	-	-	0.23	0.12	-	-	-	-	-	-	-	-	0.12	LIII
V1046 Cyg	4.94	-	-	-	0.23	0.12	-	-	-	-	-	-	-	-	0.12	LIII
V1364 Cyg	12.98	-	-	-	0.29	0.18	-	-	-	-	-	-	-	-	0.18	LIII
V1397 Cyg	4.64	-	-	-	0.01	-0.10	-	-	-	-	-	-	-	-	-0.10	LIII
V347 Cyg	8.74	-	-	-	0.25	0.14	-	-	-	-	-	-	-	-	0.14	LIII
V356 Cyg	5.06	-	-	-	0.17	0.06	-	-	-	-	-	-	-	-	0.06	LIII
V396 Cyg	33.25	-	-	-	0.11	0.00	-	-	-	-	-	-	-	-	0.00	LIII
V438 Cyg	11.21	-	-	-	0.33	0.22	-	-	-	-	-	-	-	-	0.22	LIII
V459 Cyg	7.25	-	-	-	0.09	-0.02	-	-	-	-	-	-	-	-	-0.02	LIII
V492 Cyg	7.58	-	-	-	0.24	0.13	-	-	-	-	-	-	-	-	0.13	LIII
V495 Cyg	6.72	-	-	-	0.24	0.13	-	-	-	-	-	-	-	-	0.13	LIII
V514 Cyg	5.10	-	-	-	0.18	0.07	-	-	-	-	-	-	-	-	0.07	LIII
V520 Cyg	4.05	-	-	-	0.08	-0.03	-	-	-	-	-	-	-	-	-0.03	LIII
V538 Cyg	6.12	-	-	-	0.05	-0.06	-	-	-	-	-	-	-	-	-0.06	LIII
V547 Cyg	6.23	-	-	-	0.15	0.04	-	-	-	-	-	-	-	-	0.04	LIII
V609 Cyg	31.07	-	-	-	0.22	0.11	-	-	-	-	-	-	-	-	0.11	LIII
V621 Cyg	5.86	-	-	-	0.12	0.01	-	-	-	-	-	-	-	-	0.01	LIII
EK Del	2.05	-	-	-	-1.54	-1.65	-	-	-	-	-	-	-	-	-1.65	LIII
DF Lac	4.48	-	-	-	0.04	-0.07	-	-	-	-	-	-	-	-	-0.07	LIII
FQ Lac	11.27	-	-	-	-0.20	-0.31	-	-	-	-	-	-	-	-	-0.31	LIII
V411 Lac	2.91	-	-	-	0.02	-0.09	-	-	-	-	-	-	-	-	-0.09	LIII
CS Mon	6.73	-	-	-	-0.08	-0.19	-	-	-	-	-	-	-	-	-0.19	LIII
V446 Mon	1.92	-	-	-	-0.30	-0.41	-	-	-	-	-	-	-	-	-0.41	LIII
V447 Mon	2.48	-	-	-	-0.37	-0.48	-	-	-	-	-	-	-	-	-0.48	LIII
V911 Mon	4.98	-	-	-	-0.01	-0.12	-	-	-	-	-	-	-	-	-0.12	LIII
VZ Mon	5.08	-	-	-	-0.07	-0.18	-	-	-	-	-	-	-	-	-0.18	LIII
YY Mon	3.45	-	-	-	-0.46	-0.57	-	-	-	-	-	-	-	-	-0.57	LIII
DF Ori	3.18	-	-	-	-0.28	-0.39	-	-	-	-	-	-	-	-	-0.39	LIII
AU Peg	2.40	-	-	-	0.46	0.35	-	-	-	-	-	-	-	-	0.35	LIII
DW Per	3.65	-	-	-	-0.05	-0.16	-	-	-	-	-	-	-	-	-0.16	LIII
HZ Per	11.28	-	-	-	-0.25	-0.36	-	-	-	-	-	-	-	-	-0.36	LIII
QQ Per	11.17	-	-	-	-0.67	-0.78	-	-	-	-	-	-	-	-	-0.78	LIII
SX Per	4.29	-	-	-	-0.03	-0.14	-	-	-	-	-	-	-	-	-0.14	LIII
UY Per	5.37	-	-	-	0.18	0.07	-	-	-	-	-	-	-	-	0.07	LIII
V891 Per	3.22	-	-	-	0.09	-0.02	-	-	-	-	-	-	-	-	-0.02	LIII
VY Per	5.53	-	-	-	0.04	-0.07	-	-	-	-	-	-	-	-	-0.07	LIII
DV Ser	23.06	-	-	-	0.47	0.36	-	-	-	-	-	-	-	-	0.36	LIII
DG Sge	4.44	-	-	-	0.13	0.02	-	-	-	-	-	-	-	-	0.02	LIII
GX Sge	12.90	-	-	-	0.29	0.18	-	-	-	-	-	-	-	-	0.18	LIII
GY Sge	51.06	-	-	-	0.29	0.18	-	-	-	-	-	-	-	-	0.18	LIII
AS Vul	12.22	-	-	-	0.22	0.11	-	-	-	-	-	-	-	-	0.11	LIII
DG Vul	13.61	-	-	-	0.19	0.08	-	-	-	-	-	-	-	-	0.08	LIII
SS CMa	12.36	-	-	-	0.07	-0.04	-	-	-0.02	-0.07	-	-	-	-	-0.04	LIII
TV CMa	4.67	-	-	-	0.14	0.03	-	-	0.03	-0.02	-	-	-	-	0.03	LIII
V1033 Cyg	4.94	-	-	-	0.12	0.01	-	-	0.04	-0.01	-	-	-	-	0.01	LIII
BX Sct	6.41	-	-	-	0.28	0.17	-	-	0.13	0.08	-	-	-	-	0.17	LIII
CK Sct	7.42	-	-	-	0.21	0.10	-	-	0.12	0.07	-	-	-	-	0.10	LIII
CM Sct	3.92	-	-	-	0.15	0.04	-	-	0.07	0.02	-	-	-	-	0.04	LIII
Y Sct	10.34	-	-	-	0.23	0.12	-	-	0.13	0.08	-	-	-	-	0.12	LIII
EW Aur	2.66	-	-	-	-0.54	-0.65	-	-	-	-	-	-	-0.86	-0.67	-0.65	LIII
GV Aur	5.26	-	-	-	-0.21	-0.32	-	-	-	-	-	-	-0.23	-0.04	-0.32	LIII
IN Aur	4.91	-	-	-	-0.28	-0.39	-	-	-	-	-	-	-0.48	-0.29	-0.39	LIII
FO Cas	6.80	-	-	-	-0.56	-0.67	-	-	-	-	-	-	-0.86	-0.67	-0.67	LIII
IO Cas	5.60	-	-	-	-0.49	-0.60	-	-	-	-	-	-	-0.76	-0.57	-0.60	LIII
NY Cas	2.82	-	-	-	-0.46	-0.57	-	-	-	-	-	-	-0.66	-0.47	-0.57	LIII
V484 Mon	3.14	-	-	-	-0.06	-0.17	-	-	-	-	-	-	-0.42	-0.23	-0.17	LIII
CR Ori	4.91	-	-	-	-0.19	-0.30	-	-	-	-	-	-	-0.54	-0.35	-0.30	LIII
CI Per	3.38	-	-	-	-0.32	-0.43	-	-	-	-	-	-	-1.00	-0.81	-0.43	LIII
GP Per	2.04	-	-	-	-0.80	-0.91	-	-	-	-	-	-	-0.85	-0.66	-0.91	LIII
OT Per	26.09	-	-	-	-0.07	-0.18	-	-	-	-	-	-	-0.84	-0.65	-0.18	LIII
FM Aql	6.11	-	-	-	0.24	0.13	0.08	0.04	-	-	-	-	-	-	0.13	LIII
FN Aql	9.48	-	-	-	-0.06	-0.17	-0.02	-0.06	-	-	-	-	-	-	-0.17	LIII
TT Aql	13.75	-	-	-	0.22	0.11	0.10	0.06	-	-	-	-	-	-	0.11	LIII
V1359 Aql	7.78	-	-	-	0.28	0.17	0.09	0.05	-	-	-	-	-	-	0.17	LIII
AN Aur	10.29	-	-	-	-0.10	-0.21	-0.15	-0.19	-	-	-	-	-	-	-0.21	LIII
RT Aur	3.73	-	-	-	0.13	0.02	0.06	0.02	-	-	-	-	-	-	0.02	LIII
RX Aur	11.62	-	-	-	0.10	-0.01	-0.01	-0.05	-	-	-	-	-	-	-0.01	LIII
V335 Aur	3.41	-	-	-	-0.30	-0.41	-0.27	-0.31	-	-	-	-	-	-	-0.41	LIII
AB Cam	5.79	-	-	-	-0.08	-0.19	-0.09	-0.13	-	-	-	-	-	-	-0.19	LIII
AD Cam	11.26	-	-	-	-0.25	-0.36	-0.22	-0.26	-	-	-	-	-	-	-0.36	LIII
RW Cam	16.41	-	-	-	0.11	0.00	0.09	0.05	-	-	-	-	-	-	0.00	LIII
RX Cam	7.91	-	-	-	0.11	0.00	0.04	0.00	-	-	-	-	-	-	0.00	LIII
TV Cam	5.29	-	-	-	0.04	-0.07	-0.08	-0.12	-	-	-	-	-	-	-0.07	LIII
CF Cas	4.88	-	-	-	0.02	-0.09	-0.01	-0.05	-	-	-	-	-	-	-0.09	LIII
SZ Cas	13.64	-	-	-	0.07	-0.04	0.04	0.00	-	-	-	-	-	-	-0.04	LIII
XY Cas	4.50	-	-	-	0.10	-0.01	0.03	-0.01	-	-	-	-	-	-	-0.01	LIII
CE CasA	5.14	-	-	-	-0.12	-0.23	0.18	0.14	-	-	-	-	-	-	-0.23	LIII
CE CasB	4.48	-	-	-	-0.15	-0.26	0.22	0.18	-	-	-	-	-	-	-0.26	LIII
KN Cen	34.03	-	-	-	0.41	0.30	0.35	0.31	-	-	-	-	-	-	0.30	LIII
δ Cep	5.37	-	-	-	0.12	0.01	0.09	0.05	-	-	-	-	-	-	0.01	LIII
BG Cru	3.34	-	-	-	-0.08	-0.19	0.02	-0.02	-	-	-	-	-	-	-0.19	LIII
CD Cyg	17.07	-	-	-	0.15	0.04	0.11	0.07	-	-	-	-	-	-	0.04	LIII
BB Gem	2.31	-	-	-	-0.10	-0.21	-0.09	-0.13	-	-	-	-	-	-	-0.21	LIII
W Gem	7.91	-	-	-	0.02	-0.09	-0.01	-0.05	-	-	-	-	-	-	-0.09	LIII
BB Her	7.51	-	-	-	0.26	0.15	0.15	0.11	-	-	-	-	-	-	0.15	LIII
BG Lac	5.33	-	-	-	0.07	-0.04	-0.01	-0.05	-	-	-	-	-	-	-0.04	LIII
RR Lac	6.42	-	-	-	0.04	-0.07	0.13	0.09	-	-	-	-	-	-	-0.07	LIII
V Lac	4.98	-	-	-	0.06	-0.05	0.00	-0.04	-	-	-	-	-	-	-0.05	LIII
X Lac	5.44	-	-	-	0.08	-0.03	-0.02	-0.06	-	-	-	-	-	-	-0.03	LIII
Y Lac	4.32	-	-	-	0.03	-0.08	-0.04	-0.08	-	-	-	-	-	-	-0.08	LIII

Z Lac	10.89	-	-	-	0.10	-0.01	0.01	-0.03	-	-	-	-	-	-	-0.01	LIII
V473 Lyr	1.49	-	-	-	-0.06	-0.17	-0.06	-0.10	-	-	-	-	-	-	-0.17	LIII
AA Mon	3.94	-	-	-	-0.09	-0.20	-0.21	-0.25	-	-	-	-	-	-	-0.20	LIII
AC Mon	8.01	-	-	-	-0.03	-0.14	-0.14	-0.18	-	-	-	-	-	-	-0.14	LIII
FG Mon	4.50	-	-	-	-0.14	-0.25	-0.20	-0.24	-	-	-	-	-	-	-0.25	LIII
T Mon	27.02	-	-	-	0.23	0.12	0.13	0.09	-	-	-	-	-	-	0.12	LIII
V504 Mon	2.77	-	-	-	0.01	-0.10	-0.31	-0.35	-	-	-	-	-	-	-0.10	LIII
V526 Mon	2.67	-	-	-	-0.17	-0.28	-0.13	-0.17	-	-	-	-	-	-	-0.28	LIII
AS Per	4.97	-	-	-	0.14	0.03	0.10	0.06	-	-	-	-	-	-	0.03	LIII
AW Per	6.46	-	-	-	0.04	-0.07	0.01	-0.03	-	-	-	-	-	-	-0.07	LIII
BM Per	22.95	-	-	-	0.23	0.12	0.02	-0.02	-	-	-	-	-	-	0.12	LIII
MM Per	4.12	-	-	-	-0.07	-0.18	-0.01	-0.05	-	-	-	-	-	-	-0.18	LIII
SV Per	11.13	-	-	-	0.06	-0.05	0.01	-0.03	-	-	-	-	-	-	-0.05	LIII
UX Per	4.57	-	-	-	-0.05	-0.16	-0.21	-0.25	-	-	-	-	-	-	-0.16	LIII
VX Per	10.89	-	-	-	0.06	-0.05	-0.04	-0.08	-	-	-	-	-	-	-0.05	LIII
V335 Pup	4.86	-	-	-	0.09	-0.02	-0.01	-0.05	-	-	-	-	-	-	-0.02	LIII
SS Sct	3.67	-	-	-	0.14	0.03	0.06	0.02	-	-	-	-	-	-	0.03	LIII
AE Tau	3.90	-	-	-	-0.18	-0.29	-0.19	-0.23	-	-	-	-	-	-	-0.29	LIII
S Vul	68.46	-	-	-	0.12	0.01	-0.01	-0.05	-	-	-	-	-	-	0.01	LIII
U Vul	7.99	-	-	-	0.19	0.08	0.09	0.05	-	-	-	-	-	-	0.08	LIII
CY Aur	13.85	-	-	-	-0.12	-0.23	-0.40	-0.44	-	-	-	-	-0.47	-0.28	-0.23	LIII
ER Aur	15.69	-	-	-	-0.27	-0.38	-0.34	-0.38	-	-	-	-	-0.60	-0.41	-0.38	LIII
CU Mon	4.71	-	-	-	-0.23	-0.34	-0.26	-0.30	-	-	-	-	-0.52	-0.33	-0.34	LIII
EE Mon	4.81	-	-	-	-0.52	-0.63	-0.51	-0.55	-	-	-	-	-0.49	-0.30	-0.63	LIII
FI Mon	3.29	-	-	-	-0.11	-0.22	-0.18	-0.22	-	-	-	-	-0.31	-0.12	-0.22	LIII
HQ Per	8.64	-	-	-	-0.35	-0.46	-0.31	-0.35	-	-	-	-	-0.43	-0.24	-0.46	LIII
η Aql	7.18	-	-	-	-	-	0.08	0.04	-	-	-	-	-	-	0.04	LII
FF Aql	4.47	-	-	-	-	-	0.04	0.00	-	-	-	-	-	-	0.00	LII
V1162 Aql	5.38	-	-	-	-	-	0.01	-0.03	-	-	-	-	-	-	-0.03	LII
V496 Aql	6.81	-	-	-	-	-	0.05	0.01	-	-	-	-	-	-	0.01	LII
V600 Aql	7.24	-	-	-	-	-	0.03	-0.01	-	-	-	-	-	-	-0.01	LII
V733 Aql	6.18	-	-	-	-	-	0.08	0.04	-	-	-	-	-	-	0.04	LII
BD Cas	3.65	-	-	-	-	-	-0.07	-0.11	-	-	-	-	-	-	-0.11	LII
CH Cas	15.09	-	-	-	-	-	0.17	0.13	-	-	-	-	-	-	0.13	LII
CY Cas	14.38	-	-	-	-	-	0.06	0.02	-	-	-	-	-	-	0.02	LII
DD Cas	9.81	-	-	-	-	-	0.10	0.06	-	-	-	-	-	-	0.06	LII
DF Cas	3.83	-	-	-	-	-	0.13	0.09	-	-	-	-	-	-	0.09	LII
DL Cas	8.00	-	-	-	-	-	-0.01	-0.05	-	-	-	-	-	-	-0.05	LII
FM Cas	5.81	-	-	-	-	-	-0.09	-0.13	-	-	-	-	-	-	-0.13	LII
RW Cas	14.79	-	-	-	-	-	0.22	0.18	-	-	-	-	-	-	0.18	LII
RY Cas	12.14	-	-	-	-	-	0.26	0.22	-	-	-	-	-	-	0.22	LII
SU Cas	1.95	-	-	-	-	-	0.06	0.02	-	-	-	-	-	-	0.02	LII
SW Cas	5.44	-	-	-	-	-	0.13	0.09	-	-	-	-	-	-	0.09	LII
SY Cas	4.07	-	-	-	-	-	0.04	0.00	-	-	-	-	-	-	0.00	LII
V379 Cas	4.31	-	-	-	-	-	0.06	0.02	-	-	-	-	-	-	0.02	LII
V636 Cas	8.38	-	-	-	-	-	0.07	0.03	-	-	-	-	-	-	0.03	LII
CP Cep	17.86	-	-	-	-	-	-0.01	-0.05	-	-	-	-	-	-	-0.05	LII
CR Cep	6.23	-	-	-	-	-	-0.06	-0.10	-	-	-	-	-	-	-0.10	LII
IR Cep	2.11	-	-	-	-	-	0.05	0.01	-	-	-	-	-	-	0.01	LII
V351 Cep	2.81	-	-	-	-	-	0.02	-0.02	-	-	-	-	-	-	-0.02	LII
VZ CMa	3.13	-	-	-	-	-	-0.06	-0.10	-	-	-	-	-	-	-0.10	LII
BZ Cyg	10.14	-	-	-	-	-	0.19	0.15	-	-	-	-	-	-	0.15	LII
DT Cyg	2.50	-	-	-	-	-	0.10	0.06	-	-	-	-	-	-	0.06	LII
MW Cyg	5.95	-	-	-	-	-	0.09	0.05	-	-	-	-	-	-	0.05	LII
SU Cyg	3.85	-	-	-	-	-	-0.03	-0.07	-	-	-	-	-	-	-0.07	LII
SZ Cyg	15.11	-	-	-	-	-	0.09	0.05	-	-	-	-	-	-	0.05	LII
TX Cyg	14.71	-	-	-	-	-	0.20	0.16	-	-	-	-	-	-	0.16	LII
V1154 Cyg	4.93	-	-	-	-	-	-0.10	-0.14	-	-	-	-	-	-	-0.14	LII
V1334 Cyg	3.33	-	-	-	-	-	0.03	-0.01	-	-	-	-	-	-	-0.01	LII
V1726 Cyg	4.24	-	-	-	-	-	-0.02	-0.06	-	-	-	-	-	-	-0.06	LII
V386 Cyg	5.26	-	-	-	-	-	0.11	0.07	-	-	-	-	-	-	0.07	LII
V402 Cyg	4.36	-	-	-	-	-	0.02	-0.02	-	-	-	-	-	-	-0.02	LII
V532 Cyg	3.28	-	-	-	-	-	-0.04	-0.08	-	-	-	-	-	-	-0.08	LII
V924 Cyg	5.57	-	-	-	-	-	-0.09	-0.13	-	-	-	-	-	-	-0.13	LII
VX Cyg	20.13	-	-	-	-	-	0.09	0.05	-	-	-	-	-	-	0.05	LII
VY Cyg	7.86	-	-	-	-	-	0.00	-0.04	-	-	-	-	-	-	-0.04	LII
VZ Cyg	4.86	-	-	-	-	-	0.05	0.01	-	-	-	-	-	-	0.01	LII
X Cyg	16.39	-	-	-	-	-	0.10	0.06	-	-	-	-	-	-	0.06	LII
TX Del	6.17	-	-	-	-	-	0.24	0.20	-	-	-	-	-	-	0.20	LII
V440 Per	7.57	-	-	-	-	-	-0.04	-0.08	-	-	-	-	-	-	-0.08	LII
S Sge	8.38	-	-	-	-	-	0.08	0.04	-	-	-	-	-	-	0.04	LII
AP Sgr	5.06	-	-	-	-	-	0.10	0.06	-	-	-	-	-	-	0.06	LII
U Sgr	6.75	-	-	-	-	-	0.08	0.04	-	-	-	-	-	-	0.04	LII
V350 Sgr	5.15	-	-	-	-	-	0.18	0.14	-	-	-	-	-	-	0.14	LII
W Sgr	7.59	-	-	-	-	-	0.02	-0.02	-	-	-	-	-	-	-0.02	LII
YZ Sgr	9.55	-	-	-	-	-	0.06	0.02	-	-	-	-	-	-	0.02	LII
EF Tau	3.45	-	-	-	-	-	-0.74	-0.78	-	-	-	-	-	-	-0.78	LII
EU Tau	2.10	-	-	-	-	-	-0.06	-0.10	-	-	-	-	-	-	-0.10	LII
SZ Tau	3.15	-	-	-	-	-	0.07	0.03	-	-	-	-	-	-	0.03	LII
SV Vul	44.99	-	-	-	-	-	0.05	0.01	-	-	-	-	-	-	0.01	LII
T Vul	4.44	-	-	-	-	-	0.01	-0.03	-	-	-	-	-	-	-0.03	LII
X Vul	6.32	-	-	-	-	-	0.07	0.03	-	-	-	-	-	-	0.03	LII
TU Cas	2.14	-	-	-	-	-	0.03	-0.01	-	-	0.23	0.06	-	-	-0.01	LII
BD-04 4569	13.84	-	-	-	-	-	-	-	0.08	0.03	-	-	-	-	0.03	MAR
ASAS J171305-4323.0	9.56	-	-	-	-	-	-	-	0.32	0.27	-	-	-	-	0.27	MAR
SU Sct	1.47	-	-	-	-	-	-	-	0.27	0.22	-	-	-	-	0.22	MAR
V5567 Sgr	9.76	-	-	-	-	-	-	-	0.07	0.02	-	-	-	-	0.02	MAR
V701 Car	4.32	-	-	-	-	-	-	-	-	-	0.21	0.04	-	-	0.04	SZI
V1048 Cen	0.92	-	-	-	-	-	-	-	-	-	0.21	0.04	-	-	0.04	SZI
V1210 Cen	4.09	-	-	-	-	-	-	-	-	-	0.21	0.04	-	-	0.04	SZI
HQ Car	14.07	-	-	-	-	-	-	-	-	-	-	-	-0.37	-0.18	-0.18	YON
XZ CMa	2.56	-	-	-	-	-	-	-	-	-	-	-	-0.53	-0.34	-0.34	YON

7.6 Metallicity Gradient

The last task of the current thesis was to get the metallicity gradient. In order to do this, the only further information required were the Galactocentric radii (distances), i.e. R_G. These data were collected indirectly from the FEROS base table by taking the heliocentric distances given therein and SIMBAD [35][36] Galactic longi- and latitudes and subsequently calculating the Galactocentric radius with the formulas given in Vivas (2006, [106]). The X-, Y- and Z-coordinates were also computed in this process. For the distance of the Sun to the Galactic center, a value of 7.94 kpc was adopted ([78]).

The heliocentric distances of five objects (BD-04 4569, CE Cas A, CE Cas B, ASAS J171305-4323.0 and V5567 Sgr) were not present in the FEROS base table and therefore calculated using brand-new period-wesenheit-relations from Inno (2016, submitted in ApJ). These relations provided the correct zero-intercept for computing the heliocentric distances. They could also be calculated by means of the Large Magellanic Cloud (LMC) PWRs from Inno (2013, [12]) and recalibrating the zero-point.

For the typical uncertainty on R_G, the average error of the heliocentric distances was taken, since the uncertainties on the Galactic longi- and latitude as well as the Galactocentric distance of the Sun were assumed negligible. Using the standard deviations of Fe I and Fe II of the single spectra and propagating these errors, the error on the metallicities for the single targets was calculated. By averaging the corresponding values, the typical uncertainty on [Fe/H] was derived.

The variability classes of several objects (BC Aql, HQ Car, HK Cas, DR Cep, EK Del, TX Del, QQ Per and V507 Sco) with either Z beyond +/-1 kpc from the Galactic plane, X and Y such that they would be located behind the Galactic center (seen from the solar perspective), $R_G > 20$ kpc or [Fe/H] $<$ -1.0 dex were rechecked, since those targets might be type II (and thus not classical) Cepheids. For this purpose, the GCVS variability type was compared with that given in the paper of the corresponding sample (if present). In case of disagreement, the variability class of the publication has been taken. On the basis of this check, three objects (HQ Car, TX Del and QQ Per) were found to be W Virginis stars and therefore type II Cepheids. Those stars were excluded from the entire analysis of this section. Please note that type II Cepheids could still be present in the remaining sample, but identifying them requires a thorough analysis that exceeds the scope of the thesis. However, they should be statistically irrelevant considering the total number of objects and thus have negligible influence on the derived results.

Plotting the abundances vs. the Galactocentric distance, figure 7.3 was created. It shows the Galactic metallicity gradient of the homogeneous database presented in section 7.5. The TS sample was divided into those stars for which metallicities were provided for the first time (TS (new)) and the ones for which literature values were present (TS (lit.)).

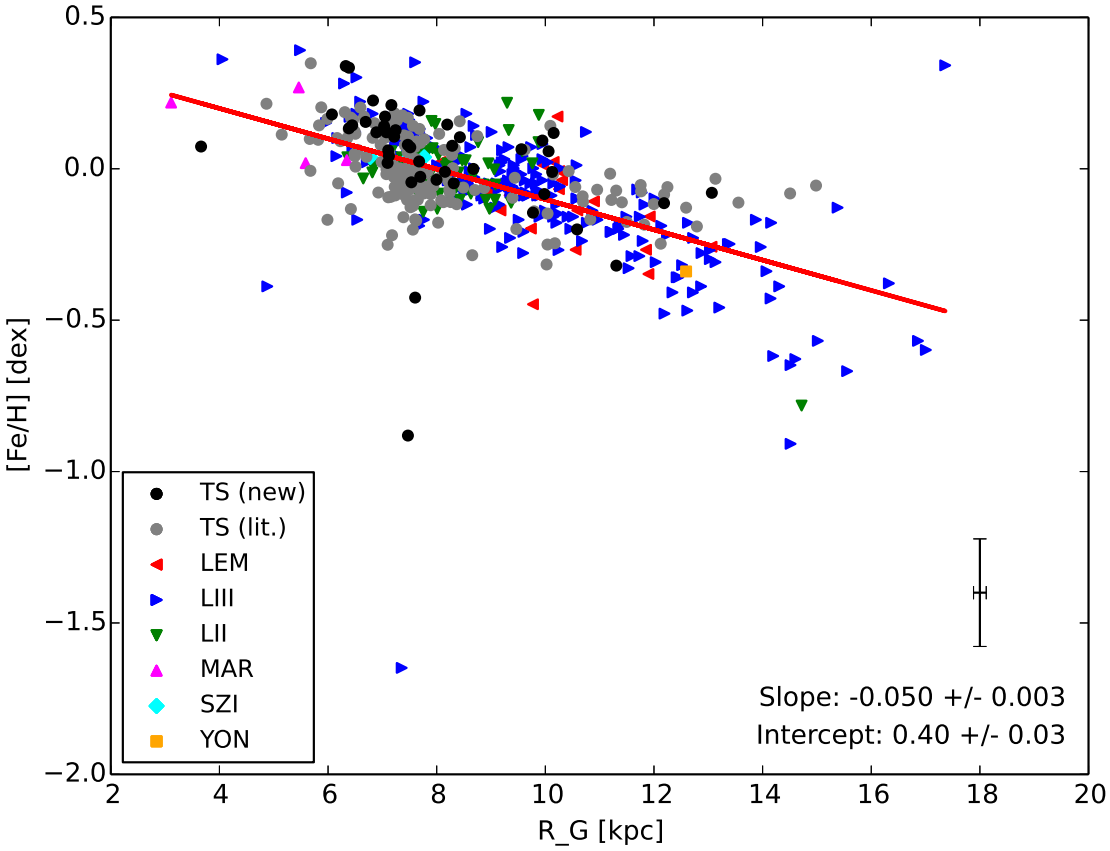

Figure 7.3: Metallicity gradient of the Milky Way. The plot shows the single data points as well as the slope and the intercept of the linear fit given by the red line (including the corresponding errors). The average error on R_G and [Fe/H] is visible in the lower right part of the figure.

The indicated slope and intercepts of the metallicity gradient indicate a decrease in iron content when moving further away from the Galactic center and agree well with the gradients given in Genovali (2014, [10]). The measurements that were obtained support and confirm the overall trend found so far and its implications.

The polar distribution of the Cepheids in the Galaxy is depicted in figure 7.4. Please note that the coordinate system has been rotated by 90° with respect to the one given in Vivas (2006, [106]). For simplicity, the Sun has furthermore been set at the coordinate origin, dividing the galactic plane into four quadrants. The vertical distribution of the Cepheids in the Milky Way can be seen in figure 7.5.

Similarly to Genovali (2013, [37]), the existence of asymmetries within these quadrants was checked by creating histograms of the objects belonging to each quadrant and fitting a Gaussian to them. These histograms are shown in figure 7.6. A comparison was made by means of a similar analysis for the variables listed in the paper of Genovali (2014, [10]), using the metallicities given therein. Figure 7.7 depicts the corresponding histograms.

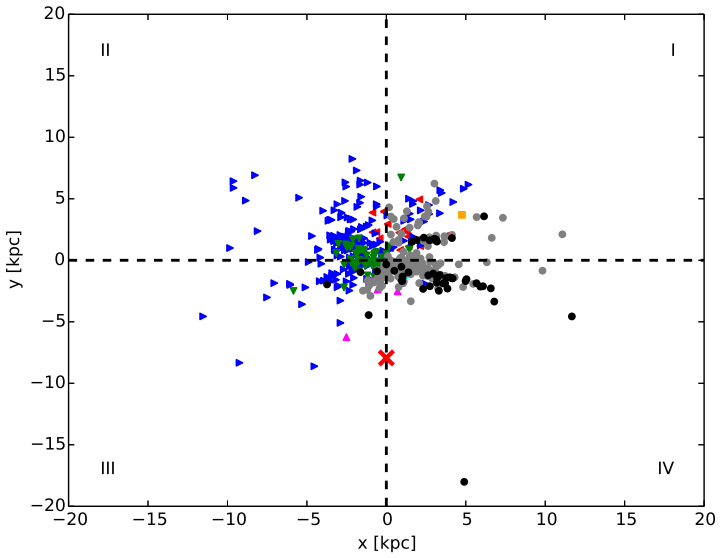

Figure 7.4: Polar Cepheid distribution of the Milky Way. The Sun is located at the intersection of the dashed black lines and the y-axis gives the direction from the Galactic center (denoted by the red cross) to the Sun. Roman numbers (I - IV) indicate the four different quadrants. The legend is the same as that of figure 7.3.

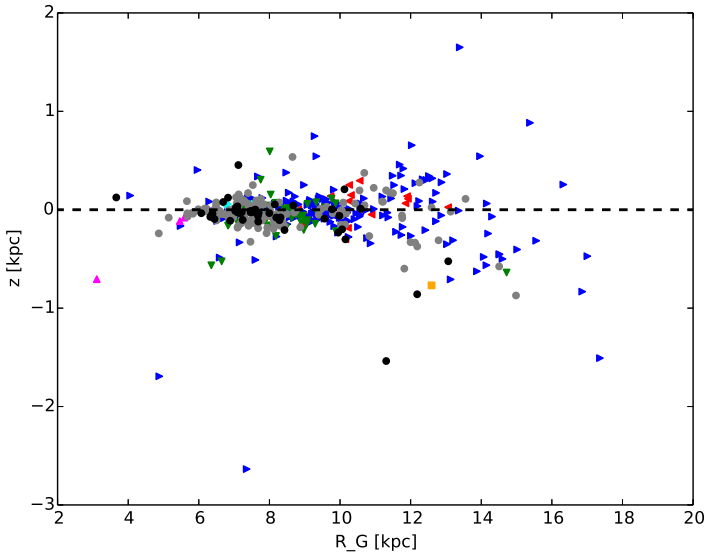

Figure 7.5: Vertical Cepheid distribution of the Milky Way. The dashed black line marks the location of the Galactic plane. The legend is the same as that of figure 7.3.

Cepheids are usually located within 1 kpc from the Galactic plane. Although on the plot five points are beyond these limits, indeed the bulk of the objects follows this rule. 467 out of 494 variables (i.e. 95 %) lie within 500 pc, while a 300 pc zone around the zero plane still comprises 433 Cepheids (88 %).

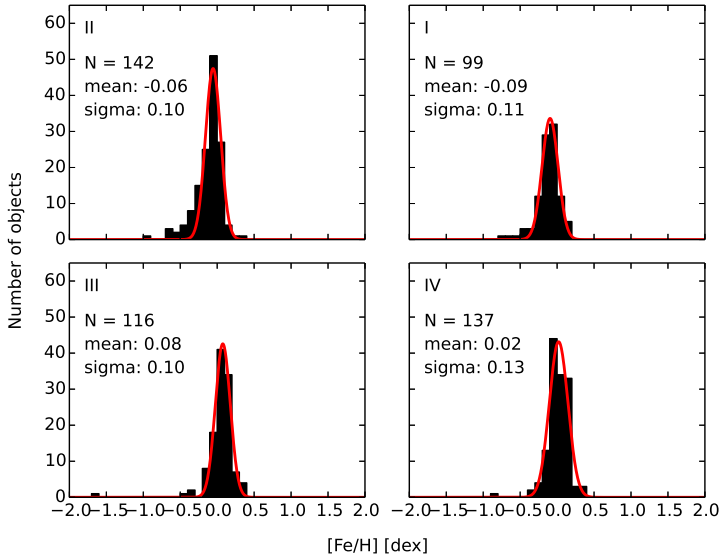

Figure 7.6: Cepheid histograms for the quadrants defined in figure 7.4. The number of objects in each quadrant and the mean as well as the standard deviation of the Gaussian fits (red lines) are indicated in the different panels. A bin size of 0.15 dex was used for the histograms.

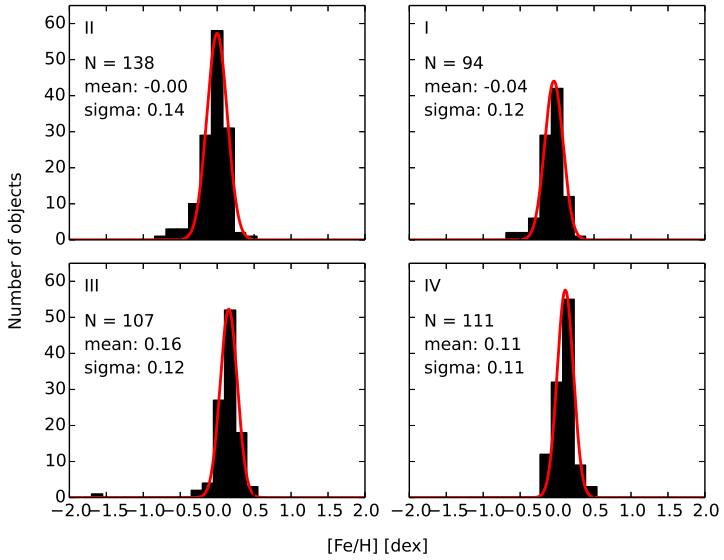

Figure 7.7: Same as figure 7.6, but for the Genovali objects and metallicities (see [10]).

The quadrants I and III are slightly underrepresented in the TS sample w.r.t II and IV. Genovali's sample shows asymmetries as well, with quadrant II being dominant over the other three. Compared to Genovali, the new targets fall mostly into quadrant IV. The widths of the Gaussians in the two datasets are well in agreement with each other ($\sim$ 0.11 and 0.12 dex, respectively). While the single mean metallicities differ slightly between TS and Genovali (since a new metallicity scale is used in this study), the differences are within the errors given

in the previous sections. Using a bin size to 0.1 dex or selecting only the objects within circles of radii ranging from 7 to 10 kpc (to discard the tail of the metallicity distribution) affected the mean abundances in either quadrant only insignificantly ($\sim$ 0.01 - 0.02 dex). As written in Genovali (2013, [37]), a slight asymmetry in the polar distribution (increasing iron abundances in the sequence I-II-IV-III) might be indicated by the histograms, but the trend is too weak (in both samples less than 0.2 dex difference between the minimum and maximum average metallicities) to make definitive statements.

Finally, in figure 7.8, the slopes of different metallicity gradients from the literature are compared to TS. These radial gradients are based on different stellar tracers, i.e. Cepheids, open clusters (OCs) and HII regions.

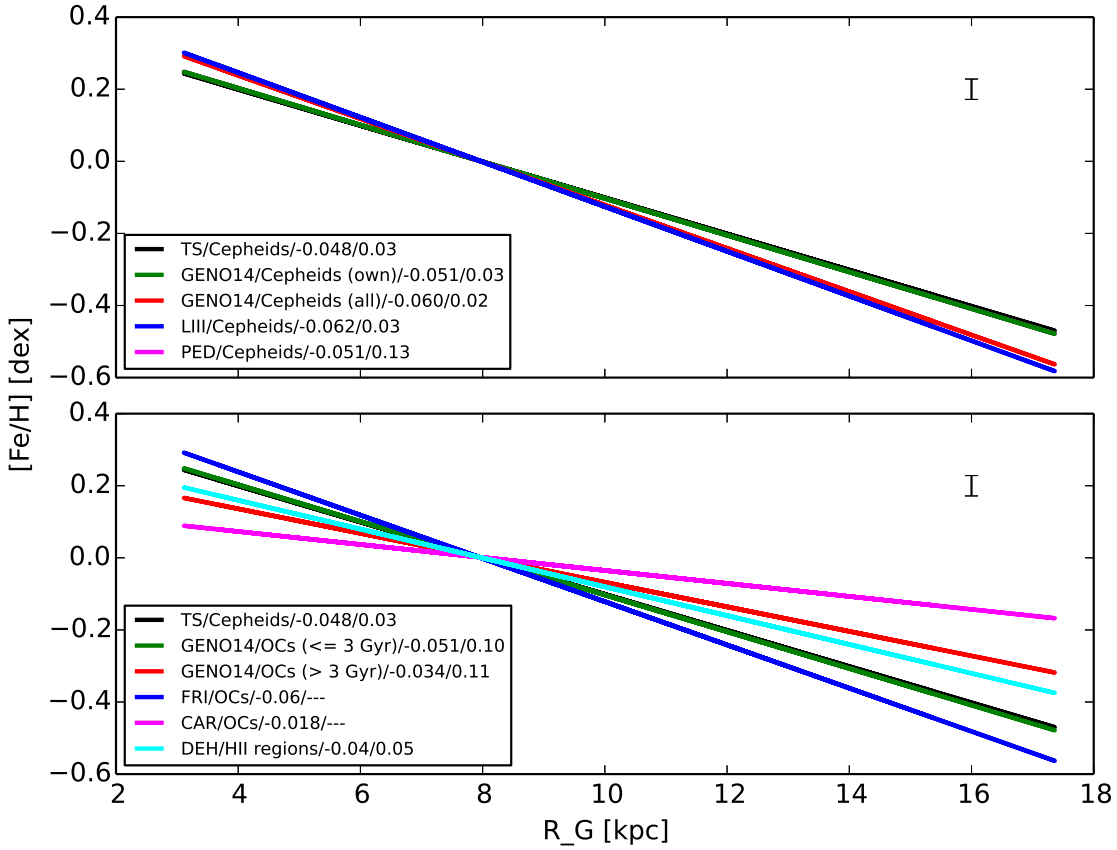

Figure 7.8: Slopes of metallicity gradients taken from the literature, set in comparison with the one obtained in this thesis (TS). In the top and bottom panel TS is compared to metallicity gradients based on Cepheids and other stellar tracers, respectively. The legend gives the publication in which the gradient was described together with the stellar tracer that had been used to derive it and the value of the slope as well as the fit uncertainties. These standard deviations were either calculated by summing the squares of the uncertainties on the slope and on the intercepts (TS, GENO14, LIII, DEH) or taken directly from the corresponding paper (PED). For TS the error on the gradient is given in the upper right part of the plot. For better comparability the zero-intercepts had been fixed such that all literature gradients intersect the TS one at the solar position (7.94 kpc). Used references are Genovali (2014, [10], GENO14), Luck (2011a, [99], LIII), Pedicelli (2009, [107], PED), Friel (2002, [108], FRI), Carraro (2007, [109], CAR) and Deharveng (2000, [110], DEH).

It can be seen that the error attributed to the TS gradient agrees well with previous literature data. The σ is slightly higher for gradients not derived using Cepheids, very likely also because of the number of typically used targets. More importantly, the various tracers have different typical ages. This could be an explanation why the slopes of different metallicity gradients in the bottom panel vary quite strongly and why they show a larger spread than the gradients derived from Cepheid metallicities. The age-dependency of the metallicity gradient is still subject of debate, however, and has also been recently discussed in Genovali (2014, [10]).

Chapter 8

Summary and Outlook

This study has dealt with the homogeneous determination of metallicities for a large sample of Galactic classical Cepheids. After having collected the necessary, prereduced spectra, they were continuum-normalized and the radial velocity was obtained via cross-correlation (using IRAF). Subsequently, their S/N ratio and their usability for the analysis was checked.

Using general parameter configurations, with ARES equivalent widths were then measured for the spectra. On the basis of these results, the line-depth-ratio method developed by Kovtyukh could be applied and effective temperatures were retrieved for the target exposures. Special care was given here since they were of crucial importance for the later steps.

For the outliers that had a high dispersion, the EW fits were rechecked and in some cases the results could be improved by performing the fitting process better, giving different input parameters. The retrieved effective temperatures agreed very well with those of Genovali.

Next, both MARCS and Kurucz/Castelli atmospheres were downloaded and interpolated with scripts provided by T. Masseron and R. da Silva. Combined with the measured EWs and a set of stellar input parameters, MOOG enabled me to calculate iron abundances. The MARCS atmospheres were discarded due to unreliable results when used together with MOOG.

A self-written wrapper performed several fits in order to fulfil different physical conditions, thus improving the input parameters until convergence was reached. After several validations of the approach, the output abundances were combined.

Literature values for objects not contained in my sample significantly enlarged the amount of information available. Finally the Galactic iron gradient could be determined and validated and a huge database of abundances based on a homogeneous metallicity scale was presented.

With all that said, there are nonetheless a lot of interesting points worth of examination. The remarks suggested below are manifold and all go beyond the scope of this thesis, either due to time or complexity limits. Potential starting points for future works include:

- larger datasets to increase Cepheid coverage even more
- a more detailed, in-depth S/N analysis
- checking the measurability of lines given in the iron linelists
- an optimal selection of input parameters for ARES equivalent width fits
- different ways of clipping temperature calibrations
- tracing the MARCS abundance discontinuities and solving that problem
- solving the MOOG wavelength step size error
- conceptual approach of linearized stellar parameter optimizations
- extending the abundance determination functionality, alpha-element results
- differences to other abundance determination algorithms (FAMA and StePar), comparison of results

Acknowledgements

First of all, I want to thank my supervisor, Giuseppe Bono. He supported me at all times during the data analysis and the writing of this thesis. Whenever I had any questions, whether urgent or not, his door was always open and his advice was more than welcome. His vision enlightened the path that I followed and guided me around the obstacles in my way. My sincere gratitude also goes to Davide Magurno, Vittorio Braga and Ronaldo da Silva, whose ideas, more often than not, helped me find the way back from whichever dead end I found myself in. They faced the many discussions with me with unsurpassable calmness and truly deserve my deepest respect. The same applies to Michele Fabrizio, who showed me how to use MOOG and make sense of its results. Furthermore, I owe Chris Sneden, the creator of that routine. His genuine interest in my findings and appreciation of my suggestions on how to improve his script was motivating. Many thanks go to Elena Valenti and John Pritchard, whose guidance during my ESO internship laid the foundations of this work. Valery Kovtyukh receives my gratitude for his perfectly working and simple-to-use LDR method and his detailed research in that field. Further thanks are dedicated to Norbert Przybilla as well as Miguel Urbaneja for their non-LTE approach and to Laura Inno, Bertrand Lemasle and Thomas Masseron for helpful interaction during the thesis work. I would like to express my gratitude also to the coordinators of the Erasmus Mundus Joint Master Programme in Astrophysics (AstroMundus) for giving me this wonderful opportunity to participate in an internationally renowned astrophyics master program.

Last but not least, I want to mention my family and friends. They accompanied me during the sunny and the rainy days (more sunny ones in Rome), gave me relief when I was stressed and pushed me forwards when necessary. They broadened my perspective when I was too narrow-minded, helped me focus in case of over-generalizing and distracted me whenever it was required. Without their never-ending support this work would not have been possible.

Bibliography

[1] J. P. Cox. *Theory of Stellar Pulsation*. Princeton University Press, 1980.

[2] H. S. Leavitt and E. C. Pickering. Periods of 25 Variable Stars in the Small Magellanic Cloud. *Harvard College Observatory Circular*, 173:1–3, 03 1912.

[3] E. Hubble. A Relation between Distance and Radial Velocity among Extra-Galactic Nebulae. *PNAS*, 15(3):168–173, 03 1929.

[4] S. Perlmutter, G. Aldering, G. Goldhaber, et al. Measurements of Ω and Λ from 42 High- Redshift Supernovae. *ApJ*, 517(2):565–586, 06 1999.

[5] A. Riess, A. V. Filippenko, P. Challis, et al. Observational Evidence from Supernovae for an Accelerating Universe and a Cosmological Constant. *ApJ*, 116(3):1009–1038, 1998.

[6] R. Anderson, N. Mowlavi, and L. Eyer. The Galactic Cepheid period-luminosity relation revisited using bona fide cluster Cepheids. *Advancing the Physics of Cosmic Distances, Proceedings of the International Astronomical Union, IAU Symposium*, 289:153–156, 02 2013.

[7] C.-C. Ngeow, S. Sarkar, A. Bhardwaj, et al. Updated 24 μm Period-Luminosity Relation Derived from Galactic Cepheids. *ApJ*, 813/1(57), 11 2015.

[8] D. G. Turner, D. J. Majaess, D. J. Lane, et al. The Galactic Calibration of the Cepheid Period-Luminosity Relation and its Implications for the Universal Distance Scale. *Odessa Astronomical Publications*, 23:119, 12 2010.

[9] D. Turner. APASS as a Tool for Calibrating the Cepheid Period-Luminosity Relation (Abstract). *AAVSO*, 44(1):83, 06 2016.

[10] K. Genovali, B. Lemasle, G. Bono, et al. On the fine structure of the Cepheid metallicity gradient in the Galactic thin disk. *A&A*, 566(A37), 06 2014.

[11] M. Romaniello, F. Primas, M. Mottini, et al. The influence of chemical composition on the properties of Cepheid stars. II. The iron content. *A&A*, 488(2):731–747, 09 2008.

[12] L. Inno, N. Matsunaga, G. Bono, et al. On the Distance of the Magellanic Clouds Using Cepheid NIR and Optical-NIR Period-Wesenheit Relations. *ApJ*, 764/1(84), 02 2013.

[13] N. Matsunaga, T. Kawadu, S. Nishiyama, et al. Three classical Cepheid variable stars in the nuclear bulge of the Milky Way. *Nature*, 477(7363):188–190, 09 2011.

[14] G. Bono, N. Matsunaga, L. Inno, et al. Stellar Populations in the Galactic Center. *Cosmic Rays in Star-Forming Environments, Astrophysics and Space Science Proceedings*, 34, 2013.

[15] G. Bono, K. Genovali, B. Lemasle, et al. The Transition between the Inner Disc and the Innermost Galactic Regions. *ASP Conference Series*, 491:148, 05 2015.

[16] G. Bono, L. Inno, N. Matsunaga, et al. Classical Cepheids, what else? *Advancing the Physics of Cosmic Distances, Proceedings of the International Astronomical Union, IAU Symposium*, 289:116–129, 02 2013.

[17] G. Cescutti, F. Matteucci, P. François, et al. Abundance gradients in the Milky Way for α elements, iron peak elements, barium, lanthanum, and europium. *A&A*, 462(3):943–951, 02 2007.

[18] G. Cescutti, F. Matteucci, G. A. Lanfranchi, et al. The chemical evolution of manganese in different stellar systems. *A&A*, 491(2):401–405, 11 2008.

[19] D. G. Turner. The PL calibration for Milky Way Cepheids and its implications for the distance scale. *ApSS*, 326(2):219–231, 04 2010.

[20] D. Majaess, L. Sturch, C. Moni Bidin, et al. Anchors for the cosmic distance scale: the Cepheid QZ Normae in the open cluster NGC 6067. *ApSS*, 347(1):61–70, 09 2013.

[21] D. Majaess, G. Carraro, C. Moni Bidin, et al. Anchors for the cosmic distance scale: the Cepheids U Sagittarii, CF Cassiopeiae, and CEab Cassiopeiae. *A&A*, 560(A22), 12 2013.

[22] I. Minchev, C. Chiappini, and M. Martig. Chemodynamical evolution of the Milky Way disk. I. The solar vicinity. *A&A*, 558(A9), 10 2013.

[23] I. Minchev, C. Chiappini, and M. Martig. Chemodynamical evolution of the Milky Way disk. II. Variations with Galactic radius and height above the disk plane. *A&A*, 572(A92), 12 2014.

[24] H. Dekker, S. D'Odorico, A. Kaufer, et al. Design, construction, and performance of UVES, the echelle spectrograph for the UT2 Kueyen Telescope at the ESO Paranal Observatory, 08 2000.

[25] `https://www.eso.org/sci/facilities/lasilla/instruments/harps/inst/description.html`.

[26] M. Mayor, F. Pepe, D. Queloz, et al. Setting New Standards with HARPS. *The Messenger*, 114:20–24, 12 2003.

[27] P. François, O. Schuez, B. Conn, et al. FEROS-II User Manual. `https://www.eso.org/sci/facilities/lasilla/instruments/feros/doc/manual/P78/FEROSII-UserManual-78.0.pdf`, 10 2006.

[28] A. Kaufer, O. Stahl, S. Tubbesing, et al. Commissioning FEROS, the new high-resolution spectrograph at La-Silla. *The Messenger*, 95:8–12, 03 1999.

[29] K. Genovali, B. Lemasle, R. da Silva, et al. On the α-element gradients of the Galactic thin disk using Cepheids. *A&A*, 580(A17), 08 2015.

[30] `http://www.eso.org/observing/dfo/quality/PHOENIX/UVES_ECH/processing.html`.

[31] V. Kovtyukh, B. Lemasle, F. Chekhonadskikh, et al. The chemical composition of Galactic beat Cepheids. *MNRAS*, 460(2), 08 2016.

[32] `http://www.ipac.caltech.edu/2mass/releases/allsky/index.html`.

[33] M. F. Skrutskie, R. M. Cutri, R. Stiening, et al. The Two Micron All Sky Survey (2MASS). *AJ*, 131(2):1163–1183, 02 2006.

[34] R. da Silva, B. Lemasle, G. Bono, et al. Neutron-capture elements across the Galactic thin disk using Cepheids. *A&A*, 586(A125), 02 2016.

[35] `http://simbad.u-strasbg.fr/simbad/`.

[36] M. Wenger, F. Ochsenbein, D. Egret, et al. The SIMBAD astronomical database. The CDS reference database for astronomical objects. *A&A Supplement*, 143(1):9–22, 04 2000.

[37] K. Genovali, B. Lemasle, G. Bono, et al. On the metallicity distribution of classical Cepheids in the Galactic inner disk. *A&A*, 554(A132), 06 2013.

[38] `http://www.eso.org/observing/dfo/quality/UVES/pipeline/pipe_reduc.html#UVES`.

[39] `http://www.eso.org/observing/dfo/quality/reproUVES/processing.html`.

[40] `http://www.eso.org/observing/dfo/quality/ALL/ref_frames/ref_uves.html`.

[41] C. Ledoux, A. Kaufer, and S. Mieske. UVES calibration plan. `http://www.eso.org/sci/facilities/paranal/instruments/uves/doc/VLT-PLA-ESO-13200-1123_v98.pdf`, 01 2016.

[42] `http://iraf.noao.edu/`.

[43] D. Tody. The IRAF Data Reduction and Analysis System. Instrumentation in astronomy VI; Proceedings of the Meeting, 01 1986.

[44] D. Tody. IRAF in the Nineties. Astronomical Data Analysis Software and Systems II, A.S.P. Conference Series, vol. 52, 01 1993.

[45] `http://iraf.noao.edu/docs/spectra.html`.

[46] `http://www.eso.org/sci/software/esomidas/`.

[47] `http://www.eso.org/sci/software/esomidas/doc/index.html`.

[48] P. Ballester, A. Modigliani, O. Boitquin, et al. The UVES Data Reduction Pipeline. *The Messenger*, 101:31–36, 09 2000.

[49] V. Forchì, T. Bierwirth, and M. Péron. Reflex User Manual. `ftp://ftp.eso.org/pub/dfs/reflex/ReflexUserManual-3.8.pdf`, 10 2015.

[50] `http://www.eso.org/observing/dfo/quality/UVES/pipeline/recipe_science.html`.

[51] K. Horne. An optimal extraction algorithm for CCD spectroscopy. *PASP*, 98:609–617, 06 1986.

[52] T. R. Marsh. The extraction of highly distorted spectra. *PASP*, 101:1032–1037, 11 1989.

[53] K. Mukai. Optimal extraction of cross-dispersed spectra. *PASP*, 102:183–189, 02 1990.

[54] J. M. Larsen, A. Modigliani, D. Bramich, et al. UVES Pipeline User Manual. `ftp://ftp.eso.org/pub/dfs/pipelines/uves/uves-pipeline-manual-22.12.pdf`, 03 2016.

[55] https://www.eso.org/sci/facilities/lasilla/instruments/feros/tools/DRS.html.

[56] http://eso.org/~jpritcha/jFEROS-DRS/index.html.

[57] http://www.eso.org/sci/facilities/lasilla/instruments/feros/inst/CCDTests/index-BIAS.html.

[58] http://www.eso.org/sci/facilities/lasilla/instruments/feros/inst/CCDTests.html.

[59] http://www.astro.up.pt/~sousasag/ares/.

[60] http://www.astro.up.pt/~sousasag/ares/Online_Doc.pdf.

[61] S. G. Sousa, N. C. Santos, G. Israelian, et al. A new code for automatic determination of equivalent widths: Automatic Routine for line Equivalent widths in stellar Spectra (ARES). *A&A*, 469(2):783–791, 07 2007.

[62] S. G. Sousa, N. C. Santos, V. Adibekyan, et al. ARES v2: new features and improved performance. *A&A*, 577(A67), 05 2015.

[63] L. Szabados. The orbital period of the Cepheid binaries XX Cen, X Sgr and V350 Sgr. *MNRAS*, 242:285–288, 01 1990.

[64] N. R. Evans. A magnitude-limited survey of Cepheid companions in the ultraviolet. *ApJ*, 384:220–233, 01 1992.

[65] M. A. T. Groenewegen. Baade-Wesselink distances and the effect of metallicity in classical cepheids. *A&A*, 488(1):25–35, 09 2008.

[66] G. Li Causi, S. Antoniucci, G. Bono, et al. On the binarity of the classical Cepheid X Sagittarii from interferometric observations. *A&A*, 549(A64), 01 2013.

[67] L. Szabados. Database on Binaries among Galactic Classical Cepheids. *IBVS*, 5394, 03 2003.

[68] D. D. Sasselov and J. B. Lester. Infrared spectroscopy of Cepheids. II - Line profiles from different atmospheric layers. *ApJ*, 362:333–345, 10 1990.

[69] N. Nardetto, W. Gieren, P. Kervella, et al. High-resolution spectroscopy for Cepheids distance determination. V. Impact of the cross-correlation method on the p-factor and the γ-velocities. *MNRAS*, 502(3):951–956, 08 2009.

[70] http://vald.astro.uu.se/~vald/php/vald.php.

[71] T. Ryabchikova, N. Piskunov, R. L. Kurucz, et al. A major upgrade of the VALD database. *Physica Scripta*, 90/5(054005), 5 2015.

[72] V. V. Kovtyukh and N. I. Gorlova. Precise temperatures of classical Cepheids and yellow supergiants from line-depth ratios. *A&A*, 358:587–592, 06 2000.

[73] V. V. Kovtyukh. High-precision effective temperatures of 161 FGK supergiants from line-depth ratios. *MNRAS*, 378(2):617–624, 06 2007.

[74] http://www.astro.utoronto.ca/DDO/research/cepheids/cepheids.html.

[75] J. D. Fernie, N. R. Evans, B. Beattie, et al. A Database of Galactic Classical Cepheids. *IBVS*, 4148, 01 1995.

[76] `http://www.sai.msu.su/gcvs/gcvs/`.

[77] N. N. Samus and O. V. et al. Durlevich. VizieR Online Data Catalog: General Catalogue of Variable Stars (Samus+2007-2013). VizieR On-line Data Catalog: B/gcvs, 2009.

[78] M. A. T. Groenewegen, A. Udalski, and G. Bono. The distance to the Galactic centre based on Population II Cepheids and RR Lyrae stars. *A&A*, 481(2):441–448, 04 2008.

[79] J. Storm, W. Gieren, P. Fouqué, et al. Calibrating the Cepheid period-luminosity relation from the infrared surface brightness technique. I. The p-factor, the Milky Way relations, and a universal K-band relation. *A&A*, 534(A94), 10 2011.

[80] N. L. Maza and N. Nieva, M.-F.; Przybilla. A non-LTE spectral analysis of the ^{3}He and ^{4}He isotopes in the HgMn star κ Cancri. *A&A*, 572(A112), 12 2014.

[81] P. Kervella, D. Bersier, D. Mourard, et al. Cepheid distances from infrared long-baseline interferometry. III. Calibration of the surface brightness-color relations. *A&A*, 428, 12 2004.

[82] J. Storm, W. P. Gieren, P. Fouqué, et al. The near-IR surface brightness method applied to six Cepheids in the young LMC cluster NGC 1866. *A&A*, 440(2):487–498, 09 2005.

[83] J. Storm, W. Gieren, P. Fouqué, et al. Calibrating the Cepheid period-luminosity relation from the infrared surface brightness technique. II. The p-factor, the Milky Way relations, and a universal K-band relation. *A&A*, 534(A95), 10 2011.

[84] L. Magrini, S. Randich, E. Friel, et al. FAMA: An automatic code for stellar parameter and abundance determination. *A&A*, 558(A38), 10 2013.

[85] H. M. Tabernero, J. I. González Hernández, and D. Montes. StePar: an automatic code for stellar parameter determination. `http://pendientedemigracion.ucm.es/info/Astrof/users/dmg/papers/SEA_X_StePar_poster_Hugo_A4.pdf`.

[86] H. M. Tabernero, J. I. González Hernández, and D. Montes. StePar: an automatic code for stellar parameter determination. *Highlights of Spanish Astrophysics VII, Proceedings of the X Scientific Meeting of the Spanish Astronomical Society (SEA)*, page 673, 05 2013.

[87] C. Sneden. The nitrogen abundance of the very metal-poor star HD 122563. *ApJ*, 184:839–849, 09 1973.

[88] `http://kurucz.harvard.edu/grids.html`.

[89] `http://wwwuser.oats.inaf.it/castelli/grids.html`.

[90] F. Castelli and R. L. Kurucz. New Grids of ATLAS9 Model Atmospheres. `https://arxiv.org/pdf/astro-ph/0405087v1.pdf,wwwuser.oats.inaf.it/castelli/grids/paper/paper.ps,availableonCD`, 05 2004.

[91] `http://marcs.astro.uu.se/`.

[92] B. Gustafsson, B. Edvardsson, K. Eriksson, et al. A grid of MARCS model atmospheres for late-type stars. I. Methods and general properties. *A&A*, 486(3):951–970, 08 2008.

[93] marcs.astro.uu.se/documents/auxiliary/interpol_marcs.tar.gz.

[94] T. Masseron. PhD thesis, Observatoire de Paris, France, 2006.

[95] C. Sneden. MOOG - An LTE Stellar Line Analysis Program. www.as.utexas.edu/~chris/codes/WRITEMOOG.ps, 04 2002.

[96] B. Lemasle, P. François, K. Genovali, et al. Galactic abundance gradients from Cepheids. α and heavy elements in the outer disk. *A&A*, 516(A31), 10 2013.

[97] B. Lemasle, P. François, A. Piersimoni, et al. Galactic abundance gradients from Cepheids. On the iron abundance gradient around 10-12 kpc. *A&A*, 490(2):613–623, 11 2008.

[98] B. Lemasle, P. François, G. Bono, et al. Detailed chemical composition of Galactic Cepheids. A determination of the Galactic abundance gradient in the 8-12 kpc region. *A&A*, 467(1):283–294, 05 2007.

[99] R. E. Luck and D. L. Lambert. The Distribution of the Elements in the Galactic Disk. III. A Reconsideration of Cepheids from l = 30° to 250°. *AJ*, 142/4(136), 10 2011.

[100] R. E. Luck, S. M. Andrievsky, V. V. Kovtyukh, et al. The Distribution of the Elements in the Galactic Disk. II. Azimuthal and Radial Variation in Abundances from Cepheids. *AJ*, 142/2(51), 08 2011.

[101] R. P. Martin, S. M. Andrievsky, V. V. Kovtyukh, et al. Oxygen, α-element and iron abundance distributions in the inner part of the Galactic thin disc. *MNRAS*, 449(4):4071–4078, 06 2015.

[102] K. Sziládi, J. Vinkó, E. Poretti, et al. New homogeneous iron abundances of double-mode Cepheids from high-resolution echelle spectroscopy. *A&A*, 473(2):579–587, 10 2007.

[103] D. Yong, B. W. Carney, M. L. Teixera de Almeida, et al. Elemental Abundance Ratios in Stars of the Outer Galactic Disk. III. Cepheids. *ApJ*, 131(4):2256–2273, 04 2006.

[104] S. Pedicelli, B. Lemasle, M. Groenewegen, et al. New Baade-Wesselink distances and radii for four metal-rich Galactic Cepheids. *A&A*, 518(A11), 07 2010.

[105] B. M. Lasker, C. R. Sturch, B. J. McLean, et al. The Guide Star Catalog. I - Astronomical foundations and image processing. *AJ*, 99:2019–2058,2173–2178, 06 1990.

[106] A. K. Vivas and R. Zinn. The QUEST RR Lyrae Survey. II. The Halo Overdensities in the First Catalog. *AJ*, 132(2):714–728, 08 2006.

[107] S. Pedicelli, G. Bono, B. Lemasle, et al. On the metallicity gradient of the Galactic disk. *A&A*, 504(1), 09 2009.

[108] E. D. Friel, K. A. Janes, M. Tavarez, et al. Metallicities of Old Open Clusters. *AJ*, 124(5):2693–2720, 11 2002.

[109] G. Carraro, D. Geisler, S. Villanova, et al. Old open clusters in the outer Galactic disk. *A&A*, 476(1):217–227, 12 2007.

[110] L. Deharveng, M. Peña, J. Caplan, et al. Oxygen and helium abundances in Galactic Hii regions - II. Abundance gradients. *MNRAS*, 311(2):329–345, 01 2000.

[111] V. V. Kovtyukh, C. Soubiran, R. E. Luck, et al. Reddenings of FGK supergiants and classical Cepheids from spectroscopic data. *MNRAS*, 389(3):1336–1344, 09 2008.

[112] N. Nardetto, D. Mourard, P. Mathias, et al. High-resolution spectroscopy for Cepheids distance determination. II. A period-projection factor relation. *A&A*, 471(2):661–669, 08 2007.

[113] G. Bono, F. Caputo, V. Castellani, et al. Theoretical Models for Classical Cepheids. II. Period- Luminosity, Period-Color, and Period-Luminosity-Color Relations. *ApJ*, 512(2):711–723, 02 1999.

[114] F. Caputo, M. Marconi, and I. Musella. The Cepheid Period-Luminosity Relation and the Maser Distance to NGC 4258. *ApJ*, 566(2):833–837, 02 2002.

[115] G. Fiorentino, F. Caputo, M. Marconi, et al. Theoretical Models for Classical Cepheids. VIII. Effects of Helium and Heavy-Element Abundance on the Cepheid Distance Scale. *ApJ*, 576(1):402–412, 09 2002.

[116] I. Musella, M. Marconi, P. B. Stetson, et al. The Cepheids of NGC 1866: a precise benchmark for the extragalactic distance scale and stellar evolution from modern UBVI photometry. *MNRAS*, 457(3):3084–3095, 04 2016.

App. A: Spectra without Metallicity Determination

Out of 1136 spectra (in total), 655 different ones are listed in table 6.1. The remaining 481 are found below:

Table A1: All spectra of the thesis that have not been used for metallicity determination. As indicated in the last column, spectra have not been given in table 6.1 because of unreliable continuum fits (a), too low S/N (b), too little lines (either for temperature or metallicity) (c), too high effective temperature standard deviation (d), problems during metallicity determination (e), due to not being targeted for abundance measurements (f) or not being reduced yet (g).

Spectrum	Object	Dataset	Notes
ADP.2013-09-25T22:59:21.050	ER Car	UVES TS	c
ADP.2013-09-25T22:59:21.123	ER Car	UVES TS	c
ADP.2013-09-25T22:59:21.130	ER Car	UVES TS	c
ADP.2013-09-25T22:59:21.170	ER Car	UVES TS	c
ADP.2013-09-25T22:59:21.177	ER Car	UVES TS	c
ADP.2013-09-25T22:59:21.303	ER Car	UVES TS	c
ADP.2013-09-25T22:59:21.337	ER Car	UVES TS	c
ADP.2013-09-25T22:59:21.343	ER Car	UVES TS	c
ADP.2013-09-25T22:59:21.350	ER Car	UVES TS	c
ADP.2013-09-24T23:09:16.213	BF Oph	UVES TS	c
ADP.2013-09-24T23:09:16.267	BF Oph	UVES TS	c
ADP.2013-09-24T23:09:16.540	BF Oph	UVES TS	c
ADP.2013-09-24T23:09:16.573	BF Oph	UVES TS	c
ADP.2013-09-24T23:09:16.640	BF Oph	UVES TS	c
ADP.2013-09-24T23:09:16.707	BF Oph	UVES TS	c
ADP.2013-09-24T23:09:16.773	BF Oph	UVES TS	c
ADP.2013-09-24T23:09:16.227	BB Sgr	UVES TS	c
ADP.2013-09-24T23:09:16.320	BB Sgr	UVES TS	c
ADP.2013-09-24T23:09:16.427	BB Sgr	UVES TS	c
ADP.2013-09-24T23:09:16.567	BB Sgr	UVES TS	c
ADP.2013-09-24T23:09:16.613	BB Sgr	UVES TS	c
ADP.2013-09-24T23:09:16.720	BB Sgr	UVES TS	c
ADP.2013-09-24T23:09:16.787	BB Sgr	UVES TS	c
ADP.2014-07-23T11:47:41.227	IU Aql	UVES Inno	a
ADP.2014-07-23T11:47:41.233	IU Aql	UVES Inno	a
ADP.2014-07-23T11:47:41.260	IU Aql	UVES Inno	a
ADP.2014-05-16T05:52:31.523	V475 Ara	UVES Inno	a
ADP.2014-05-16T05:52:31.557	V475 Ara	UVES Inno	a
ADP.2014-05-16T05:52:31.663	V475 Ara	UVES Inno	a
ADP.2014-05-16T05:52:31.717	V475 Ara	UVES Inno	a
ADP.2014-04-07T15:30:11.003	FH Car	UVES Inno	a
ADP.2014-04-07T15:39:53.810	FH Car	UVES Inno	a
ADP.2014-04-07T15:39:53.907	FH Car	UVES Inno	a
ADP.2014-04-07T15:39:53.953	FH Car	UVES Inno	a
ADP.2014-04-07T15:35:11.720	V686 Cen	UVES Inno	a
ADP.2014-04-07T15:35:11.780	V686 Cen	UVES Inno	a
ADP.2014-04-07T15:35:11.987	V686 Cen	UVES Inno	a
ADP.2014-04-07T15:39:53.757	SU Cru	UVES Inno	a
ADP.2014-04-07T15:39:53.777	SU Cru	UVES Inno	a
ADP.2014-04-07T15:39:53.823	DW Mus	UVES Inno	a
ADP.2014-04-07T15:39:53.920	DW Mus	UVES Inno	a
ADP.2014-04-07T15:39:53.967	DW Mus	UVES Inno	a
ADP.2014-04-07T15:36:11.587	UX Mus	UVES Inno	a
ADP.2014-04-07T15:36:11.600	UX Mus	UVES Inno	a
ADP.2014-04-07T15:36:11.620	UX Mus	UVES Inno	a
ADP.2014-04-07T15:36:11.640	UX Mus	UVES Inno	a
ADP.2014-04-07T15:39:13.407	V567 Sco	UVES Inno	a
ADP.2014-04-07T15:39:13.473	V567 Sco	UVES Inno	a
ADP.2014-04-07T15:39:13.500	V567 Sco	UVES Inno	a
ADP.2014-05-16T06:11:57.103	V742 Sco	UVES Inno	a
ADP.2014-05-16T06:11:57.310	V742 Sco	UVES Inno	a
ADP.2014-05-16T06:11:57.403	V742 Sco	UVES Inno	a
ADP.2014-05-16T06:11:57.450	V742 Sco	UVES Inno	a
ADP.2014-05-16T06:11:56.990	V708 Sco	UVES Inno	c
ADP.2014-05-16T06:11:57.030	V708 Sco	UVES Inno	c
ADP.2014-05-16T06:11:57.203	V708 Sco	UVES Inno	c
ADP.2014-05-16T06:11:57.550	V708 Sco	UVES Inno	c
ADP.2014-05-16T06:18:30.930	SU Sct	UVES Inno	c
ADP.2014-05-16T06:18:30.950	SU Sct	UVES Inno	c
ADP.2014-05-16T06:18:30.983	SU Sct	UVES Inno	c
ADP.2014-05-16T06:18:31.023	SU Sct	UVES Inno	c
ADP.2014-06-05T06:43:45.953	V800 Aql	UVES Inno	d
ADP.2014-06-05T06:43:45.980	V800 Aql	UVES Inno	d
ADP.2014-06-05T06:43:45.987	V800 Aql	UVES Inno	d
ADP.2014-06-05T06:43:46.013	V800 Aql	UVES Inno	d
ADP.2014-06-05T06:47:08.420	V800 Aql	UVES Inno	d
ADP.2014-06-05T06:47:08.427	V800 Aql	UVES Inno	d
ADP.2014-06-05T06:47:08.460	V800 Aql	UVES Inno	d
ADP.2014-06-05T06:47:08.513	V800 Aql	UVES Inno	d
ADP.2014-04-07T15:34:03.703	IK Car	UVES Inno	d
ADP.2014-04-07T15:34:03.750	IK Car	UVES Inno	d
ADP.2014-04-07T15:34:03.917	IK Car	UVES Inno	d
ADP.2014-04-07T15:34:03.977	IK Car	UVES Inno	d
ADP.2014-04-07T15:35:11.867	IU Cen	UVES Inno	d
ADP.2014-04-07T15:35:11.947	IU Cen	UVES Inno	d
ADP.2014-04-07T15:35:11.973	IU Cen	UVES Inno	d
ADP.2014-05-16T05:52:31.510	V706 Sco	UVES Inno	d
ADP.2014-05-16T05:52:31.630	V706 Sco	UVES Inno	d
ADP.2014-05-16T05:52:31.683	V706 Sco	UVES Inno	d
ADP.2014-05-16T05:52:31.703	V706 Sco	UVES Inno	d
ADP.2014-05-16T06:11:57.250	GK Sgr	UVES Inno	d
ADP.2014-05-16T06:11:57.270	GK Sgr	UVES Inno	d

ADP.2014-05-16T06:11:57.570	GK Sgr	UVES Inno	d
ADP.2014-05-16T06:11:57.610	GK Sgr	UVES Inno	d
KNCen_15_00	KN Cen	UVES Geno	e
science20060719-0224_botzfxsEcd	η Aql	STELLA	f
science20060720-0002_botzfxsEcd	η Aql	STELLA	f
science20060728-0001_botzfxsEcd	η Aql	STELLA	f
science20060731-0006_botzfxsEcd	η Aql	STELLA	f
science20060802-0004_botzfxsEcd	η Aql	STELLA	f
science20060802-0116_botzfxsEcd	η Aql	STELLA	f
science20060803-0110_botzfxsEcd	η Aql	STELLA	f
science20060805-0102_botzfxsEcd	η Aql	STELLA	f
science20060811-0128_botzfxsEcd	η Aql	STELLA	f
science20060812-0000_botzfxsEcd	η Aql	STELLA	f
science20060815-0000_botzfxsEcd	η Aql	STELLA	f
science20140429B-0019_botzfxsEcd	δ Cep	STELLA	f
science20140504B-0012_botzfxsEcd	δ Cep	STELLA	f
science20140509B-0012_botzfxsEcd	δ Cep	STELLA	f
science20140510B-0011_botzfxsEcd	δ Cep	STELLA	f
science20140513B-0012_botzfxsEcd	δ Cep	STELLA	f
science20140518B-0012_botzfxsEcd	δ Cep	STELLA	f
science20140519B-0012_botzfxsEcd	δ Cep	STELLA	f
science20140523B-0006_botzfxsEcd	δ Cep	STELLA	f
science20140524B-0014_botzfxsEcd	δ Cep	STELLA	f
science20140601B-0009_botzfxsEcd	δ Cep	STELLA	f
science20140602B-0011_botzfxsEcd	δ Cep	STELLA	f
science20140607B-0005_botzfxsEcd	δ Cep	STELLA	f
science20140610B-0004_botzfxsEcd	δ Cep	STELLA	f
science20140612B-0005_botzfxsEcd	δ Cep	STELLA	f
science20140613B-0009_botzfxsEcd	δ Cep	STELLA	f
science20070905-0035_botzfxsEcd	ζ Gem	STELLA	f
science20070925-0027_botzfxsEcd	ζ Gem	STELLA	f
science20070930-0025_botzfxsEcd	ζ Gem	STELLA	f
science20071113-0073_botzfxsEcd	ζ Gem	STELLA	f
science20071114-0038_botzfxsEcd	ζ Gem	STELLA	f
science20071114-0039_botzfxsEcd	ζ Gem	STELLA	f
science20071114-0046_botzfxsEcd	ζ Gem	STELLA	f
science20071117-0024_botzfxsEcd	ζ Gem	STELLA	f
science20071119-0025_botzfxsEcd	ζ Gem	STELLA	f
science20071204-0034_botzfxsEcd	ζ Gem	STELLA	f
science20071228-0034_botzfxsEcd	ζ Gem	STELLA	f
science20071229-0015_botzfxsEcd	ζ Gem	STELLA	f
science20071231-0015_botzfxsEcd	ζ Gem	STELLA	f
science20080106-0015_botzfxsEcd	ζ Gem	STELLA	f
science20080121-0022_botzfxsEcd	ζ Gem	STELLA	f
science20080205-0022_botzfxsEcd	ζ Gem	STELLA	f
science20080206-0000_botzfxsEcd	ζ Gem	STELLA	f
science20080229-0013_botzfxsEcd	ζ Gem	STELLA	f
science20080401-0142_botzfxsEcd	ζ Gem	STELLA	f
science20080823-0022_botzfxsEcd	ζ Gem	STELLA	f
science20080824-0022_botzfxsEcd	ζ Gem	STELLA	f
science20080824-0023_botzfxsEcd	ζ Gem	STELLA	f
science20080825-0023_botzfxsEcd	ζ Gem	STELLA	f
science20080825-0024_botzfxsEcd	ζ Gem	STELLA	f
science20080826-0023_botzfxsEcd	ζ Gem	STELLA	f
science20080826-0025_botzfxsEcd	ζ Gem	STELLA	f
science20080827-0024_botzfxsEcd	ζ Gem	STELLA	f
science20080827-0025_botzfxsEcd	ζ Gem	STELLA	f
science20080828-0022_botzfxsEcd	ζ Gem	STELLA	f
science20080828-0024_botzfxsEcd	ζ Gem	STELLA	f
science20080828-0025_botzfxsEcd	ζ Gem	STELLA	f
science20080828-0026_botzfxsEcd	ζ Gem	STELLA	f
science20080829-0025_botzfxsEcd	ζ Gem	STELLA	f
science20080830-0022_botzfxsEcd	ζ Gem	STELLA	f
science20080831-0023_botzfxsEcd	ζ Gem	STELLA	f
science20080831-0028_botzfxsEcd	ζ Gem	STELLA	f
science20080831-0029_botzfxsEcd	ζ Gem	STELLA	f
science20080902-0022_botzfxsEcd	ζ Gem	STELLA	f
science20080902-0023_botzfxsEcd	ζ Gem	STELLA	f
science20080903-0020_botzfxsEcd	ζ Gem	STELLA	f
science20080903-0021_botzfxsEcd	ζ Gem	STELLA	f
science20080903-0026_botzfxsEcd	ζ Gem	STELLA	f
science20080904-0027_botzfxsEcd	ζ Gem	STELLA	f
science20080905-0020_botzfxsEcd	ζ Gem	STELLA	f
science20080905-0021_botzfxsEcd	ζ Gem	STELLA	f
science20080905-0028_botzfxsEcd	ζ Gem	STELLA	f
science20080920-0025_botzfxsEcd	ζ Gem	STELLA	f
science20081011-0030_botzfxsEcd	ζ Gem	STELLA	f
science20081015-0032_botzfxsEcd	ζ Gem	STELLA	f
science20081015-0034_botzfxsEcd	ζ Gem	STELLA	f
science20081021-0015_botzfxsEcd	ζ Gem	STELLA	f
science20081021-0016_botzfxsEcd	ζ Gem	STELLA	f
science20081021-0017_botzfxsEcd	ζ Gem	STELLA	f
science20081021-0018_botzfxsEcd	ζ Gem	STELLA	f
science20081021-0019_botzfxsEcd	ζ Gem	STELLA	f
science20081021-0020_botzfxsEcd	ζ Gem	STELLA	f
science20081021-0023_botzfxsEcd	ζ Gem	STELLA	f
science20081021-0024_botzfxsEcd	ζ Gem	STELLA	f
science20081021-0027_botzfxsEcd	ζ Gem	STELLA	f
science20081021-0028_botzfxsEcd	ζ Gem	STELLA	f
science20081021-0029_botzfxsEcd	ζ Gem	STELLA	f
science20081023-0036_botzfxsEcd	ζ Gem	STELLA	f
science20081107-0019_botzfxsEcd	ζ Gem	STELLA	f
science20081118-0149_botzfxsEcd	ζ Gem	STELLA	f
science20081118-0150_botzfxsEcd	ζ Gem	STELLA	f
science20081119-0002_botzfxsEcd	ζ Gem	STELLA	f
science20081119-0003_botzfxsEcd	ζ Gem	STELLA	f
science20081119-0004_botzfxsEcd	ζ Gem	STELLA	f
science20081122-0125_botzfxsEcd	ζ Gem	STELLA	f
science20081122-0126_botzfxsEcd	ζ Gem	STELLA	f
science20081123-0001_botzfxsEcd	ζ Gem	STELLA	f
science20081123-0161_botzfxsEcd	ζ Gem	STELLA	f
science20081123-0162_botzfxsEcd	ζ Gem	STELLA	f
science20081124-0156_botzfxsEcd	ζ Gem	STELLA	f
science20081127-0178_botzfxsEcd	ζ Gem	STELLA	f
science20081128-0136_botzfxsEcd	ζ Gem	STELLA	f
science20081128-0137_botzfxsEcd	ζ Gem	STELLA	f
science20081129-0173_botzfxsEcd	ζ Gem	STELLA	f
science20081129-0174_botzfxsEcd	ζ Gem	STELLA	f

science20081130-0148_botzfxsEcd	ζ Gem	STELLA	f
science20081222-0035_botzfxsEcd	ζ Gem	STELLA	f
science20090730-0228_botzfxsEcd	X Sgr	STELLA	f
science20100121-0043_botzfxsEcd	X Sgr	STELLA	f
science20100206-0015_botzfxsEcd	X Sgr	STELLA	f
science20100315-0032_botzfxsEcd	X Sgr	STELLA	f
science20100319-0096_botzfxsEcd	X Sgr	STELLA	f
science20100327-0024_botzfxsEcd	X Sgr	STELLA	f
science20100330-0029_botzfxsEcd	X Sgr	STELLA	f
science20100411-0021_botzfxsEcd	X Sgr	STELLA	f
science20100412-0024_botzfxsEcd	X Sgr	STELLA	f
science20100505-0004_botzfxsEcd	X Sgr	STELLA	f
science20100506-0018_botzfxsEcd	X Sgr	STELLA	f
science20100707B-0180_botzfxsEcd	X Sgr	STELLA	f
science20100722B-0197_botzfxsEcd	X Sgr	STELLA	f
science20110421B-0007_botzfxsEcd	X Sgr	STELLA	f
science20110422B-0010_botzfxsEcd	X Sgr	STELLA	f
science20110507B-0015_botzfxsEcd	X Sgr	STELLA	f
science20110508B-0015_botzfxsEcd	X Sgr	STELLA	f
science20110508B-0016_botzfxsEcd	X Sgr	STELLA	f
science20110508B-0030_botzfxsEcd	X Sgr	STELLA	f
science20110509B-0004_botzfxsEcd	X Sgr	STELLA	f
science20110510B-0003_botzfxsEcd	X Sgr	STELLA	f
science20110629B-0215_botzfxsEcd	X Sgr	STELLA	f
science20110719B-0097_botzfxsEcd	X Sgr	STELLA	f
science20110725B-0213_botzfxsEcd	X Sgr	STELLA	f
science20070529-0019_botzfxsEcd	Y Sgr	STELLA	f
science20070615-0010_botzfxsEcd	Y Sgr	STELLA	f
science20070620-0010_botzfxsEcd	Y Sgr	STELLA	f
ADP.2014-10-06T10:04:43.180	Y Sgr	HARPS	b
ADP.2014-10-01T10:22:07.337	RS Pup	HARPS	d
FEROS.2004-05-31T00:44:42.609	V701 Car	FEROS Kov	g
FEROS.2004-06-02T04:20:58.745	V1210 Cen	FEROS Kov	g
FEROS.2005-05-30T05:18:45.099	V340 Ara	FEROS	b
FEROS.2005-05-31T05:06:10.147	V340 Ara	FEROS	b
FEROS.2005-06-01T05:02:43.510	V340 Ara	FEROS	b
FEROS.2005-06-02T06:22:08.244	V340 Ara	FEROS	b
FEROS.2005-06-03T03:54:26.053	V340 Ara	FEROS	b
FEROS.2005-06-28T07:17:16.380	V340 Ara	FEROS	b
FEROS.2005-06-29T03:40:37.820	V340 Ara	FEROS	b
FEROS.2005-06-30T04:39:05.981	V340 Ara	FEROS	b
FEROS.2005-06-30T06:33:25.940	V340 Ara	FEROS	b
FEROS.2005-07-01T07:17:30.350	V340 Ara	FEROS	b
FEROS.2005-07-05T07:35:16.551	V340 Ara	FEROS	b
FEROS.2005-07-05T07:39:43.340	V340 Ara	FEROS	b
FEROS.2005-08-15T00:53:55.150	V340 Ara	FEROS	b
FEROS.2005-08-17T02:20:24.880	V340 Ara	FEROS	b
FEROS.2005-08-19T02:46:46.770	V340 Ara	FEROS	b
FEROS.2005-08-20T02:37:31.090	V340 Ara	FEROS	b
FEROS.2005-08-21T02:38:18.890	V340 Ara	FEROS	b
FEROS.2005-08-27T00:54:34.170	V340 Ara	FEROS	b
FEROS.2005-08-27T01:01:06.790	V340 Ara	FEROS	b
FEROS.2005-09-02T00:38:26.051	V340 Ara	FEROS	b
FEROS.2005-09-03T01:17:16.691	V340 Ara	FEROS	b
FEROS.2005-09-04T01:40:15.050	V340 Ara	FEROS	b
FEROS.2005-09-05T01:17:02.041	V340 Ara	FEROS	b
FEROS.2005-09-06T01:08:10.781	V340 Ara	FEROS	b
FEROS.2005-09-08T03:01:02.430	V340 Ara	FEROS	b
FEROS.2007-03-30T00:51:20.023	CR Ori	FEROS	b
FEROS.2007-03-30T01:22:11.582	CR Ori	FEROS	b
FEROS.2012-12-28T07:23:34.978	BM Pup	FEROS	b
FEROS.2007-03-30T02:43:05.091	HW Pup	FEROS	b
FEROS.2007-03-30T03:28:56.616	HW Pup	FEROS	b
FEROS.2007-03-30T04:14:49.020	HW Pup	FEROS	b
FEROS.2012-12-28T07:37:14.258	WY Pup	FEROS	b
FEROS.2005-05-30T05:58:21.742	EV Sct	FEROS	b
FEROS.2005-05-31T05:45:24.050	EV Sct	FEROS	b
FEROS.2005-06-01T05:48:29.642	EV Sct	FEROS	b
FEROS.2005-06-02T07:00:11.265	EV Sct	FEROS	b
FEROS.2005-06-03T04:47:06.928	EV Sct	FEROS	b
FEROS.2005-06-28T07:57:20.110	EV Sct	FEROS	b
FEROS.2005-06-29T04:19:00.410	EV Sct	FEROS	b
FEROS.2005-06-30T06:52:55.340	EV Sct	FEROS	b
FEROS.2005-07-01T07:48:27.200	EV Sct	FEROS	b
FEROS.2005-07-05T08:52:27.690	EV Sct	FEROS	b
FEROS.2005-07-05T08:56:05.090	EV Sct	FEROS	b
FEROS.2005-07-26T06:58:36.401	EV Sct	FEROS	b
FEROS.2005-08-27T02:07:00.650	EV Sct	FEROS	b
FEROS.2005-08-27T02:10:55.561	EV Sct	FEROS	b
FEROS.2005-09-02T01:16:29.520	EV Sct	FEROS	b
FEROS.2005-09-04T03:19:30.161	EV Sct	FEROS	b
FEROS.2005-09-05T04:14:57.681	EV Sct	FEROS	b
FEROS.2005-09-06T04:08:00.440	EV Sct	FEROS	b
FEROS.2005-09-07T04:14:22.070	EV Sct	FEROS	b
FEROS.2005-05-30T05:49:03.522	UZ Sct	FEROS	b
FEROS.2005-05-31T05:35:44.936	UZ Sct	FEROS	b
FEROS.2005-06-01T05:39:29.229	UZ Sct	FEROS	b
FEROS.2005-06-02T06:50:04.526	UZ Sct	FEROS	b
FEROS.2005-06-03T04:37:21.024	UZ Sct	FEROS	b
FEROS.2005-06-28T07:48:29.800	UZ Sct	FEROS	b
FEROS.2005-06-29T04:09:12.951	UZ Sct	FEROS	b
FEROS.2005-06-30T05:43:00.551	UZ Sct	FEROS	b
FEROS.2005-06-30T05:50:10.160	UZ Sct	FEROS	b
FEROS.2005-06-30T05:56:24.251	UZ Sct	FEROS	b
FEROS.2005-06-30T06:02:38.040	UZ Sct	FEROS	b
FEROS.2005-07-01T07:37:47.591	UZ Sct	FEROS	b
FEROS.2005-07-05T08:33:15.771	UZ Sct	FEROS	b
FEROS.2005-07-05T08:40:39.540	UZ Sct	FEROS	b
FEROS.2005-07-26T06:50:07.410	UZ Sct	FEROS	b
FEROS.2005-08-20T03:13:06.021	UZ Sct	FEROS	b
FEROS.2005-08-21T03:14:03.250	UZ Sct	FEROS	b
FEROS.2005-08-27T01:50:02.341	UZ Sct	FEROS	b
FEROS.2005-08-27T01:57:26.691	UZ Sct	FEROS	b
FEROS.2005-09-02T01:07:49.820	UZ Sct	FEROS	b
FEROS.2005-09-03T02:24:03.921	UZ Sct	FEROS	b
FEROS.2005-09-04T03:25:09.201	UZ Sct	FEROS	b
FEROS.2005-09-05T04:06:27.860	UZ Sct	FEROS	b
FEROS.2005-09-06T03:58:48.130	UZ Sct	FEROS	b

FEROS.2005-09-07T04:02:42.330	UZ Sct	FEROS	b
FEROS.2005-09-08T00:51:55.930	UZ Sct	FEROS	b
FEROS.2005-05-30T05:27:18.437	AV Sgr	FEROS	b
FEROS.2005-05-31T05:15:44.906	AV Sgr	FEROS	b
FEROS.2005-06-01T05:11:37.090	AV Sgr	FEROS	b
FEROS.2005-06-02T06:29:31.913	AV Sgr	FEROS	b
FEROS.2005-06-03T04:00:39.860	AV Sgr	FEROS	b
FEROS.2005-06-28T07:27:49.980	AV Sgr	FEROS	b
FEROS.2005-06-29T03:46:51.720	AV Sgr	FEROS	b
FEROS.2005-06-30T03:59:32.060	AV Sgr	FEROS	b
FEROS.2005-06-30T04:14:40.231	AV Sgr	FEROS	b
FEROS.2005-06-30T06:42:24.770	AV Sgr	FEROS	b
FEROS.2005-07-01T07:54:25.620	AV Sgr	FEROS	b
FEROS.2005-07-05T07:49:16.061	AV Sgr	FEROS	b
FEROS.2005-07-05T08:04:16.790	AV Sgr	FEROS	b
FEROS.2005-07-26T06:15:20.531	AV Sgr	FEROS	b
FEROS.2005-08-15T01:00:43.640	AV Sgr	FEROS	b
FEROS.2005-08-17T02:28:00.601	AV Sgr	FEROS	b
FEROS.2005-08-21T02:52:20.890	AV Sgr	FEROS	b
FEROS.2005-08-27T01:08:23.890	AV Sgr	FEROS	b
FEROS.2005-08-27T01:17:23.070	AV Sgr	FEROS	b
FEROS.2005-09-02T00:45:50.471	AV Sgr	FEROS	b
FEROS.2005-09-03T02:04:20.421	AV Sgr	FEROS	b
FEROS.2005-09-04T02:59:39.480	AV Sgr	FEROS	b
FEROS.2005-09-05T03:41:25.541	AV Sgr	FEROS	b
FEROS.2005-09-06T03:33:25.461	AV Sgr	FEROS	b
FEROS.2005-09-07T03:39:49.521	AV Sgr	FEROS	b
FEROS.2005-05-30T05:37:35.841	VY Sgr	FEROS	b
FEROS.2005-05-31T05:24:52.650	VY Sgr	FEROS	b
FEROS.2005-06-02T06:38:38.515	VY Sgr	FEROS	b
FEROS.2005-06-03T04:26:36.018	VY Sgr	FEROS	b
FEROS.2005-06-28T07:36:51.550	VY Sgr	FEROS	b
FEROS.2005-06-30T04:56:20.960	VY Sgr	FEROS	b
FEROS.2005-06-30T05:08:26.300	VY Sgr	FEROS	b
FEROS.2005-06-30T05:24:18.860	VY Sgr	FEROS	b
FEROS.2005-07-01T07:26:15.821	VY Sgr	FEROS	b
FEROS.2005-07-05T08:13:13.861	VY Sgr	FEROS	b
FEROS.2005-07-05T08:21:55.371	VY Sgr	FEROS	b
FEROS.2005-07-26T06:25:31.310	VY Sgr	FEROS	b
FEROS.2005-08-15T01:09:18.680	VY Sgr	FEROS	b
FEROS.2005-08-17T02:37:04.560	VY Sgr	FEROS	b
FEROS.2005-08-19T04:16:55.190	VY Sgr	FEROS	b
FEROS.2005-08-20T03:02:33.040	VY Sgr	FEROS	b
FEROS.2005-08-21T03:02:15.660	VY Sgr	FEROS	b
FEROS.2005-08-27T01:28:27.410	VY Sgr	FEROS	b
FEROS.2005-08-27T01:38:19.591	VY Sgr	FEROS	b
FEROS.2005-09-02T00:54:52.211	VY Sgr	FEROS	b
FEROS.2005-09-04T03:09:01.770	VY Sgr	FEROS	b
FEROS.2005-09-05T03:56:25.800	VY Sgr	FEROS	b
FEROS.2005-09-06T03:44:32.781	VY Sgr	FEROS	b
FEROS.2005-09-07T03:50:08.330	VY Sgr	FEROS	b
FEROS.2010-03-25T08:20:27.288	KN Cen	FEROS	e
FEROS.2006-06-20T08:24:40.155	V1359 Aql	FEROS	g
FEROS.2007-03-27T04:50:49.194	V340 Ara	FEROS	g
FEROS.2007-03-27T05:21:39.731	V340 Ara	FEROS	g
FEROS.2001-12-22T07:05:43.000	GZ Car	FEROS	g
FEROS.2001-12-22T04:47:53.000	Y Car	FEROS	g
FEROS.2001-12-28T09:08:11.000	Y Car	FEROS	g
FEROS.2001-12-22T07:18:11.000	BB Cen	FEROS	g
FEROS.2001-12-22T07:12:42.000	BK Cen	FEROS	g
FEROS.2012-08-02T03:05:10.226	TX Cen	FEROS	g
FEROS.2005-02-02T06:24:05.426	AX Cir	FEROS	g
FEROS.2001-12-29T02:42:57.000	DZ Cma	FEROS	g
FEROS.2003-01-20T08:04:12.000	SS Cma	FEROS	g
FEROS.2012-02-09T08:21:03.141	AG Cru	FEROS	g
FEROS.2005-01-03T08:32:12.928	BG Cru	FEROS	g
FEROS.2010-03-30T01:00:53.484	BG Cru	FEROS	g
FEROS.2010-03-30T01:02:30.045	BG Cru	FEROS	g
FEROS.2010-03-30T01:04:07.386	BG Cru	FEROS	g
FEROS.2012-02-09T08:54:34.823	X Cru	FEROS	g
FEROS.2004-10-14T07:05:26.520	β Dor	FEROS	g
FEROS.2001-12-22T06:52:57.000	DX Gem	FEROS	g
FEROS.2001-12-23T03:07:59.000	DX Gem	FEROS	g
FEROS.2001-12-25T01:35:12.000	DX Gem	FEROS	g
FEROS.2001-11-30T04:35:33.000	AA Mon	FEROS	g
FEROS.2001-12-02T05:29:08.000	AC Mon	FEROS	g
FEROS.2003-01-20T02:20:33.000	AC Mon	FEROS	g
FEROS.2001-12-23T03:12:12.000	CV Mon	FEROS	g
FEROS.2001-12-27T00:36:17.000	CV Mon	FEROS	g
FEROS.2001-12-27T00:38:10.000	CV Mon	FEROS	g
FEROS.2001-12-27T00:40:17.000	CV Mon	FEROS	g
FEROS.2001-12-27T00:42:45.000	CV Mon	FEROS	g
FEROS.2001-12-27T00:43:54.000	CV Mon	FEROS	g
FEROS.2001-12-27T00:45:15.000	CV Mon	FEROS	g
FEROS.2001-12-29T02:49:53.000	CV Mon	FEROS	g
FEROS.2001-12-29T02:50:51.000	CV Mon	FEROS	g
FEROS.2001-12-29T02:52:02.000	CV Mon	FEROS	g
FEROS.2001-12-29T02:53:31.000	CV Mon	FEROS	g
FEROS.2001-12-29T02:54:26.000	CV Mon	FEROS	g
FEROS.2001-12-29T02:55:35.000	CV Mon	FEROS	g
FEROS.2001-12-29T02:57:07.000	CV Mon	FEROS	g
FEROS.2001-12-29T02:58:10.000	CV Mon	FEROS	g
FEROS.2001-12-29T02:59:29.000	CV Mon	FEROS	g
FEROS.2001-12-30T02:56:26.000	CV Mon	FEROS	g
FEROS.2001-12-30T02:57:21.000	CV Mon	FEROS	g
FEROS.2001-12-30T02:58:29.000	CV Mon	FEROS	g
FEROS.2001-12-30T02:59:37.000	CV Mon	FEROS	g
FEROS.2001-12-30T03:02:50.000	CV Mon	FEROS	g
FEROS.2001-12-30T03:03:46.000	CV Mon	FEROS	g
FEROS.2003-01-19T01:07:16.000	CV Mon	FEROS	g
FEROS.2001-12-02T03:21:28.000	EE Mon	FEROS	g
FEROS.2001-12-02T04:31:34.000	EE Mon	FEROS	g
FEROS.2001-11-30T02:48:36.000	EK Mon	FEROS	g
FEROS.2001-11-29T04:21:52.000	SV Mon	FEROS	g
FEROS.2001-12-22T06:48:56.000	T Mon	FEROS	g
FEROS.2001-12-23T03:05:28.000	T Mon	FEROS	g
FEROS.2001-12-25T01:22:22.000	T Mon	FEROS	g
FEROS.2001-12-25T01:25:17.000	T Mon	FEROS	g

FEROS.2001-12-25T01:54:56.000	T Mon	FEROS	g
FEROS.2001-12-26T01:07:36.000	T Mon	FEROS	g
FEROS.2003-01-20T00:41:01.000	T Mon	FEROS	g
FEROS.2001-11-29T07:02:09.000	TX Mon	FEROS	g
FEROS.2001-12-22T06:57:48.000	TX Mon	FEROS	g
FEROS.2001-12-25T01:27:58.000	TX Mon	FEROS	g
FEROS.2003-01-19T02:35:39.000	TX Mon	FEROS	g
FEROS.2003-01-19T03:19:57.000	TX Mon	FEROS	g
FEROS.2001-11-30T03:44:18.000	TZ Mon	FEROS	g
FEROS.2001-12-01T07:45:11.000	V495 Mon	FEROS	g
FEROS.2003-01-19T04:05:48.000	V495 Mon	FEROS	g
FEROS.2003-01-19T04:48:27.000	V495 Mon	FEROS	g
FEROS.2003-01-19T05:31:42.000	V495 Mon	FEROS	g
FEROS.2003-01-19T06:14:20.000	V495 Mon	FEROS	g
FEROS.2001-11-30T05:23:38.000	V504 Mon	FEROS	g
FEROS.2001-11-29T06:07:03.000	V508 Mon	FEROS	g
FEROS.2003-01-19T01:51:58.000	V508 Mon	FEROS	g
FEROS.2001-12-01T06:38:55.000	XX Mon	FEROS	g
FEROS.2003-01-20T03:04:21.000	XX Mon	FEROS	g
FEROS.2003-01-20T04:27:34.000	XX Mon	FEROS	g
FEROS.2003-01-20T05:10:13.000	XX Mon	FEROS	g
FEROS.2010-06-26T02:22:41.109	S Nor	FEROS	g
FEROS.2012-08-02T04:51:03.298	U Nor	FEROS	g
FEROS.2001-11-29T04:59:44.000	CS Ori	FEROS	g
FEROS.2001-11-30T06:32:19.000	AD Pup	FEROS	g
FEROS.2001-11-30T07:19:36.000	BN Pup	FEROS	g
FEROS.2003-01-19T08:15:29.000	BN Pup	FEROS	g
FEROS.2001-12-01T05:30:10.000	HW Pup	FEROS	g
FEROS.2003-01-20T05:55:18.000	HW Pup	FEROS	g
FEROS.2003-01-20T06:37:53.000	HW Pup	FEROS	g
FEROS.2003-01-20T07:20:35.000	HW Pup	FEROS	g
FEROS.2004-10-27T05:54:32.562	MY Pup	FEROS	g
FEROS.2005-01-26T04:35:04.511	MY Pup	FEROS	g
FEROS.2001-12-01T03:17:27.000	VW Pup	FEROS	g
FEROS.2001-12-01T03:24:29.000	VW Pup	FEROS	g
FEROS.2001-12-22T04:37:54.000	VX Pup	FEROS	g
FEROS.2001-12-23T03:15:31.000	VX Pup	FEROS	g
FEROS.2001-12-25T01:45:24.000	VX Pup	FEROS	g
FEROS.2001-12-28T08:52:55.000	VX Pup	FEROS	g
FEROS.2001-12-28T08:53:53.000	VX Pup	FEROS	g
FEROS.2001-12-28T08:55:05.000	VX Pup	FEROS	g
FEROS.2001-12-28T08:56:30.000	VX Pup	FEROS	g
FEROS.2001-12-28T08:57:26.000	VX Pup	FEROS	g
FEROS.2001-12-28T08:58:35.000	VX Pup	FEROS	g
FEROS.2001-12-28T09:00:05.000	VX Pup	FEROS	g
FEROS.2001-12-28T09:00:59.000	VX Pup	FEROS	g
FEROS.2001-12-28T09:02:06.000	VX Pup	FEROS	g
FEROS.2001-12-28T09:03:28.000	VX Pup	FEROS	g
FEROS.2001-12-29T02:46:36.000	VX Pup	FEROS	g
FEROS.2003-01-19T06:58:12.000	VZ Pup	FEROS	g
FEROS.2001-12-01T04:32:25.000	WW Pup	FEROS	g
FEROS.2001-12-03T02:52:44.000	WY Pup	FEROS	g
FEROS.2003-01-19T07:32:16.000	WY Pup	FEROS	g
FEROS.2012-08-02T04:17:17.777	KQ Sco	FEROS	g
FEROS.2005-03-03T07:52:36.988	X Sgr	FEROS	g
FEROS.2011-04-16T07:24:20.305	XX Sgr	FEROS	g
FEROS.2011-04-17T07:32:51.094	XX Sgr	FEROS	g
FEROS.2011-04-18T07:36:43.058	XX Sgr	FEROS	g
FEROS.2011-04-19T08:25:32.869	XX Sgr	FEROS	g
FEROS.2001-11-29T03:29:26.000	AE Tau	FEROS	g
FEROS.2001-12-23T00:14:17.000	SZ Tau	FEROS	g
FEROS.2004-10-28T06:17:16.235	AH Vel	FEROS	g
FEROS.2010-03-30T00:51:29.543	AH Vel	FEROS	g
FEROS.2010-03-30T00:53:20.595	AH Vel	FEROS	g
FEROS.2010-03-30T00:55:11.597	AH Vel	FEROS	g
FEROS.2001-12-22T04:42:39.000	AP Vel	FEROS	g
FEROS.2001-12-23T09:10:12.000	AP Vel	FEROS	g
FEROS.2001-12-28T09:05:45.000	AP Vel	FEROS	g
FEROS.2001-12-29T07:08:50.000	AP Vel	FEROS	g
FEROS.2001-12-22T04:40:37.000	AX Vel	FEROS	g
FEROS.2001-12-29T07:12:12.000	AX Vel	FEROS	g
FEROS.2007-03-26T00:58:53.435	CP Vel	FEROS	g
FEROS.2007-03-26T01:29:45.804	CP Vel	FEROS	g
FEROS.2007-03-26T02:00:37.712	CP Vel	FEROS	g
FEROS.2003-01-19T09:12:42.000	SW Vel	FEROS	g

App. B: Linelists for EW Measurements

Table A2: All linelists used for the thesis (thus including Kovtyukh, Fe and α-element lines).

λ	χ	log(gf)	Element	Num	Source
5348.30	1.00	-	CrI	24.00	KOV2
5373.71	4.47	-	FeI	26.00	KOV2
5410.91	4.47	-	FeI	26.00	KOV2
5497.52	1.01	-	FeI	26.00	KOV2
5501.46	0.96	-	FeI	26.00	KOV2
5506.78	0.99	-	FeI	26.00	KOV2
5554.89	4.55	-	FeI	26.00	KOV2
5565.71	4.61	-	FeI	26.00	KOV2
5578.72	1.68	-	NiI	28.00	KOV2
5633.97	4.99	-	FeI	26.00	KOV2
5645.62	4.93	-	SiI	14.00	KOV2
5670.86	1.08	-	VI	23.00	KOV2
5690.43	4.93	-	SiI	14.00	KOV2
5754.68	1.93	-	NiI	28.00	KOV2
5772.15	5.08	-	SiI	14.00	KOV3
5778.47	2.59	-	FeI	26.00	KOV3
5793.08	4.93	-	SiI	14.00	KOV3
5793.92	4.22	-	FeI	26.00	KOV2
5805.23	4.17	-	NiI	28.00	KOV2
5809.25	3.88	-	FeI	26.00	KOV2
5847.00	1.68	-	NiI	28.00	KOV3
5862.36	4.55	-	FeI	26.00	KOV3
5866.45	1.07	-	TiI	22.00	KOV3
5905.67	4.65	-	FeI	26.00	KOV3
5934.66	3.93	-	FeI	26.00	KOV2
5956.70	0.86	-	FeI	26.00	KOV3
5983.69	4.55	-	FeI	26.00	KOV3
5984.79	4.73	-	FeI	26.00	KOV3
5987.05	4.80	-	FeI	26.00	KOV3
6003.03	3.88	-	FeI	26.00	KOV3
6007.96	4.65	-	FeI	26.00	KOV3
6008.56	3.88	-	FeI	26.00	KOV2
6021.79	3.08	-	MnI	25.00	KOV3
6024.07	4.55	-	FeI	26.00	KOV3
6039.73	1.06	-	VI	23.00	KOV3
6046.00	7.86	-	SI	16.00	KOV3
6052.67	7.87	-	SI	16.00	KOV3
6055.99	4.73	-	FeI	26.00	KOV3
6062.89	2.18	-	FeI	26.00	KOV3
6078.50	4.80	-	FeI	26.00	KOV3
6079.02	4.65	-	FeI	26.00	KOV3
6081.44	1.05	-	VI	23.00	KOV3
6082.72	2.22	-	FeI	26.00	KOV3
6085.27	2.76	-	FeI	26.00	KOV3
6086.29	4.27	-	NiI	28.00	KOV2
6090.21	1.08	-	VI	23.00	KOV2
6091.18	2.27	-	TiI	22.00	KOV3
6091.92	5.87	-	SiI	14.00	KOV3
6093.14	1.74	-	CoI	27.00	KOV2
6093.66	4.61	-	FeI	26.00	KOV2
6108.12	1.68	-	NiI	28.00	KOV3
6122.23	1.89	-	CaI	20.00	KOV2
6125.03	5.61	-	SiI	14.00	KOV3
6126.22	1.07	-	TiI	22.00	KOV3
6128.99	1.68	-	NiI	28.00	KOV3
6130.17	4.27	-	NiI	28.00	KOV3
6135.36	1.05	-	VI	23.00	KOV3
6136.61	2.45	-	FeI	26.00	KOV3
6142.49	5.62	-	SiI	14.00	KOV3
6145.02	5.61	-	SiI	14.00	KOV3
6150.16	0.30	-	VI	23.00	KOV2
6151.62	2.18	-	FeI	26.00	KOV3
6155.14	5.62	-	SiI	14.00	KOV3
6162.18	1.90	-	CaI	20.00	KOV2
6165.37	4.14	-	FeI	26.00	KOV2
6170.49	4.80	-	FeI	26.00	KOV3
6176.81	4.09	-	NiI	28.00	KOV3
6180.22	2.73	-	FeI	26.00	KOV3
6189.01	1.71	-	CoI	27.00	KOV3
6200.32	2.61	-	FeI	26.00	KOV2
6215.15	4.19	-	FeI	26.00	KOV2
6216.37	0.28	-	VI	23.00	KOV2
6219.28	2.20	-	FeI	26.00	KOV2
6232.65	3.65	-	FeI	26.00	KOV3
6237.33	5.61	-	SiI	14.00	KOV3
6240.66	2.22	-	FeI	26.00	KOV3
6243.11	0.30	-	VI	23.00	KOV3
6243.81	5.61	-	SiI	14.00	KOV3
6244.48	5.61	-	SiI	14.00	KOV3
6258.10	1.44	-	TiI	22.00	KOV3
6258.71	1.46	-	TiI	22.00	KOV3
6261.10	1.43	-	TiI	22.00	KOV2
6327.60	1.68	-	NiI	28.00	KOV2
6330.13	0.94	-	CrI	24.00	KOV2
6330.86	4.73	-	FeI	26.00	KOV2
6355.04	2.85	-	FeI	26.00	KOV2
6358.69	0.86	-	FeI	26.00	KOV3
6380.75	4.19	-	FeI	26.00	KOV2
6392.55	2.28	-	FeI	26.00	KOV2
6414.99	5.87	-	SiI	14.00	KOV3
6419.98	4.73	-	FeI	26.00	KOV2
6439.08	2.52	-	CaI	20.00	KOV3
6498.95	0.96	-	FeI	26.00	KOV3
6538.60	8.05	-	SI	16.00	KOV2
6597.61	4.80	-	FeI	26.00	KOV2
6608.03	2.28	-	FeI	26.00	KOV3
6609.12	2.56	-	FeI	26.00	KOV3
6680.15	4.16	-	CrI	24.00	KOV1
6703.57	2.76	-	FeI	26.00	KOV3
6710.31	1.49	-	FeI	26.00	KOV3

6713.76	4.79	-	FeI	26.00	KOV1
6717.69	2.71	-	CaI	20.00	KOV2
6721.85	5.86	-	SiI	14.00	KOV3
6748.84	7.87	-	SI	16.00	KOV2
6750.15	2.42	-	FeI	26.00	KOV2
6757.17	7.87	-	SI	16.00	KOV3
6767.77	1.83	-	NiI	28.00	KOV2
6771.04	1.88	-	CoI	27.00	KOV3
6806.85	2.73	-	FeI	26.00	KOV1
6839.83	2.56	-	FeI	26.00	KOV3
6848.57	5.86	-	SiI	14.00	KOV1
7022.390	4.30	-	FeI	26.00	KOV4
7022.954	4.19	-	FeI	26.00	KOV4
7034.901	5.87	-	SiI	14.00	KOV4
7071.880	4.60	-	FeI	26.00	KOV4
7090.384	4.23	-	FeI	26.00	KOV4
7110.896	1.93	-	NiI	28.00	KOV4
7112.180	2.99	-	FeI	26.00	KOV4
7130.922	4.21	-	FeI	26.00	KOV4
7132.986	4.07	-	FeI	26.00	KOV4
7142.517	4.95	-	FeI	26.00	KOV4
7181.194	4.22	-	FeI	26.00	KOV4
7216.183	1.44	-	TiI	22.00	KOV4
7221.202	4.55	-	FeI	26.00	KOV4
7251.708	1.43	-	TiI	22.00	KOV4
7327.648	3.79	-	NiI	28.00	KOV4
7357.727	1.44	-	TiI	22.00	KOV4
7375.246	6.19	-	SiI	14.00	KOV4
7445.749	4.25	-	FeI	26.00	KOV4
7461.521	2.55	-	FeI	26.00	KOV4
7468.312	10.33	-	NI	7.00	KOV4
7491.647	4.30	-	FeI	26.00	KOV4
7495.066	4.22	-	FeI	26.00	KOV4
7507.266	4.41	-	FeI	26.00	KOV4
7511.021	4.17	-	FeI	26.00	KOV4
7531.144	4.37	-	FeI	26.00	KOV4
7540.430	2.72	-	FeI	26.00	KOV4
7563.010	4.83	-	FeI	26.00	KOV4
7583.788	3.01	-	FeI	26.00	KOV4
7586.018	4.31	-	FeI	26.00	KOV4
7680.266	5.86	-	SiI	14.00	KOV4
7710.365	4.22	-	FeI	26.00	KOV4
7714.270	-	-	NiI	28.00	KOV4
7723.208	2.27	-	FeI	26.00	KOV4
7748.269	2.94	-	FeI	26.00	KOV4
7780.557	4.47	-	FeI	26.00	KOV4
7788.95	-	-	NiI	28.00	KOV4
7832.195	4.43	-	FeI	26.00	KOV4
7849.966	6.19	-	SiI	14.00	KOV4
7912.867	0.85	-	FeI	26.00	KOV4
7932.348	5.96	-	SiI	14.00	KOV4
7944.001	5.98	-	SiI	14.00	KOV4
8426.507	0.82	-	TiI	22.00	KOV4
4757.58	3.27	-2.04	FeI	26.0	TS
4772.80	1.56	-2.90	FeI	26.0	TS
4779.44	3.41	-2.02	FeI	26.0	TS
4780.81	3.25	-3.36	FeI	26.0	TS
4787.83	3.00	-2.53	FeI	26.0	TS
4788.76	3.24	-1.76	FeI	26.0	TS
4789.65	3.55	-0.96	FeI	26.0	TS
4793.96	3.05	-3.53	FeI	26.0	TS
4794.35	2.42	-4.05	FeI	26.0	TS
4799.41	3.64	-2.23	FeI	26.0	TS
4802.52	4.61	-1.82	FeI	26.0	TS
4802.87	3.69	-2.03	FeI	26.0	TS
4802.88	3.64	-1.51	FeI	26.0	TS
4808.15	3.25	-2.79	FeI	26.0	TS
4809.94	3.57	-2.72	FeI	26.0	TS
4811.03	3.07	-3.50	FeI	26.0	TS
4869.46	3.55	-2.52	FeI	26.0	TS
4872.14	2.88	-0.57	FeI	26.0	TS
4872.69	4.26	-2.51	FeI	26.0	TS
4872.91	4.22	-2.30	FeI	26.0	TS
4873.75	3.30	-3.06	FeI	26.0	TS
4874.35	3.07	-3.03	FeI	26.0	TS
4875.88	3.33	-2.02	FeI	26.0	TS
4877.60	3.00	-3.15	FeI	26.0	TS
4882.14	3.42	-1.64	FeI	26.0	TS
4885.43	3.88	-1.02	FeI	26.0	TS
4891.49	2.85	-0.11	FeI	26.0	TS
4892.86	4.22	-1.29	FeI	26.0	TS
4896.44	3.88	-2.05	FeI	26.0	TS
4903.31	2.88	-0.93	FeI	26.0	TS
4905.13	3.93	-2.05	FeI	26.0	TS
4907.73	3.43	-1.84	FeI	26.0	TS
4917.23	4.19	-1.18	FeI	26.0	TS
4918.01	4.23	-1.36	FeI	26.0	TS
4920.50	2.83	0.07	FeI	26.0	TS
4924.77	2.28	-2.24	FeI	26.0	TS
4927.42	3.57	-2.07	FeI	26.0	TS
4932.08	4.65	-1.48	FeI	26.0	TS
4935.41	3.64	-3.43	FeI	26.0	TS
4938.81	2.88	-1.08	FeI	26.0	TS
4939.69	0.86	-3.34	FeI	26.0	TS
4946.39	3.37	-1.17	FeI	26.0	TS
4950.11	3.42	-1.67	FeI	26.0	TS
4952.64	4.21	-2.31	FeI	26.0	TS
4957.30	2.85	-0.41	FeI	26.0	TS
4961.91	3.63	-2.29	FeI	26.0	TS
4962.57	4.18	-1.18	FeI	26.0	TS
4966.09	3.33	-0.87	FeI	26.0	TS
4967.90	4.19	-0.49	FeI	26.0	TS
4969.92	4.22	-0.71	FeI	26.0	TS
4973.10	3.96	-0.95	FeI	26.0	TS
4979.59	3.64	-2.58	FeI	26.0	TS
4985.25	3.93	-0.56	FeI	26.0	TS
4985.55	2.87	-1.33	FeI	26.0	TS
4986.22	4.22	-1.39	FeI	26.0	TS

4987.62	4.18	-2.72	FeI	26.0	TS
4992.79	4.26	-2.35	FeI	26.0	TS
4993.68	4.21	-1.47	FeI	26.0	TS
4994.13	0.91	-3.08	FeI	26.0	TS
4995.41	4.26	-1.89	FeI	26.0	TS
4999.11	4.19	-1.74	FeI	26.0	TS
5001.86	3.88	0.01	FeI	26.0	TS
5002.79	3.40	-1.58	FeI	26.0	TS
5012.69	4.28	-1.79	FeI	26.0	TS
5014.94	3.94	-0.30	FeI	26.0	TS
5016.48	4.26	-1.69	FeI	26.0	TS
5022.24	3.98	-0.53	FeI	26.0	TS
5023.19	4.28	-1.60	FeI	26.0	TS
5023.50	4.31	-1.71	FeI	26.0	TS
5025.30	4.28	-2.04	FeI	26.0	TS
5028.13	3.57	-1.12	FeI	26.0	TS
5029.62	3.41	-2.05	FeI	26.0	TS
5031.91	4.37	-1.67	FeI	26.0	TS
5036.92	3.02	-2.99	FeI	26.0	TS
5044.21	2.85	-2.04	FeI	26.0	TS
5048.44	3.96	-1.03	FeI	26.0	TS
5049.82	2.28	-1.36	FeI	26.0	TS
5054.64	3.64	-1.92	FeI	26.0	TS
5056.84	4.26	-1.96	FeI	26.0	TS
5058.50	3.64	-2.83	FeI	26.0	TS
5060.08	0.00	-5.46	FeI	26.0	TS
5067.15	4.22	-0.97	FeI	26.0	TS
5068.77	2.94	-1.04	FeI	26.0	TS
5072.67	4.22	-0.83	FeI	26.0	TS
5074.75	4.22	-0.20	FeI	26.0	TS
5079.22	2.20	-2.07	FeI	26.0	TS
5079.74	0.99	-3.22	FeI	26.0	TS
5083.34	0.96	-2.96	FeI	26.0	TS
5088.15	4.15	-1.78	FeI	26.0	TS
5090.77	4.26	-0.40	FeI	26.0	TS
5104.44	4.28	-1.69	FeI	26.0	TS
5107.45	0.99	-3.09	FeI	26.0	TS
5107.64	1.56	-2.42	FeI	26.0	TS
5109.65	4.30	-0.98	FeI	26.0	TS
5115.78	3.57	-2.74	FeI	26.0	TS
5119.90	3.88	-3.05	FeI	26.0	TS
5126.19	4.26	-1.08	FeI	26.0	TS
5127.36	0.91	-3.31	FeI	26.0	TS
5129.63	3.94	-1.85	FeI	26.0	TS
5131.47	2.22	-2.52	FeI	26.0	TS
5133.69	4.18	0.14	FeI	26.0	TS
5141.74	2.42	-1.96	FeI	26.0	TS
5143.72	2.20	-3.79	FeI	26.0	TS
5150.84	0.99	-3.00	FeI	26.0	TS
5151.91	1.01	-3.32	FeI	26.0	TS
5159.06	4.28	-0.82	FeI	26.0	TS
5162.27	4.18	0.02	FeI	26.0	TS
5166.28	0.00	-4.20	FeI	26.0	TS
5171.60	1.48	-1.79	FeI	26.0	TS
5180.06	4.47	-1.26	FeI	26.0	TS
5187.91	4.14	-1.37	FeI	26.0	TS
5194.94	1.56	-2.09	FeI	26.0	TS
5195.47	4.22	-0.09	FeI	26.0	TS
5196.06	4.26	-0.49	FeI	26.0	TS
5197.94	4.30	-1.64	FeI	26.0	TS
5198.71	2.22	-2.14	FeI	26.0	TS
5206.80	4.28	-2.53	FeI	26.0	TS
5213.34	4.39	-2.24	FeI	26.0	TS
5213.81	3.94	-2.76	FeI	26.0	TS
5215.18	3.27	-0.87	FeI	26.0	TS
5216.27	1.61	-2.15	FeI	26.0	TS
5217.39	3.21	-1.07	FeI	26.0	TS
5223.18	3.64	-1.78	FeI	26.0	TS
5225.53	0.11	-4.79	FeI	26.0	TS
5228.38	4.22	-1.29	FeI	26.0	TS
5229.84	3.28	-0.96	FeI	26.0	TS
5232.94	2.94	-0.06	FeI	26.0	TS
5235.39	4.08	-0.85	FeI	26.0	TS
5236.20	4.19	-1.50	FeI	26.0	TS
5241.90	4.42	-1.67	FeI	26.0	TS
5242.49	3.63	-0.97	FeI	26.0	TS
5243.78	4.26	-1.15	FeI	26.0	TS
5247.05	0.09	-4.95	FeI	26.0	TS
5250.21	0.12	-4.94	FeI	26.0	TS
5250.65	2.20	-2.18	FeI	26.0	TS
5253.02	2.28	-3.94	FeI	26.0	TS
5253.46	3.28	-1.57	FeI	26.0	TS
5257.65	3.57	-2.75	FeI	26.0	TS
5262.88	3.25	-2.66	FeI	26.0	TS
5263.31	3.27	-0.88	FeI	26.0	TS
5267.27	4.37	-1.60	FeI	26.0	TS
5269.54	0.86	-1.32	FeI	26.0	TS
5273.16	3.29	-0.99	FeI	26.0	TS
5279.65	3.30	-3.44	FeI	26.0	TS
5281.79	3.04	-0.83	FeI	26.0	TS
5285.13	4.43	-1.64	FeI	26.0	TS
5288.52	3.69	-1.51	FeI	26.0	TS
5293.96	4.14	-1.87	FeI	26.0	TS
5294.55	3.64	-2.86	FeI	26.0	TS
5295.31	4.42	-1.69	FeI	26.0	TS
5300.40	4.59	-1.75	FeI	26.0	TS
5302.30	3.28	-0.72	FeI	26.0	TS
5307.36	1.61	-2.99	FeI	26.0	TS
5308.68	4.26	-2.50	FeI	26.0	TS
5310.46	5.09	-1.72	FeI	26.0	TS
5315.07	4.37	-1.55	FeI	26.0	TS
5320.04	3.64	-2.54	FeI	26.0	TS
5321.11	4.43	-0.95	FeI	26.0	TS
5322.04	2.28	-2.80	FeI	26.0	TS
5324.18	3.21	-0.10	FeI	26.0	TS
5326.14	3.57	-2.07	FeI	26.0	TS
5326.79	4.42	-2.10	FeI	26.0	TS
5339.93	3.27	-0.65	FeI	26.0	TS

5358.11	3.30	-3.67	FeI	26.0	TS
5361.62	4.42	-1.43	FeI	26.0	TS
5364.87	4.45	0.23	FeI	26.0	TS
5365.40	3.57	-1.02	FeI	26.0	TS
5367.47	4.42	0.44	FeI	26.0	TS
5369.96	4.37	0.54	FeI	26.0	TS
5373.71	4.47	-0.86	FeI	26.0	TS
5376.83	4.29	-2.31	FeI	26.0	TS
5379.57	3.69	-1.51	FeI	26.0	TS
5383.37	4.31	0.65	FeI	26.0	TS
5385.58	3.69	-2.97	FeI	26.0	TS
5386.33	4.15	-1.77	FeI	26.0	TS
5389.48	4.42	-0.41	FeI	26.0	TS
5391.46	4.15	-0.78	FeI	26.0	TS
5393.17	3.24	-0.72	FeI	26.0	TS
5395.22	4.45	-2.17	FeI	26.0	TS
5397.13	0.91	-1.99	FeI	26.0	TS
5397.62	3.63	-2.48	FeI	26.0	TS
5398.28	4.45	-0.67	FeI	26.0	TS
5400.50	4.37	-0.16	FeI	26.0	TS
5401.27	4.32	-1.92	FeI	26.0	TS
5405.77	0.99	-1.84	FeI	26.0	TS
5406.77	4.37	-1.72	FeI	26.0	TS
5409.13	4.37	-1.30	FeI	26.0	TS
5410.91	4.47	0.40	FeI	26.0	TS
5412.78	4.43	-1.72	FeI	26.0	TS
5415.20	4.39	0.64	FeI	26.0	TS
5417.03	4.42	-1.68	FeI	26.0	TS
5421.85	4.55	-1.78	FeI	26.0	TS
5422.15	4.32	-2.26	FeI	26.0	TS
5424.07	4.32	0.52	FeI	26.0	TS
5429.50	4.19	-1.02	FeI	26.0	TS
5429.70	0.96	-1.88	FeI	26.0	TS
5429.84	4.47	-1.01	FeI	26.0	TS
5432.95	4.45	-1.04	FeI	26.0	TS
5434.52	1.01	-2.12	FeI	26.0	TS
5436.29	4.39	-1.54	FeI	26.0	TS
5436.59	2.28	-2.96	FeI	26.0	TS
5441.34	4.31	-1.73	FeI	26.0	TS
5443.41	4.10	-2.95	FeI	26.0	TS
5445.04	4.39	-0.02	FeI	26.0	TS
5452.09	3.64	-2.86	FeI	26.0	TS
5455.39	4.47	-0.75	FeI	26.0	TS
5455.45	4.32	0.33	FeI	26.0	TS
5455.61	1.01	-2.09	FeI	26.0	TS
5460.87	3.07	-3.58	FeI	26.0	TS
5461.55	4.45	-1.90	FeI	26.0	TS
5463.28	4.43	0.11	FeI	26.0	TS
5464.28	4.14	-1.40	FeI	26.0	TS
5466.40	4.37	-0.63	FeI	26.0	TS
5466.99	3.57	-2.23	FeI	26.0	TS
5470.09	4.45	-1.81	FeI	26.0	TS
5472.71	4.21	-1.50	FeI	26.0	TS
5473.16	4.19	-2.14	FeI	26.0	TS
5473.90	4.15	-0.76	FeI	26.0	TS
5476.56	4.10	-0.45	FeI	26.0	TS
5481.24	4.10	-1.24	FeI	26.0	TS
5483.10	4.15	-1.41	FeI	26.0	TS
5487.15	4.42	-1.53	FeI	26.0	TS
5491.83	4.19	-2.19	FeI	26.0	TS
5494.46	4.08	-2.09	FeI	26.0	TS
5496.56	4.91	-1.73	FeI	26.0	TS
5497.52	1.01	-2.85	FeI	26.0	TS
5501.46	0.96	-3.05	FeI	26.0	TS
5506.78	0.99	-2.80	FeI	26.0	TS
5521.28	4.43	-2.39	FeI	26.0	TS
5522.45	4.21	-1.55	FeI	26.0	TS
5524.25	4.15	-2.83	FeI	26.0	TS
5525.54	4.23	-1.08	FeI	26.0	TS
5528.90	4.47	-2.02	FeI	26.0	TS
5531.98	4.91	-1.61	FeI	26.0	TS
5534.66	3.64	-2.58	FeI	26.0	TS
5536.58	2.83	-3.81	FeI	26.0	TS
5538.52	4.22	-3.04	FeI	26.0	TS
5539.28	3.64	-2.66	FeI	26.0	TS
5539.82	4.29	-2.53	FeI	26.0	TS
5543.15	3.69	-1.57	FeI	26.0	TS
5543.94	4.22	-1.14	FeI	26.0	TS
5546.51	4.37	-1.31	FeI	26.0	TS
5546.99	4.22	-1.91	FeI	26.0	TS
5549.95	3.69	-2.91	FeI	26.0	TS
5552.69	4.96	-1.99	FeI	26.0	TS
5553.58	4.43	-1.41	FeI	26.0	TS
5554.89	4.55	-0.44	FeI	26.0	TS
5559.64	4.99	-1.83	FeI	26.0	TS
5560.21	4.43	-1.19	FeI	26.0	TS
5561.24	4.61	-1.20	FeI	26.0	TS
5562.71	4.43	-0.64	FeI	26.0	TS
5565.70	4.61	-0.21	FeI	26.0	TS
5567.39	2.61	-2.56	FeI	26.0	TS
5568.81	3.64	-2.95	FeI	26.0	TS
5569.62	3.42	-0.49	FeI	26.0	TS
5572.84	3.40	-0.28	FeI	26.0	TS
5573.10	4.19	-1.32	FeI	26.0	TS
5576.09	3.43	-1.00	FeI	26.0	TS
5577.02	5.03	-1.55	FeI	26.0	TS
5579.34	4.23	-2.40	FeI	26.0	TS
5584.76	3.57	-2.32	FeI	26.0	TS
5586.76	3.37	-0.12	FeI	26.0	TS
5587.57	4.14	-1.85	FeI	26.0	TS
5594.65	4.55	-0.66	FeI	26.0	TS
5595.06	5.06	-1.77	FeI	26.0	TS
5597.06	4.99	-2.17	FeI	26.0	TS
5600.22	4.26	-1.42	FeI	26.0	TS
5607.66	4.15	-2.27	FeI	26.0	TS
5608.97	4.21	-2.40	FeI	26.0	TS
5609.96	3.64	-3.24	FeI	26.0	TS
5611.36	3.64	-2.99	FeI	26.0	TS

5615.64	3.33	0.05	FeI	26.0	TS
5618.63	4.21	-1.28	FeI	26.0	TS
5619.22	3.69	-3.27	FeI	26.0	TS
5619.60	4.39	-1.70	FeI	26.0	TS
5622.94	3.64	-3.07	FeI	26.0	TS
5624.02	4.39	-1.48	FeI	26.0	TS
5633.95	4.99	-0.27	FeI	26.0	TS
5635.82	4.26	-1.89	FeI	26.0	TS
5636.70	3.64	-2.61	FeI	26.0	TS
5638.26	4.22	-0.87	FeI	26.0	TS
5640.31	4.64	-1.37	FeI	26.0	TS
5641.43	4.26	-1.18	FeI	26.0	TS
5646.68	4.26	-2.50	FeI	26.0	TS
5649.99	5.10	-0.92	FeI	26.0	TS
5650.71	5.09	-0.96	FeI	26.0	TS
5651.47	4.47	-2.00	FeI	26.0	TS
5652.32	4.26	-1.95	FeI	26.0	TS
5653.86	4.39	-1.64	FeI	26.0	TS
5655.18	5.06	-0.64	FeI	26.0	TS
5658.82	3.40	-0.79	FeI	26.0	TS
5659.57	5.09	-0.99	FeI	26.0	TS
5661.02	4.58	-2.43	FeI	26.0	TS
5661.34	4.28	-1.74	FeI	26.0	TS
5662.52	4.18	-0.57	FeI	26.0	TS
5667.52	4.18	-1.58	FeI	26.0	TS
5677.68	4.10	-2.70	FeI	26.0	TS
5678.38	3.88	-3.02	FeI	26.0	TS
5678.60	2.42	-4.67	FeI	26.0	TS
5679.02	4.65	-0.92	FeI	26.0	TS
5680.24	4.19	-2.58	FeI	26.0	TS
5686.53	4.55	-0.45	FeI	26.0	TS
5691.50	4.30	-1.52	FeI	26.0	TS
5693.62	4.96	-2.64	FeI	26.0	TS
5696.09	4.55	-1.72	FeI	26.0	TS
5698.02	3.64	-2.68	FeI	26.0	TS
5701.54	2.56	-2.22	FeI	26.0	TS
5704.73	5.03	-1.43	FeI	26.0	TS
5705.46	4.30	-1.36	FeI	26.0	TS
5707.05	3.64	-2.40	FeI	26.0	TS
5715.09	4.28	-2.31	FeI	26.0	TS
5717.83	4.28	-1.13	FeI	26.0	TS
5720.89	4.55	-1.95	FeI	26.0	TS
5724.45	4.28	-2.64	FeI	26.0	TS
5731.76	4.26	-1.30	FeI	26.0	TS
5732.30	4.99	-1.56	FeI	26.0	TS
5734.56	4.96	-1.48	FeI	26.0	TS
5738.23	4.22	-2.34	FeI	26.0	TS
5741.85	4.26	-1.85	FeI	26.0	TS
5742.96	4.18	-2.51	FeI	26.0	TS
5752.03	4.55	-1.17	FeI	26.0	TS
5754.40	3.64	-2.70	FeI	26.0	TS
5759.26	4.65	-2.07	FeI	26.0	TS
5760.34	3.64	-2.49	FeI	26.0	TS
5769.32	4.61	-2.26	FeI	26.0	TS
5775.08	4.22	-1.30	FeI	26.0	TS
5778.45	2.59	-3.43	FeI	26.0	TS
5784.66	3.40	-2.53	FeI	26.0	TS
5793.91	4.22	-1.70	FeI	26.0	TS
5806.72	4.61	-1.05	FeI	26.0	TS
5809.22	3.88	-1.84	FeI	26.0	TS
5811.91	4.14	-2.43	FeI	26.0	TS
5814.81	4.28	-1.97	FeI	26.0	TS
5815.22	4.15	-2.62	FeI	26.0	TS
5827.88	3.28	-3.41	FeI	26.0	TS
5835.10	4.26	-2.37	FeI	26.0	TS
5837.70	4.29	-2.34	FeI	26.0	TS
5838.37	3.94	-2.34	FeI	26.0	TS
5844.92	4.15	-2.94	FeI	26.0	TS
5845.29	5.03	-1.82	FeI	26.0	TS
5848.13	4.61	-1.06	FeI	26.0	TS
5849.68	3.69	-2.99	FeI	26.0	TS
5852.22	4.55	-1.33	FeI	26.0	TS
5853.15	1.48	-5.28	FeI	26.0	TS
5855.08	4.61	-1.48	FeI	26.0	TS
5856.09	4.29	-1.33	FeI	26.0	TS
5858.78	4.22	-2.26	FeI	26.0	TS
5859.59	4.55	-0.42	FeI	26.0	TS
5861.11	4.28	-2.45	FeI	26.0	TS
5862.36	4.55	-0.13	FeI	26.0	TS
5873.21	4.26	-2.14	FeI	26.0	TS
5877.79	4.18	-2.23	FeI	26.0	TS
5879.49	4.61	-2.14	FeI	26.0	TS
5880.03	4.56	-1.94	FeI	26.0	TS
5881.28	4.61	-1.84	FeI	26.0	TS
5883.82	3.96	-1.36	FeI	26.0	TS
5898.22	4.73	-1.83	FeI	26.0	TS
5902.47	4.59	-1.81	FeI	26.0	TS
5905.67	4.65	-0.73	FeI	26.0	TS
5909.97	3.21	-2.59	FeI	26.0	TS
5916.25	2.45	-2.99	FeI	26.0	TS
5927.79	4.65	-1.09	FeI	26.0	TS
5929.68	4.55	-1.41	FeI	26.0	TS
5930.18	4.65	-0.23	FeI	26.0	TS
5933.80	4.64	-2.23	FeI	26.0	TS
5934.65	3.93	-1.17	FeI	26.0	TS
5940.99	4.18	-2.15	FeI	26.0	TS
5947.51	4.61	-2.42	FeI	26.0	TS
5952.72	3.98	-1.44	FeI	26.0	TS
5956.69	0.86	-4.61	FeI	26.0	TS
5958.33	2.18	-4.18	FeI	26.0	TS
5961.92	4.22	-3.16	FeI	26.0	TS
5969.56	4.28	-2.73	FeI	26.0	TS
5975.35	4.83	-0.69	FeI	26.0	TS
5976.78	3.94	-1.24	FeI	26.0	TS
5983.68	4.55	-0.49	FeI	26.0	TS
5984.81	4.73	-0.20	FeI	26.0	TS
5987.06	4.80	-0.43	FeI	26.0	TS
5997.78	4.61	-1.04	FeI	26.0	TS

6003.01	3.88	-1.12	FeI	26.0	TS
6005.54	2.59	-3.60	FeI	26.0	TS
6007.96	4.65	-0.60	FeI	26.0	TS
6008.56	3.88	-0.98	FeI	26.0	TS
6012.21	2.22	-4.04	FeI	26.0	TS
6015.24	2.22	-4.68	FeI	26.0	TS
6019.37	3.57	-3.36	FeI	26.0	TS
6020.17	4.61	-0.27	FeI	26.0	TS
6024.06	4.55	-0.12	FeI	26.0	TS
6027.05	4.08	-1.09	FeI	26.0	TS
6034.03	4.31	-2.42	FeI	26.0	TS
6035.34	4.29	-2.59	FeI	26.0	TS
6054.07	4.37	-2.31	FeI	26.0	TS
6056.00	4.73	-0.46	FeI	26.0	TS
6062.85	2.18	-4.14	FeI	26.0	TS
6065.48	2.61	-1.53	FeI	26.0	TS
6078.49	4.80	-0.32	FeI	26.0	TS
6079.01	4.65	-1.12	FeI	26.0	TS
6082.71	2.22	-3.57	FeI	26.0	TS
6085.26	2.76	-3.10	FeI	26.0	TS
6089.59	4.58	-3.62	FeI	26.0	TS
6093.64	4.61	-1.50	FeI	26.0	TS
6094.37	4.65	-1.94	FeI	26.0	TS
6096.66	3.98	-1.93	FeI	26.0	TS
6098.24	4.56	-1.88	FeI	26.0	TS
6105.13	4.55	-2.05	FeI	26.0	TS
6120.25	0.91	-5.95	FeI	26.0	TS
6127.91	4.14	-1.40	FeI	26.0	TS
6136.61	2.45	-1.40	FeI	26.0	TS
6136.99	2.20	-2.95	FeI	26.0	TS
6137.69	2.59	-1.40	FeI	26.0	TS
6139.64	2.59	-4.50	FeI	26.0	TS
6145.41	3.37	-3.70	FeI	26.0	TS
6151.62	2.18	-3.30	FeI	26.0	TS
6157.73	4.08	-1.26	FeI	26.0	TS
6159.37	4.61	-2.37	FeI	26.0	TS
6165.36	4.14	-1.47	FeI	26.0	TS
6170.51	4.80	-0.44	FeI	26.0	TS
6173.33	2.22	-2.88	FeI	26.0	TS
6180.20	2.73	-2.59	FeI	26.0	TS
6187.40	2.83	-4.16	FeI	26.0	TS
6187.99	3.94	-1.72	FeI	26.0	TS
6191.56	2.43	-1.42	FeI	26.0	TS
6199.51	2.56	-4.43	FeI	26.0	TS
6200.31	2.61	-2.44	FeI	26.0	TS
6213.43	2.22	-2.48	FeI	26.0	TS
6215.14	4.19	-1.32	FeI	26.0	TS
6219.28	2.20	-2.43	FeI	26.0	TS
6220.78	3.88	-2.46	FeI	26.0	TS
6221.67	0.86	-5.97	FeI	26.0	TS
6226.73	3.88	-2.22	FeI	26.0	TS
6229.23	2.85	-2.81	FeI	26.0	TS
6230.72	2.56	-1.28	FeI	26.0	TS
6232.64	3.65	-1.22	FeI	26.0	TS
6240.65	2.22	-3.23	FeI	26.0	TS
6246.32	3.60	-0.73	FeI	26.0	TS
6252.55	2.40	-1.69	FeI	26.0	TS
6253.83	4.73	-1.66	FeI	26.0	TS
6254.26	2.28	-2.44	FeI	26.0	TS
6265.13	2.18	-2.55	FeI	26.0	TS
6270.22	2.86	-2.46	FeI	26.0	TS
6271.28	3.33	-2.70	FeI	26.0	TS
6280.62	0.86	-4.39	FeI	26.0	TS
6290.54	2.59	-4.33	FeI	26.0	TS
6290.96	4.73	-0.77	FeI	26.0	TS
6293.92	4.83	-1.72	FeI	26.0	TS
6297.79	2.22	-2.74	FeI	26.0	TS
6301.50	3.65	-0.72	FeI	26.0	TS
6302.49	3.69	-0.97	FeI	26.0	TS
6303.46	4.32	-2.66	FeI	26.0	TS
6311.50	2.83	-3.14	FeI	26.0	TS
6315.81	4.08	-1.71	FeI	26.0	TS
6318.02	2.45	-2.26	FeI	26.0	TS
6322.68	2.59	-2.43	FeI	26.0	TS
6330.85	4.73	-1.74	FeI	26.0	TS
6335.33	2.20	-2.18	FeI	26.0	TS
6336.82	3.69	-0.86	FeI	26.0	TS
6338.88	4.80	-1.06	FeI	26.0	TS
6344.15	2.43	-2.92	FeI	26.0	TS
6353.84	0.91	-6.17	FeI	26.0	TS
6355.03	2.85	-2.35	FeI	26.0	TS
6358.70	0.86	-4.47	FeI	26.0	TS
6364.36	4.80	-1.43	FeI	26.0	TS
6380.74	4.19	-1.38	FeI	26.0	TS
6385.72	4.73	-1.77	FeI	26.0	TS
6392.54	2.28	-4.03	FeI	26.0	TS
6393.60	2.43	-1.43	FeI	26.0	TS
6400.00	3.60	-0.29	FeI	26.0	TS
6400.32	0.91	-4.32	FeI	26.0	TS
6408.02	3.69	-1.02	FeI	26.0	TS
6411.11	4.73	-1.94	FeI	26.0	TS
6411.65	3.65	-0.60	FeI	26.0	TS
6419.95	4.73	-0.24	FeI	26.0	TS
6421.35	2.28	-2.03	FeI	26.0	TS
6430.84	2.18	-2.01	FeI	26.0	TS
6436.41	4.19	-2.46	FeI	26.0	TS
6464.66	0.96	-8.12	FeI	26.0	TS
6469.19	4.83	-0.77	FeI	26.0	TS
6475.62	2.56	-2.94	FeI	26.0	TS
6481.87	2.28	-2.98	FeI	26.0	TS
6483.94	1.48	-4.84	FeI	26.0	TS
6494.98	2.40	-1.27	FeI	26.0	TS
6495.74	4.83	-0.94	FeI	26.0	TS
6496.47	4.80	-0.57	FeI	26.0	TS
6498.94	0.96	-4.70	FeI	26.0	TS
6509.62	4.08	-2.97	FeI	26.0	TS
6518.37	2.83	-2.46	FeI	26.0	TS
6533.93	4.56	-1.46	FeI	26.0	TS

6546.24	2.76	-1.54	FeI	26.0	TS
6569.21	4.73	-0.13	FeI	26.0	TS
6574.23	0.99	-5.02	FeI	26.0	TS
6575.02	2.59	-2.71	FeI	26.0	TS
6581.21	1.48	-4.68	FeI	26.0	TS
6591.31	4.59	-2.07	FeI	26.0	TS
6592.91	2.73	-1.47	FeI	26.0	TS
6593.87	2.43	-2.42	FeI	26.0	TS
6597.56	4.80	-1.07	FeI	26.0	TS
6608.02	2.28	-4.03	FeI	26.0	TS
6609.11	2.56	-2.69	FeI	26.0	TS
6625.02	1.01	-5.35	FeI	26.0	TS
6627.54	4.55	-1.68	FeI	26.0	TS
6633.41	4.83	-1.49	FeI	26.0	TS
6633.75	4.56	-0.80	FeI	26.0	TS
6634.11	4.80	-1.43	FeI	26.0	TS
6646.93	2.61	-3.99	FeI	26.0	TS
6648.08	1.01	-5.43	FeI	26.0	TS
6653.85	4.15	-2.52	FeI	26.0	TS
6667.42	2.45	-4.40	FeI	26.0	TS
6667.71	4.58	-2.11	FeI	26.0	TS
6677.98	2.69	-1.42	FeI	26.0	TS
6699.14	4.59	-2.10	FeI	26.0	TS
6703.57	2.76	-3.16	FeI	26.0	TS
6704.48	4.22	-2.66	FeI	26.0	TS
6705.10	4.61	-1.38	FeI	26.0	TS
6707.43	4.61	-3.71	FeI	26.0	TS
6710.32	1.48	-4.88	FeI	26.0	TS
6713.05	4.61	-0.96	FeI	26.0	TS
6713.19	4.14	-2.97	FeI	26.0	TS
6713.74	4.80	-1.60	FeI	26.0	TS
6715.38	4.61	-1.64	FeI	26.0	TS
6716.24	4.58	-1.92	FeI	26.0	TS
6725.36	4.10	-2.30	FeI	26.0	TS
6726.67	4.61	-1.09	FeI	26.0	TS
6730.29	4.91	-0.62	FeI	26.0	TS
6732.06	4.58	-2.21	FeI	26.0	TS
6733.15	4.64	-1.58	FeI	26.0	TS
6737.98	4.56	-1.75	FeI	26.0	TS
6739.52	1.56	-4.79	FeI	26.0	TS
6745.10	4.58	-2.16	FeI	26.0	TS
6745.96	4.08	-2.77	FeI	26.0	TS
6746.95	2.61	-4.35	FeI	26.0	TS
6750.15	2.42	-2.62	FeI	26.0	TS
6752.71	4.64	-1.20	FeI	26.0	TS
6753.46	4.56	-2.29	FeI	26.0	TS
6783.70	2.59	-3.98	FeI	26.0	TS
6786.86	4.19	-2.07	FeI	26.0	TS
6793.26	4.08	-2.33	FeI	26.0	TS
6796.12	4.14	-2.53	FeI	26.0	TS
6804.27	4.58	-1.81	FeI	26.0	TS
6806.84	2.73	-3.21	FeI	26.0	TS
6810.26	4.61	-0.99	FeI	26.0	TS
6820.37	4.64	-1.32	FeI	26.0	TS
6828.59	4.64	-0.92	FeI	26.0	TS
6833.23	4.64	-2.08	FeI	26.0	TS
6837.01	4.59	-1.69	FeI	26.0	TS
6839.83	2.56	-3.45	FeI	26.0	TS
6841.34	4.61	-0.75	FeI	26.0	TS
6842.69	4.64	-1.32	FeI	26.0	TS
6843.65	4.55	-0.93	FeI	26.0	TS
8514.07	2.20	-2.23	FeI	26.0	TS
8515.11	3.02	-2.07	FeI	26.0	TS
8527.85	5.02	-1.61	FeI	26.0	TS
8571.80	5.01	-1.39	FeI	26.0	TS
8582.26	2.99	-2.13	FeI	26.0	TS
8592.95	4.96	-1.09	FeI	26.0	TS
8598.83	4.39	-1.09	FeI	26.0	TS
8611.80	2.85	-1.93	FeI	26.0	TS
8613.94	4.99	-1.25	FeI	26.0	TS
8616.28	4.91	-0.71	FeI	26.0	TS
8621.60	2.95	-2.32	FeI	26.0	TS
8674.75	2.83	-1.80	FeI	26.0	TS
8688.62	2.18	-1.21	FeI	26.0	TS
8699.45	4.96	-0.38	FeI	26.0	TS
8757.19	2.85	-2.06	FeI	26.0	TS
8763.97	4.65	-0.15	FeI	26.0	TS
8784.44	4.96	-1.59	FeI	26.0	TS
8793.34	4.61	-0.09	FeI	26.0	TS
8824.22	2.20	-1.54	FeI	26.0	TS
8846.74	5.01	-0.78	FeI	26.0	TS
8868.43	3.02	-2.91	FeI	26.0	TS
8922.65	4.99	-1.70	FeI	26.0	TS
4893.81	2.83	-4.27	FeII	26.1	TS
4923.92	2.89	-1.32	FeII	26.1	TS
4993.35	2.81	-3.64	FeII	26.1	TS
5000.73	2.78	-4.54	FeII	26.1	TS
5018.44	2.89	-1.22	FeII	26.1	TS
5100.65	2.81	-4.17	FeII	26.1	TS
5132.66	2.81	-3.98	FeII	26.1	TS
5136.80	2.84	-4.29	FeII	26.1	TS
5169.03	2.89	-1.25	FeII	26.1	TS
5197.57	3.23	-2.10	FeII	26.1	TS
5234.62	3.22	-2.23	FeII	26.1	TS
5256.93	2.89	-4.18	FeII	26.1	TS
5264.80	3.23	-3.12	FeII	26.1	TS
5272.40	5.96	-2.03	FeII	26.1	TS
5284.10	2.89	-2.99	FeII	26.1	TS
5316.61	3.15	-1.85	FeII	26.1	TS
5316.78	3.22	-2.76	FeII	26.1	TS
5325.55	3.22	-3.12	FeII	26.1	TS
5337.72	3.23	-3.79	FeII	26.1	TS
5362.86	3.20	-2.62	FeII	26.1	TS
5414.07	3.22	-3.54	FeII	26.1	TS
5425.25	3.20	-3.16	FeII	26.1	TS
5427.82	6.72	-1.58	FeII	26.1	TS
5525.12	3.27	-3.95	FeII	26.1	TS
5534.84	3.24	-2.73	FeII	26.1	TS

5627.49	3.39	-4.13	FeII	26.1	TS
5932.05	3.20	-5.05	FeII	26.1	TS
5991.37	3.15	-3.54	FeII	26.1	TS
6084.10	3.20	-3.78	FeII	26.1	TS
6113.32	3.22	-4.11	FeII	26.1	TS
6129.70	3.20	-4.74	FeII	26.1	TS
6147.73	3.89	-2.83	FeII	26.1	TS
6149.25	3.89	-2.72	FeII	26.1	TS
6238.39	3.89	-2.75	FeII	26.1	TS
6239.94	3.89	-3.57	FeII	26.1	TS
6247.56	3.89	-2.31	FeII	26.1	TS
6369.46	2.89	-4.16	FeII	26.1	TS
6383.72	5.55	-2.07	FeII	26.1	TS
6407.24	3.89	-3.85	FeII	26.1	TS
6416.92	3.89	-2.65	FeII	26.1	TS
6432.68	2.89	-3.52	FeII	26.1	TS
6442.96	5.55	-2.67	FeII	26.1	TS
6446.41	6.22	-1.96	FeII	26.1	TS
6456.38	3.90	-2.10	FeII	26.1	TS
6516.08	2.89	-3.32	FeII	26.1	TS
6300.30	0.00	-9.71	OI	8.0	TS
6363.77	0.02	-10.20	OI	8.0	TS
5688.21	2.10	-0.40	NaI	11.0	TS
6154.23	2.10	-1.55	NaI	11.0	TS
6160.75	2.10	-1.25	NaI	11.0	TS
5711.09	4.35	-1.83	MgI	12.0	TS
8712.69	5.93	-1.37	MgI	12.0	TS
8736.02	5.95	-0.36	MgI	12.0	TS
6696.02	3.14	-1.57	AlI	13.0	TS
6698.67	3.14	-1.87	AlI	13.0	TS
7835.31	4.02	-0.65	AlI	13.0	TS
7836.13	4.02	-0.49	AlI	13.0	TS
8772.87	4.02	-0.17	AlI	13.0	TS
8773.90	4.02	-0.02	AlI	13.0	TS
5665.56	4.92	-1.94	SiI	14.0	TS
5690.43	4.93	-1.77	SiI	14.0	TS
5948.54	5.08	-1.13	SiI	14.0	TS
6125.03	5.61	-1.46	SiI	14.0	TS
6155.14	5.62	-0.75	SiI	14.0	TS
6244.48	5.62	-1.09	SiI	14.0	TS
6414.98	5.87	-1.03	SiI	14.0	TS
6741.63	5.98	-1.65	SiI	14.0	TS
7034.90	5.87	-0.88	SiI	14.0	TS
7375.25	6.19	-1.05	SiI	14.0	TS
7423.50	5.62	-0.18	SiI	14.0	TS
7680.27	5.86	-0.69	SiI	14.0	TS
7849.97	6.19	-0.72	SiI	14.0	TS
7932.35	5.96	-0.47	SiI	14.0	TS
7944.00	5.98	-0.31	SiI	14.0	TS
6538.60	8.05	-0.93	SI	16.0	TS
6748.84	7.87	-0.60	SI	16.0	TS
6757.17	7.87	-0.31	SI	16.0	TS
9237.54	6.53	0.04	SI	16.0	TS
4578.56	2.52	-0.70	CaI	20.0	TS
4685.27	2.93	-0.88	CaI	20.0	TS
5349.47	2.71	-0.31	CaI	20.0	TS
5581.97	2.52	-0.55	CaI	20.0	TS
5590.11	2.52	-0.57	CaI	20.0	TS
5601.28	2.53	-0.52	CaI	20.0	TS
5867.56	2.93	-1.57	CaI	20.0	TS
6166.44	2.52	-1.14	CaI	20.0	TS
6471.66	2.53	-0.69	CaI	20.0	TS
4721.02	7.05	-0.78	CaII	20.1	TS
4020.90	0.43	-2.07	CoI	27.0	TS
4110.53	1.05	-1.08	CoI	27.0	TS
4118.77	1.05	-0.49	CoI	27.0	TS
4121.31	0.92	-0.32	CoI	27.0	TS
5342.69	4.02	0.69	CoI	27.0	TS
5408.12	2.28	-2.19	CoI	27.0	TS
5454.57	4.07	-0.24	CoI	27.0	TS
5483.34	1.71	-1.49	CoI	27.0	TS
5530.77	1.71	-2.06	CoI	27.0	TS
5590.72	2.04	-1.87	CoI	27.0	TS
5647.23	2.28	-1.56	CoI	27.0	TS
5915.55	2.13	-2.00	CoI	27.0	TS
6005.02	1.71	-3.32	CoI	27.0	TS
6117.00	1.78	-2.49	CoI	27.0	TS
6189.00	1.71	-2.45	CoI	27.0	TS
6454.99	3.63	-0.25	CoI	27.0	TS
6632.43	2.28	-2.00	CoI	27.0	TS
6771.03	1.88	-1.97	CoI	27.0	TS
6814.94	1.95	-1.70	CoI	27.0	TS
7154.67	2.04	-2.42	CoI	27.0	TS
7354.58	1.88	-2.67	CoI	27.0	TS
7417.37	2.04	-2.07	CoI	27.0	TS
7437.14	1.95	-2.88	CoI	27.0	TS
5105.54	1.39	-1.52	CuI	29.0	TS
5700.24	1.64	-2.31	CuI	29.0	TS
5782.13	1.64	-1.72	CuI	29.0	TS
4722.15	4.03	-0.34	ZnI	30.0	TS
4810.53	4.08	-0.14	ZnI	30.0	TS
4607.33	0.00	0.28	SrI	38.0	TS
5119.12	0.99	-1.36	YII	39.1	TS
5289.81	1.03	-1.85	YII	39.1	TS
5402.77	1.84	-0.63	YII	39.1	TS
5509.91	0.99	-0.95	YII	39.1	TS
5728.89	1.84	-1.12	YII	39.1	TS
6795.41	1.74	-1.03	YII	39.1	TS
7881.88	1.84	-0.57	YII	39.1	TS
4687.81	0.73	0.55	ZrI	40.0	TS
4739.48	0.65	0.23	ZrI	40.0	TS
6127.48	0.15	-1.06	ZrI	40.0	TS
6134.59	0.00	-1.28	ZrI	40.0	TS
6143.25	0.07	-1.10	ZrI	40.0	TS
8070.12	0.73	-0.79	ZrI	40.0	TS
8133.01	0.69	-1.13	ZrI	40.0	TS
8389.49	0.60	-1.76	ZrI	40.0	TS
9276.97	0.69	-1.00	ZrI	40.0	TS

4208.98	0.71	-0.51	ZrII	40.1	TS
5112.28	1.66	-0.85	ZrII	40.1	TS
4554.04	0.00	0.17	BaII	56.1	TS
5853.69	0.60	-0.91	BaII	56.1	TS
6141.71	0.70	-0.03	BaII	56.1	TS
6496.89	0.60	-0.41	BaII	56.1	TS
5114.56	0.23	-1.03	LaII	57.1	TS
5290.82	0.00	-1.65	LaII	57.1	TS
5805.77	0.13	-1.56	LaII	57.1	TS
6262.29	0.40	-1.22	LaII	57.1	TS
6390.48	0.32	-1.41	LaII	57.1	TS
6774.27	0.13	-1.71	LaII	57.1	TS
5044.02	1.21	-0.07	CeI	58.0	TS
4486.91	0.29	-0.26	CeII	58.1	TS
4562.37	0.48	0.23	CeII	58.1	TS
5518.49	1.15	-0.67	CeII	58.1	TS
6043.39	1.21	-0.48	CeII	58.1	TS
4959.12	0.06	-0.80	NdII	60.1	TS
5092.79	0.38	-0.61	NdII	60.1	TS
5130.59	1.30	0.45	NdII	60.1	TS
5181.17	0.86	-0.74	NdII	60.1	TS
5431.52	1.12	-0.47	NdII	60.1	TS
6740.08	0.06	-1.53	NdII	60.1	TS
6437.64	1.32	-0.32	EuII	63.1	TS
6645.13	1.38	0.12	EuII	63.1	TS

App. C: Calibrations for Effective Temperature Estimation

Table A3: All effective temperature calibrations used for the thesis.

λ_1	λ_2	ΔT	a	b	c	d	e	f	Source	Function
5348.30	5554.89	7200-7700	8120	-919.996	-	-	-	-	KOV2	a+b*r
5348.30	5565.71	7200-7700	7940	-646.94	-	-	-	-	KOV2	a+b*r
5373.71	5501.46	7200-7700	6757	1603.21	-	-	-	-	KOV2	a+b*r
5410.91	5501.46	7200-7700	6748	463.441	-	-	-	-	KOV2	a+b*r
5497.52	5554.89	7200-7700	8065	-295.956	-	-	-	-	KOV2	a+b*r
5501.46	5554.89	7200-7700	8490	-809.128	-	-	-	-	KOV2	a+b*r
5501.46	5565.71	7200-7700	8487	-805.207	-	-	-	-	KOV2	a+b*r
5501.46	5633.97	7200-7700	8473	-557.534	-	-	-	-	KOV2	a+b*r
5506.78	5554.89	7200-7700	8673	-767.096	-	-	-	-	KOV2	a+b*r
5506.78	5565.71	7200-7700	8986	-968.498	-	-	-	-	KOV2	a+b*r
5506.78	5633.97	7200-7700	8639	-521.982	-	-	-	-	KOV2	a+b*r
5578.72	5645.62	5400-6300	9486.76	0.653644	0.283943	-	-	-	KOV2	$a*b^{1/r}*r^c$
5578.72	5805.23	5600-6750	7343	-975.039	-74.7727	-	-	-	KOV2	$a+b*r+c*r^2$
5670.86	5690.43	3700-6400	7113	-7600.38	11646.9	-9095.52	3251.54	-433.007	KOV2	$a+b*r+c*r^2+d*r^3+e*r^4+f*r^5$
5754.68	5772.15	7200-7700	8101	-941.716	-	-	-	-	KOV2	a+b*r
5754.68	5772.15	5400-7000	7553	-906.095	-319.209	-	-	-	KOV2	$a+b*r+c*r^2$
5772.15	5778.47	5000-6500	4870.26	0.991324	0.177759	-	-	-	KOV2	$a*b^r*r^c$
5772.15	5778.47	3600-5000	2733	1889.61	-	-	-	-	KOV2	a+b*r
5772.15	5847.00	3750-6400	5600.3858	0.859917	7.6436205	-	-	-	KOV3	$a*b^{1/r}*r^c$
5772.15	5866.45	3750-6400	5844.6836	0.89753238	0.36660117	-	-	-	KOV3	$a*b^r*r^c$
5778.47	5793.08	4700-6550	5150.2198	-0.19395103	-0.20263094	-	-	-	KOV3	$a*(r-b)^c$
5793.08	5793.92	4600-6900	1828	4179.03	-1318.34	150.31	-	-	KOV2	$a+b*r+c*r^2+d*r^3$
5793.08	5847.00	3750-6400	5292.4677	188.04705	-431.74828	-	-	-	KOV3	$a+b*r+c/r^2$
5793.08	5866.45	3750-6900	6385.3741	0.85596741	0.047715024	-	-	-	KOV3	$a*b^{1/r}*r^c$
5809.25	6046.00	5300-6900	7849	-2708.78	1124.64	-187.28	-	-	KOV2	$a+b*r+c*r^2+d*r^3$
5809.25	6052.67	5450-6900	7543	-2173.24	763.632	-96.4729	-	-	KOV2	$a+b*r+c*r^2+d*r^3$
5847.00	5862.36	4800-6400	4732.753	0.9950455	-0.14769983	-	-	-	KOV3	$a*b^{1/r}*r^c$
5847.00	5905.67	4800-6350	6972.3012	-4507.1987	3736.2682	-1279.5186	-	-	KOV3	$a+b*r+c*r^2+d*r^3$
5847.00	5987.05	4800-6350	6952.0126	-5341.52	5624.8112	-2521.265	-	-	KOV3	$a+b*r+c*r^2+d*r^3$
5847.00	6003.03	4800-6350	6988.9083	-6964.1741	9499.6138	-5413.4344	-	-	KOV3	$a+b*r+c*r^2+d*r^3$
5847.00	6046.00	4800-6900	5548.4816	0.9885989	-0.081945655	-	-	-	KOV3	$a*b^r*r^c$
5862.36	5866.45	3750-6400	6394.1552	0.7536621	0.033678894	-	-	-	KOV3	$a*b^{1/r}*r^c$
5866.45	5905.67	4800-6350	6727.9816	-597.326	-1541.8658	727.53509	-	-	KOV3	$a+b*r+c*r^2+d*r^3$
5866.45	5983.69	4800-6900	0.0001341342	7.8919307E-005	-1.4266169E-005	-	-	-	KOV3	$1/(a+b*r+c*r^2)$
5866.45	5984.79	4800-6900	6164.4205	0.79631902	-0.062253009	-	-	-	KOV3	$a*b^r*r^c$
5866.45	6003.03	4800-6900	7219.8944	-3585.8283	1210.6378	-	-	-	KOV3	$a+b*r+c*r^2$
5866.45	6021.79	4800-6700	7201.1881	-3234.7364	754.27062	-	-	-	KOV3	$a+b*r+c*r^2$
5866.45	6046.00	4700-6900	6034.8217	-0.27055898	-0.14115708	-	-	-	KOV3	$a*(r-b)^c$
5866.45	6055.99	4800-6900	7099.5674	-2781.3457	770.38101	-	-	-	KOV3	$a+b*r+c*r^2$
5934.66	6046.00	7200-7700	8390	-978.164	-	-	-	-	KOV2	a+b*r
5934.66	6052.67	7200-7700	8221	-918.937	-	-	-	-	KOV2	a+b*r
5956.70	5983.69	3700-6900	7286	-2865.02	1353.68	-396.557	-	-	KOV2	$a+b*r+c*r^2+d*r^3$
5956.70	6142.49	3750-6450	7052.7128	-1014.7929	97.242351	-3.3812526	-	-	KOV3	$a+b*r+c*r^2+d*r^3$
5987.05	6216.37	3600-5700	1179	6441.65	-3564.96	709.834	-	-	KOV2	$a+b*r+c*r^2+d*r^3$
6003.03	6052.67	5550-7000	6283.25	1.083756	-0.1341008	-	-	-	KOV2	$a*b^{1/r}*r^c$
6003.03	6052.67	7200-7700	8037	-551.182	-	-	-	-	KOV2	a+b*r
6007.96	6082.72	3750-6350	5459.2622	305.72716	-787.01683	-	-	-	KOV3	$a+b*r+c/r^2$
6008.56	6046.00	5600-7000	7155.97	-0.241376	-	-	-	-	KOV2	$a*r^b$
6021.79	6046.00	5700-7000	7944	-1437.72	260.697	-19.1727	-	-	KOV2	$a+b*r+c*r^2+d*r^3$
6021.79	6052.67	5700-7000	7749	-1312.04	221.004	-13.474	-	-	KOV2	$a+b*r+c*r^2+d*r^3$
6024.07	6082.72	3750-6550	5388.3579	150.09207	-1263.9396	-	-	-	KOV3	$a+b*r+c/r^2$
6039.73	6046.00	3700-5400	5569	-345.093	5.36966	-	-	-	KOV2	$a+b*r+c*r^2$
6039.73	6078.50	3750-5400	5590.5654	-1140.171	-197.64575	139.85301	-	-	KOV3	$a+b*r+c*r^2+d*r^3$
6039.73	6079.02	3750-5750	5349.3333	0.87139818	-0.06060133	-	-	-	KOV3	$a*b^r*r^c$
6039.73	6091.92	3800-6050	5060.286	0.97817533	-0.11128624	-	-	-	KOV3	$a*b^r*r^c$
6039.73	6145.02	3750-5650	5144.3594	0.95420384	-0.073702513	-	-	-	KOV3	$a*b^r*r^c$
6039.73	6155.14	3750-5450	-555860.5	-92075392	-16835.861	-3465.0764	-	-	KOV3	$(a+b*r)/(1+c*r+d*r^2)$
6039.73	6237.33	3750-5500	5188.6032	0.89874901	-0.055517417	-	-	-	KOV3	$a*b^r*r^c$
6046.00	6062.89	4600-6400	5470.5386	0.99518466	0.10524197	-	-	-	KOV3	$a*b^r*r^c$
6046.00	6081.44	4450-6400	5166.8456	-0.15189352	0.10673444	-	-	-	KOV3	$a*(r-b)^c$
6046.00	6082.72	4450-6550	5786.2114	0.98639057	0.1266466	-	-	-	KOV3	$a*b^r*r^c$
6046.00	6085.27	4450-6900	5846.0931	0.98556293	0.13541182	-	-	-	KOV3	$a*b^r*r^c$
6046.00	6086.29	4800-6800	6156.77	0.954343	0.218591	-	-	-	KOV2	$a*b^r*r^c$
6046.00	6091.18	4450-6350	4581.1358	619.83166	-82.470124	3.8980452	-	-	KOV3	$a+b*r+c*r^2+d*r^3$
6046.00	6108.12	4800-6700	6384.08	0.97804	0.0987979	-	-	-	KOV2	$a*b^{1/r}*r^c$
6046.00	6126.22	4450-6650	4243.1981	6981.8997	1.0296664	-0.0051885512	-	-	KOV3	$(a+b*r)/(1+c*r+d*r^2)$
6046.00	6130.17	4600-6350	4305.295	976.14392	-64.570196	-18.376814	-	-	KOV3	$a+b*r+c*r^2+d*r^3$
6046.00	6151.62	4450-6900	3802.3885	16046.227	2.3423486	-0.030215793	-	-	KOV3	$(a+b*r)/(1+c*r+d*r^2)$
6046.00	6165.37	4950-6500	5953.195	0.9938577	0.153777	-	-	-	KOV2	$a*b^{1/r}*r^c$
6046.00	6176.81	7200-7700	6075	877.871	-	-	-	-	KOV2	a+b*r
6046.00	6180.22	4950-6700	6383.75	0.96151	0.170212	-	-	-	KOV2	$a*b^r*r^c$
6046.00	6215.15	7200-7700	6896	358.445	-	-	-	-	KOV2	a+b*r
6046.00	6240.66	4450-6900	4016.0153	12659.012	1.8004153	-0.011523382	-	-	KOV3	$(a+b*r)/(1+c*r+d*r^2)$
6046.00	6243.11	4450-6350	5536.7477	0.99676933	0.089085045	-	-	-	KOV3	$a*b^r*r^c$
6046.00	6258.10	4750-6700	6037.88	0.98653	0.110763	-	-	-	KOV2	$a*b^{1/r}*r^c$
6052.67	6082.72	4600-6550	5731.2095	0.99327876	0.096572399	-	-	-	KOV3	$a*b^{1/r}*r^c$
6052.67	6108.12	5250-6800	6293.6	0.984529	0.129272	-	-	-	KOV2	$a*b^r*r^c$
6052.67	6108.12	7200-7700	6558	246.382	-	-	-	-	KOV2	a+b*r
6052.67	6122.23	7200-7700	6905	1649.06	-	-	-	-	KOV2	a+b*r
6052.67	6136.61	7200-7700	6866	1219.4	-	-	-	-	KOV2	a+b*r
6052.67	6151.62	5000-6800	6074.89	0.984276	0.127801	-	-	-	KOV2	$a*b^r*r^c$
6052.67	6162.18	7200-7700	6821	2178.43	-	-	-	-	KOV2	a+b*r
6052.67	6176.81	7200-7700	7016	265.574	-	-	-	-	KOV2	a+b*r
6052.67	6180.22	5000-6700	6224.77	0.979038	0.142497	-	-	-	KOV2	$a*b^r*r^c$
6052.67	6215.15	7200-7700	7025	239.858	-	-	-	-	KOV2	a+b*r
6052.67	6219.28	7200-7700	7140	302.498	-	-	-	-	KOV2	a+b*r
6052.67	6240.66	5050-6750	6057.77	0.986549	0.126622	-	-	-	KOV2	$a*b^r*r^c$

6052.67	6258.10	5000-6750	5924	688.557	-	-	-	-	KOV2	a+b*log(r)
6055.99	6062.89	3700-4850	9851.19	0.473424	-0.446733	-	-	-	KOV2	$a*b^{1/r}*r^c$
6055.99	6062.89	5000-6000	-21.6837	418.865	4532	-	-	-	KOV2	$a+b*r+c*r^2$
6055.99	6082.72	3750-3550	5357.431	264.82251	-770.39303	-	-	-	KOV3	$a+b*r+c/r^2$
6055.99	6085.27	4900-6750	5140.04	0.96892	0.257266	-	-	-	KOV2	$a*b^r*r^c$
6055.99	6085.27	3600-4900	2405	2480.21	-	-	-	-	KOV2	a+b*r
6055.99	6151.62	3750-6700	5765.9039	289.50467	-885.53492	-	-	-	KOV3	$a+b*r+c/r^2$
6055.99	6180.22	3750-6550	6311.9278	167.30491	-1248.4987	-	-	-	KOV3	$a+b*r+c/r^2$
6055.99	6243.11	3750-6350	5143.6204	180.91218	-340.54146	-	-	-	KOV3	$a+b*r+c/r^2$
6062.89	6078.50	4800-6400	7023.5296	-6273.8558	6896.536	-2897.7313	-	-	KOV3	$a+b*r+c*r^2+d*r^3$
6062.89	6091.92	3800-6500	5594.0551	0.95024411	-0.11399896	-	-	-	KOV3	$a*b^r*r^c$
6062.89	6145.02	4750-6500	7037.1654	-3469.1523	2026.3339	-438.42083	-	-	KOV3	$a+b*r+c*r^2+d*r^3$
6062.89	6237.33	4750-6350	6986.3819	-4788.9303	4169.7261	-1434.1114	-	-	KOV3	$a+b*r+c*r^2+d*r^3$
6078.50	6082.72	3750-6400	5293.1184	268.82143	-733.04741	-	-	-	KOV3	$a+b*r+c/r^2$
6078.50	6085.27	4900-6800	5935.8	0.824949	0.0896904	-	-	-	KOV2	$a*b^{1/r}*r^c$
6078.50	6085.27	3600-4950	2484	2374.49	-	-	-	-	KOV2	a+b*r
6078.50	6243.11	3750-6350	5152.999	173.02512	-349.42793	-	-	-	KOV3	$a+b*r+c/r^2$
6078.50	6258.10	3750-6400	6707.9691	0.74607455	0.057018238	-	-	-	KOV3	$a*b^{1/r}*r^c$
6078.50	6258.71	3900-6900	8385.9963	0.57382889	-	-	-	-	KOV3	a*r/(b+r)
6081.44	6145.02	3750-5700	547550.54	13399692	2584.0445	211.68131	-	-	KOV3	$(a+b*r)/(1+c*r+d*r^2)$
6081.44	6155.14	3750-5500	5751.571	-1528.4472	503.44595	-90.6585	-	-	KOV3	$a+b*r+c*r^2+d*r^3$
6081.44	6176.81	3800-5500	5537.8688	-984.85259	11.202499	-	-	-	KOV3	$a+b*r+c/r^2$
6081.44	6237.33	3750-5900	1264810.5	55029420	10277.115	1582.781	-	-	KOV3	$(a+b*r)/(1+c*r+d*r^2)$
6081.44	6243.81	3750-5900	1276671.6	41437376	7844.3312	1018.2459	-	-	KOV3	$(a+b*r)/(1+c*r+d*r^2)$
6082.72	6091.92	3800-6550	6255.7979	0.91578628	-0.089526206	-	-	-	KOV3	$a*b^r*r^c$
6082.72	6125.03	4800-6550	7189.7511	-1996.0635	425.19285	-	-	-	KOV3	$a+b*r+c*r^2$
6082.72	6142.49	3750-6550	8026.8322	-1.2495207	-0.4271677	-	-	-	KOV3	$a*(r-b)^c$
6082.72	6145.02	3750-6550	6039.2179	0.9182164	-0.098249267	-	-	-	KOV3	$a*b^r*r^c$
6082.72	6155.14	4800-6550	5145.1625	-0.14258724	-0.20952186	-	-	-	KOV3	$a*(r-b)^c$
6082.72	6170.49	4800-6600	5771.2091	-0.55350322	-0.42594585	-	-	-	KOV3	$a*(r-b)^c$
6082.72	6237.33	3750-6550	7072.4147	-3032.6104	1513.9486	-371.04912	-	-	KOV3	$a+b*r+c*r^2+d*r^3$
6082.72	6243.81	3750-6550	7196.6943	-2751.3448	1087.5405	-213.44259	-	-	KOV3	$a+b*r+c*r^2+d*r^3$
6085.27	6086.29	4200-6700	7683	-2129.69	114.528	-	-	-	KOV2	$a+b*r+c*r^2$
6085.27	6091.92	3800-6650	7252.8278	-1703.6908	311.72639	-21.895353	-	-	KOV3	$a+b*r+c*r^2+d*r^3$
6085.27	6142.49	3750-6650	7634.692	630.77421	0.44872922	-0.018371584	-	-	KOV3	$(a+b*r)/(1+c*r+d*r^2)$
6085.27	6155.14	3750-6900	5708.4483	0.8720183	-0.10554208	-	-	-	KOV3	$a*b^r*r^c$
6085.27	6237.33	3750-6900	8222.8194	-1.2533326	-0.56289765	-	-	-	KOV3	$a*(r-b)^c$
6090.21	6091.92	3700-5800	6585	-1215.97	185.711	-11.2669	-	-	KOV2	$a+b*r+c*r^2+d*r^3$
6090.21	6155.14	3700-5750	5638.22	0.866727	-0.0731712	-	-	-	KOV2	$a*b^r*r^c$
6090.21	6330.86	3700-5550	7359	-1844.03	213.264	-	-	-	KOV2	$a+b*r+c*r^2$
6091.18	6125.03	4800-6350	4277.4717	1.139652	-0.22374728	-	-	-	KOV3	$a*b^r*r^c$
6091.18	6145.02	3750-5750	4980.2378	0.96649545	-0.11349399	-	-	-	KOV3	$a*b^r*r^c$
6091.18	6155.14	3750-5450	5153.6733	0.8565174	-0.054459935	-	-	-	KOV3	$a*b^r*r^c$
6091.18	6237.33	3750-5750	4928.1186	0.91700085	-0.1017638	-	-	-	KOV3	$a*b^r*r^c$
6091.92	6219.28	7200-7700	6935	1346.25	-	-	-	-	KOV2	a+b*r
6091.92	6243.11	3800-6350	5625.0556	0.96931038	0.092095843	-	-	-	KOV3	$a*b^{1/r}*r^c$
6093.14	6093.66	3700-6200	6679	-3868.72	3130.89	-1022.74	-	-	KOV2	$a+b*r+c*r^2+d*r^3$
6108.12	6125.03	5600-7000	7910.42	0.821822	0.0421413	-	-	-	KOV2	$a*b^r*r^c$
6108.12	6145.02	4000-7000	7598	-1309.78	90.231	-	-	-	KOV2	$a+b*r+c*r^2$
6108.12	6155.14	4600-6900	7023.0844	-614.59734	-1541.5092	661.13611	-	-	KOV3	$a+b*r+c*r^2+d*r^3$
6108.12	6237.33	5400-7000	7549	-1908.86	283.413	-	-	-	KOV2	$a+b*r+c*r^2$
6125.03	6126.22	4400-6650	5571.4418	0.95872488	0.2433342	-	-	-	KOV3	$a*b^r*r^c$
6125.03	6151.62	5600-6600	6834.79	0.892416	0.0563776	-	-	-	KOV2	$a*b^{1/r}*r^c$
6125.03	6243.11	4800-6350	4414.6542	1216.2187	-311.79239	31.88682	-	-	KOV3	$a+b*r+c*r^2+d*r^3$
6125.03	6358.69	7200-7700	8295	-505.937	-	-	-	-	KOV2	a+b*r
6126.22	6145.02	3750-6900	5541.4767	-0.22966992	-0.23199881	-	-	-	KOV3	$a*(r-b)^c$
6126.22	6155.14	3750-6550	5192.2074	0.91920445	-0.12146185	-	-	-	KOV3	$a*b^r*r^c$
6126.22	6237.33	3750-6550	5343.9359	0.92516671	-0.12840343	-	-	-	KOV3	$a*b^r*r^c$
6128.99	6237.33	3750-6550	6934.9822	-3307.7598	2018.2402	-577.34869	-	-	KOV3	$a+b*r+c*r^2+d*r^3$
6135.36	6142.49	3700-5300	5575	-656.539	35.5005	-	-	-	KOV2	$a+b*r+c*r^2$
6135.36	6237.33	3750-5650	5193.125	0.8986041	-0.044948334	-	-	-	KOV3	$a*b^r*r^c$
6136.61	6243.11	3750-6350	5226.9903	78.711256	-1353.7489	-	-	-	KOV3	$a+b*r+c/r^2$
6142.49	6243.11	3750-6350	5575.6374	0.97029759	0.097815165	-	-	-	KOV3	$a*b^{1/r}*r^c$
6145.02	6151.62	3750-6700	7414.7921	0.24285202	-	-	-	-	KOV3	a*r/(b+r)
6145.02	6180.22	3700-5000	2382	5416.72	-	-	-	-	KOV2	a+b*r
6145.02	6243.11	3750-6350	5515.3062	0.96712503	0.09179199	-	-	-	KOV3	$a*b^{1/r}*r^c$
6145.02	6258.10	3700-6700	2870	5476.94	-3256.51	800.595	-	-	KOV2	$a+b*r+c*r^2+d*r^3$
6150.16	6237.33	3700-4900	5505	-770.29	-	-	-	-	KOV2	a+b*r
6150.16	6380.75	3700-4800	6126	-1611.92	-	-	-	-	KOV2	a+b*r
6151.62	6155.14	3750-6900	6727.799	0.7737723	-0.036684239	-	-	-	KOV3	$a*b^r*r^c$
6151.62	6237.33	3750-6900	7156.5565	-1767.765	146.61902	-	-	-	KOV3	$a+b*r+c*r^2$
6155.14	6180.22	3750-6900	-14407.078	75426.24	10.641479	-0.09935597	-	-	KOV3	$(a+b*r)/(1+c*r+d*r^2)$
6155.14	6240.66	3750-6900	6784.9875	0.76711376	0.026378813	-	-	-	KOV3	$a*b^{1/r}*r^c$
6155.14	6243.11	3750-6350	5393.2959	0.92019335	0.073807492	-	-	-	KOV3	$a*b^{1/r}*r^c$
6155.14	6358.69	3700-6700	6642.5	0.85674	0.086193	-	-	-	KOV2	$a*b^{1/r}*r^c$
6170.49	6180.22	5150-6850	380	7413.41	-3207.31	501.652	-	-	KOV2	$a+b*r+c*r^2+d*r^3$
6176.81	6243.11	3800-6350	5094.4861	234.05509	-315.52803	-	-	-	KOV3	$a+b*r+c/r^2$
6176.81	6258.10	3700-6200	6317.32	0.812411	0.611525	-	-	-	KOV2	$a*b^r*r^c$
6176.81	6261.10	4700-6700	2011	3758	-753.8	-	-	-	KOV1	$a+b*r+c*r^2$
6180.22	6237.33	3750-6900	7361.1377	-1749.5269	52.616694	-	-	-	KOV3	$a+b*r+c*r^2$
6189.01	6237.33	3750-5400	5602.0793	-1172.9134	370.85881	-109.56462	-	-	KOV3	$a+b*r+c*r^2+d*r^3$
6189.01	6244.48	3750-5500	5421.6284	-616.52128	9.4613246	-	-	-	KOV3	$a+b*r+c/r^2$
6200.32	6237.33	5300-6900	7936	-1668.99	-	-	-	-	KOV2	a+b*r
6219.28	6414.99	7200-7700	8068	-364.285	-	-	-	-	KOV2	a+b*r
6232.65	6243.11	3750-6350	5105.7991	177.4715	-513.57204	-	-	-	KOV3	$a+b*r+c/r^2$
6237.33	6240.66	3750-6900	32620441	-168828320	-25019.24	389.82997	-	-	KOV3	$(a+b*r)/(1+c*r+d*r^2)$
6237.33	6243.11	3750-6350	5509.5994	0.92783258	0.074721402	-	-	-	KOV3	$a*b^{1/r}*r^c$
6237.33	6258.10	4700-6700	6691.94	0.808588	0.0677634	-	-	-	KOV2	$a*b^{1/r}*r^c$
6237.33	6258.71	4800-6700	2379	5481.69	-2484.04	406.352	-	-	KOV2	$a+b*r+c*r^2+d*r^3$
6237.33	6358.69	3750-6900	7336.2706	0.82039503	0.021229756	-	-	-	KOV3	$a*b^{1/r}*r^c$
6240.66	6243.81	3750-6900	7448.8726	0.77089127	-	-	-	-	KOV3	$a*b^r$
6240.66	6244.48	4500-6900	7340.2	0.793709	-0.0153904	-	-	-	KOV2	$a*b^r*r^c$
6240.66	6414.99	4000-6900	6892.895	0.84853114	-0.039046311	-	-	-	KOV3	$a*b^r*r^c$
6243.11	6243.81	4800-5900	6561.787	-2261.2405	1032.1541	-171.36594	-	-	KOV3	$a+b*r+c*r^2+d*r^3$
6243.11	6244.48	4800-5900	6564.3353	-2186.4868	956.13517	-145.40885	-	-	KOV3	$a+b*r+c*r^2+d*r^3$
6243.11	6414.99	4800-5900	6478.4211	-1881.5917	820.5678	-141.74283	-	-	KOV3	$a+b*r+c*r^2+d*r^3$

6243.11	6439.08	4000-5500	6265.953	-4949.8037	7534.6692	-4708.8282	-	-	KOV3	$a+b*r+c*r^2+d*r^3$
6243.81	6261.10	3700-5600	2952	3689.04	-1068.2	-	-	-	KOV2	$a+b*r+c*r^2$
6243.81	6358.69	3700-7000	7757.8	0.81203	0.00385864	-	-	-	KOV2	$a*b^{1/r}*r^c$
6244.48	6258.10	4700-6600	2199	6096	3216	634.3	-	-	KOV1	$a+b*r+c*r^2+d*r^3$
6327.60	6414.99	3700-6900	6080.41	0.906332	-0.0951967	-	-	-	KOV2	$a*b^r*r^c$
6330.13	6330.86	4700-6700	7190	-2042	307.6	-	-	-	KOV1	$a+b*r+c*r^2$
6330.13	6414.99	3700-6000	5526.66	0.937233	-0.111614	-	-	-	KOV2	$a*b^r*r^c$
6355.04	6414.99	3700-7000	7780	-1298.65	-	-	-	-	KOV2	$a+b*r$
6355.04	6419.98	3700-7000	7433	-1541.58	7.58844	-464.06	-	-	KOV2	$a+b*r+c*r^2+d*r^3$
6358.69	6414.99	4400-7000	7527	-1283.15	99.1835	-	-	-	KOV2	$a+b*r+c*r^2$
6358.69	6419.98	3700-7000	7482	-2075.08	143.949	-	-	-	KOV2	$a+b*r+c*r^2$
6392.55	6414.99	3700-6200	6889	-4485.89	4193.86	-1917.35	294.546	-	KOV2	$a+b*r+c*r^2+d*r^3+e*r^4$
6414.99	6498.95	4200-6550	6204.5377	0.91929415	0.066862673	-	-	-	KOV3	$a*b^{1/r}*r^c$
6498.95	6597.61	4850-6600	8132	-4988.98	4606.31	-2274.22	408.814	-	KOV2	$a+b*r+c*r^2+d*r^3+e*r^4$
6538.60	6609.12	5600-7000	4943	4959.69	-4809.9	1698.54	-	-	KOV2	$a+b*r+c*r^2+d*r^3$
6597.61	6608.03	4700-6500	3853	1195	-225	15.9	-	-	KOV1	$a+b*r+c*r^2+d*r^3$
6608.03	6721.85	4700-6550	0.0001475568	8.19176E-005	-2.7477373E-005	-	-	-	KOV3	$1/(a+b*r+c*r^2)$
6609.12	6748.84	5000-7000	6073.03	0.994752	-0.118793	-	-	-	KOV2	$a*b^{1/r}*r^c$
6609.12	6757.17	4400-6900	5845.1056	1.0058528	-0.12878833	-	-	-	KOV3	$a*b^r*r^c$
6680.15	6703.57	4800-6500	3635	2633	-967	130.6	-	-	KOV1	$a+b*r+c*r^2+d*r^3$
6703.57	6721.85	4700-6550	6825.2988	-840.26077	-1038.0854	496.98698	-	-	KOV3	$a+b*r+c*r^2+d*r^3$
6710.31	6713.76	4800-6300	6674	-1353	233.29	-	-	-	KOV1	$a+b*r+c*r^2$
6710.31	6721.85	3750-5700	6105.508	-1551.6196	691.66748	-176.15435	-	-	KOV3	$a+b*r+c*r^2+d*r^3$
6710.31	6767.77	3700-6000	6949	-10279.7	20503.9	-15335.9	-	-	KOV2	$a+b*r+c*r^2+d*r^3$
6717.69	6757.17	5300-6800	5926.58	1.17997	-0.138265	-	-	-	KOV2	$a*b^{1/r}*r^c$
6717.69	6757.17	7200-7700	8158	-686.136	-	-	-	-	KOV2	$a+b*r$
6721.85	6771.04	3750-6250	5554.4503	0.91377129	0.060535721	-	-	-	KOV3	$a*b^{1/r}*r^c$
6721.85	6839.83	4800-6400	3783.9506	1939.4483	-521.88679	49.382188	-	-	KOV3	$a+b*r+c*r^2+d*r^3$
6748.84	6750.15	4900-6800	6194.06	1.004298	0.138792	-	-	-	KOV2	$a*b^{1/r}*r^c$
6748.84	6767.77	5000-6800	6307.54	1.005136	0.148183	-	-	-	KOV2	$a*b^{1/r}*r^c$
6750.15	6757.17	4700-7000	6044.21	1.00735	-0.125622	-	-	-	KOV2	$a*b^{1/r}*r^c$
6757.17	6767.77	4800-6700	6169.4	1.00416	0.145267	-	-	-	KOV2	$a*b^{1/r}*r^c$
6806.85	6848.57	4700-6700	7116	-790.9	-	-	-	-	KOV1	$a+b*r$
7110.90	7022.39	5300-6500	6492	-791.06341	-	-	-	-	KOV4	$a+b*\log(r)$
7110.90	7022.95	3500-6600	7775	-5150.6755	325.81723	6084.4549	-4007.2797	-	KOV4	$a+b*r+c*r^2+d*r^3+e*r^4$
7110.90	7034.90	4500-6700	5677.678	0.9068567	-0.090936813	-	-	-	KOV4	$a*b^r*r^c$
7110.90	7071.88	5050-6500	6066	-1076.6458	-	-	-	-	KOV4	$a+b*\log(r)$
7110.90	7090.38	3900-6500	6957	796.9239	-16020.09	25423.295	-12379.132	-	KOV4	$a+b*r+c*r^2+d*r^3+e*r^4$
7110.90	7130.92	4300-7000	7740.5691	-8974.467	12385.913	-6956.3501	-	-	KOV4	$a+b*r+c*r^2+d*r^3$
7110.90	7132.99	5500-6050	5989.5842	748.53279	-1124.968	-	-	-	KOV4	$a+b*r+c*r^2$
7110.90	7181.19	4200-7000	7926.6838	-8555.0465	10974.93	-5542.4826	-	-	KOV4	$a+b*r+c*r^2+d*r^3$
7112.18	7022.95	4300-6000	7924.3779	-8118.8128	8946.0425	-4311.6523	-	-	KOV4	$a+b*r+c*r^2+d*r^3$
7112.18	7034.90	3800-6700	7348.5613	-5185.4006	3691.6343	-967.50273	-	-	KOV4	$a+b*r+c*r^2+d*r^3$
7216.18	7132.99	3500-5900	6365.0976	-2170.5471	1242.9243	-491.89608	-	-	KOV4	$a+b*r+c*r^2+d*r^3$
7216.18	7181.19	3500-5800	6463.9587	-4488.1749	5325.8248	-2628.69	-	-	KOV4	$a+b*r+c*r^2+d*r^3$
7216.18	7221.20	3500-5800	6284.6629	-1527.7419	-	-	-	-	KOV4	$a+b*r$
7251.71	7142.52	4200-6800	7654.0242	-3858.2697	2899.9181	-1135.2843	-	-	KOV4	$a+b*r+c*r^2+d*r^3$
7251.71	7181.19	4300-6900	5441.5977	-0.4745018	-0.39033324	-	-	-	KOV4	$a*(r-b)^c$
7327.65	7375.25	3500-5250	5833.1952	-1992.5838	1774.5887	-857.75968	-	-	KOV4	$a+b*r+c*r^2+d*r^3$
7357.73	7445.75	4400-5400	5781.7635	-1570.4442	-	-	-	-	KOV4	$a+b*r$
7461.52	7491.65	4400-5800	6414.7319	-1800.1392	-	-	-	-	KOV4	$a+b*r$
7461.52	7495.07	4400-5800	6152.7548	-2318.461	-	-	-	-	KOV4	$a+b*r$
7461.52	7507.27	4400-5900	7604.3548	-7135.3851	8481.292	-4440.1886	-	-	KOV4	$a+b*r+c*r^2+d*r^3$
7540.43	7511.02	4700-6000	6613.917	-14032.5	41178.67	-45064.2	-	-	KOV4	$a+b*r+c*r^2+d*r^3$
7540.43	7563.01	5000-6300	5198.713	-0.1799965	-	-	-	-	KOV4	$a*r^b$
7583.79	7468.31	5700-7000	7052.4777	-895.819	234.25416	-30.425818	1.4601492	-	KOV4	$a+b*r+c*r^2+d*r^3+e*r^4$
7583.79	7531.14	3500-6600	5973.5196	3784.5656	-4235.942	-	-	-	KOV4	$a+b*r+c*r^2$
7583.79	7586.02	3500-6900	11021.68	-38217.372	138605.19	-248399.82	209495.81	-67865.923	KOV4	$a+b*r+c*r^2+d*r^3+e*r^4+f*r^5$
7714.27	7680.27	3500-6900	7193	-29.77509	-1681.5027	731.7729	-95.782326	-	KOV4	$a+b*r+c*r^2+d*r^3+e*r^4$
7714.27	7780.56	5900-7000	9319.357	0.5872613	0.108473	-	-	-	KOV4	$a*b^r*r^c$
7714.27	7780.56	3600-7000	7831.5986	-3202.7715	2050.2954	-1218.1437	-	-	KOV4	$a+b*r+c*r^2+d*r^3$
7723.21	7680.27	3500-6000	7282.2329	-4432.9632	2956.9517	-776.4689	-	-	KOV4	$a+b*r+c*r^2+d*r^3$
7748.27	7680.27	6500-7150	7979	-1601.28	-	-	-	-	KOV4	$a+b*r$
7748.27	7680.27	4600-7000	13167.773	-21440.335	27243.5	-15901.87	3287.8501	-	KOV4	$a+b*r+c*r^2+d*r^3+e*r^4$
7748.27	7832.20	3500-6800	8443	-5245.24	6015.251	-4029.735	-	-	KOV4	$a+b*r+c*r^2+d*r^3$
7788.95	7680.27	3500-7000	7554.168	-2001.119	252.7902	-	-	-	KOV4	$a+b*r+c*r^2$
7788.95	7780.56	3500-7000	7889.0498	-4728.7165	4151.1333	-2183.3018	-	-	KOV4	$a+b*r+c*r^2+d*r^3$
7788.95	7832.20	3500-7000	8477.5756	-7634.1137	8209.1666	-4105.5848	-	-	KOV4	$a+b*r+c*r^2+d*r^3$
7788.95	7849.97	5200-7000	9151.883	-5400.7313	3647.6843	-991.87973	-	-	KOV4	$a+b*r+c*r^2+d*r^3$
7788.95	7932.35	3500-7000	12176.034	-1.8245293	-0.73875711	-	-	-	KOV4	$a*(r-b)^c$
7788.95	7944.00	4200-7000	11254.539	-30436.921	78629.353	-103193.97	64744.83	-15594.876	KOV4	$a+b*r+c*r^2+d*r^3+e*r^4+f*r^5$
7912.87	7680.27	5200-6800	7033.8179	-3523.7759	2431.6723	-589.24672	-	-	KOV4	$a+b*r+c*r^2+d*r^3$
7912.87	7710.37	5300-6800	7433.4687	-3131.7646	1119.1743	-	-	-	KOV4	$a+b*r+c*r^2$
8426.51	7680.27	5300-6400	6963.6582	-2717.0084	967.28678	-	-	-	KOV4	$a+b*r+c*r^2$